Applications of Gold Catalysis for the Synthesis of Carbocycles

Alyson Poyser

Thesis submitted to the University of Ottawa
in partial fulfillment of the requirements for the
Master's degree in Chemistry

Department of Chemistry and Biomolecular Sciences
Faculty of Science
University of Ottawa

Abstract

Terpenoid natural products are important synthetic targets due to their abundance and broad range of physiological activity. Herein, we report a method taking advantage of the divergent nature of gold(I)-catalyzed cyclization reactions to reach a range of complex polycycles.

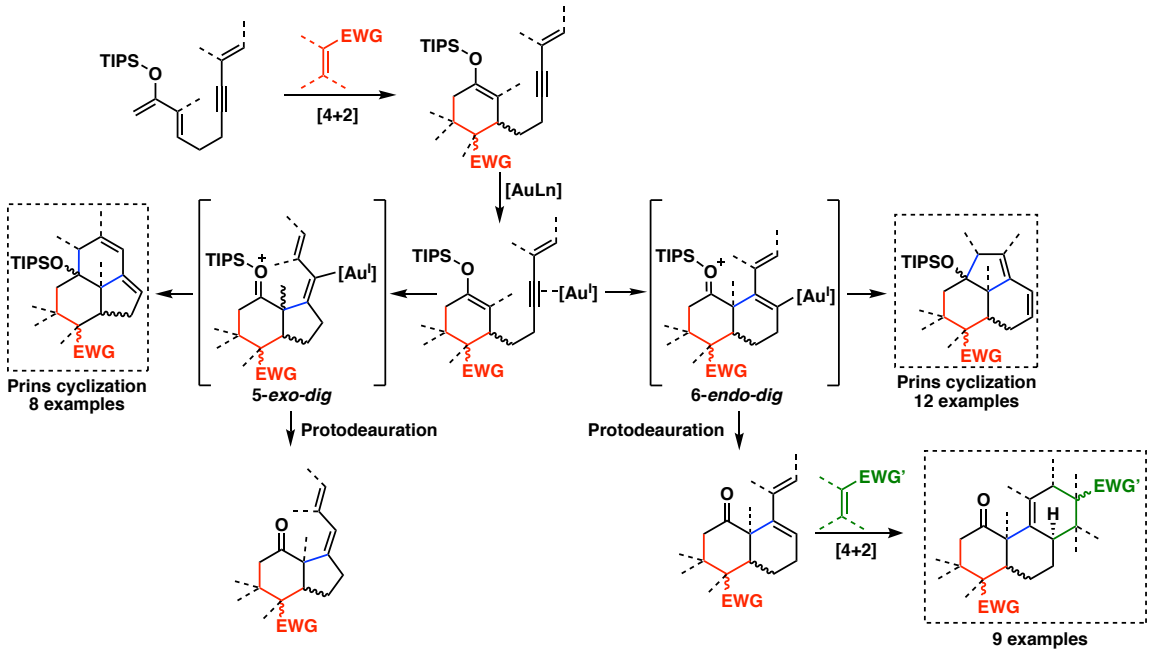

Gold(I) complexes have been investigated to selectively modulate the regioselectivity of the cyclization reaction of a silyl enol ether onto a tethered alkyne. The resulting vinyl gold intermediates can then undergo a Prins-type cyclization or protodeauration. The diene generated from the 6-*endo-dig* cyclization/ protodeauration can react in a subsequent Diels-Alder reaction, forming tri and tetracyclic products. Overall, three efficient one-pot sequences were developed to selectively synthesize carbocycles from a common starting material.

In addition, investigations into gold photoredox using dimeric catalyst $[Au_2[\mu\text{-dppm}]_2]X_2$ were also carried out for the synthesis of cyclic molecules.

Acknowledgements

First and foremost, I would like to thank Prof. Louis Barriault for giving me the opportunity to complete my honours project, as well as my graduate studies in his research group. I would not have discovered my passion for research had I not been given this chance. Thank you for allowing me to pursue my personal goals and for giving me guidance throughout this entire process. I have learned so much from this experience and you are to thank for that.

I would also like to thank all of the faculty members and support staff I have had the chance to encounter and work with. Thank you, Josée Rouleau, Annette Campeau and Chloé Lagacé for handling the administrative side of everything and answering all of my questions. Thank you, Dr. Glenn Facey, for maintaining the NMR facilities, Dr. B. Gabidullin and Dr. J. Ovens for X-ray analyses, and Sharon Curtis for managing the mass spectroscopy centre. Finally, I would like to thank my committee members, Prof. Stephen Newman and Prof. Fabien Gagosz, for your time and valuable input on my work.

The last two years would not have been the same without everybody I met in the Barriault and Gagosz labs along the way. A special thank you to Huy for taking me under his wing during my honours project. You were an incredible mentor and I'm so glad to have been able to work on a project with you. Avery, Montse, André, Julie, Sam, Phil, Martin, Dominic, Terry, David and Victor, I consider myself very fortunate to

have worked alongside all of you. You've all become good friends and I wish you all the best in your current and future endeavours.

Last but not least, I couldn't thank my family and friends enough for all the support they've given me. My parents, Jackie and Daniel, thank you for giving me so many opportunities and encouraging me from a front row seat in everything that I do. My sister, Alex, you're always there when I need it, and you have reassured and supported me through it all. Larry, you push me to be my best every single day and none of this would have been the same without you by my side. I love you all and I am so lucky to have you in my life.

Contribution statement

The project presented in chapter 2 was conducted under the supervision of Louis Barriault in collaboration with Huy Tran. Throughout the project, the synthesis of starting materials was shared between Huy Tran and I. In section 2.2.2, my contributions include the Co(III)-catalyzed Diels-Alder reaction optimization, solvent optimization of the gold(I)-catalyzed cyclization reaction and further investigations into the one-pot reactions. Dienophile optimization was shared with Huy Tran and he also completed all studies involving the gold(I) cyclization with the Diels-Alder product prepared with methyl vinyl ketone.

In chapter 2.2.3, Huy Tran completed catalyst and solvent optimizations, as well as control studies of the Diels-Alder reaction. He also carried out the ligand optimization for the gold-catalyzed cyclization reaction. The synthesis and optimization of Evan's auxiliaries for the Diels-Alder reaction was completed in collaboration. I completed the solvent optimization of the Diels-Alder/cyclization sequence, along with the second Diels-Alder reaction studies and the complete one-pot sequences presented. I also participated in preparing the steroid-like carbocycles scope. Characterization of compounds that were synthesized by Huy Tran will not appear in this thesis.

From section 2.3, I carried out the catalyst optimization for the 6-*endo*-*dig* cyclization/Prins reaction. Both scopes were shared and the molecules prepared by myself are highlighted and included in the characterization chapter.

As for chapter 3, the project was conceived by Prof. Louis Barriault and the work presented was completed by myself.

Table of Contents

List of Figures

List of Schemes

List of Tables

Abbreviations

Ac	acetate
Ad	adamantyl
AIBN	2,2'-azobisisobutyronitrile
AO	atomic orbital
Ar	aryl
Bn	benzyl
BOX	bis(oxazoline)
Bpy	2,2'-bipyridine
$CDCl_3$	deuterated chloroform
CFL	compact fluorescent light bulb
DABCO	1,4-diazabicyclo[2.2.2]octane
DCE	dichloroethane
DCM	dichloromethane
DIBAL-H	diisobutylaluminum hydride
DIPEA	N,N-diisopropylethylamine
Dppm	bis(diphenylphosphino)methane
dr	diastereoisomeric excess
Dtbbpy	di-*tert*-butyl-2,2'-bipyridine
EDG	electron donating group
ee	enantiomeric excess
equiv	equivalents
Et	ethyl
EtOAc	ethyl acetate
EWG	electron withdrawing group
h	hours
HOMO	highest occupied molecular orbital
HRMS	high-resolution mass spectroscopy
*i*Pr	isopropyl
IR	infrared

ISC	intersystem crossing
LA	Lewis acid
LBA	Lewis acid and chiral Brønsted acid system
LED	light-emitting diode
LUMO	lowest occupied molecular orbital
Me	methyl
MeCN	acetonitrile
MeOAc	methyl acetate
MeOH	methanol
MLCT	metal to ligand charge transfer
MS	molecular sieves
NMR	nuclear magnetic resonance
OTf	triflate
PCC	pyridinium chlorochromate
Ph	phenyl
Ppy	2-phenylpyridinate
RBF	round bottom flask
rt	room temperature
SET	single electron transfer
TBDPS	*tert*-butyldiphenylsilyl
TBS	*tert*-butyldimethylsilyl
*t*Bu	*tert*-butyl
*t*BuOH	*tert*-butanol
TEA	triethylamine
TFA	trifluoroacetic acid
THF	tetrahydrofuran
TIPS	tri-isopropylsilyl
TLC	thin layer chromatography
TMS	trimethylsilyl
TS	transition state
UVA	ultraviolet A

Chapter 1. Gold Catalysis

1.1 Properties of gold

Gold has been valued for thousands of years and has been used for currency, jewellery and valuable art due to its high oxidation potential. The unusual inherent stability of gold led scientific researchers to believe that it had little to no synthetic utility, and these common misconceptions have unfortunately delayed the evolution of gold chemistry. It wasn't until the early 1990's when its potential for application in organic synthesis was uncovered, leading to increased awareness and attention from the scientific community.

The Schrodinger equation is a well-known tool to determine quantum mechanical behaviour of physical systems. Applied to chemistry, this equation can define the energy levels of atoms and can generate functions describing the probability of finding particles in a specific position. However, the Schrodinger equation cannot account for systems in which the velocity of electrons approaches the speed of light (c). This phenomenon occurs when the atomic nuclear charge (Z) of an element is elevated and increases in return the velocity and mass of electrons.[1] Due to this drawback, British physicist, Paul Dirac, developed a new equation incorporating relativity. For the first time, quantum mechanics and the laws of special relativity were combined to describe particles in what we now call the Dirac equation. Properties resulting from this law are known as relativistic effects and provide clarity on the electronic structure and reactivity of elements. Gold, which has an atomic number of 79, is greatly affected by relativistic effects and derives from them its most

valued properties: strong π-Lewis acidity and the capability to stabilize neighbouring cations.[2]

An important distinction between the Schrodinger equation and the Dirac equation is the mass correction. An increase in velocity leads to an increase in mass of electrons, which has an inversely proportional relation to the Bohr radius. As Z increases, the atomic radius becomes smaller and the s and p orbitals contract, further shielding outer electrons from the nucleus. Due to this increase in shielding, the f and d orbitals experience less effective nuclear charge and expand.[1] The respective expansion and contraction of 6s and 5d orbitals are principally responsible for relativistic effects exhibited by gold complexes.[2] The contraction of the 6s orbital is responsible for the superior π-acidity of gold complexes, and the expansion of the 5d orbital can lead to backdonation of electron density and stabilization of carbocations.

1.2 Gold Reactivity

Ever since studies revealed the potential for gold in synthetic chemistry, an abundance of research has endeavoured to develop new chemical reactivity. It is a common misconception that gold-based catalysts are more expensive than other routinely used metals, such as palladium and ruthenium. In truth, the cost of a catalyst is often driven by the cost of the ligand, rather than the metal. Furthermore, gold catalysts are no more challenging to prepare. The ability of gold to tolerate acidic protons and oxygen allows for reactions to operate with high functional group

tolerance under mild conditions, such as ambient temperatures and in the presence of air and moisture.[3]

The first example of homogeneous gold catalysis was reported in 1986 by Ito and Hayashi for an asymmetric aldol reaction using a ferrocenylphosphine-gold(I) complex.[4] Later, in 1998 and 2002, Teles and Tanaka respectively reported the first applications of gold catalysis towards the addition of alcohols and water to alkynes (**Scheme 1.1**).[5,6] The use of gold(I) catalysts for the electrophilic activation of alkynes replaced the need for toxic metals, such as mercury, and played a key role in broadening the field of gold chemistry.

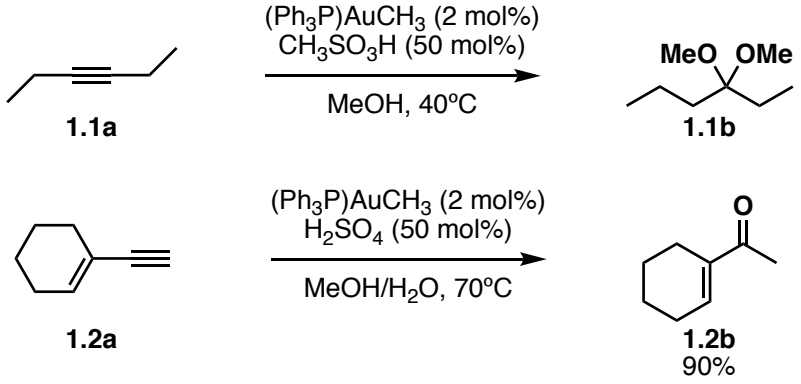

Scheme 1.1. *First applications of gold catalysis.*

1.2.1 Mechanism of gold(I)-catalyzed nucleophilic additions

Nucleophilic additions to gold-activated multiple bonds are the most common application of gold catalysis. Gold(I) is a soft Lewis acid that preferentially interacts with soft nucleophiles, such as π systems. This controlled reactivity has been applied to the activation of alkenes, allenes and alkynes. Gold is especially the metal of choice when it comes to alkyne-involved reactions, as it has the ability to chemoselectively

activate them in the presence of alkenes. The proposed explanation of the observed alkynophilicity is the lower in energy LUMO of Au-alkyne complexes when compared to Au-alkene complexes.[1]

The first stage of gold-catalyzed nucleophilic addition reactions involves electrophilic activation of a C–C multiple bond (**1.3a**) by means of coordination of the gold catalyst (**1.3b**) (**Scheme 1.2**). Then, the addition of a nucleophile proceeds in an anti manner, leading to the formation of vinyl gold species **1.3c**. Finally, the trans-alkenyl gold complex interacts with a proton through protodeauration to release the catalyst and desired product (**1.3d**). It is important to note that C–Au intermediates are not susceptible to *ß*-hydride elimination, contributing to their selective reactivity.

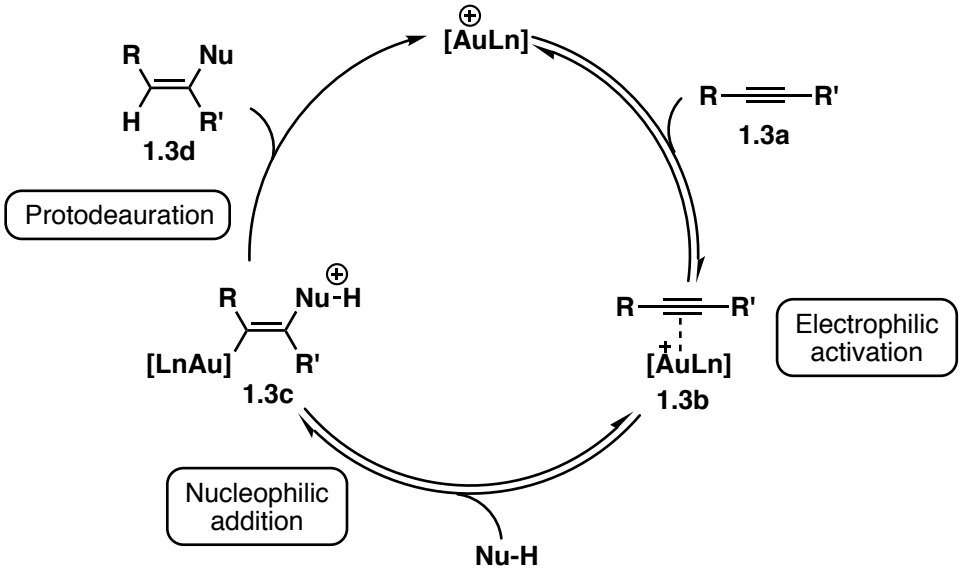

Scheme 1.2. *Stages of Gold Catalysis.*

In 2012, Xu and Hammond studied ligand effects on the reaction steps of Au-catalyzed reactions.[7] The authors found that electron poor ligands facilitate π-bond

activation by increasing the cationic nature of the gold species, thereby rendering it more electrophilic. In reactions between poorly activated substrates and weak nucleophiles, this activation step is expected to be rate determining and electron poor ligands are favorable. Protodeauration kinetics were also examined and a large influence was correlated between the ligands and the rate of the step. Sterically bulky and electron poor Ar_3P ligands seemed to decrease the rate of protodeauration, while electron rich phosphine ligands, as well as NHC ligands, led to increased rates.

1.2.2 Formation of C–C bonds

One of the most studied gold-catalyzed transformations for the creation of C–C bonds is the cycloisomerization of 1,n-enynes.[8] In the past, metals such as palladium were used as electrophilic activators for enynes to undergo Alder-ene reactions. However, this is not applicable to gold as it is not as easily oxidized from gold(I) to gold(III). Accordingly, cycloisomerization of 1,6-enynes instead involves gold(I) coordination to alkyne **1.4** and formation of a (η^2-alkyne)gold complex (**Scheme 1.3**). The electrophilically activated alkyne can then interact with the alkene and lead to cyclopropyl gold carbenes **1.5a** and **1.6a,** through a 5-*exo*-*dig* or 6-*endo*-*dig* pathway, respectively. These intermediates can be highly delocalized and can also be present as gold(I)-stabilized carbocations, due to poor π-backdonation from the gold(I). From here, various pathways can lead to a range of products.

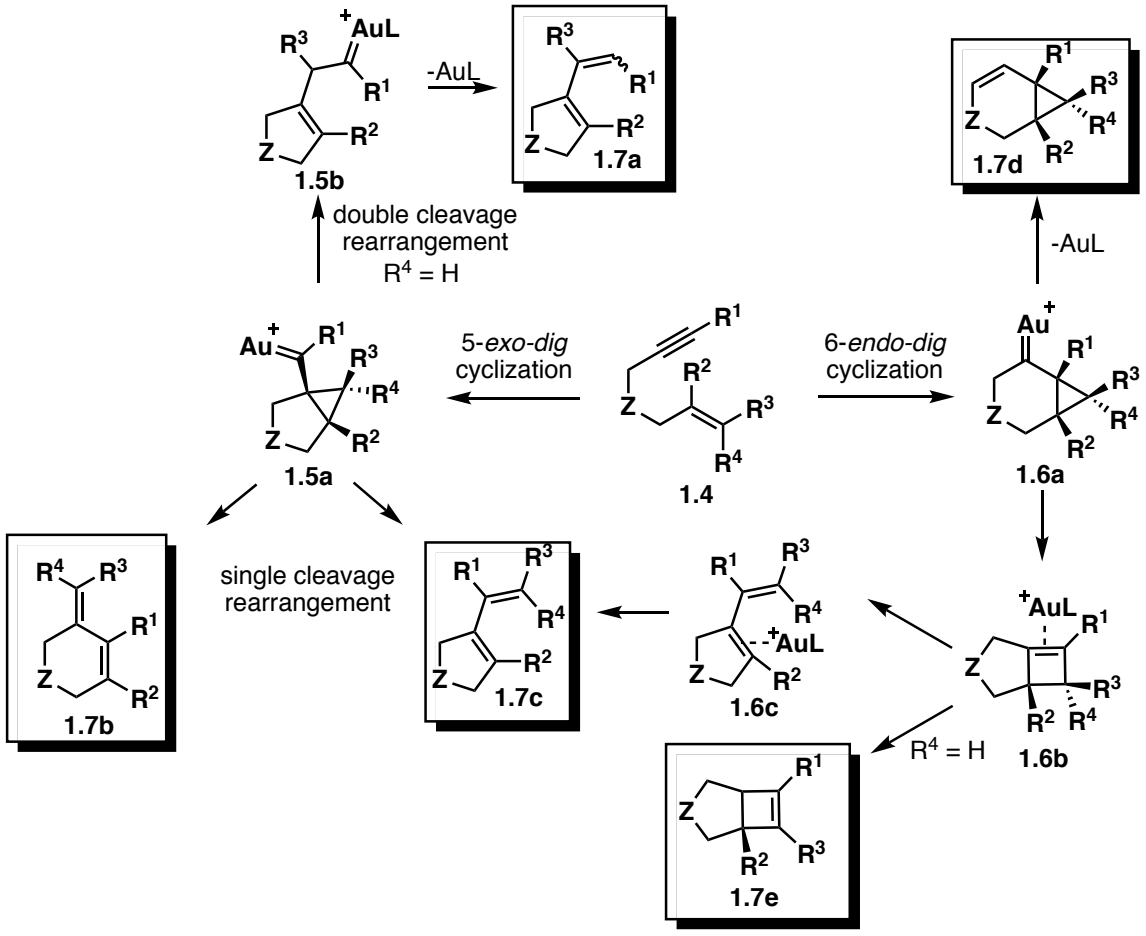

Scheme 1.3. *Reaction pathways for the cycloisomerization of 1,6-enynes.*

From intermediate **1.5a**, a 1,3-migration of the terminal carbon of the alkene, followed by a single bond cleavage, can lead to the formation of 1,3-diene **1.7c**. Following a similar 1,3-migration, an intramolecular double cleavage rearrangement involving both the alkyne and alkene, followed by proton elimination and protodeauration, can generate diene **1.7a**. A third product can also be formed by a single cleavage rearrangement, however the initial 1,3-migration involves the displacement of the internal alkene carbon. In addition, when the regioselectivity of the initial cyclization favors 6-*endo-dig* intermediate **1.6a**, the possibility of generated

products is further increased. Bicyclic product **1.7d** can be directly formed through protodemetalation. Alternatively, ring expansion of the cyclopropane intermediate forms (η^2-cyclobutene)-gold(I) complex **1.6b**, which can isomerize to produce cyclobutene **1.7e** or precursor **1.6c** through ring opening of the gold(I) complex. Over the years, different strategies have been employed to control the selectivity of these reactions.[9, 10] Modifications of the gold catalyst can largely affect the initial cyclization, and substrate design can affect the stability and reactivity of intermediates.

As an efficient approach to form C–C bonds, gold catalysis has established its place in total synthesis.[11] In 2009, the Barriault group reported the development of a Au-catalyzed cyclization method to generate bicyclo[*m.n.*1]alkenone frameworks (**Scheme 1.4**).[12] The synthetic strategy was focused on the affinity of phosphino gold(I) salts for alkyne moieties (**1.8**), targeting a 6-*endo-dig* cyclization pathway to generate the desired fused carbocyclic rings (**1.9**).

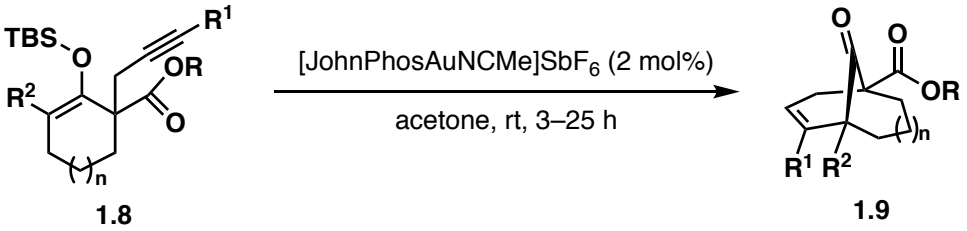

Scheme 1.4. *Optimized conditions for the formation of bicyclo[m.n.1]alkenone frameworks.*

The main challenge here was controlling the reactivity of the silyl enol ether towards the alkyne, rather than having the ester moiety cyclize in a 5-*exo-dig* manner, which could lead to bicycle **1.11** following hydrolysis. Then, cyclization

regioselectivity was important to avoid formation of the 5-*exo-dig* carbocyclic product **1.10** (**Scheme 1.5**).

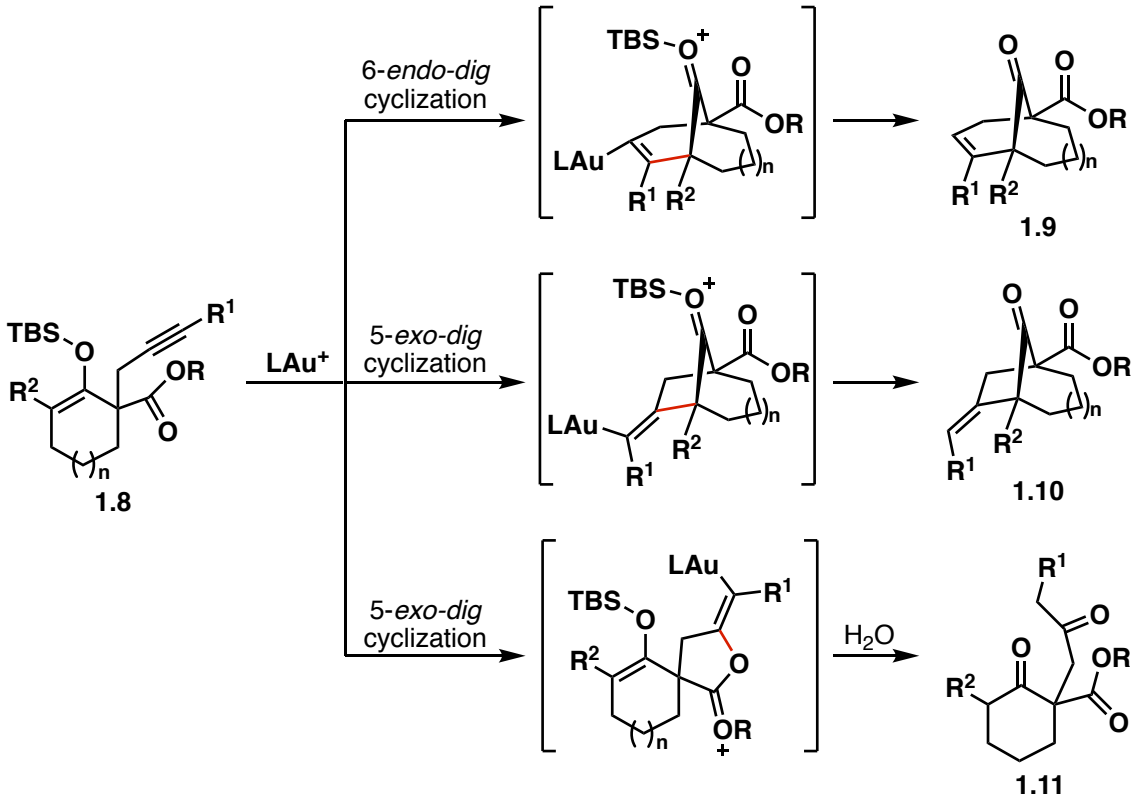

Scheme 1.5. *Alternative cyclization pathways.*

Investigations of gold catalysts revealed the ability of phosphino ligands to govern the cyclization reactivity, favoring the 6-*endo-dig* pathway. Et_3P ligand greatly improved the conversion and selectivity from Ph_3P and varying the counterion also had an important effect on regioselectivity. Further optimization targeting Buchwald ligands uncovered JohnPhos as an optimal ligand, leading to 100% conversion with excellent selectivity. Moreover, this methodology was later employed in the total synthesis of hyperforin, and papuaforins A, B, and C (**Figure 1.1**).[13]

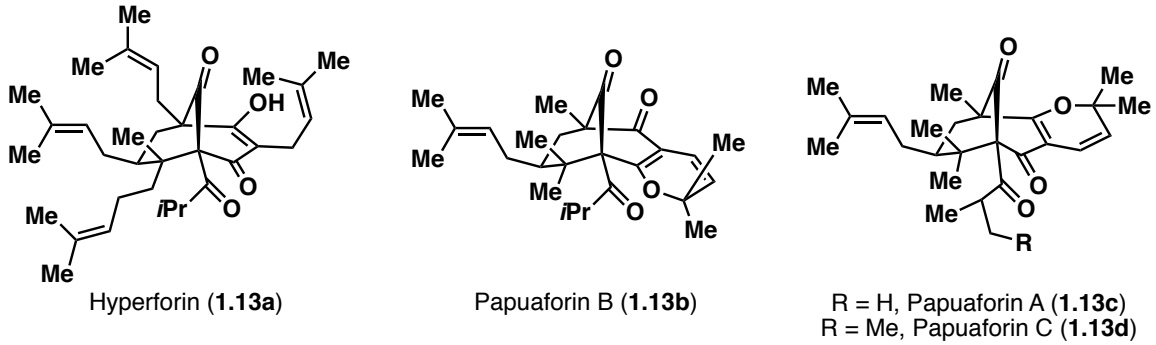

Figure 1.1. *Structures of natural products hyperforin and papuaforins A, B, and C.*

1.2.3 Formation of C-X bonds

Similar to the first examples of hydroalkoxylation achieved by Teles and Tanaka, a variety of heteronucleophile additions to multiple bonds have been developed.[14] In 2006, Genêt and Michelet reported the first gold-catalyzed cyclization of acetylenic acids (**Scheme 1.6**).[15] In general, previous methods for the addition of acids to alkynes required high temperatures, the incorporation of ligands or additives, and in some cases, Hg salts.[16] The use of AuCl in acetonitrile realized *exo*-methylene lactones in 90% yield (**1.14b**) at room temperature and in short reaction times. Ag(I) and Sc(III) were used in comparison and demonstrated the superiority of gold(I) by leading to respective product yields of 10% and 0%. The reaction conditions showed compatibility with a variety of substrate substituents, including ester, alkenyl, chloro, alkynyl, alcohol and protected alcohol moieties.

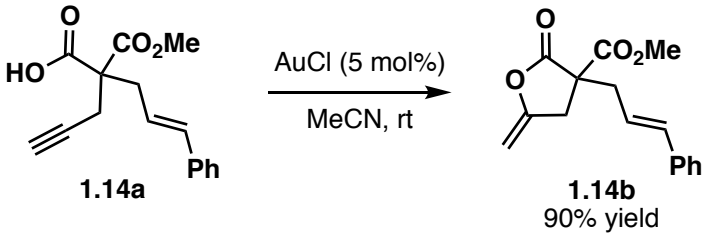

Scheme 1.6. *Cyclization of acetylenic acids reported by Genêt and Michelet.*

In 2009, Aponick and co-workers studied the intramolecular cyclization of alkynediols using PPh_3AuNTf_2, which was generated *in situ* from PPh_3AuCl and $AgNTf_2$ (**Scheme 1.7**).[17,18] Under mild conditions, the formation of highly substituted furans was performed in minutes. Catalyst loadings could be as low as 0.05% to prompt the cyclization of the alcohol onto the alkyne, forming intermediate **1.15b** and product **1.15c** following the elimination of water.

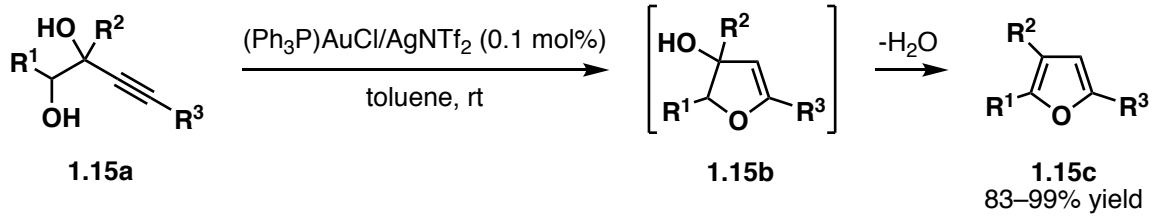

Scheme 1.7. *Intramolecular cyclization of alkynediols.*

A similar synthetic strategy as shown above was exploited to initiate a cascade cyclization reaction in the synthesis of the reported structures of curcusones I and J.[19] Through a furan formation/ [4+3] cycloaddition sequence, the distinctive 5,7-fused ring system with an oxa-bridge was achieved (**Scheme 1.8**). The first hetereocyclic ring was formed through a Au-catalyzed 5-*endo-dig* cyclization of enyne alcohol **1.16**. Buchwald ligands realized the desired transformation and optimal conditions

involved a JohnPhosAuNTf$_2$ catalyst. Rapid isomerization of the cyclization product to furan intermediate **1.17a,** and allene activation by the Au(I) catalyst (**1.17b**), prompted subsequent [4+3] cycloaddition. Furthermore, the reaction cascade was completed on large scale (5 g, 46%). Unfortunately, spectral data of the final synthesized curcusone structures (**1.19a–b**) were not compatible with reported data for the natural products, which now remain ambiguous.

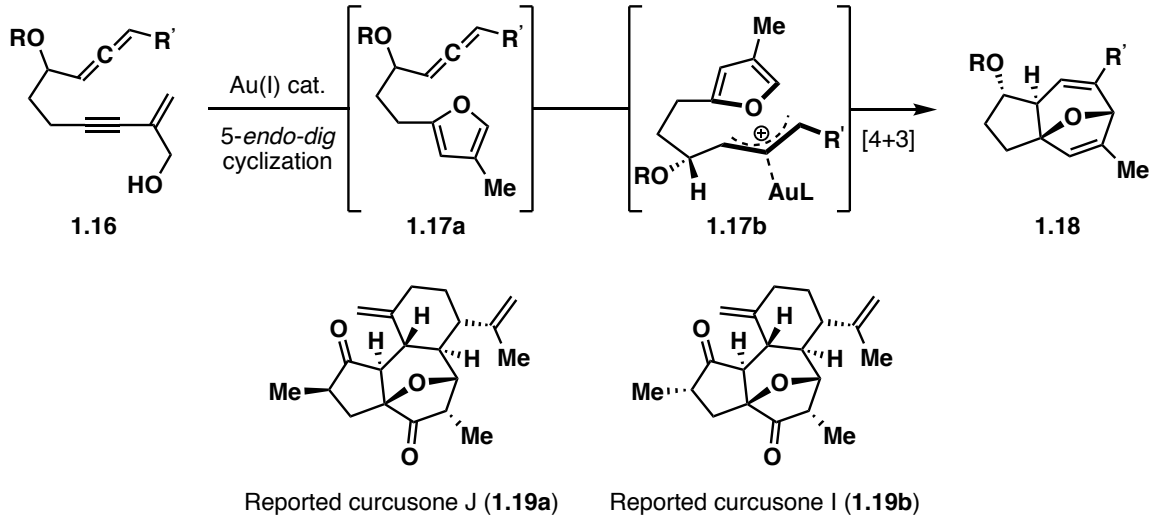

Scheme 1.8. *General reaction scheme of the Au-catalyzed tandem furan formation and [4+3] cycloaddition for the synthesis of reported curcusones I and J.*

Intramolecular hydroamination of alkynes was accomplished by Nozaki, Utimoto *et al.* under mild conditions (**Scheme 1.9**).[20, 21] Sodium tetrachloroaurate was chosen to prompt the cyclization of an amine onto a tethered alkyne. The initial enamine (**1.21a–b**) was formed through a 6-*exo-dig* cyclization or a 5-*exo-dig* cyclization, respectively from 5-alkylnylamines (**1.20a**) or 4-alkynylamines (**1.20b**). Successive tautomerization delivered the thermodynamically favored imine products (**1.22a–b**).

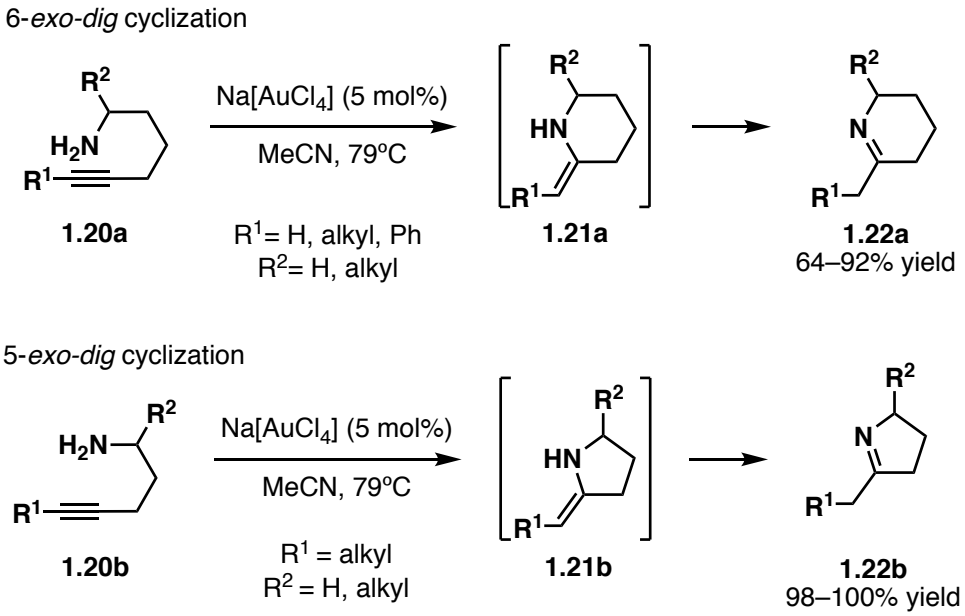

Scheme 1.9. *Intramolecular hydroamination of alkynes.*

While the intramolecular alkyne hydroamination was well developed, it wasn't until 2003 that Hayashi and Tanaka demonstrated the first application of an intermolecular alkyne hydroamination (**Scheme 1.10**).[22] The formation of imines from anilines and alkynes was accomplished using catalyst loadings as low as 0.1%. Markovnikov regioselectivity was observed from reactions involving terminal alkynes.

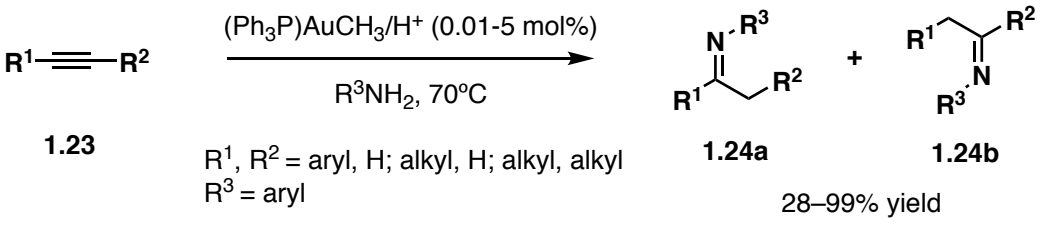

Scheme 1.10. *First example of intermolecular alkyne hydroamination.*

Gold catalysis was also exploited for C–N bond formation in the protecting-group-free total syntheses of natural products rhazinilam and rhazinicine.[23] A 6-*endo-dig* cyclization/ 5-*exo-trig* cyclization/ aromatization sequence was accomplished under catalytic gold conditions to generate mutual alkaloid intermediate **1.27** (**Scheme 1.11**). Gold coordination to the alkyne moiety (**1.25**) triggered the initial 6-*exo-dig* cyclization, generating enamide intermediate **1.26a**. The formation of oxocarbenium ion **1.26b** under acidic conditions further prompted the 5-*exo-trig* cyclization of the enamide to form intermediate **1.26c**. The latter spontaneously aromatized and desired product **1.27** was realized. The authors proposed that the use of microwave irradiation and acidic additive was especially necessary in the transformation of **1.25** due to the steric bulk of the quaternary center neighboring the alkyne. The cascade was also achieved on less substituted substrates solely in the presence of the gold(I) catalyst at 80˚C.

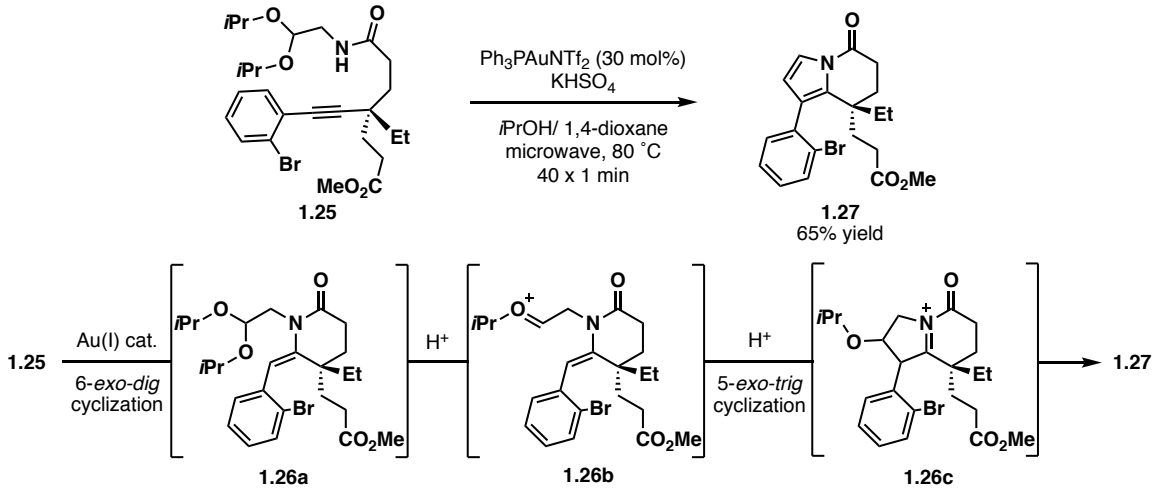

Scheme 1.11. *6-endo-dig cyclization/5-exo-trig cyclization/aromatization sequence in the protecting-group-free total syntheses of rhazinilam and rhazinicine.*

1.3 Gold catalyst binding model and ligand/counterion effects

It is apparent from transformations involving gold catalysis that the substrates and ligands have an indisputable effect on the efficiency and selectivity of the reactions.[24] Many reaction pathways have been proposed to explain these differences, based mostly on gold-stabilized carbocations and gold carbene intermediates. In 2009, Toste and coworkers investigated these theories to better understand the true character of gold–substrate intermediates.[25] When studying ligand effects, it is important to consider the components of the Au–ligand and Au–substrate bonds which can be depicted as three components, demonstrated in **figure 1.2**.

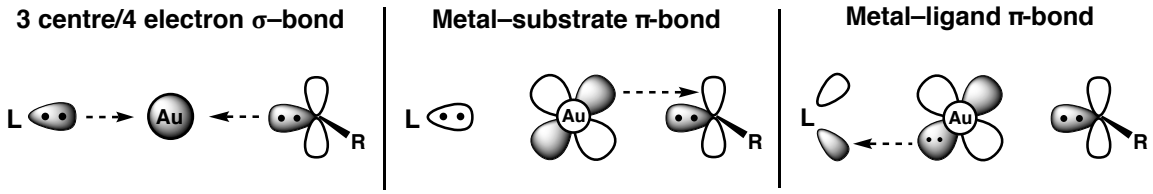

Figure 1.2. *Components of bonding interactions of gold(I) catalysts with ligands and substrates.*

First, the only vacant valence orbital on gold is the 6*s* AO which leads to a three-center-four-electron σ–hyperbond. However, this does not always equate to matching bond lengths, and increasing *trans* ligand σ–donation seemingly leads to decreased bond order between the Au center and the substrate. In addition, the π bond can be formed by electron donation from filled d-orbitals on the metal center into empty π-acceptor orbitals of the ligand and the substrate. Toste describes these gold intermediates as a continuum ranging between the singlet carbene and the metal-coordinated carbocation, suggesting these π-bonds are not mutually exclusive.

Consequently, electron density from the gold center is shared and the nature of the ligand can influence the scale (**Figure 1.3**). For example, highly π–acidic ligands will lead to stronger π-donation from the gold center to the ligand, and therefore stronger Au-stabilized carbocation reactivity.

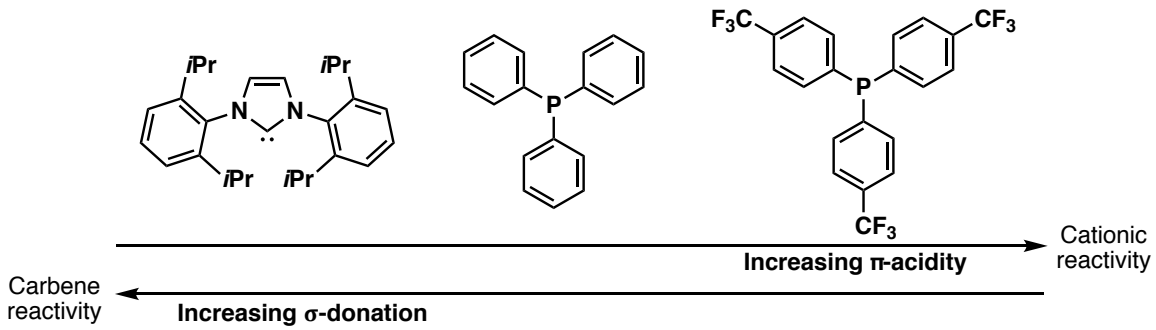

Figure 1.3. *Common gold complex ligands in increasing π-donating ability.*

Further experiments were conducted to determine the effect of the substrate on the state of cationic gold intermediates. Experiments involving measurements of π–bond rotation energy barriers were conducted for different gold-carbene complexes to approximate their strength. Through computational methods, it was suggested that the reactivity was highly dependent on stabilization of the intermediate by substituents. For example, the presence of stabilizing oxygen atoms proximate to the carbocation can decrease the bond rotation energy barrier, suggesting these substrates may preferably react as cationic intermediates.

Counterion effects on gold catalyst reactivity have also been examined. In 2017, Xu and Hammond published their works and concluded that coordinating counterions with low dissociation energies generally exhibit high reactivity.[26] This is

due to the lesser energy required to overcome Coulombic attractions and produce a charge separation between the gold and the counterion in the reaction's transition state. In **figure 1.4**, counterions are listed by decreasing affinity to gold.

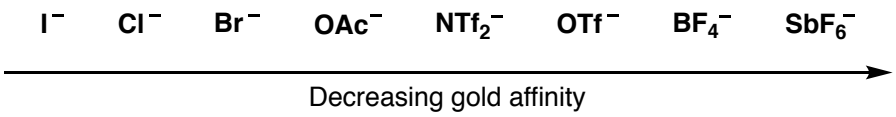

Figure 1.4. *Counterions and their affinity to gold.*

1.4. Gold as a photocatalyst

The discovery of $[Au_2(\mu\text{-dppm})_2]Cl_2$ as a photocatalyst was significant, as photochemistry gained popularity as an efficient method for the formation of C–C bonds (**Figure 1.5**). The synthesis of dimeric Au(I) complexes was first described in 1977 by Schmidbaur.[27] Although gold(I) has a [$5d^{10}$] closed-shell configuration and would only be expected to exhibit van der Waals interactions, studies demonstrated that there is a Au–Au interaction with similar strength to hydrogen bonding, between 20–50 kJ/mol.[28]

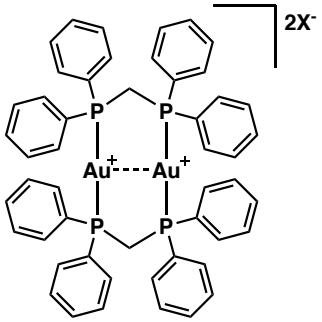

Figure 1.5. *Structure of dimeric gold complex* $[Au_2(\mu\text{-dppm})_2]X_2$.

The photophysical properties of dinuclear gold complexes were first reported in 1988 by Che *et al.*, and have been further studied since.[29–32] Investigations into

cationic species $[Au_2(\mu\text{-dppm})_2]^{2+}$ elucidated its capability to absorb light with an absorption maxima of 295 nm. Through transient absorption spectroscopy and computational experiments, it was found that the excitation of the cationic species involves the transition of an electron from the $5d_{z^2}$ anti-bonding orbital to a $6s/6p_z$ bonding orbital. The singlet excited state is not long lived, as it undergoes intersystem crossing within approximately 0.15 picoseconds to ^{3}5ds*6ps. The Au–Au bond order, which was previously 0 in the ground state, then becomes 1 in the excited state and the relative interatomic distance decreases from 2.962 Å to 2.677 Å. The dimeric catalyst was described as having great potential for photocatalysis, as it possesses a lifetime of 850 nanoseconds in its triplet excited state and has the most negative reduction potential in comparison to other commonly used catalysts. These photophysical discoveries led to a better understanding of cationic gold dimers and attracted attention to their application in photochemistry. Further studies and applications will be explored in Chapter 3.

1.5 Summary

The literature has demonstrated various applications of gold catalysis, from the electrophilic activation of π systems to the photochemical properties of dimeric gold species. The fascinating reactivity of gold is namely due to its superior π-acidic properties and its ability to stabilize carbocations. The objective of this thesis is to demonstrate the prominence of gold catalysis through different applications under thermal and photochemical conditions.

1.6 References

[1] Gorin, D. J.; Toste, F. D. Relativistic effects in homogeneous gold catalysis. *Nature*, **2007**, *446* (7136), 395–403.

[2] Bartlett, N. Relativistic Effects and the Chemistry of Gold. *Gold Bull.* **1998**, *31* (1), 22–25.

[3] Hashmi, A. S. K. Gold-Catalyzed Organic Reactions. *Chem. Rev*. **2007**, *107* (7), 3180−3211.

[4] Ito, Y.; Sawamura, M.; Hayashi, T. Catalytic Asymmetric Aldol Reaction: Reaction of Aldehydes with Isocyanate Catalyzed by a Chiral Ferrocenylphosphine-Gold(I) Complex. *J. Am. Chem. Soc*. **1986**, *108* (20), 6405–6406.

[5] Teles, J. H.; Brode, S.; Chabanas, M. Cationic Gold(I) Complexes: Highly Efficient Catalysts for the Additions of Alcohols to Alkynes. *Angew. Chem., Int. Ed.* **1998**, *37* (10), 1415–1418.

[6] Mizushima, E.; Sato, K.; Hayashi, T.; Tanaka, M. Highly Efficient Au^{I}-Catalyzed Hydration of Alkynes*. Angew. Chem., Int. Ed*. **2002**, *41* (23), 4563–4565.

[7] Wang, W.; Hammond, G. B.; Xu, B. Ligand Effects and Ligand Design in Homogeneous Gold(I) Catalysis. *J. Am. Chem. Soc*. **2012**, *134* (12), 5697−5705.

[8] Nieto-Oberhuber, C.; Lopez, S.; Mūnoz, M. P.; Cardenas, D. J.; Būnuel, E.; Nevado, C.; Echavarren, A. M. Divergent Mechanisms for the Skeletal Rearrangement and [2+2] Cycloaddition of Enynes Catalyzed by Gold. *Angew. Chem., Int. Ed.* **2005**, *44* (38), 6146–6148.

[9] Obradors, C.; Echavarren, A. M. Gold-catalyzed rearrangements and beyond. *Acc. Chem. Res.* **2014**, *47* (3), 902–912.

[10] Jiménez-Núñez, E.; Echavarren, A. M. Gold-Catalyzed Cycloisomerizations of Enynes: A Mechanistic Perspective. *Chem. Rev.* **2008**, *108* (8), 3326–3350.

[11] Dorel, R.; Echavarren, A. M. Gold(I)-Catalyzed Activation of Alkynes for the Construction of Molecular Complexity. *Chem. Rev*. **2015**, *115* (17), 9028−9072.

[12] Barabé, F.; Bétournay, G.; Bellavance, G.; Barriault, L. Gold-Catalyzed Synthesis of Carbon-Bridged Medium Sized Rings. *Org. Lett.* **2009**, *11* (18), 4236–4238.

[13] Bellavance, G.; Barriault, L. Modular Total Syntheses of Hyperforin, Papuaforins A, B and C via Gold(I)-Catalyzed Carbocyclization. *J. Org. Chem.* **2018**, 83 (*13*) 7215–7230.

[14] Corma, A.; Leyva-Pérez, A.; Sabater, M. J. Gold-Catalyzed Carbon-Heteroatom Bond-Forming Reactions. *Chem. Rev.* **2011**, *111* (3), 1657–1712.

[15] Genin, E.; Tullec, P. Y.; Antoniotti, S.; Brancour, C.; Genêt, J.-P.; Michelet, V. Room Temperature Au(I)-Catalyzed Exo-Selective Cycloisomerization of Acetylenic Acids: An Entry to Functionalized Gamma-Lactones. *J. Am. Chem. Soc.* **2006**, *128* (10), 3112–3113.

[16] Alonso, F.; Beletskaya, I. P.; Yus, M. Transition-Metal-Catalyzed Addition of Heteroatom-Hydrogen bonds to Alkynes. *Chem. Rev.* **2004**, *104* (6), 3079–3160.

[17] Aponick, A.; Li, C.-Y.; Malinge, J.; Marques, E. F. An Extremely Facile Synthesis of Furans, Pyrroles, and Thiophenes by the Dehydrative Cyclization of Propargyl Alcohols. *Org. Lett.* **2009**, *11* (20), 4624–4627.

[18] Egi, M.; Azechi, K.; Akai, S. Cationic Gold(I)-Mediated Intramolecular Cyclization of 3-Alkyne-1,2-diols and 1-Amino-3-alkyn-2-ols: A Practical Route to Furans and Pyrroles. *Org. Lett.* **2009**, *11* (21), 5002–5005.

[19] Li, Y.; Dai, M. Total Syntheses of the Reported Structures of Curcusones I and J through Tandem Gold Catalysis. *Angew. Chem., Int. Ed.* **2017**, *56* (38), 11624–11627.

[20] Fukuda, Y.; Utimoto, K.; Nozaki, H. Preparation of 2,3,4,5-tetrahydropyridines from 5-Alkynylamines under the Catalytic Action of Au(III). *Heterocycles*, **1987**, *25* (1), 297–300.

[21] Fukuda, Y.; Utimoto, K.; Preparation of 2,3,4,5-Tetrahydropyridines from 5-Alkynylamines Under the Catalytic Action of Gold(III) Salts. *Synthesis*, **1991**, *1991* (11), 975–978.

[22] Mizushima, E.; Hayashi, T.; Tanaka, M. Au(I)-Catalyzed Highly Efficient Intermolecular Hydroamination of Alkynes. *Org. Lett.* **2003**, *5* (18), 3349–3352.

[23] Sugimoto, K.; Toyoshima, K.; Nonaka, S.; Kotaki K.; Ueda, H.; Tokuyama, H. Natural Products Protecting-Group-Free Total Synthesis of (–)-Rhazinilam and (–)-Rhazinicine using a Gold-Catalyzed Cascade Cyclization. *Angew. Chem., Int. Ed.* **2013**, *52* (28), 7168–7171.

[24] Gorin, D. J.; Sherry, B. D.; Toste, F. D. Ligand Effects in Homogeneous Au Catalysis. *Chem. Rev.* **2008**, *108* (8), 3351–3378.

[25] Benitez, D.; Shapiro, N. D.; Tkatchouk, E.; Wang, Y.; Goddard, W. A.; Toste, D. F. A bonding model for gold(I) carbene complexes. *Nat. Chem.* **2009**, *1* (6), 482–486.

[26] Lu, Z.; Han, J.; Okoromoba, O. E.; Shimizu, N.; Amii, H.; Tormen, C. F.; Hammon, G. B.; Xu, B. Predicting Counterion Effects Using a Gold Affinity Index and a Hydrogen Bonding Basicity Index. *Org. Lett.* **2017**, *19* (21), 5848–5851.

[27] Schmidbaur, H.; Wohlleben, A.; Wagner, F.; Orama, O.; Huttner, G. Synthese und Kristallstruktur zweikerniger Gold(1)-Ver bindungen. *Chem. Ber.* **1977**, *110* (8), 1748–1754.

[28] Schmidbaur, H.; Schier, A. Aurophilic interactions as a subject of current research: an up-date. *Chem. Soc. Rev.*, **2012**, *41* (1), 370–412.

[29] Che, C.-M.; Kwong, H.-L.; Yam.; Cho, K.-C. Spectroscopic properties and redox chemistry of the phosphorescent excited state of $[Au_2(dppm)_2]^{2+}$[dppm = bis(diphenylphosphino)methane]. *J. Chem. Soc., Chem. Commun.,* **1989**, (13), 885–886.

[30] Li, D.; Che, C.-M.; Kwong, H.-L.; Yam, V. W.-W. Photoinduced C–C– Bond Formation from Alkyl Halides catalyzed by Luminescent Dinuclear Gold(I) and Copper(I) Complexes. *J. Chem. Soc. Dalton Trans.* **1992**, (23), 3325–3329.

[31] Fu, W.-F.; Chan, K.-C.; Miskowski V. M.; Che, C.-M. Die innere ^{3}[dσ*pσ]-Emission zweikerniger Gold(I)-Komplexe mit zwei verbrückenden Diphosphan-Liganden liegt im nahen UV-Bereich, Emissionen im sichtbaren Bereich sind auf Exciplexe zurückzuführen. *Angew. Chem.,* **1999**, *111* (18), 2953–2955.

[32] Ma, C.; Chan, C. T.-L.; To, W.-P.; Kwok, W.-M.; Che, C.-M. Deciphering Photoluminescence Dynamics and Reactivity of the Luminescent Metal–Metal-Bonded Excited State of a Binuclear Gold(I) Phosphine Complex Containing Open Coordination Sites. *Chem. Eur. J.,* **2015**, *21* (40), 13888–13893.

Chapter 2. Divergent strategies for the formation of fused carbocycles

2.1 Introduction

From the development of synthetic methodologies, to the design of new molecular systems and the study of biological properties, natural product synthesis is a key research area that encompasses many fields of science. It has become a highlight in organic chemistry for many years, especially due to the importance of natural products and natural product-derived compounds in the pharmaceutical industry. The structural complexity of natural products has made them interesting targets for synthetic organic chemists, leading the modern field of chemistry in pursuit of highly selective and efficient methods.

2.1.1 Introduction to terpenoids

Terpenoids represent a large class of naturally derived products from terpene precursors. These compounds are highly relevant as they have a large range of biological activity. Steroids in particular are very effective because they often play a major role in cell signalling by coordinating basic cellular activity.[33] They are commonly used for contraception, hormone replacement therapy, or as immunosuppressants for the treatments of diseases such as rheumatoid arthritis, asthma, skin diseases, allergies and cancer (**Figure 2.1**).[34]

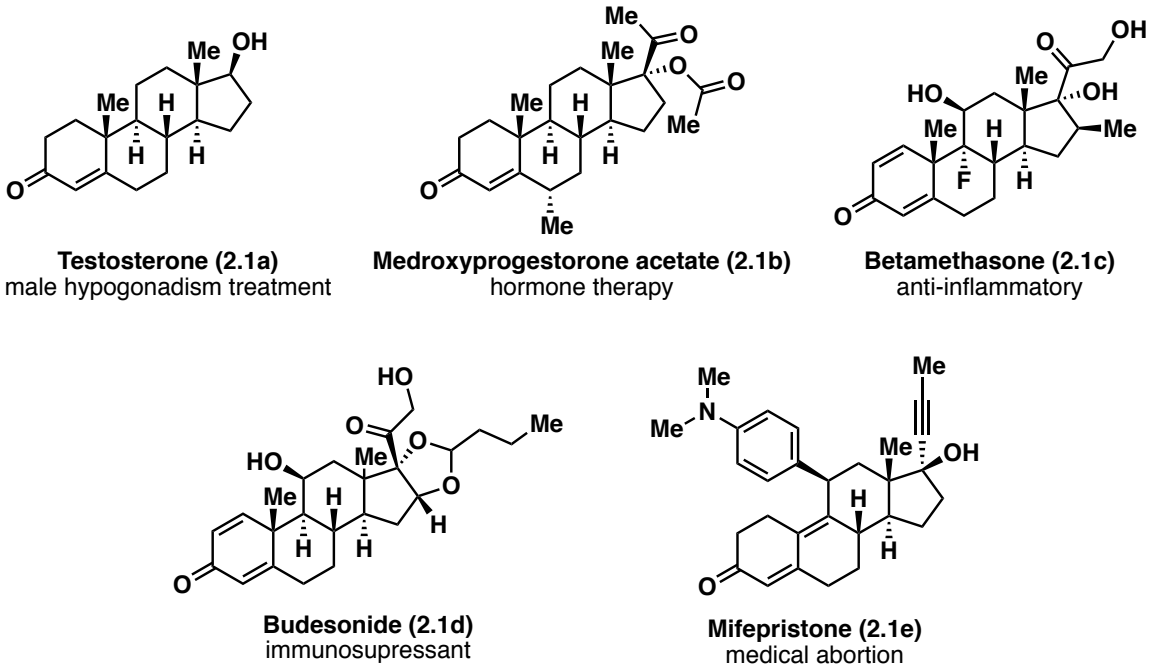

Figure 2.1. *Natural and synthetic steroids as medical treatments.*

In humans and animals, steroids are biochemically derived from lanosterol following the mevalonate pathway, an anabolic pathway using acetyl-CoA as a small building block to form polyolefins comprised of repeating isoprene units. Squalene, a 6-isoprene unit building block, undergoes an enzyme-catalyzed cyclization and skeletal rearrangement to create lanosterol (**Scheme 2.1**).[35] In the 1950's, Stork and Eschenmoser independently reported studies leading to important mechanistic and stereochemical clarification of polyolefin cyclization: both researchers suggesting that the stereoselectivity was controlled by the (*E*)-alkenes.[36]

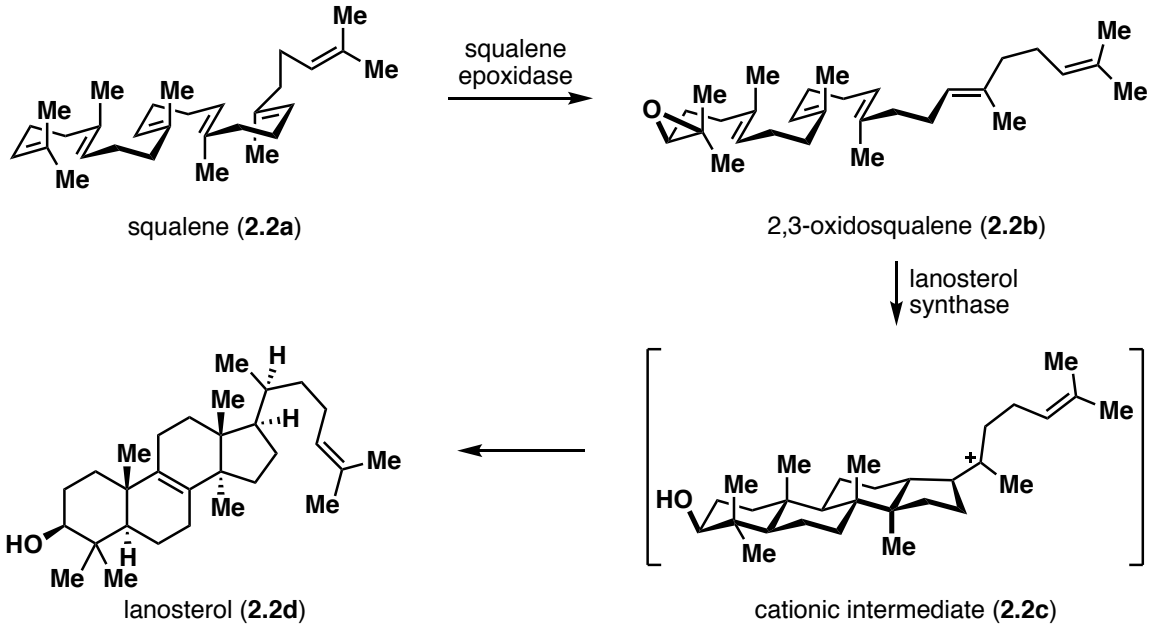

Scheme 2.1. *Biosynthetic cyclization of squalene to lanosterol.*

Inspired by Stork and Eschenmoser's work, Johnson played a major role in the synthesis of steroid scaffolds. He reported the renowned biomimetic synthesis of progesterone (**2.3c**) in 1971 through a cationic π-cyclization reaction cascade using trifluoroacetic acid (TFA) (**Scheme 2.2**).[37] Additional steps from steroid framework **2.3b** elegantly formed the natural product**.**

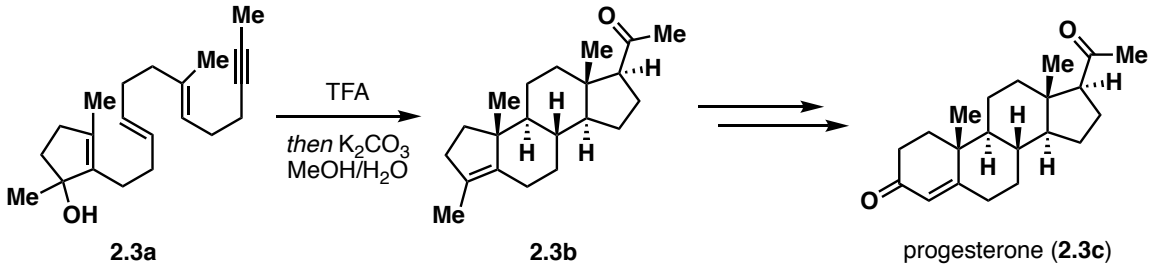

Scheme 2.2. *Cationic π-cyclization in Johnson's synthesis of progesterone.*

Similarly, Johnson achieved the first pentacyclic cyclization in the synthesis of (±)-sophoradiol (**2.4f**), generating 5 rings in a single polyolefin cyclization

transformation (**Scheme 2.3**).[38] The use of Lewis acid $SnCl_4$ led to unwanted elimination of HF, however TFA was able to generate the pentacyclic framework **2.4c** without dehydrofluoronation. From this intermediate, (±)-sophoradiol was formed in 3 steps.

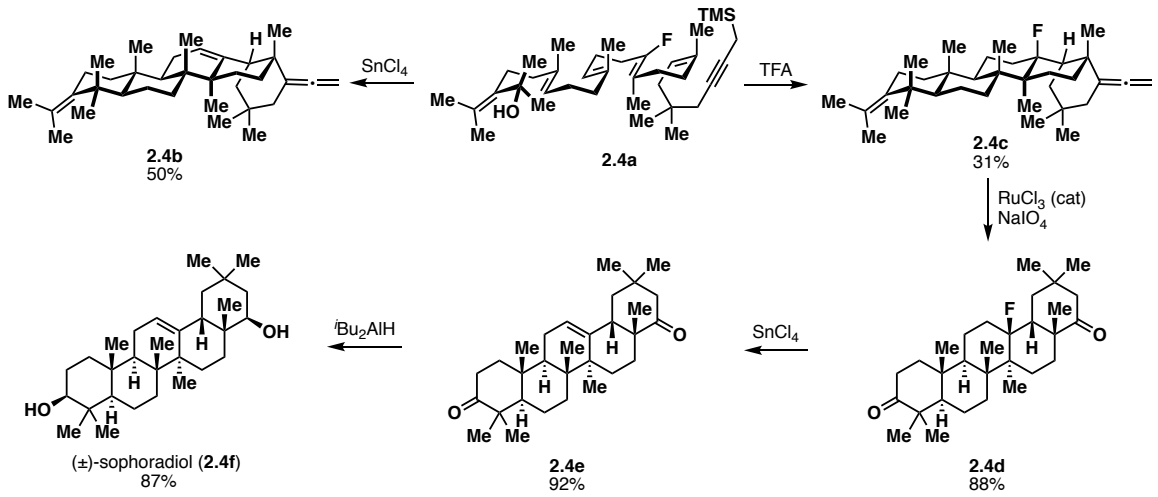

Scheme 2.3. *Synthesis of (±)-sophoradiol.*

Since then, a multitude of methods have been developed to form steroidal frameworks from linear precursors.[39] Notably, Corey completed an enantioselective total synthesis of dammarenediol II (**2.5d**) in 1996 utilizing a similar biomimetic polyolefin cyclization strategy (**Scheme 2.4**).[40] Starting compound **2.5a** was prepared from the known enantioselective dihydroxylation of E,E-farnesyl acetate in 80% yield with 98:2 enantioselectivity. Further transformations eventually generated linear precursor **2.5b** and a cyclization initiated by $MeAlCl_2$ generated framework **2.5c** in 42% yield over 3 steps. Dammarenediol II was generated in a few steps from this intermediate.

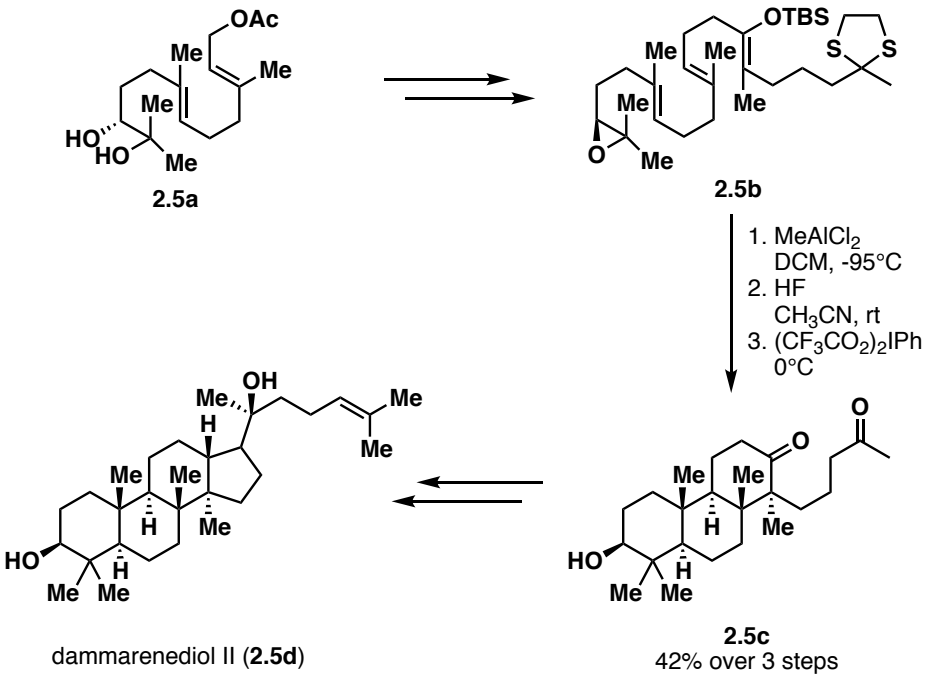

Scheme 2.4. *Total synthesis of dammarenediol II*.

In 1999, Yamamoto achieved the first enantioselective polyolefin cyclization.[41] With the objective of designing artificial geranyl and farnesyl cyclase replacements, a variety of binaphthyl derivatives comprised of a Lewis acid and Chiral Bronsted acid system (LBA) were prepared. Success was found in a BINOL•$SnCl_4$ complex (**2.6a**), which has the ability to induce asymmetric protonation of the isoprenyl moiety. As shown in **scheme 2.5**, high yields and moderate enantioselectivity were achieved. Corey further improved this method in 2012 by employing a bulkier Lewis acid, replacing $SnCl_4$ by $SbCl_5$.[42] This generated stronger coordination between a modified BINOL derivative and the LA, leading to increased acidity and in return, 84% yield and 92% enantiomeric excess of product **2.7c**.

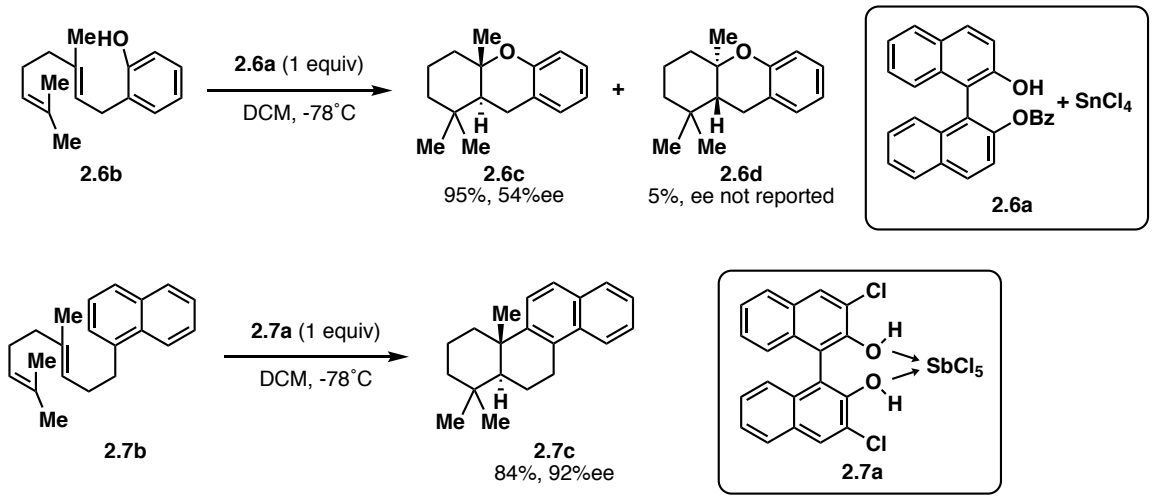

Scheme 2.5. *Enantioselective polyene cyclization by LBA catalysts.*

Following these key studies in the development of polyene cyclizations, other methods employing metal-catalysis were developed to form complex polycyclic hydrocarbon structures.[43] In 2017, Gagné and Geier reported the polycyclization of linear precursor **2.8b** using a pincer-platinum(II) catalyst (**2.8a**) (**Scheme 2.6**).[44] Pentanene 7 (**2.8c**) was formed as a single diastereoisomer in a 44% yield. Later that year, Echavarren and Rong published a similar study on the polycyclization of polyenynes by gold(I)-catalysis to form multiple C–C bonds of steroidal framework **2.9c** and a variety of other substrates in a single transformation.[45] The use of bulky biphenylphonsphine ligands was the most successful and the scope was performed using gold(I) complex **2.9a**.

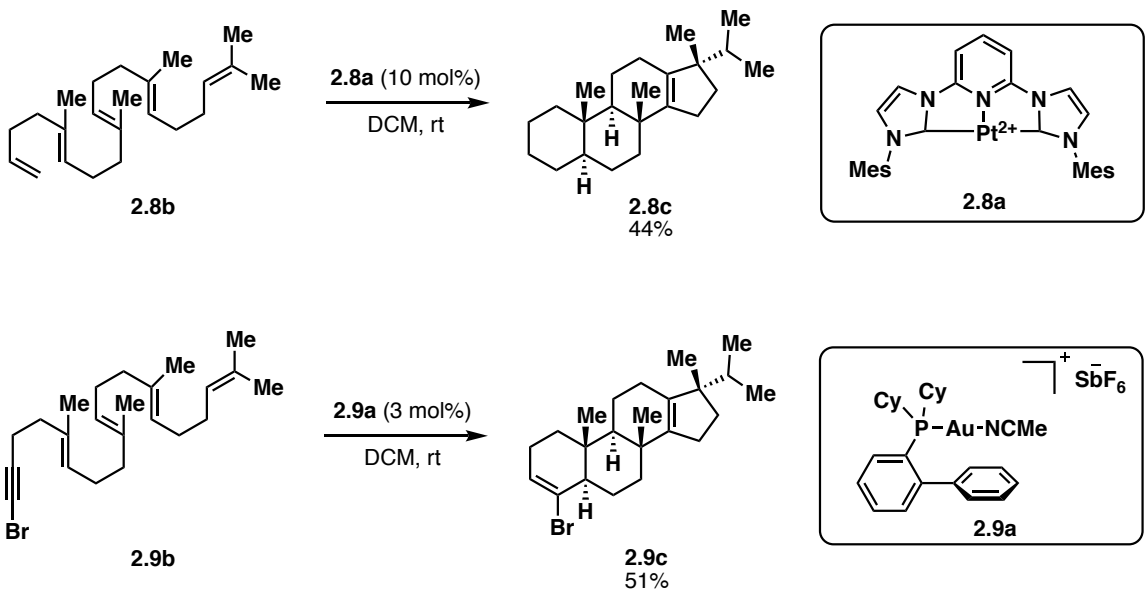

Scheme 2.6. *Metal-catalyzed polycyclization strategies for the generation of steroidal frameworks.*

More recently, the importance in the pharmaceutical industry of the synthetic methods mentioned above has declined due to semi-synthesis becoming a common strategy of choice to generate steroid-based products.[46] Partial chemical synthesis from naturally abundant precursors isolated from microbial cell cultures and/or natural plant sources can be advantageous from a financial perspective, while facilitating the synthesis of very complex frameworks. Although this method does present many advantages, difficulties remain in the incorporation of substrate modifications to produce large libraries of complex polycyclic compounds. It is therefore important to focus on continuing the development of divergent strategies that allow for the formation of a multitude of products through simple reagent modifications.

The objective of this project was to develop a method for the formation of fused carbocycles by using a strategy that could easily incorporate modified building blocks. Our envisioned approach involves a linear precursor undergoing a [4+2] cycloaddition, followed by a 6-*endo-dig* cyclization to form an internal diene. The generated intermediate could subsequently undergo a second [4+2] cycloaddition to create a terpenoid scaffold (**Scheme 2.7**).

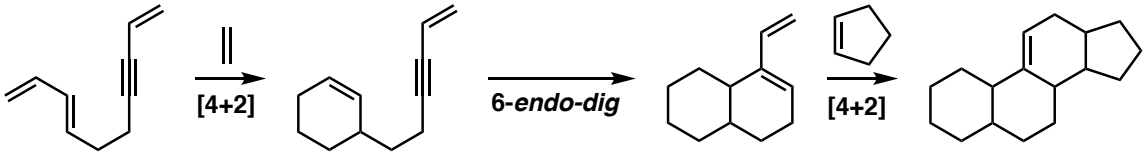

Scheme 2.7. *Envisioned approach towards the synthesis of steroid scaffolds.*

2.1.2 Previous work

The Barriault group has studied gold reactions and their application in total synthesis for many years.[47] Gold(I)-catalyzed cyclizations have been reported in the literature[48], but strategies are still lacking when it comes to forming the 6-*endo-dig* cyclization product. As visited in the previous chapter, ligands have been shown to greatly modify the reactivity and selectivity of catalytic gold reactions. In 2001, our group developed a gold(I)-catalyzed carbocyclization where both the 5-*exo-dig* and 6-*endo-dig* products were selectively formed (**Scheme 2.8**).[49] Me_4*t*BuXPhos (**L¹**) demonstrated the strongest bias towards the 6-*endo-dig* pathway during optimization studies. In the presence of [**L¹**AuNCMe]SbF_6, **2.10** undergoes a carbocyclization by nucleophilic attack of the cyclic enol ether onto the internal alkyne. Overall yields ranged from 45–91% and good to excellent regioselectivity was attained to afford product **2.11a** in up to >95:5 regioisomeric ratios (**2.11a:2.11b**).

Similarly, by using NHC ligand **L²**, the 5-*exo-dig* cyclization pathway was favored, generating products **2.11b** in 86–94% yields with excellent regioselectivity. This method demonstrated the divergent regioselectivities that could be achieved through simple modifications of the gold catalyst.

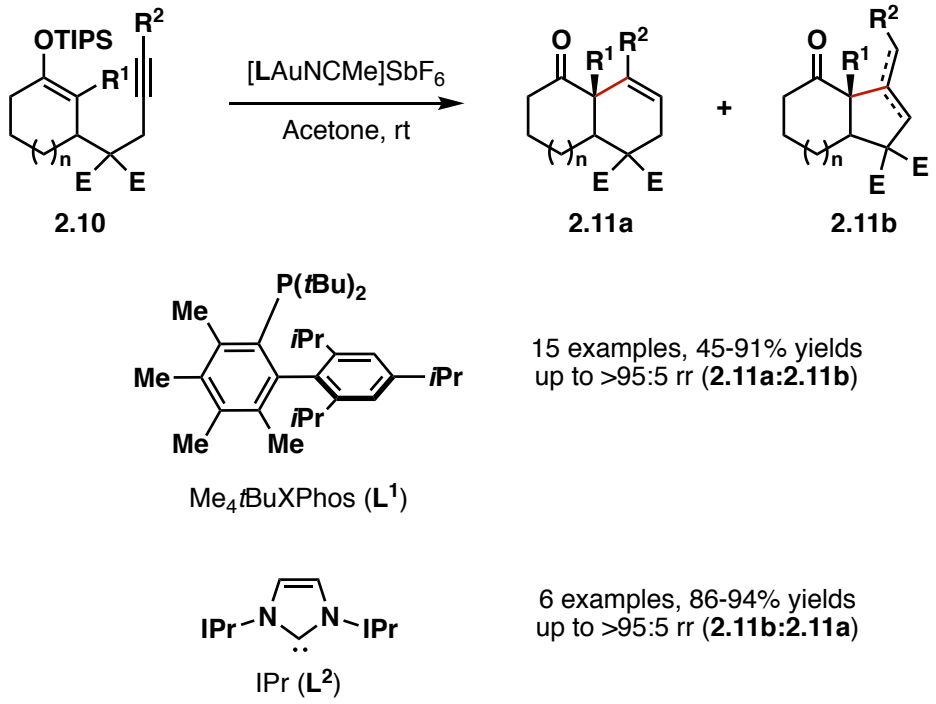

Scheme 2.8. *Intramolecular gold-catalyzed cyclization of cyclic enol ether **2.10** to selectively afford products **2.11a** and **2.11b**.*

2.1.3 Synthetic strategy

Inspired by the ability to selectively generate two cyclization products, our group envisioned a divergent synthetic method for the formation of terpenoid scaffolds (**Scheme 2.9**). First, designed precursor **2.13** could be formed through a Diels-Alder reaction from diene **2.12**. Then, both 6-*endo-dig* and 5-*exo-dig* cyclizations could occur, leading respectively to dienes **2.17** and **2.16** following

protodeauration. Complex tricyclic scaffolds **2.14** and **2.15** can also be formed from a subsequent Prins-type cyclization following the initial cyclization reaction.

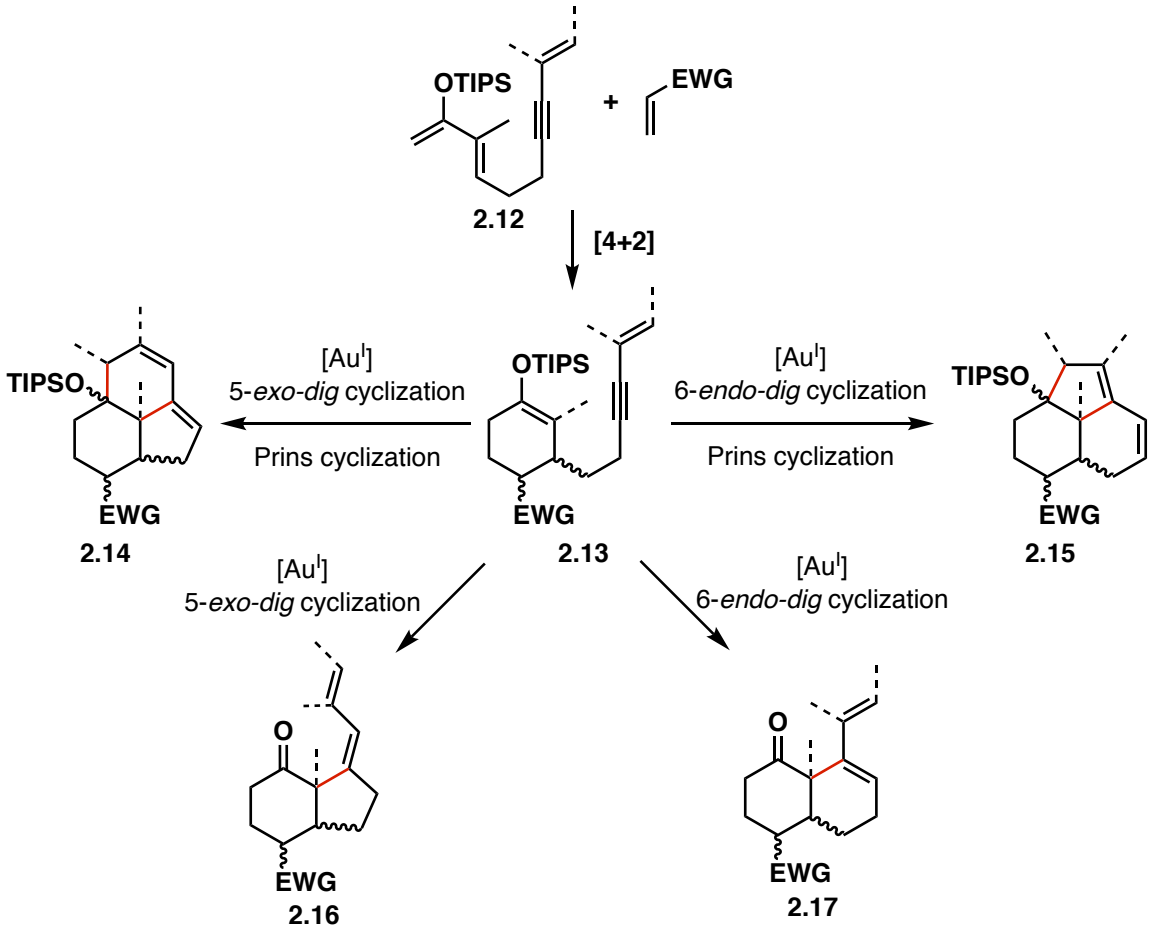

Scheme 2.9. *Alternative products from the Gold(I) cyclization reaction.*

The proposed gold cyclization mechanism begins with a gold(I) species coordinating the alkyne moity of silyl enol ether **2.13** (**Scheme 2.10**). The resulting organogold complex **2.18a** promotes an intramolecular nucleophilic attack from the silyl enol ether onto the internal alkyne, forming either the 6-*endo-dig* (**2.18b**) or the 5-*exo-dig* oxonium intermediates (**2.18c**). The targeted diene product **2.17**, as well as bicyclic product **2.16**, can subsequently be generated following proton elimination

and protodeauration. Alternatively, either oxonium intermediate (**2.18b** or **2.18c**) can undergo a Prins-type cyclization, forming an additional cycle and C–C bond. Tricyclic product **2.13** can be generated from a 1,2-H shift followed by elimination of the gold species of intermediate **2.19b**. Finally, tricycle compound **2.14** can be formed following proton elimination and protodeauration of intermediate **2.20b**.

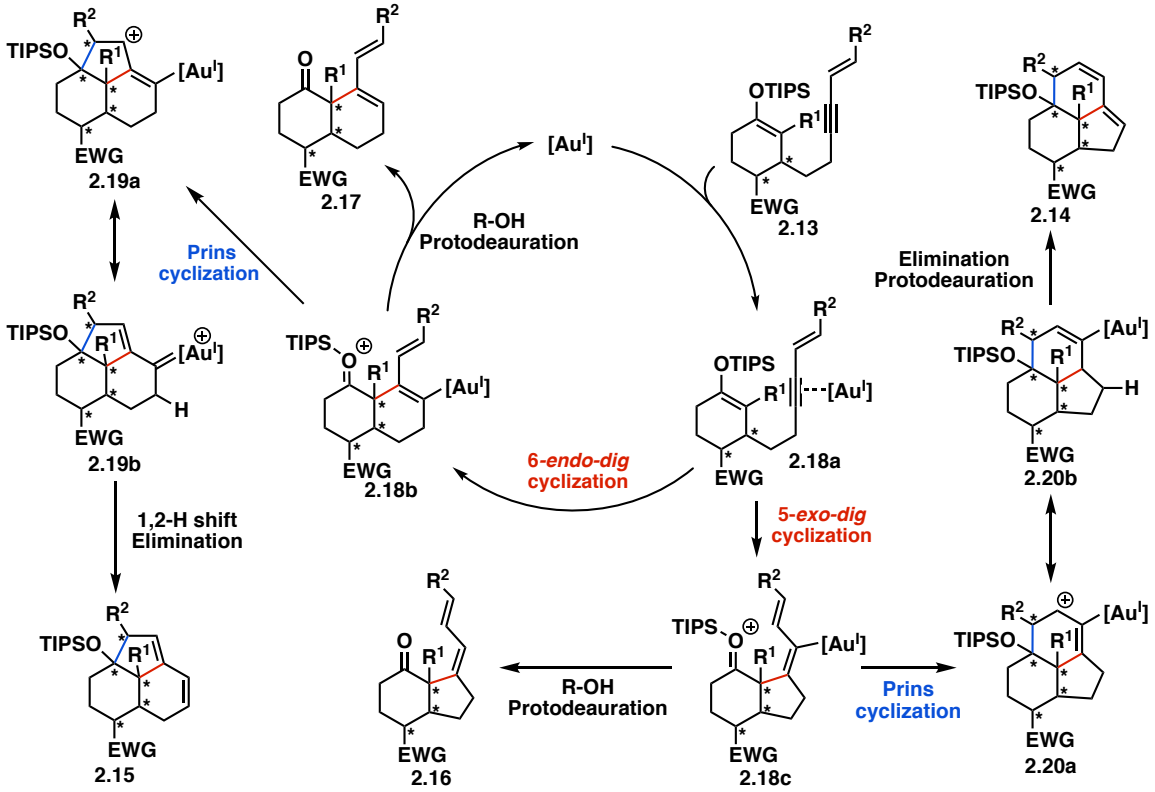

Scheme 2.10. *Gold(I) cyclization mechanism.*

This project was completed in collaboration with Huy Tran, as we further envisioned a one-pot sequence for the formation of steroid scaffolds by taking advantage of the internal diene generated in cyclization product **2.17** (**Scheme 2.11**). Silyl enol ether **2.13** could be generated through a Diels-Alder reaction from a linear diene (**2.12**), followed by the 6-*endo-dig* cyclization to form **2.17**. The generated

intermediate could subsequently undergo a second [4+2] cycloaddition to create terpenoid scaffold **2.12**. This highly efficient synthetic strategy has the potential of forming 5 C–C bonds and controlling the stereoselectivity of up to 8 stereocenters in a single one-pot multistep reaction.

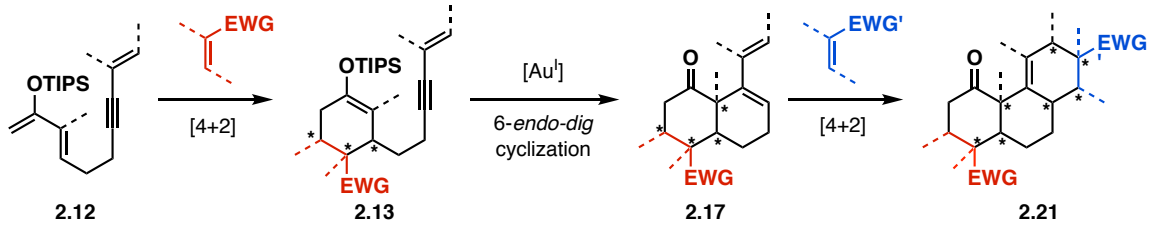

Scheme 2.11. *Synthetic scheme of one-pot reaction cascade.*

2.1.4 Substrate synthesis

The starting material of the one-pot synthesis is comprised of a diene tethered to an enyne moiety, designed to undergo the desired transformations. The formation of this scaffold followed a convergent synthesis from phosphonate **2.22** and 4-pentyn-1-al (**2.23**), the latter derived from the oxidation of 4-pentyn-1-ol (**Scheme 2.12**). A Horner-Wadsworth-Emmons transformation generated enone **2.24**, which was subsequently converted to enyne **2.25** through a Sonogashira coupling reaction. Finally, a triisopropyl silyl protecting group was installed to the enone (**2.25**) to afford diene **2.12**.

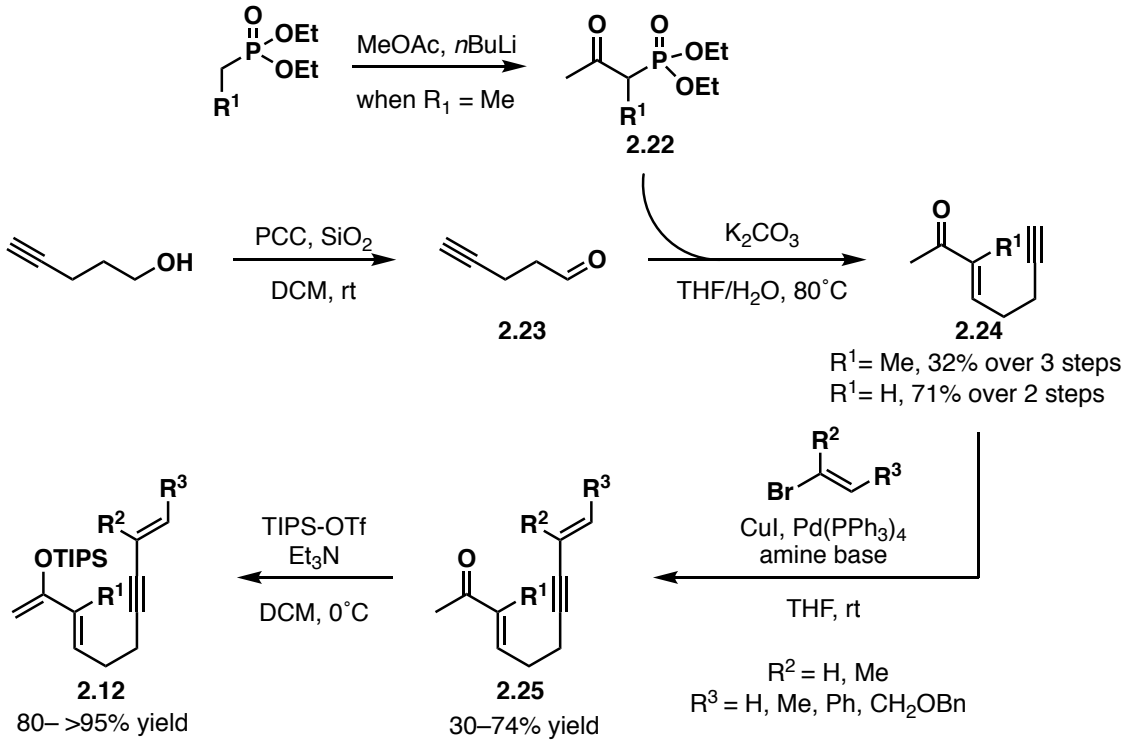

Scheme 2.12. *Synthesis of linear enol ether starting material.*

2.2 Selective formation of tri and tetracyclic carbocycles

2.2.1 Diels-Alder reactions

Diels-Alder reactions are [4+2] cycloadditions involving a conjugated diene and a dienophile. They are a well-known transformations that have had a large impact in the chemical world, advancing many total synthesis projects. The Diels-Alder reaction is favored by the energy gap between the highest occupied molecular orbital (HOMO) and lowest unoccupied molecular orbital (LUMO) of the reactants.[50] Otto Diels and Kurt Alder were awarded the Nobel prize in 1950 for their advancements on the transformation published in 1928. From a reaction between cyclopentadiene and quinone, they identified the monoadduct (**2.27a**) and bis-adduct (**2.27b**) products from a [4+2] cycloaddition (**Scheme 2.13**).[51]

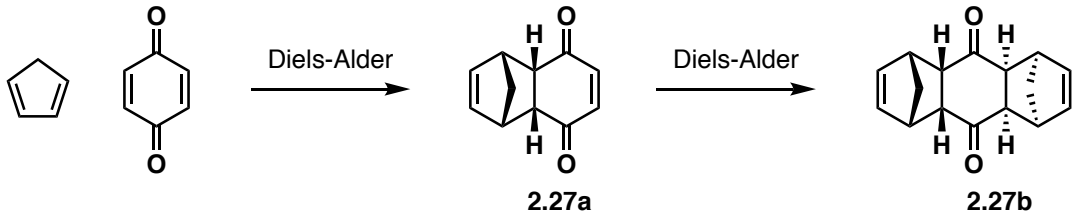

Scheme 2.13. *Diels-Alder reaction products between cyclopentadiene and quinone, identified by Otto Diels and Kurt Alder in 1928.*

Stereoselectivity of the Diels-Alder reaction is determined by the approach of the dienophile to the diene (**Scheme 2.14**). The resulting stereoisomers have been characterized as the *endo* and *exo* products. The *endo* product (**2.29b**) is generally the kinetic product, favored in intermolecular reactions when secondary orbital interactions can stabilize the transition state (**2.29a**). In contrast, the *exo* product (**2.28b**) is generally the thermodynamic product, favored in intramolecular Diels-Alder reactions where it is difficult for the molecule to force itself into a more stabilizing conformation.[52]

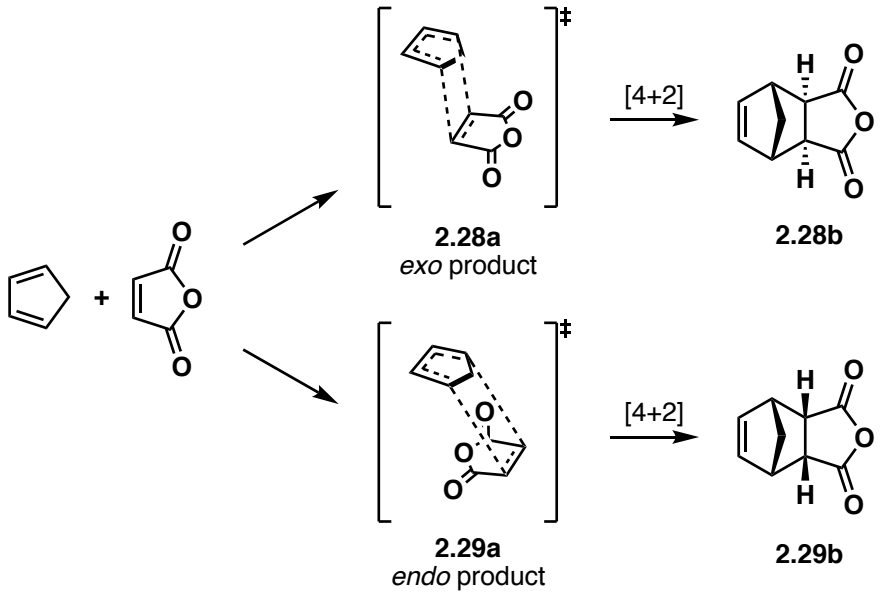

Scheme 2.14. *Endo and exo products formed in a Diels-Alder reaction between cyclopentadiene and maleic anhydride.*

A common strategy to increase Diels-Alder reactivity involves activation of the diene and dienophile to lower the energy gap between the HOMO and the LUMO. This can be done by an electron donating group (EDG) on a diene increasing the HOMO energy level, or an electron withdrawing group (EWG) on a dienophile decreasing the LUMO energy level.[53] For instance, Lewis acids have demonstrated the ability to accelerate Diels-Alder reactions by complexing the dienophile and withdrawing electron density, thus activating the substrate. In 1960, aluminum trichloride was reported to increase the rate of reaction between anthracene and maleic anhydride by 5 orders of magnitude (**Scheme 2.15**).[54] The transformation resulted in quantitative yield of product **2.30** in 1.5 minutes with one equivalent of aluminum chloride. In other cases, the addition of a Lewis acid increased the rate of reaction and allowed for it to occur under mild conditions.

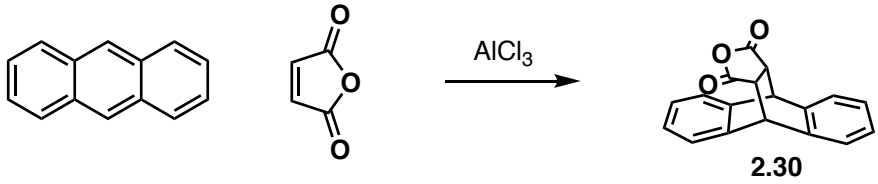

2.30

Scheme 2.15. *Diels-Alder reaction between anthracene and maleic anhydride in DCM.*

Synthetic efforts have led to many improvements of selective cycloaddition methods, notably the development of enantioselective strategies. These have been applied through a variety of approaches, such as the use of chiral catalysts and substrate-bound chiral auxiliaries. In 2002, Rawal published his findings on the application of Co(III)-salen complex **2.31a**[55] as a catalyst for an enantioselective Diels-Alder reaction (**Scheme 2.16**).[56] In this example, the Diels-Alder reaction between methacrolein and diene **2.32a** generated cycloadduct **2.32b** in 93-100%

yield with an enantiomeric excess of 97–98%. With their designed method, catalyst loadings were reduced as low as 0.05 mol% and the reactions could be run at room temperature and under air atmosphere.

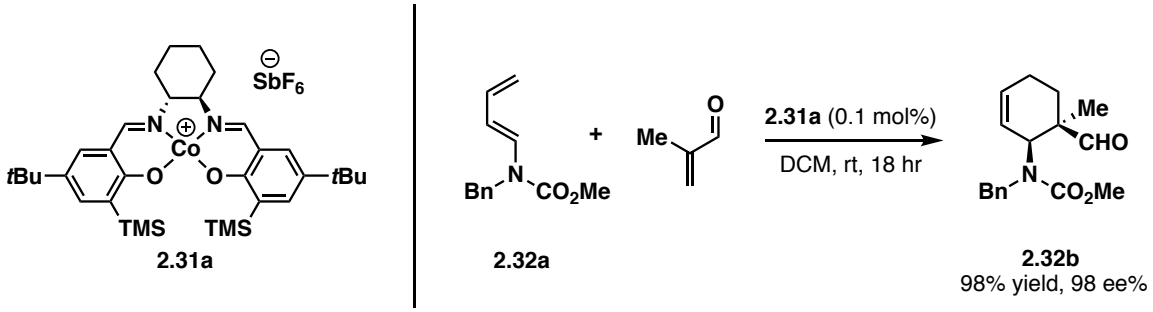

Scheme 2.16. *Diels-Alder reaction designed by Rawal generating 93-100% yields of product **2.32b**.*

2.2.2 Enal dienophiles

Initial studies of the Diels-Alder reaction performed by coworker Huy Tran and myself were based on Rawal's demonstration of the effectiveness of chiral cobalt(III) catalysts. The first optimization was performed using various cobalt(III) catalysts for the cycloaddition between diene **2.12a** and methacrolein (**Table 2.1**).

Table 2.1. *Optimization of Diels-Alder Cobalt(III) catalyst and reaction conditions.*

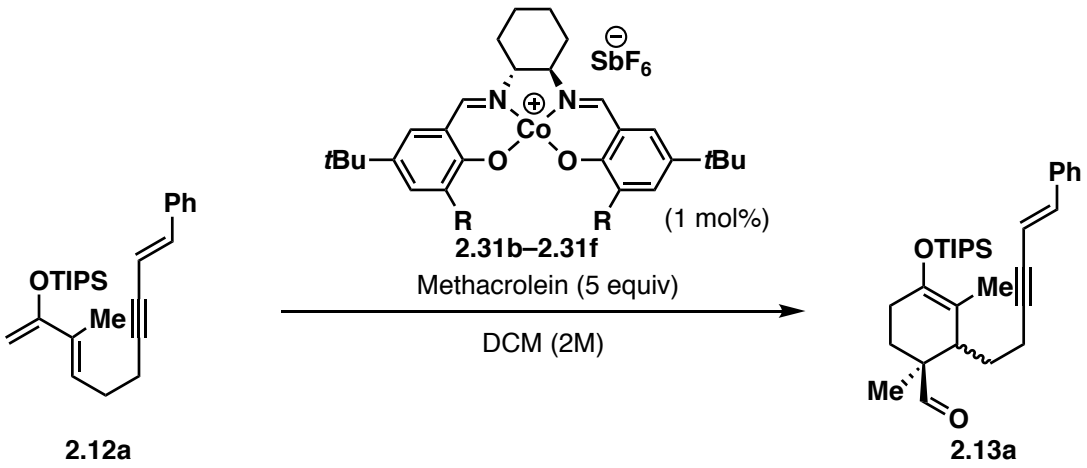

2.12a **2.13a**

Entry	R	Time (h)	Temperature (˚C)	Yield (%)	dr (*endo*:*exo*)	ee (%)
1	TBS (**2.31b**)	18	20	90	94:6	27
2[1]	TBS (**2.31b**)	18	0	46	–	41
3	TBS (**2.31b**)	5 days	-20	56	90:10	22
4	TIPS (**2.31c**)	18	20	19	94:6	6
5	TBDPS (**2.31d**)	18	20	19	93:7	6
6	Ad (**2.31e**)	18	20	degradation	–	–
7	*t*Bu (**2.31f**)	18	20	62	91:9	35

[1]Reaction was carried out with solvent concentration of 1M.

In all cases, the experimental conditions favored the formation of the *endo* cycloadduct, generating silyl enol ether **2.13a** in yields ranging from 19 to 90%. Unfortunately, only low to moderate enantioselectivity was achieved from these

reaction conditions. The Diels-Alder reaction employing catalyst **2.31b** resulted in the highest product yield of 90% at room temperature with a dr of 94:6 (*endo*:*exo*) and 27% ee (entry 1). Lowering the temperature to 0°C proved to be beneficial to obtain higher ee, but detrimental to the reaction yield (entry 2). Other Co(III) catalysts were examined without generating any substancial improvement (entries 4-6). Although the cycloaddition using **2.31f** led to the desired compound **2.13a** in good yield and moderate ee (entry 7), further experiments were conducted using **2.31b**, prioritizing the higher yield and dr.

Following catalyst optimization, experiments were completed with modifications of the diene and dienophile (**Table 2.2**). From the diene alterations, removal of the methyl group at position R^1 led to decreased yields and selectivity. Methyl vinyl ketones was also attempted as an alternate dienophile, however the yields dropped drastically and desilylated starting material was being observed.

Table 2.2. *Diene and dienophile optimization for initial Diels-Alder reaction.*

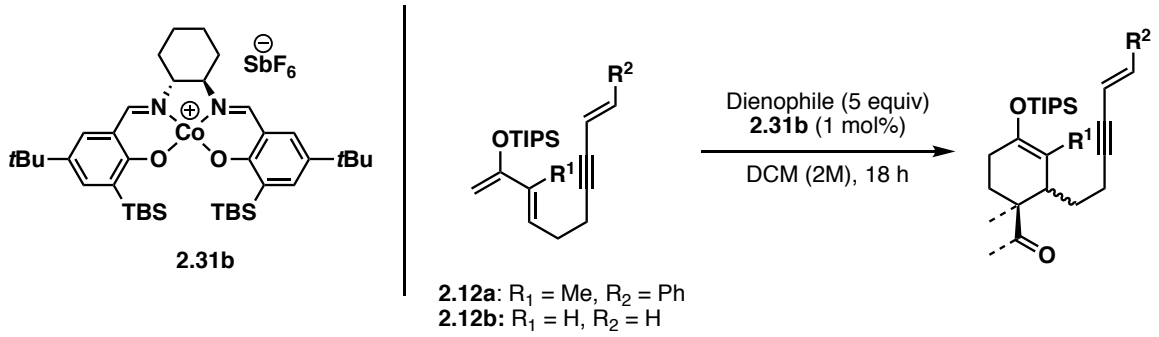

Entry	Diene	Dienophile	Product	Temperature (°C)	Yield (%)	dr (*endo*:*exo*)
1	**2.12a**	Methacrolein	**2.13a**	20	90	94:6
2	**2.12b**	Methacrolein	**2.13b**	20	62	87:13
3	**2.12a**	Methacrolein	**2.13a**	40	62	83:17
4	**2.12b**	MVK	**2.13c**	20	21	61:39
5	**2.12b**	MVK[1]	**2.13d**	20	30[2]	-
6	**2.12a**	MVK[1]	**2.13d**	20	15	82:18

[1] Methyl Vinyl Ketone was distilled prior to use.
[2] Desilylation of starting material observed.

The next step of the one-pot sequence was the gold-catalyzed cyclization to generate the 6-*endo-dig* product. First, multiple reactions were attempted using the Diels-Alder adduct **2.13b** in the presence of various phosphine gold(I) catalysts and in acetone and methanol (10:1 v/v) at room temperature. Unfortunately, in all cases, these conditions led to degradation and our first hypothesis was that this was due to the methanol. It prompted us to examine bulkier alcohols with the anticipation of preventing degradation (**Table 2.3**). The solvent optimization was performed on substrate **2.13e** with *iso*-propanol, *tert*-butanol and phenol (entries 2-4). In all cases,

these reactions catalyzed by [JohnPhosAuNCMe]SbF_6 gave tricycle **2.14a** in yields ranging from 20–26% via a 5-*exo-dig* cyclization/ Prins cyclization sequence.

Table 2.3. *Solvent optimization of the gold(I)-catalyzed cyclization.*

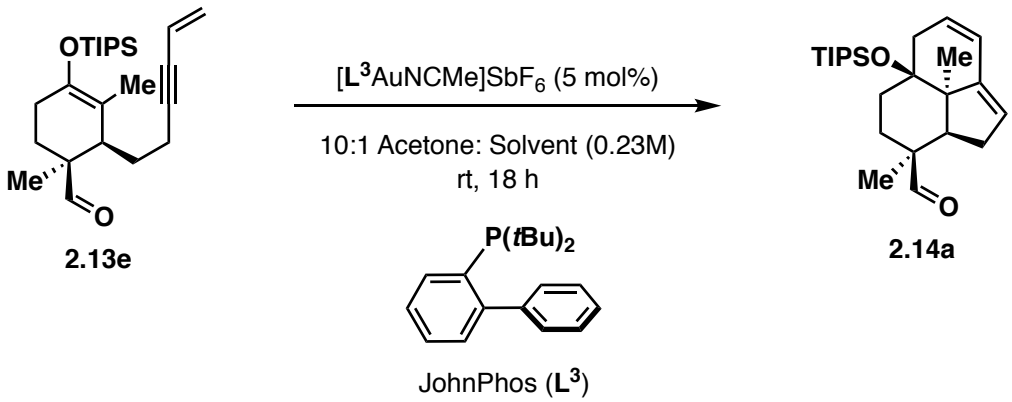

Entry	Solvent	NMR yield[1] (%)
1	MeOH	-
2	*i*Pr	26
3	*t*BuOH	20
4	Phenol	22

[1]NMR yields were determined using a mesitylene standard.

Forming the 6-*endo-dig* cyclization product remained a challenge and JohnPhos was replaced by Me_3MeO*t*BuXPhos (**L⁴**) due to its bulkiness and more electron donating properties. However, applied to a one-pot sequence, the 5-*endo-dig*/ Prins cyclization cascade product (**2.14a**) was again formed in 65% yield (**Scheme 2.17**).

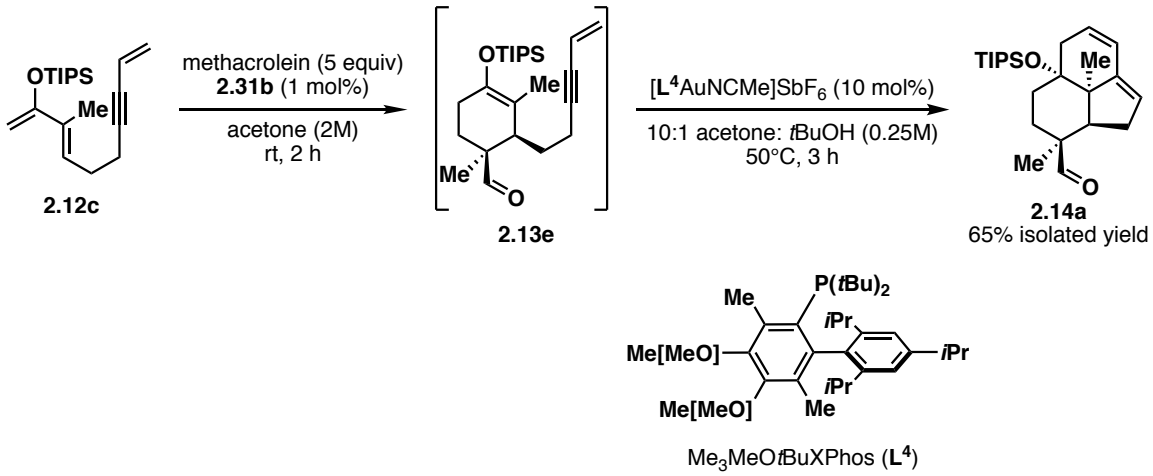

Scheme 2.17. *One-pot reaction using [Me$_3$MeOtBuXPhosAuNCMe]SbF$_6$ catalyst.*

Due to the difficulty obtaining the desired 6-*endo-dig* product, we attempted to modify the regioselectivity and prevent the Prins cyclization by increasing the reactivity and the rate of the protodeauration. In 2014, Xu and coworkers demonstrated that hydrogen bonding additives could increase reactivity when the limiting step was protodeauration, as long as weak bases, which also had low affinity for cationic gold complexes, were used.[57] Even so, they also found that incompatibility between the base and the reaction conditions could completely shut down the reactivity by inhibiting the formation of the gold-coordinated alkyne intermediate. This approach was attempted with our reaction using 1H-benzotriazole and pyridine *N*-oxide, but these were unsuccessful as no reaction progress was observed following the initial Diels-Alder reaction (**Scheme 2.18**).

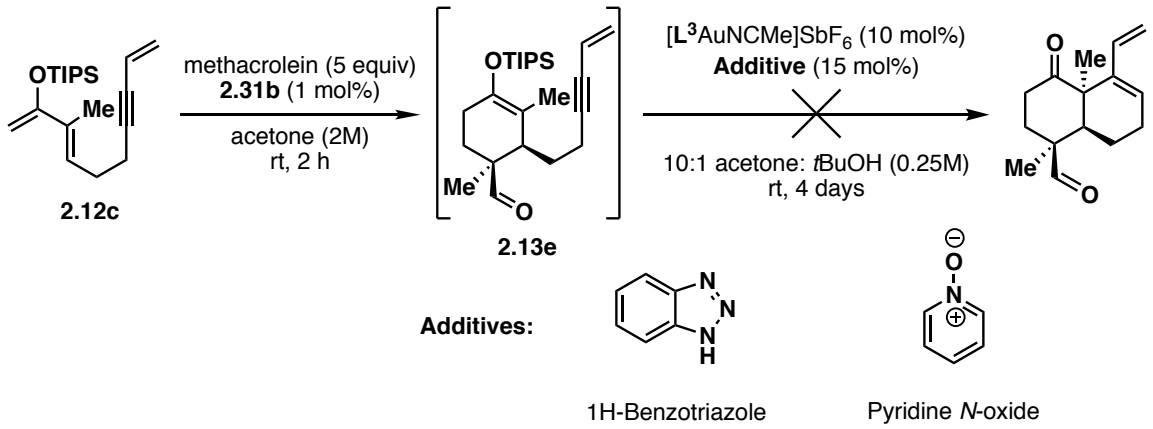

Scheme 2.18. *One-pot reactions using hydrogen bonding additives, 1H-Benzotriazole and Pyridine N-oxide.*

The next strategy to modify the reactivity of our cyclization reaction was to use a Lewis acid co-catalyst with the gold(I) catalyst. This combination has revealed in reported literature to increase reactivity by giving rise to a gold complex with even stronger acidic properties.[58] As a result, stronger binding of π-systems and promotion of the protodeauration step can be observed, however the absence of mechanistic understanding makes the effects difficult to predict. As demonstrated in **scheme 2.19**, we attempted using a combination of our gold catalyst with Lewis acids $Gd(OTf)_3$ and $In(OTf)_3$. Tricycle **2.14a** was nonetheless generated in the one-pot reaction as we were unable to modify the reactivity to favour the 6-*endo-dig* cyclization product.

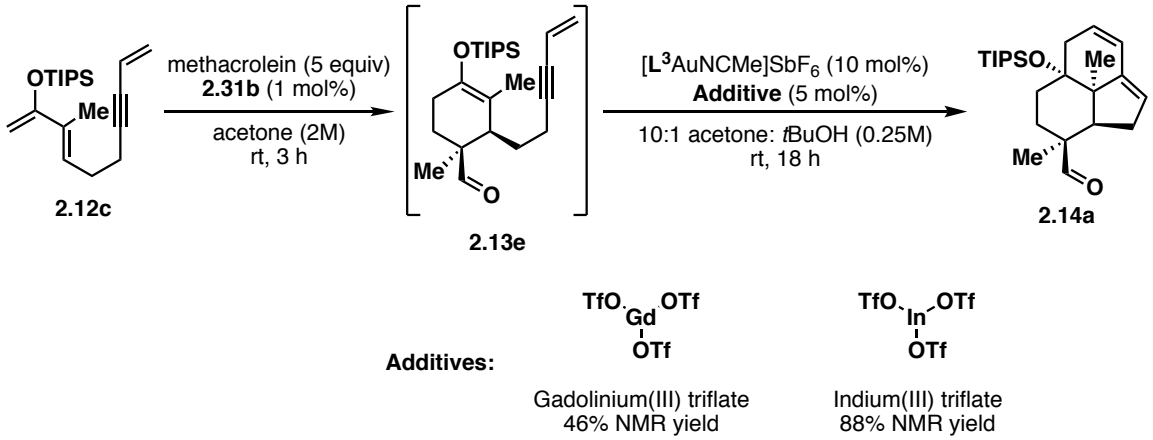

Scheme 2.19. *One-pot reaction using Lewis acid co-catalysts Gd(OTf)₃ and In(OTf)₃.*

At this point in time, the targeted 6-*endo-dig* cyclization product had not been formed from the intial Diels-Alder product using enal dienophiles. However, these one-pot reactions generated interesting tricyclic scaffolds through the 5-*exo-dig*/ Prins cyclization cascade. This method maintains the potential of being applied to the synthesis of sesquiterpenoid natural products, as these 6-6-5 fused ring systems are present in many variations in nature (**Figure 2.2**).

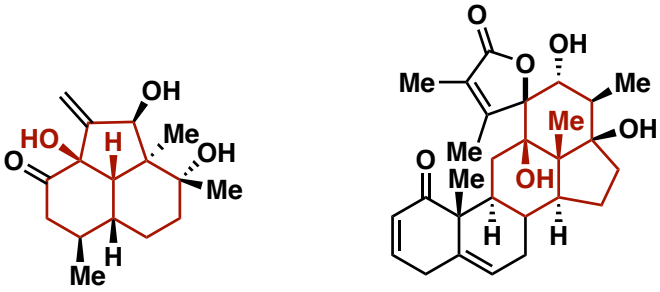

Figure 2.2. *Potential for applications of 5-exo-dig/ Prins cyclization methodology in total synthesis.*

While the investigations presented above were ongoing, co-worker Huy Tran explored the gold(I)-catalyzed cyclization reaction with Diels-Alder product **2.13d**, formed from the linear diene **2.12a** and methyl vinyl ketone. Interestingly, he found a distinct pattern of cyclization products generated from a diastereoisomeric mixture of **2.13d** (**Scheme 2.20**).

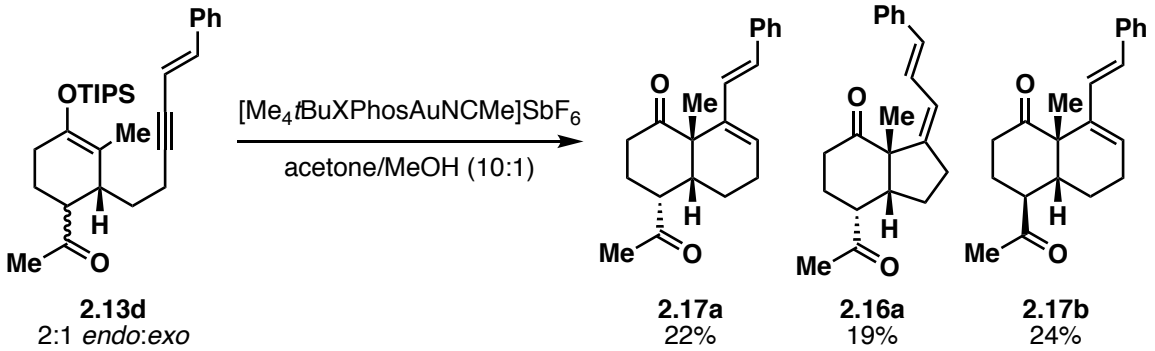

2.13d
2:1 *endo*:*exo*

2.17a
22%

2.16a
19%

2.17b
24%

Scheme 2.20. *Product distribution of gold(I)-catalyzed cyclization from diastereoisomeric mixture of cycloadduct* ***2.13d*** .

In fact, from this product distribution, we concluded that the *exo* Diels-Alder product was leading solely to the 6-*endo-dig* cyclization product (**2.17b**), while the *endo* Diels-Alder product was being transformed into a 1:1 mixture of the 5-*exo-dig* and 6-*endo-dig* cyclization products (**2.17a**, **2.16a**) (**Scheme 2.21**). From these results, we realized the importance of the Diels-Alder product conformation and the influence it was having on the gold-catalyzed cyclization.

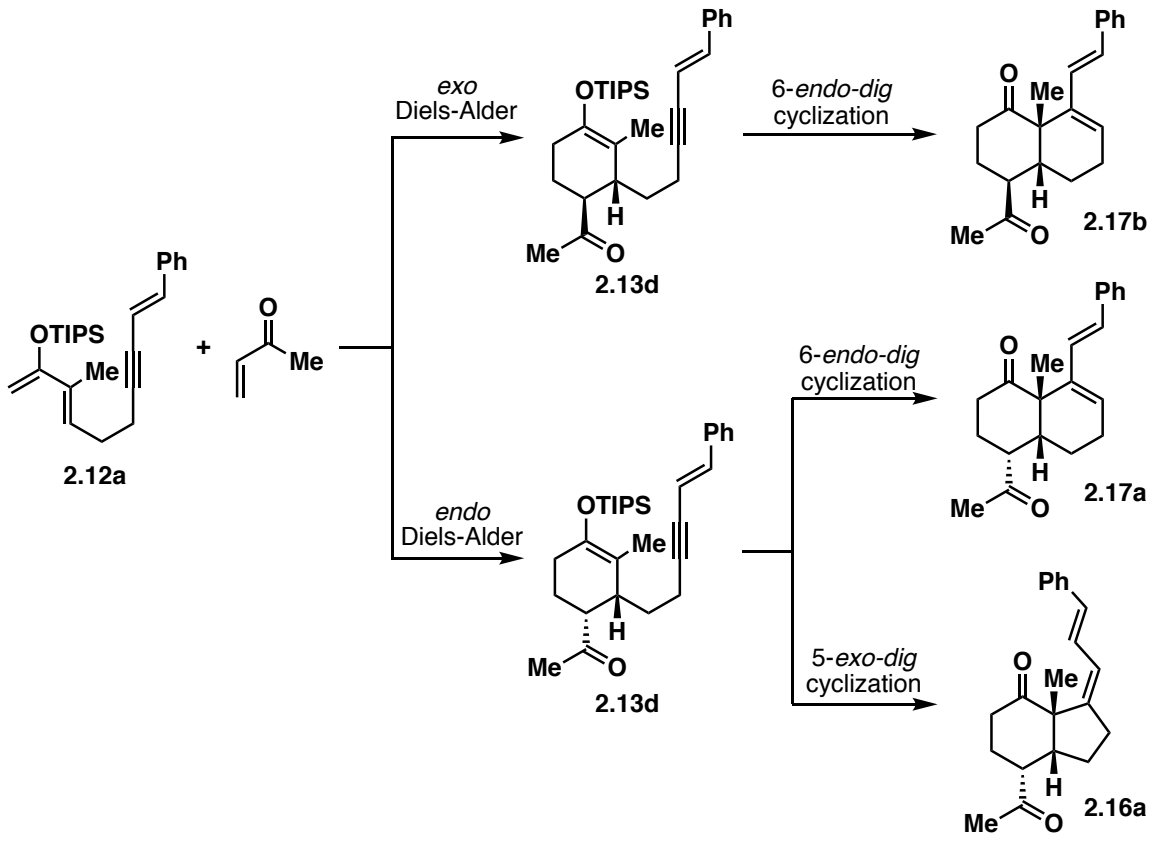

Scheme 2.21. *Cyclization product distribution from the exo and endo Diels-Alder products.*

To explain the reaction outcome, one can propose the mechanisms depicted in **schemes 2.22–2.24**. From the *endo* Diels-Alder product, one could imagine both 6-*endo-dig* and 5-*exo-dig* cyclization products being formed from two conformations (**a** and **b**) (**Scheme 2.22**)**.** From here, the silyl enol ether can cyclize onto the Au-activated alkyne at either position to generate a 6 or 5 membered cycle. From **a**, the transition states are presented as **TS1** and **TS2** to generate the 6-*endo-dig* and 5-*exo-dig* products **2.34a** and **2.34b**, respectively. Transition states **TS3** and **TS4** can be ignored given the development of steric interactions between the axial ketone and the newly formed cycle.

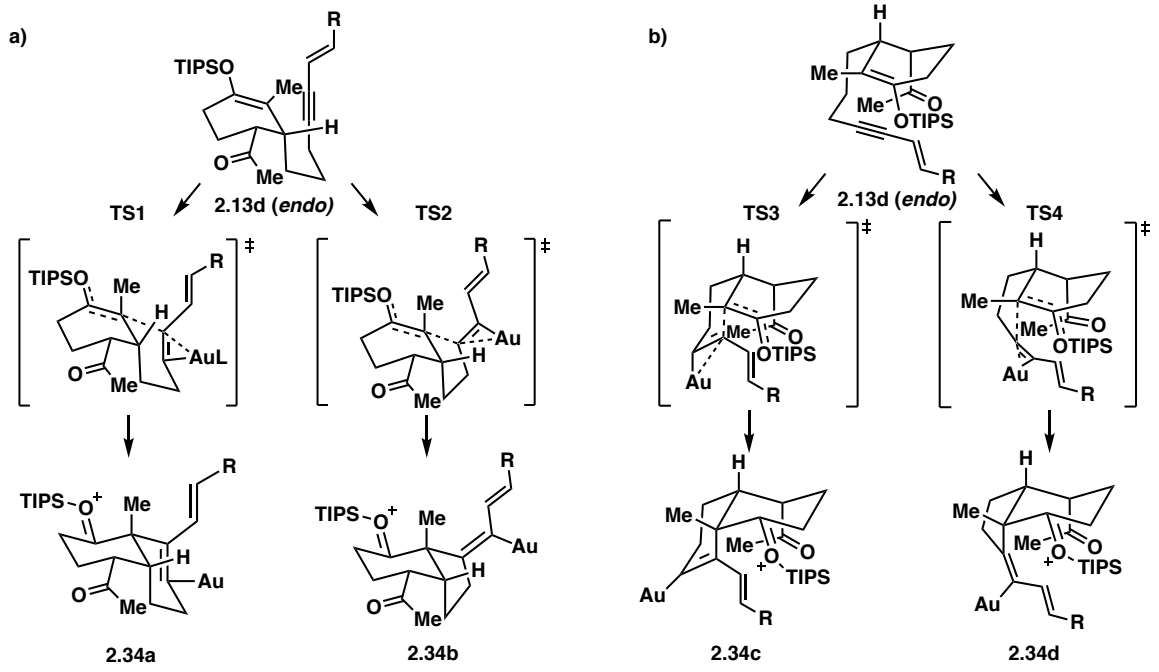

Scheme 2.22. *Proposed transition states for the Au(I)-catalyzed cyclization of (endo)-**2.13d**.*

It is also interesting to observe that the *cis*-junction is being formed, rather than the more usual and thermodynamically stable *trans*-junction. This could be explained by a highly disfavored transition state, which requires too much energy for proper orbital overlap (**Scheme 2.23**). Exclusive formation of the *cis*-junction further suggests that the cyclization is under kinetic control, highly reliant on the transition state energy barriers.

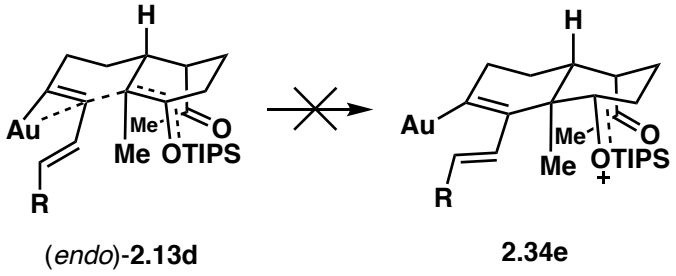

Scheme 2.23. *Transition state of the gold(I)-catalyzed cyclization to generate the trans-decalin.*

In the case of the *exo* Diels-Alder product, the cyclization can occur from **c** and **d** (**Scheme 2.24**). A cursory inspection of these paths reveals that 1,3-diaxial interactions between the methyl and the methyl ketone at the transition state favor **TS3/TS4** over **TS1/TS2**. Furthermore, based on the exclusive formation of the 6-*endo-dig* cyclization product **2.17b**, one can propose that a better orbital alignment favors **TS3** over **TS4.**

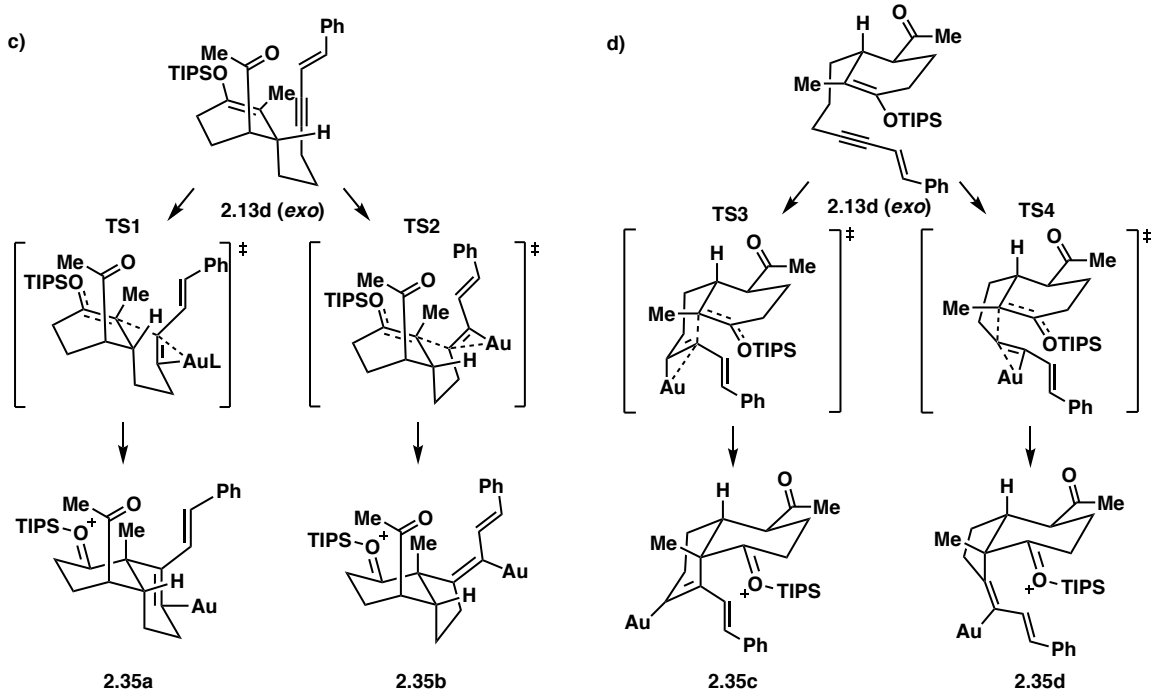

Scheme 2.24. *Proposed transition states for the Au(I)-catalyzed cyclization of (exo)-**2.13d**.*

Looking back at the Diels-Alder reaction involving a methacrolein dienophile, the generated silyl enol ether led to exclusive formation of the 5-*exo-dig* cyclization product. In this case, it is clear that **TS1** and **TS2** demonstrated in **scheme 2.25** are very high in energy due to both axial methyl groups. We could instead expect the product to be formed through conformation **f**. The regioselectivity is most likely due to more favorable orbital alignment in **TS4**, rather than **TS3**.

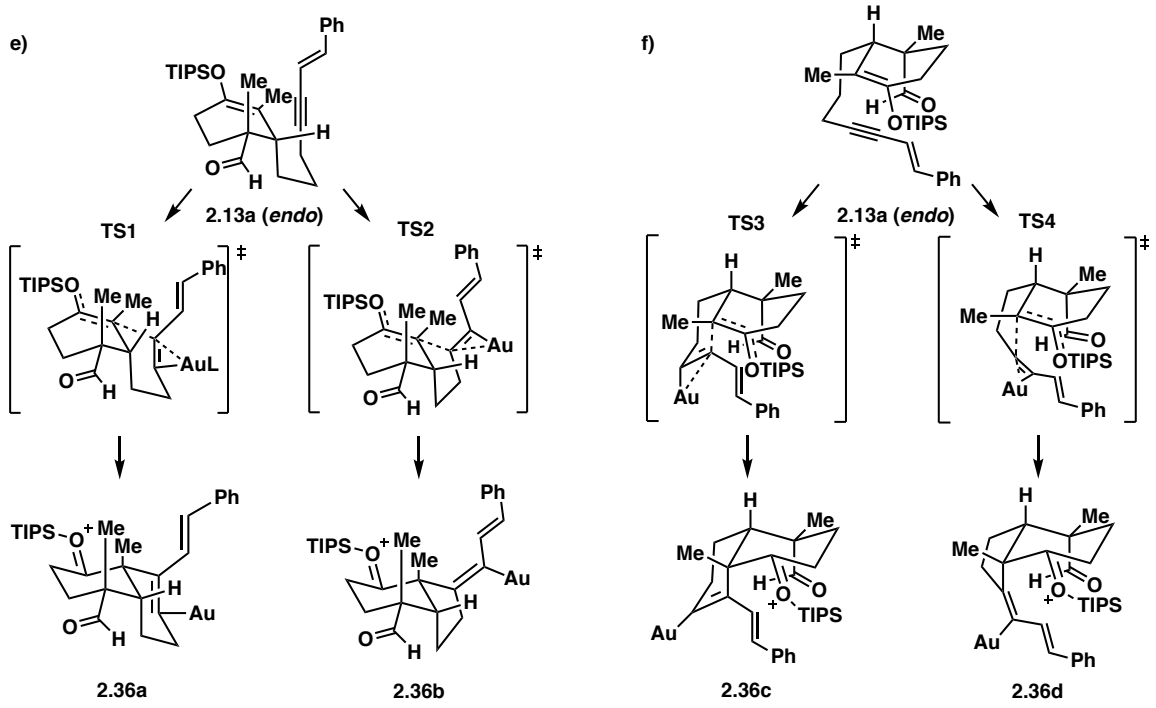

Scheme 2.25. *Proposed transition states for the Au(I)-catalyzed cyclization of (endo)-**2.13a**.*

Typically, gold(I)-catalyzed cyclizations can be highly substrate dependent, and these reactions were no different. Nonetheless, we looked to target the formation of the *exo* Diels-Alder product in hopes of directing regioselectivity for the 6-*endo-dig* product. Moving forward, we began investigating oxazolidinone dienophiles.

2.2.3 Oxazolidinone dienophiles

Bis(oxazoline) (BOX) ligands have been widely used in various chemical reactions for asymmetric synthesis. These ligands are designed to bind to a metal through bidentate chelation, forming a distorted square planar complex with a second chelated substrate (**Figure 2.3**).[59]

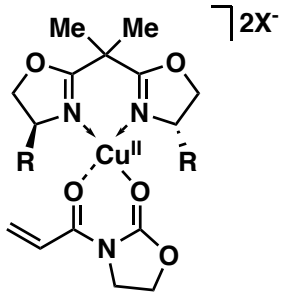

Figure 2.3. *Distorted square planar geometry of Copper(II)-BOX catalyst bound to an oxazolidinone substrate.*

Enantioselectivity in the Diels-Alder reaction is dictated by the face of approach of the dienophile to the diene. Chiral projections on the BOX ligand provoke steric interactions with the approaching diene, resulting in a preferential transition-state geometry where the diene has better access to the dienophile. C_2 symmetry of the BOX ligand also ensures that the orientation of the substrate in relation to the ligand will not affect the selectivity.[60] Moreover, counterions of the [metal-BOX] catalyst can have a large impact on the outcome of the reaction. Weakly- or non-coordinating counterions can lead to a more cationic active catalyst, allowing for stronger coordination between the metal and the dienophile.[61] Consequently, the reacting dienophile is held in a more rigid conformation for a better controlled cycloaddition.

In 1999, Evans and coworkers further explored the utility of the BOX ligand with imide dienophiles in Diels-Alder reactions.[62] Demonstrated in **scheme 2.26**, the [4+2] cycloadditions with cyclopentadiene were directed by the catalyst and afforded yields ranging from 86%–93%. Excellent diastereoselectivity of 98:2 (*endo*:*exo*) and enantiomeric excess of >98% was achieved with **2.37b**.

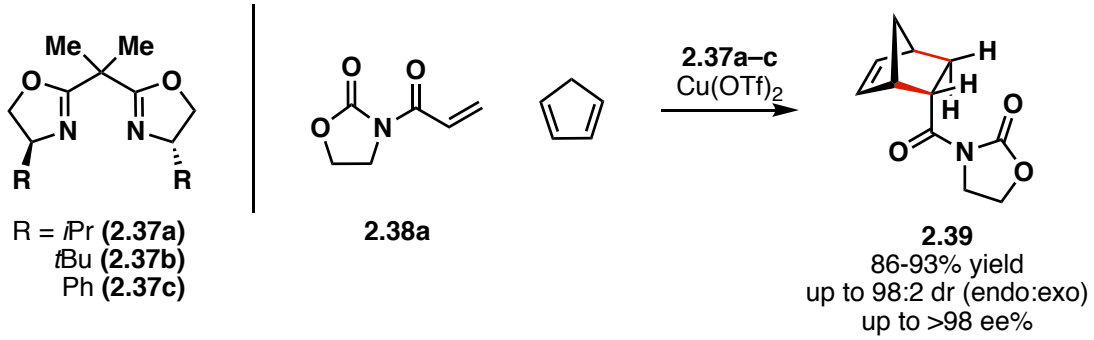

Scheme 2.26. *Application of BOX ligand in a Diels-Alder reaction between cyclopentadiene and an oxazolidionone dienophile.*

While the example above preferentially leads to the *endo* Diels-Alder product, we hoped to achieve *exo* selectivity due to the nature of our diene. We hypothesized that the *exo* selectivity of the concerted [4+2] cycloaddition could be obtained by the diene approaching the dienophile to form the lowest energy transition state by decreasing steric hindrance. In fact, the chiral *tert*-butyl group on the BOX ligand could hinder the *endo* approach if the diene contains a bulky group (**Figure 2.4**).[32] In the specific case of our diene, R^3 is a bulky OTIPS substituent.

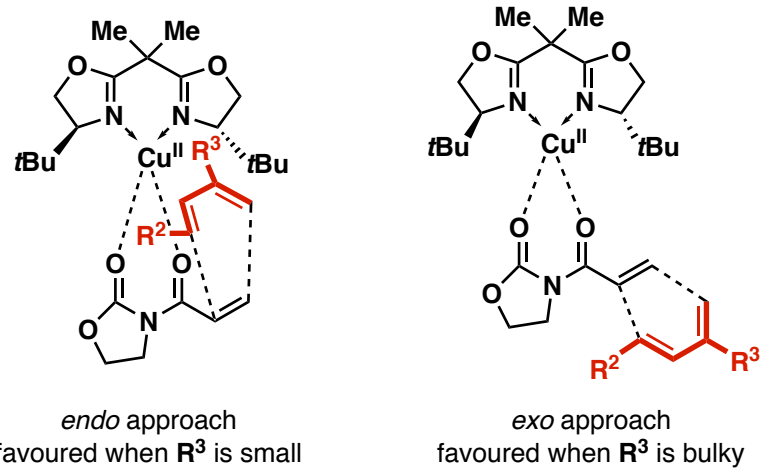

Figure 2.4. *Favored diene approach in accordance to* ***R³*** *substituent bulk.*

The first experiment based on Evan's work was carried out between our linear diene **2.12a** and an oxazolidinone dienophile (**2.38a**) with chiral BOX ligand **2.37b** and copper(II) triflate (**Table 2.4,** entry 1). These conditions proved to be successful as the desired Diels-Alder cycloadduct was obtained in 60% isolated yield, with a dr of 20:80 (*endo*:*exo*) and 72% ee. A catalyst optimization was then performed in collaboration with my colleague Huy Tran in which several metal triflates were examined. The use of Mg, Fe, Zn and Pd complexes generated poor to moderate yields of the desired Diels-Alder product and desilylation of starting material in some cases (entries 2-5). The use of Sc(III) triflate (entry 6) resulted in a yield of 70% and was the only metal to favor the *endo* product in a 70:30 ratio. To our delight, the use of other lanthanide complexes led to complete conversion of the diene after 18 hours, giving the *exo*-cycloadduct **2.13f** in 81–88% isolated yields and high diastereoselectivity (entries 8–11). Unfortunately, the reaction did not operate in an enantioselective manner.

Table 2.4. *Catalyst optimization for the initial Diels-Alder reaction.*

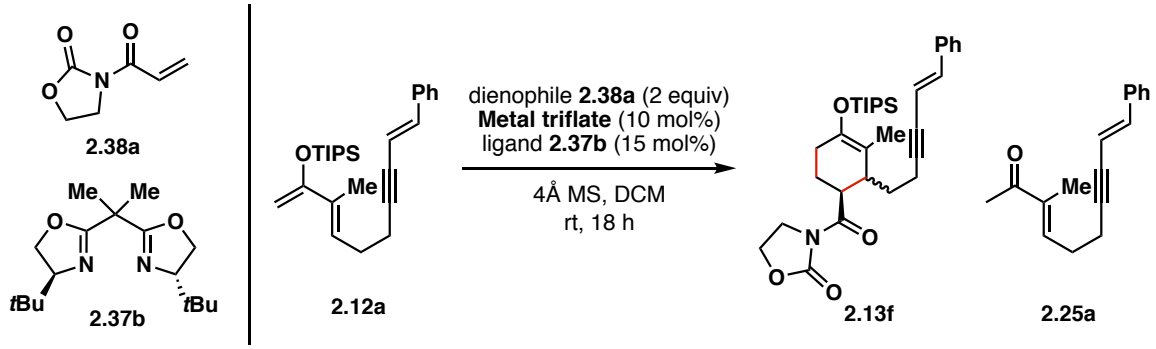

Entry	Metal triflate	NMR yield[1] (%) **2.13f**	**2.25a**	**2.12a**	dr (endo:exo)	ee% (exo)
1	Cu(II)	66 (60)	7	0	20:80	72
2	Mg(II)	10	3	77	-	-
3	Fe(III)	60	34	0	-	-
4	Zn(II)	46	6	35	-	-
5	$Pd(TFA)_2$	8	36	38	-	-
6	Sc(III)	70	18	0	70:30	8
7	In(III)	20	41	31	-	-
8	Yb(III)	95 (81)	trace	0	7:93	0
9	Gd(III)	>95 (88)	trace	0	7:93	0
10	Eu(III)	>95 (82)	trace	0	7:93	0
11	Er(III)	94 (83)	trace	0	7:93	-10

[1]NMR yields were determined using a mesitylene standard

Following the catalyst optimization, attempts to induce enantioselectivity were put on hold and gadolinium(III) triflate was applied to further Diels-Alder reactions as the Lewis Acid. A solvent optimization was then performed by Huy Tran and showed that the reaction carried out in DCM and acetone obtained the highest

yields of **2.13f** with a dr of >90:10. In DCM, the cycloaddition required 18 h for completion, compared to 5 h in acetone.

In collaboration with Huy Tran, an extensive study of the gold(I)-catalyzed 6-*endo-dig* carbocyclization was undertaken, where various ligands were screened (**Figure 2.5**). All cyclization reactions fully converted after 18 h. In general, ancillary ligands having bulky and electron rich aryl systems favored the 6-*endo-dig* cyclization pathway. It was found that Vphos ligand (**L^5**) gave the highest yield (76%) of the desired 6-*endo-dig* cyclization product. Moreover, Me_3MeO*t*BuXPhos (**L^4**) produced the desired coumpound **2.17c** in 63% yield and was the only ligand that did not lead to degradation.

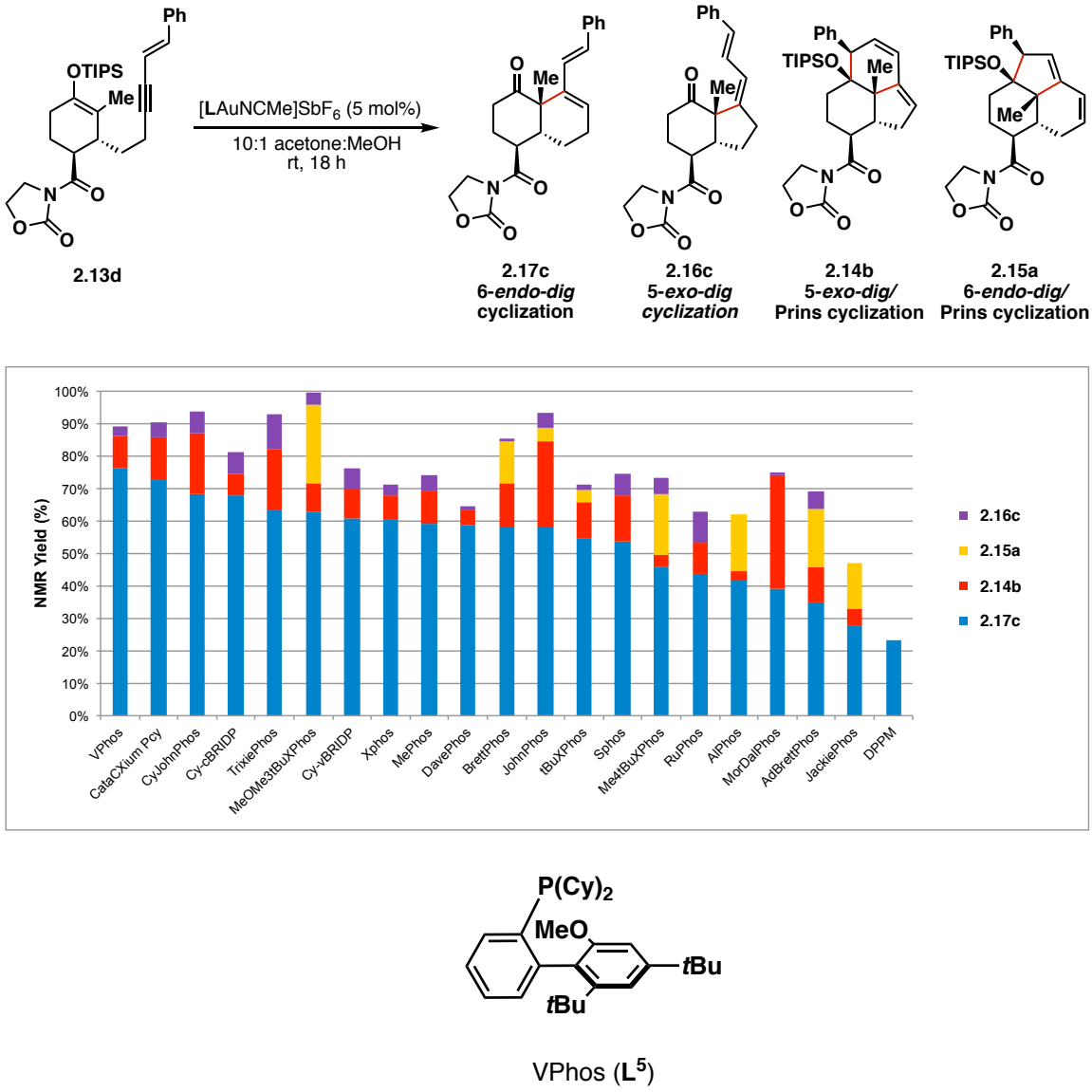

Figure 2.5. *Gold(I) catalyst ligand optimization and structure of VPhos.*

Once the Diels-Alder and gold(I)-catalyzed cyclization optimizations were complete, we envisaged a one-pot Diels-Alder/ gold-catalyzed cyclization sequence (**Table 2.5**).

Table 2.5. *Diels-Alder/Gold(I) cyclization sequence with chiral BOX ligand.*

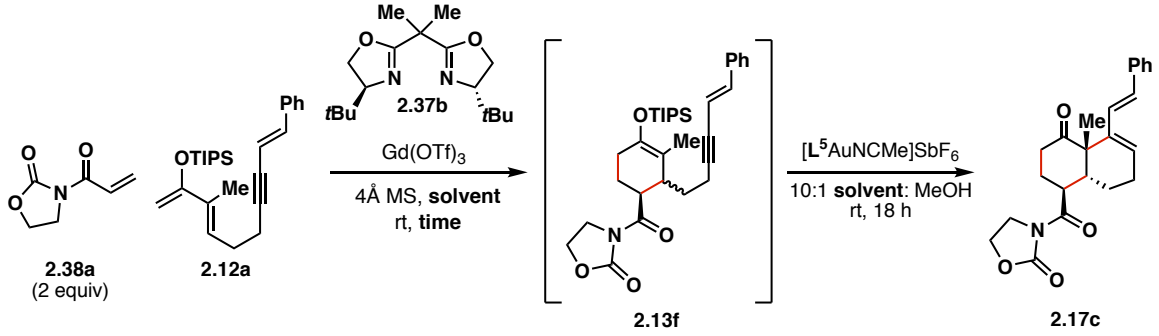

Entry	Solvent	$Gd(OTf)_3$ (mol%)	**2.37b** (mol%)	Time (h)	Au^I cat. (mol%)	NMR Yield[1] (%)
1	DCM	10	15	18	10	56
2	$CHCl_3$	10	15	18	10	36[2]
3	Acetone	5	7.5	5 d	5	41

[1] NMR yields were determined using a mesitylene standard
[2] Isolated yield

The one-pot sequences presented above led to the formation of the desired 6-*endo-dig* cyclization product (**2.17c**), with an overall yield of 56% in DCM and methanol (10:1). The incorporation of MeOH is important in these reactions as it increases the rate of protodeauration, preventing the Prins-type cyclization from occurring. In chloroform, **2.17c** was generated in 36% isolated yield. The ability to run the reactions in chloroform allows us to heat the mixtures in the final Diels-Alder step, allowing for reactivity between less activated substrates. Furthermore, elevated loadings of the ligand seemed to slow the Diels-Alder reaction, therefore the one-pot was attempted in acetone with smaller loadings of ligand and catalyst. This modification was done in order to decrease the reaction time of 5 days, however the

time of conversion did not change. Ensuing reactions were performed in DCM:MeOH (10:1 v/v).

Once we could access the 6-*endo-dig* cyclization product, the next step was to perform the second Diels-Alder reaction between diene **2.17c** and activated dienophiles (**Table 2.6**). These experiments demonstrated good conversion using tetracyanoethylene (entry 1) and *N*-methylmaleimide (entry 2) with 77% and 81% yields, respectively. Although the reacting diene is not electron rich, both of these dienophiles are activated enough for the reaction to be completed at room temperature. In the case of 1,4-benzoquinone, no cycloaddition products were observed.

Table 2.6. *Second Diels-Alder reaction scope.*

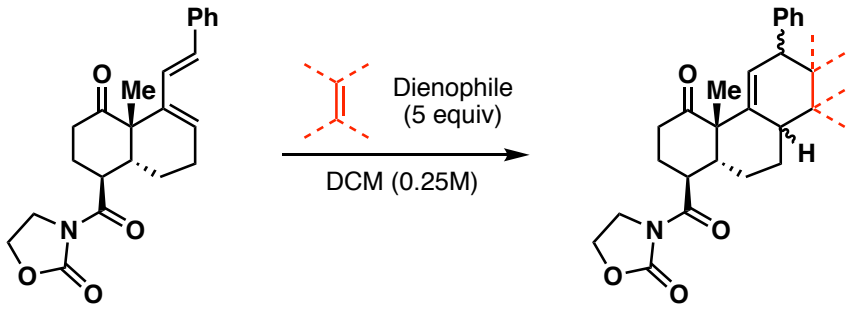

2.17c **2.21a–b**

Entry	1	2	3
Dienophile	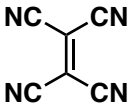	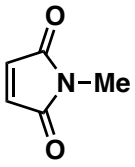	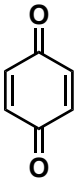
Yield (%)	77%[2] (**2.21a**)	81%[2] (**2.21b**)	n.r.[1]
dr	>20:1	2.85:1	-

[1]n.r. = no reaction.
[2] combined yield of diastereoisomers.

Prior to performing the complete one-pot reaction, the initial Diels-Alder reaction was carried out using achiral BOX ligand **2.37d**, given that the chiral group did not induce an enantioselective process (**Scheme 2.27**). Under these conditions, the *exo* cycloadduct **2.13f** was obtained in 72% yield (dr = 95:5).

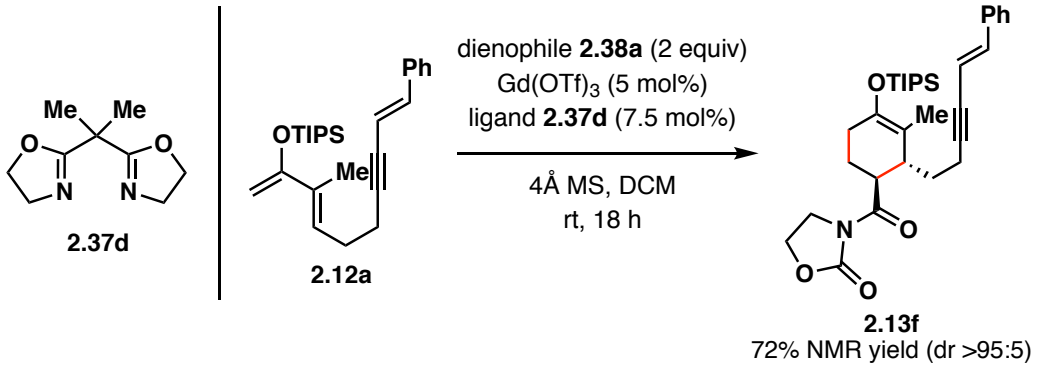

Scheme 2.27. *Diels-Alder reaction using achiral BOX ligand.*

A final three step one-pot reaction was completed with a non-chiral BOX ligand in the initial step, as shown below in **scheme 2.28**. Tetracyanoethylene was employed as the dienophile for the final step and the full sequence produced tricycle **2.21a** in 26% isolated yield.

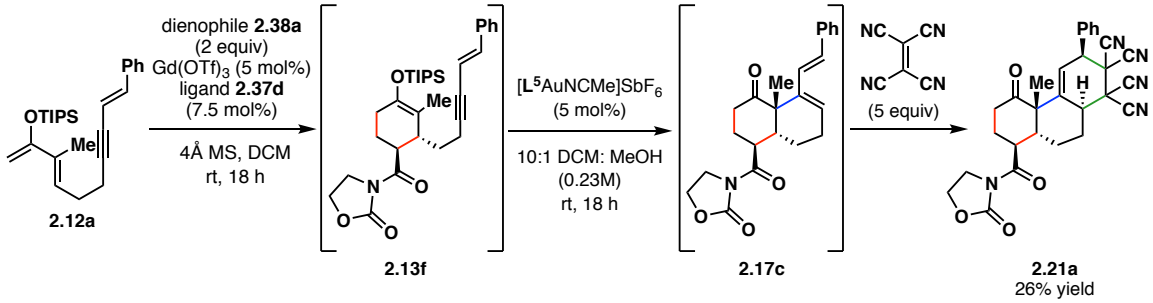

Scheme 2.28. *Diels-Alder/gold(I) cyclization/Diels-Alder one-pot reaction.*

While I completed the first 3-step one-pot sequence, Huy Tran carried out control studies of the first Diels-Alder reaction (**Table 2.7**). Without the catalyst and the BOX ligand, the conversion of the reaction was very low and only 7% of product was generated (entry 2). The control reactions also revealed that the desired product was obtained in 81% yield in the absence of the BOX ligand and molecular sieves

(entry 3). In the case where solely the BOX ligand was removed (entry 4), a 97% yield outcome confirmed that it had been having no effect on the reaction. However, molecular sieves were deemed important, preventing the starting material from desilylation and other degradation processes, and increasing the yield by 16% (entry 4).

Table 2.7. *Control reactions of Diels-Alder reaction involving Lewis acid catalyst and BOX ligand.*

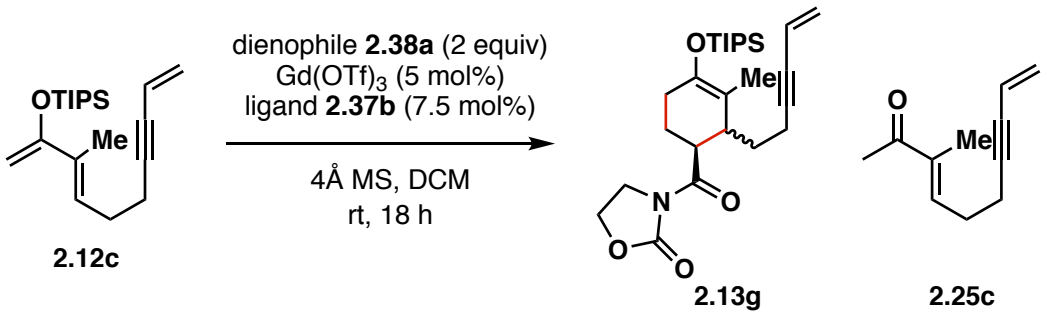

Entry	Modification	NMR Yield[1] (%)				dr (*exo*:*endo*)
		2.13g	**2.25c**	**2.12c**	Degradation	
1	No modification	92	3	2	3	95:5
2	No catalyst, no BOX ligand	7	0	84	9	-
3	No BOX ligand, no sieves	81	8	0	11	95:5
4	No BOX ligand	97	3	0	0	95:5

[1]NMR yields were determined using a mesitylene standard.

Once we knew that the BOX ligand was unecessary to achieve *exo* Diels-Alder selectivity, we concluded that the dr was influenced by the $Gd(OTf)_3$. In fact, it is possible that steric interactions between the bulky Lewis acid and substituents on the diene were enough to selectively facilitate the *exo*-cycloadduct formation (**figure 2.6**).[64]

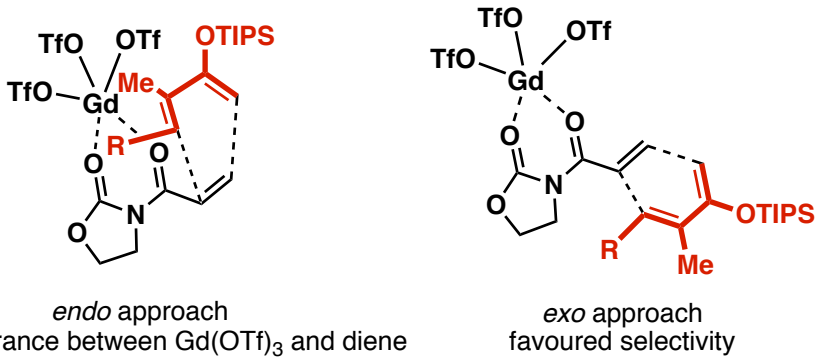

Figure 2.6. *Exo Diels-Alder selectivity from $Gd(OTf)_3$.*

2.2.4 Chiral Oxazolidinone Dienophiles

After the removal of the BOX ligand from our reaction conditions, we began exploring the use of chiral oxazolidinones as a new approach to prepare enantiopure Diels-Alder products. The possible transition states of the two *exo* cycloadducts (***exo* 1**, ***exo* 2**) are shown in **scheme 2.29**. The favored ***exo* 1** adduct goes through a non-hindered top face approach between the diene and the most stable s-cis conformer of the oxazolidinone dienophile. The disfavored transition states involve the s-trans configuration of the dienophile (**TS II**, **TS IV**), destabilized by A(1,3) strain, and/or destabilization due to steric hindrance between the chiral auxiliary and the diene (**TS II**, **TS III)**.

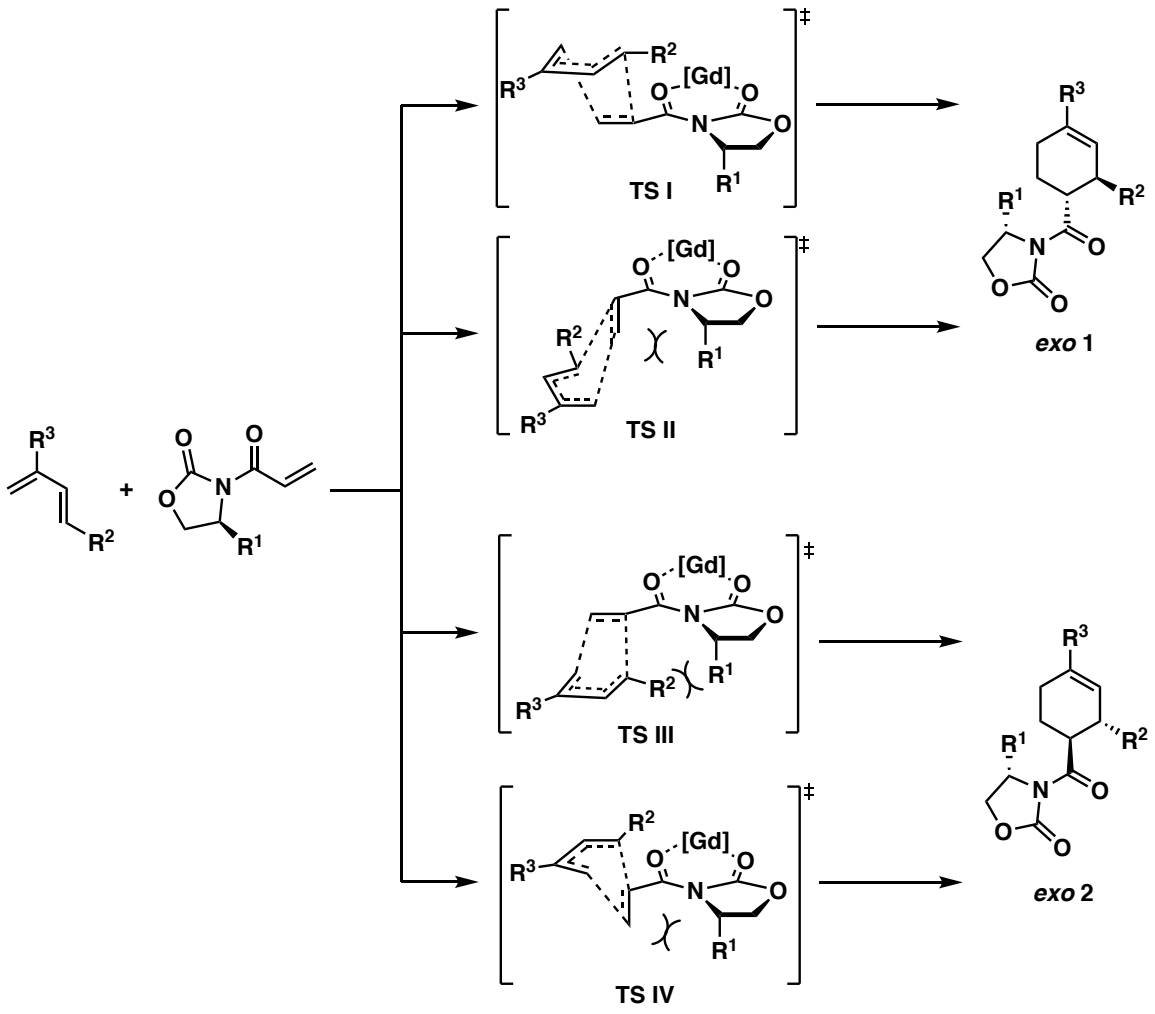

Scheme 2.29. *Transition states of exo Diels-Alder adducts with chiral oxazolidinone dienophiles.*

As shown in **table 2.8**, the Diels-Alder reaction was performed with various dienophiles in DCM and in the presence of $Gd(OTf)_3$. The chiral auxiliaries generated a range of selectivity, in which dienophile **2.38b** gave the best diastereoisomeric ratio of 10:1. However, in this particular reaction, the yield of **2.13h** was significantly reduced in comparison to **2.13h–k** and a ratio of 1:1 between the product and desilylated starting material was also observed.

Table 2.8. *Evans' auxiliary optimization for Lewis acid-catalyzed Diels-Alder reaction.*

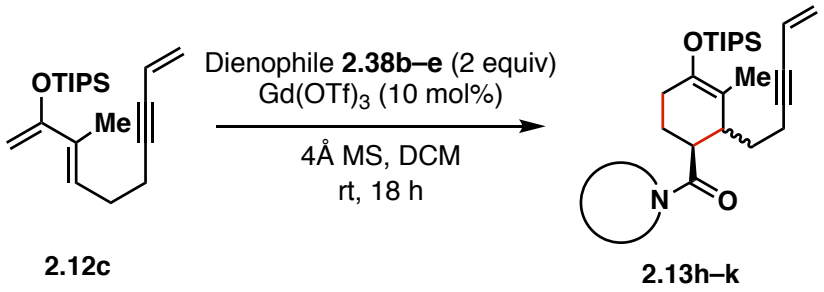

2.12c

2.13h–k

Entry	1	2	3	4
Dienophile	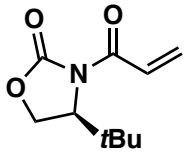 2.38b	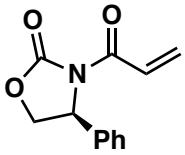 2.38c	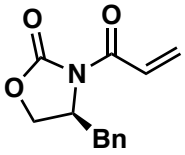 2.38d	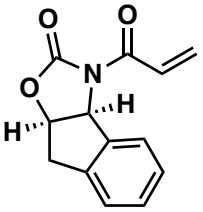 2.38e
NMR Yield[1] (%)	(37) (**2.13h**)	>95 (**2.13i**)	>95 (**2.13j**)	93 (**2.13k**)
dr (*exo*1:*exo*2)	10:1	2:1	3:1	6:1

[1]NMR yields were determined using a mesitylene standard.

Unfortunately, reproducibility of our reactions became a concern upon removal of the BOX ligand (**Table 2.8**, entry 1). Previous reaction procedures involved stirring of the BOX ligand with gadolinium triflate and molecular sieves to ensure the removal of water and binding to the metal centre. After 3 hours, the dienophile and the diene were added to the reaction mixture. In the absence of the BOX ligand, the gadolinium was stirred with molecular sieves for 3 hours before the addition of the diene and dienophile. It was later hypothesized that the gadolinium, which was not bound to the oxazolidinone, was directly involved in the desilylation

of the starting material, in competition with the Diels-Alder reaction. These results led to a modification of the procedure and the gadolinium triflate is now stirred with molecular sieves and the dienophile **2.38b** for 3 hours, before the addition of the diene. Luckily, promising results were observed with this change and a one-pot reaction was successfully performed in the absence of BOX ligand (**Scheme 2.30**). An overall yield of 46% was achieved using tetracyanoethylene as the dienophile in the final Diels-Alder step, with a dr of >95:5.

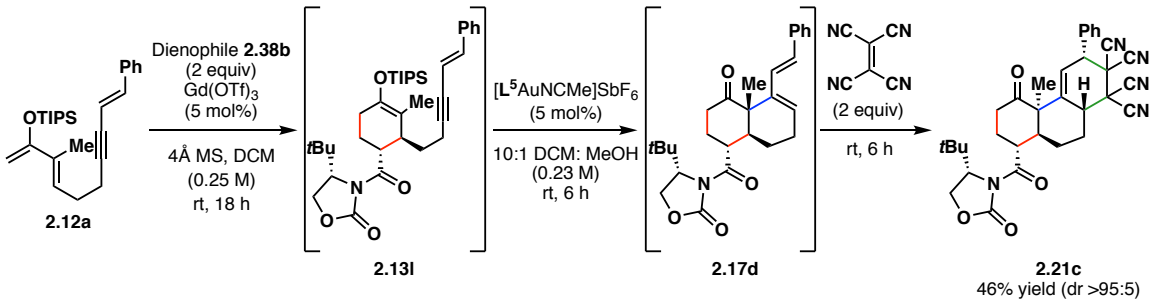

Scheme 2.30. *Final Diels-Alder/gold(I) cyclization/Diels-Alder one-pot reaction.*

2.2.5 Reaction scope

With these optimized conditions in hand, a scope was performed on the reaction with various dienes and dienophiles (**Scheme 2.31**). Difficulties arose as we made modifications to the oxazolidinone dienophiles and only *trans* electron withdrawing substituents were tolerated. On the other hand, our method allowed for more variations of the diene substrate at R^1. Substituting R^1 with a more electron withdrawing OBn functionality led to excellent diastereoselectivity and supressed the formation of the Prins cyclization product. In the case of the terminal olefin, it was more difficult to prevent the formation of the Prins-type cyclization product, however

the 2nd Diels-Alder reaction became more efficient due to the diene being less substituted. Overall, a total of nine examples were performed with yields ranging from 33% to 52% over three steps and dr ranging from 3:1 to >95:5.

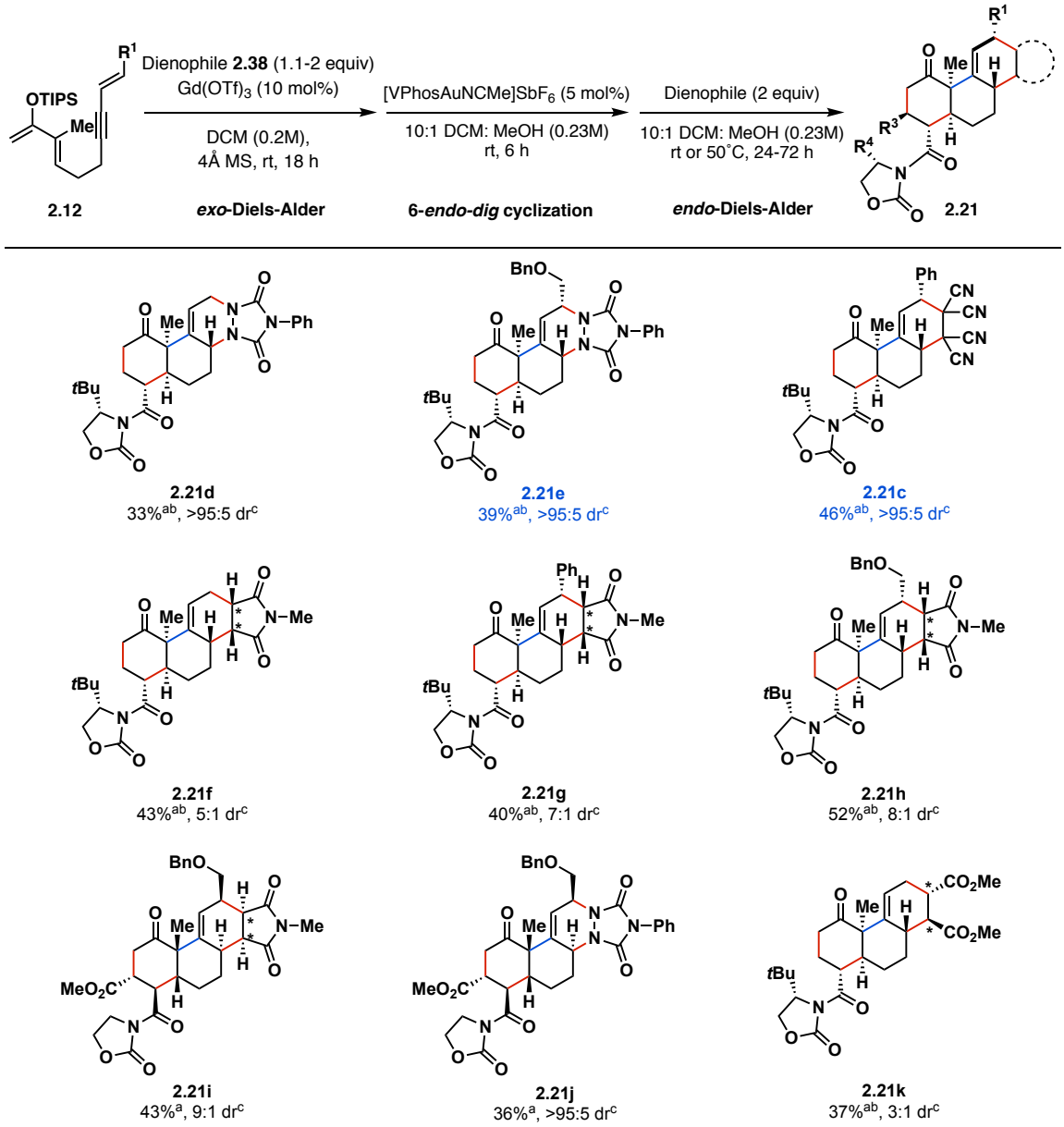

[a]Combined isolated yield. [b]Enantiopure product. [c]Diastereomeric ratio of crude mixture.

Scheme 2.31. *Scope of Diels-Alder/6-endo-dig gold(I)-catalyzed cyclization/Diels-Alder one-pot cascade.*

2.3 Selective formation of tricyclic terpenoids

Following the completion of the tri and tetracycles scope, we decided to revisit the formation of tricyclic compounds through a Diels-Alder/gold(I) cyclization/Prins cyclization cascade. As demonstrated earlier, a Prins-type cyclization can occur following the initial gold(I)-catalyzed cyclization (**Scheme 2.32**). An important modification to note from the above methodology is the removal of methanol in the gold cyclization conditions, slowing the protodeauration step and allowing for the second cyclization to occur.

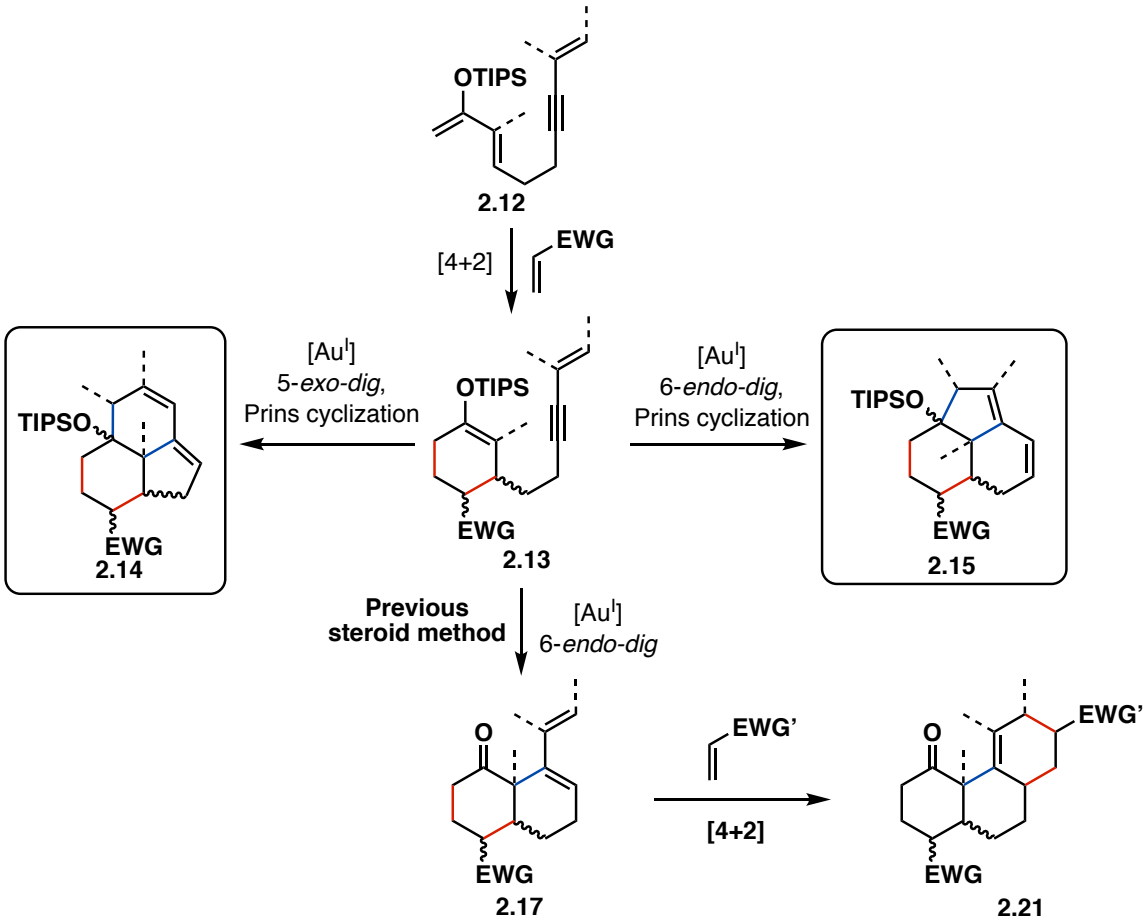

Scheme 2.32. *Divergent method to synthesize complex polycycles.*

2.3.1 Diels-Alder/6-*endo-dig* cyclization/Prins reaction cascade

The first reaction of the sequence is an intermolecular Diels-Alder reaction, followed by the 6-*endo-dig* cyclization and a Prins-type cyclization (**Scheme 2.33**). We hypothesized that the cycloadduct **2.13** would coordinate to the gold(I) catalyst to trigger a nucleophilic attack by the silyl enol ether onto the alkyne to form a second 6-membered ring through a 6-*endo-dig* cyclization process. The organogold species **2.18b** could subsequently undergo a Prins-type cyclization to produce carbocation **2.19a**. At this stage, product **2.15** could be generated through a 1,2-H shift followed by elimination of the gold species.

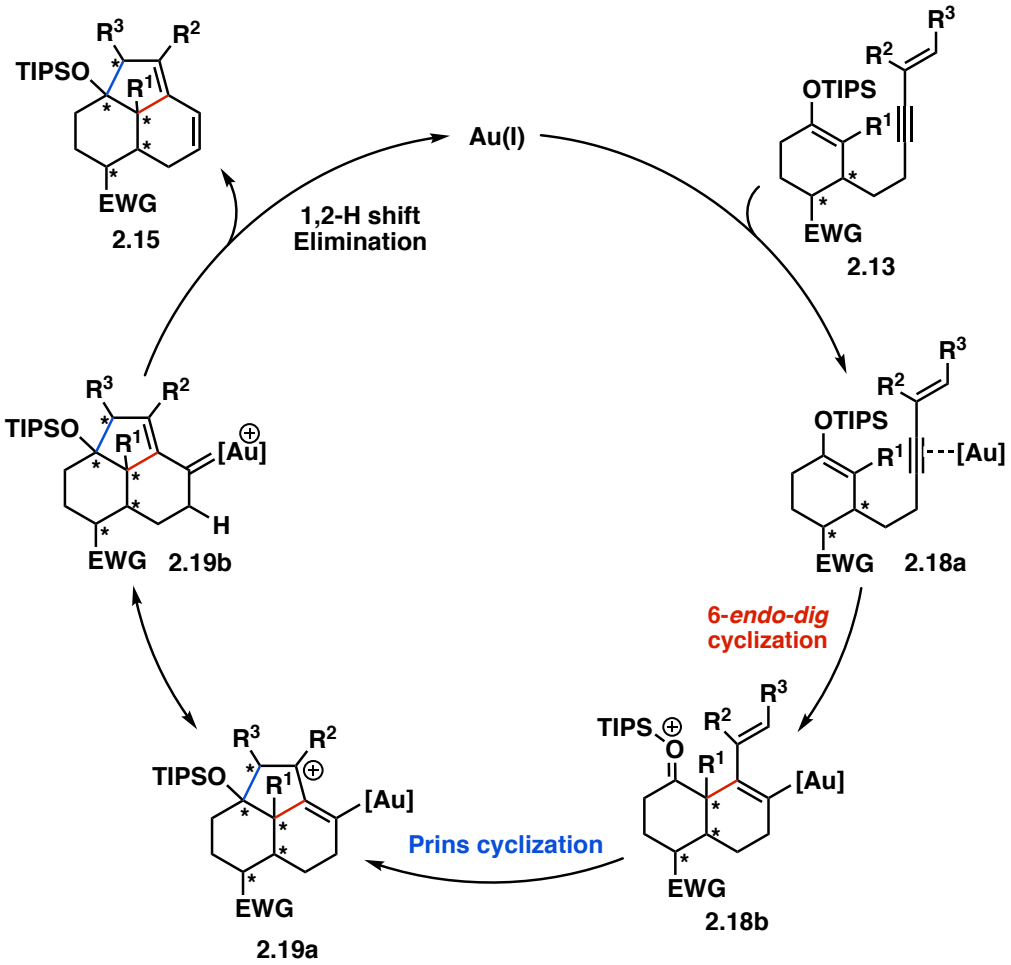

Scheme 2.33. *Catalytic cycle of Diels-Alder/6-endo-dig cyclization/Prins reaction cascade.*

We applied our Diels-Alder reaction conditions developed in chapter 2.2.2 and re-optimized the catalyst for the gold(I)-cyclization step in order to ensure high selectivity between the 5-*exo-dig* and 6-*endo-dig* cyclization products (**Table 2.9**). The optimization was completed using monosubstituted enyne diene **2.12c** and dienophile **2.37a**. A variety of phosphine ligands were screened and the best regioselectivity that we could obtain for the gold(I)-catalyzed cyclization was 2:1, favoring the 6-*endo-dig* pathway with [Me$_4$*t*BuXPhosAuNCMe]SbF$_6$. This result was in line with results previously obtained by our group.

Table 2.9. *Catalyst optimization of 6-endo-dig cyclization.*

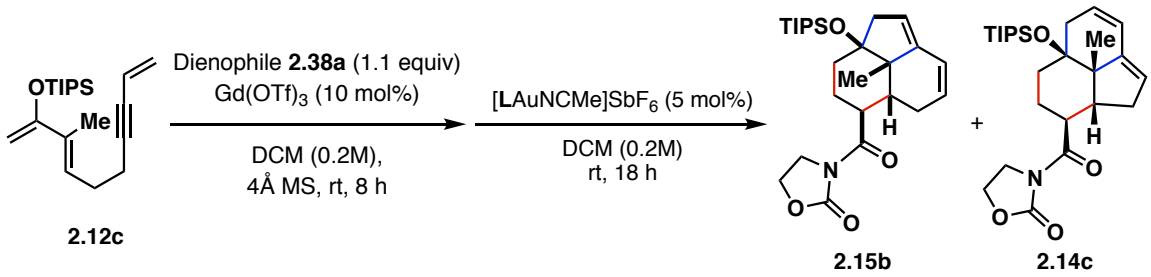

Entry	Ligand (L)	NMR yield[1,2] (%)	Regioselectivity (**2.15b:2.14c**)
1	Me$_4$*t*BuXPhos	78	2:1
2	JackiePhos	40	1:1
3	BrettPhos	39	1:1
4	DavePhos	50	35:65
5	RuPhos	26	30:70
6	AlPhos	41	3:2
7	Cy-cBRIDP	24	1:2

[1]NMR yields were determined using a mesitylene standard. [2]Yields include mixture of **2.13b** and **2.14c**.

Following optimization of the reaction conditions, a variety of dienes and oxazolidinone dienophiles were examined (**Scheme 2.34**). The *exo* Diels-Alder reaction proceeded with excellent diastereoselectivity. When it came to using disubstituted oxazolidinones, it was necessary that the additional functionality possessed electron-withdrawing properties for the initial Diels-Alder reaction to occur efficiently. The substitution of the terminal diene olefin had an important effect when it came to the regioselectivity of the cyclization reaction. The monosubstituted olefin led to poor regioselectivity of 2:1 favoring the 6-*endo-dig* and 5-*exo-dig* cyclization products (**Table 2.9**). However, once we studied di- and tri-substituted enynes, the regioselectivities highly improved, ranging from 6:1 to >95:5 selectivity in favor of the anticipated product. Notably, **2.15k** was obtained using [JohnPhosAuNCMe]SbF_6 rather than the usual gold conditions which were not leading to product formation. **2.15h** was also obtained from a different set of conditions, but interestingly, we were able to use the IPr ligand, which is the same ligand later used in the scope for the 5-*exo-dig* cyclization products. This demonstrates how strongly this particular substrate favors the 6-*endo-dig* cyclization and the extent to which these reactions can be substrate dependent.

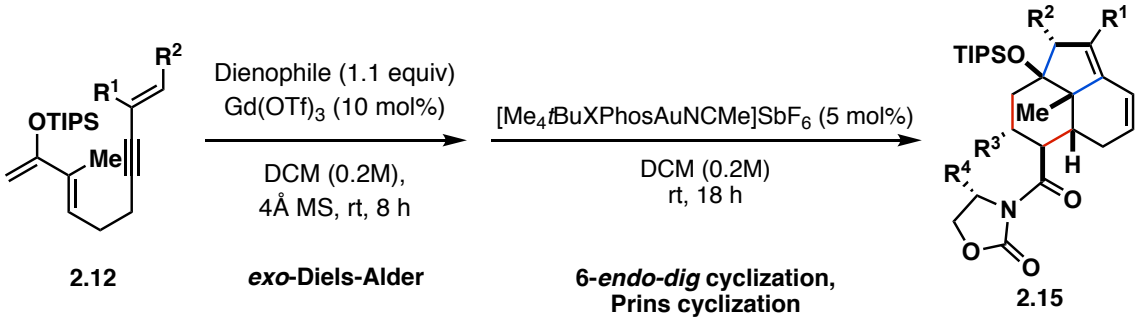

2.12 — ***exo*-Diels-Alder** — **6-*endo-dig* cyclization, Prins cyclization** — **2.15**

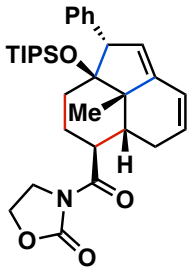

2.15a
76%[a], >95:5 dr[c], 12:1 rr[f]

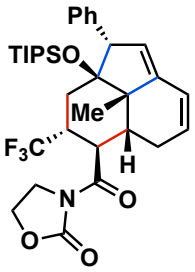

2.15c
49%[a], >95:5 dr[c], >95:5 rr[f]

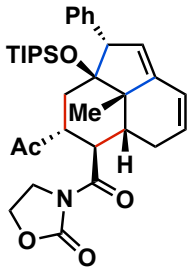

2.15d
53%[a], 9:1 dr[c], 5:1 rr[f]

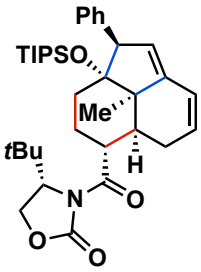

2.15e
30%[ab], >95:5 dr[c], 5:1 rr[f]

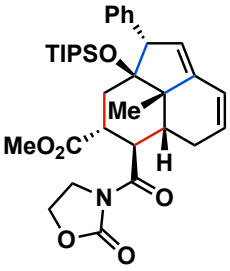

2.15f
57%[a], >95:5 dr[c], 6:1 rr[f]

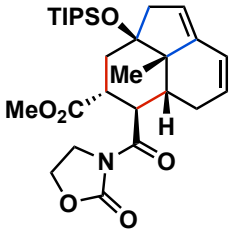

2.15g
42%[a], >95:5 dr[c], 2:1 rr[f]

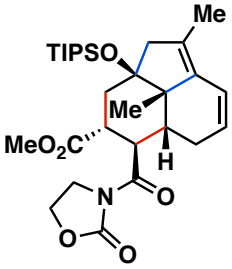

2.15h
54%[ad], >95:5 dr[c], >95:5 rr[f]

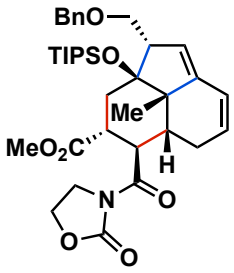

2.15i
55%[a], >95:5 dr[c], 8:1 rr[f]

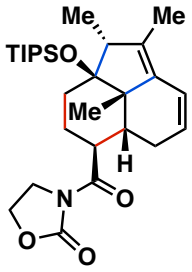

2.15j
39%[a], >95:5 dr[c], >95:5 rr[f]

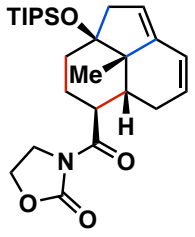

2.15b
55%[a], >95:5 dr[c], 2:1 rr[f]

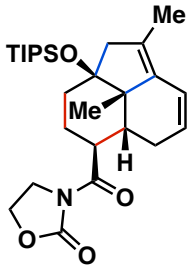

2.15k
39%[ae], >95:5 dr[c], 7:1 rr[f]

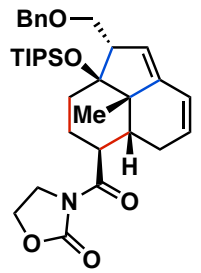

2.15l
55%[a], >95:5 dr[c], 6:1 rr[f]

[a]Combined isolated yield. [b]Enantiopure product. [c]Diastereomeric ratio of crude mixture. [d][IPrAuNCMe]SbF_6 used. [e][JohnPhosAuNCMe]SbF_6 used. [f]Regioselectivity of crude mixture.

Scheme 2.34. *Diels-Alder/6-endo-dig cyclization/Prins cyclization one-pot sequence scope.*

2.3.2 Diels-Alder/5-*exo-dig* cyclization/Prins reaction cascade

The next reaction sequence forming tricyclic compounds involved a Diels-Alder reaction followed by a 5-*exo-dig* cyclization and a Prins reaction. The mechanism is very similar to the previous cascade forming tricyclic products through a 6-*endo-dig* cyclization (**Scheme 2.35**). Once again, intermediate **2.13** is formed from the Diels-Alder reaction and undergoes a 5-*exo-dig* cyclization in the presence of a gold(I) catalyst. The organogold species **2.18c** can subsequently undergo a Prins-type cyclization to form the resulting carbocation **2.20a**. Proton elimination of resonating intermediate **2.20b**, followed by protodeauration, leads to the expected tricycle **2.14** while regenerating the Au(I) catalyst.

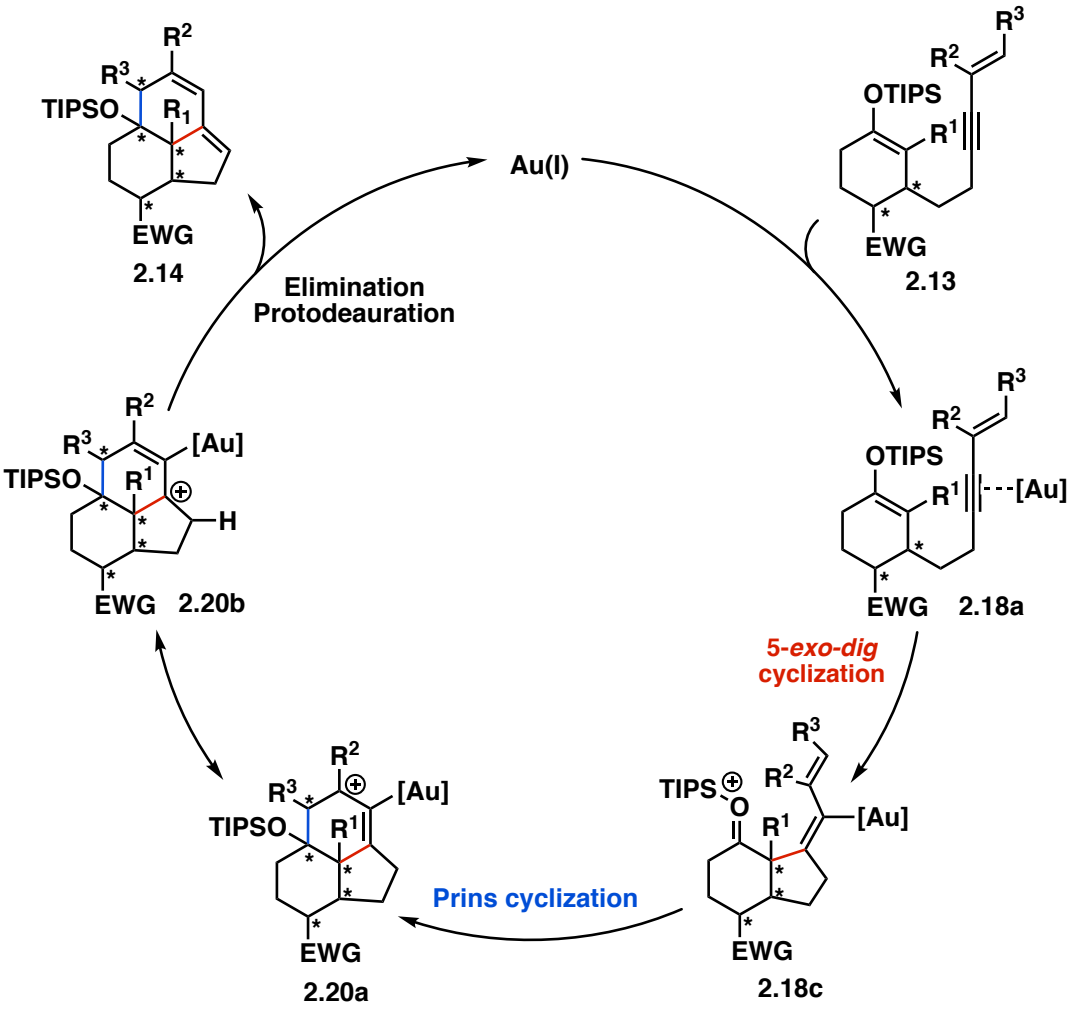

Scheme 2.35. *Catalytic cycle of Diels-Alder/5-exo-dig cyclization/Prins reaction cascade.*

The scope was completed using our usual Diels-Alder reaction conditions and an [IPrAuNCMe]SbF_6 catalyst for the gold(I) transformation (**Scheme 2.36**). Similar to our previous methods results, the *exo* Diels-Alder reactions involving chiral oxazolidinone dienophiles led to excellent diastereoselectivity of >95:5. The greater limitations were in fact observed when it came to the diene substrates. Phenyl and methyl substituents at position R^1 lead to degradation during the gold-catalyzed cyclization, limiting our scope to the terminal olefin and the benzyl-substituted

substrates. Nevertheless, the scope was expanded by a large variety of dienophiles. *Endo* Diels-Alder product **2.14a** and dehydro-Diels-Alder product **2.14i** were both generated under thermal Diels-Alder reaction conditions, with excellent regioselectivity and diastereoselectivity.

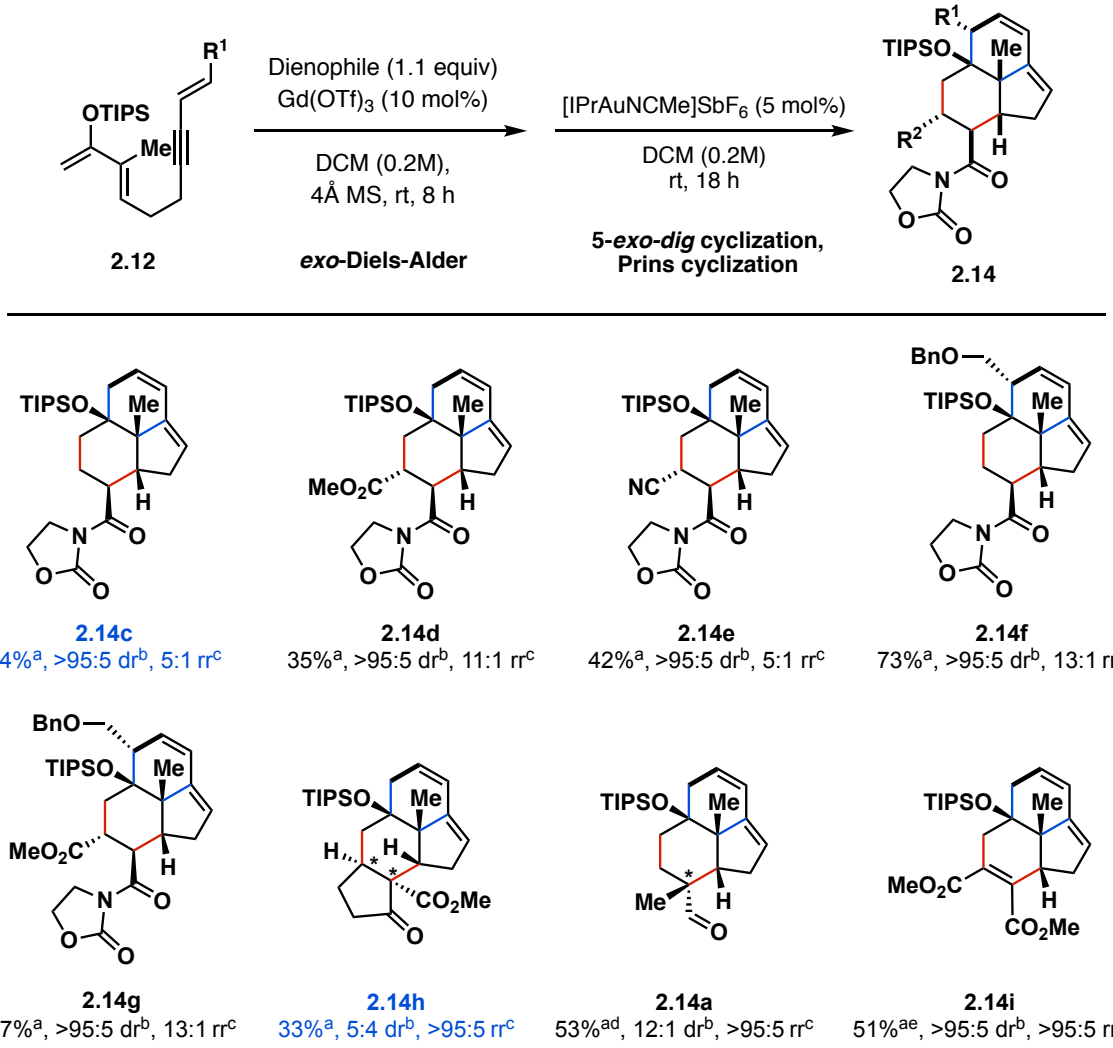

[a]Combined isolated yield. [b]Diastereomeric ratio of crude mixture. [c]Regioisomer selectivity shown. [d]Dienophile (5 equiv), DCE at 100˚C, then [JohnPhosAuNCMe]SbF_6 (5 mol%). [e]Dienophile (5 equiv), 1:1 acetone:DCE at 100˚C, then [JohnPhosAuNCMe]SbF_6 (5 mol%).

Scheme 2.36. *Diels-Alder/5-exo-dig cyclization/Prins cyclization one-pot sequence scope.*

2.4. Conclusion

In summary, the divergence of gold(I)-catalyzed cyclizations has been utilized for the generation of complex polycyclic molecules through three different reactivity pathways (**Scheme 2.37**). From a starting diene, a Diels-Alder reaction leads to the formation of a silyl enol ether tethered to an alkyne which can undergo a gold(I)-catalyzed cyclization.

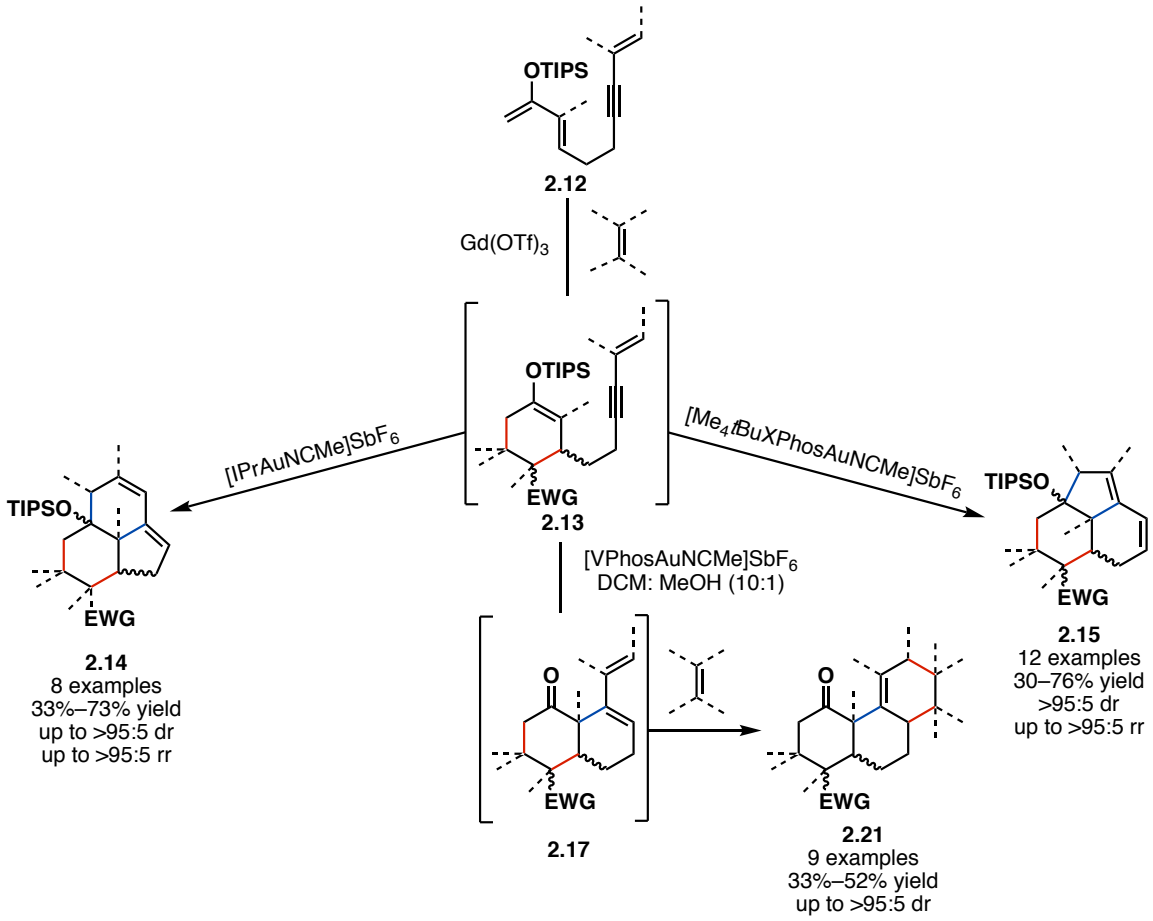

Scheme 2.37. *Divergent pathways for selective formation of complex polycycles.*

By controlling this second step of the reaction sequence, we are able to select the desired pathway to generate either tricyclic products **2.15** and **2.14**, or diene intermediate **2.17** to undergo a second Diels-alder reaction and generate **2.21**. From experimental studies, the diastereoselectivity of the initial Diels-Alder cycloadduct was deemed important. While unable to form the 6-*endo*-*dig* cyclization product from the *endo*-cycloadduct, the *exo* product led to the desired cyclized scaffold. Using [VPhosAuNCMe]SbF_6 and by incorporating MeOH in the reaction, 12 examples of tri and tetracycles were exhibited in a three-step one-pot reaction, with yields ranging from 33%–52% and dr between 3:1 and >95:5. This reactivity pathway allows for the formation of up to 5 C-C bonds, and the control of up to 8 stereocenters.

The Diels-Alder/gold-cyclization/Prins cyclization sequences were completed using an NHC IPr ligand and phosphine ligand Me_4*t*BuXPhos to respectively favor the 5-*exo*-*dig* and the 6-*endo*-*dig* cyclization pathways. Both of these transformations led to the formation of three C–C bonds and the control of up to six stereocenters. Through ligand modification, we have demonstrated the ability to control three complex divergent reactivity pathways from an easily synthesized linear substrate.

2.5 References

[33] a) Cheskis, B. J. Regulation of cell signalling cascades by steroid hormones. *J. Cell. Biochem.* **2004**, *93* (1), 20–27; b) Evans, R. M. The Steroid and Thyroid Hormone Receptor Superfamily. *Science*. **1988**, *240* (4854), 889–895.

[34] a) Ericson-Neilsen, W.; Kaye, A. D. Steroids: Pharmacology, Complications, and Practice Delivery Issues. *Ochsner J.* **2014**, *14* (2), 203–207; b) Vyas, A. R.; Singh, S. H. Molecular targets and mechanisms of cancer prevention and treatment by withaferin A, a naturally occurring steroidal lactone. *AAPS J.* **2014**, *16* (1), 1–10.

[35] Fakheri, R. J.; Javitt, N. B. Autoregulation of cholesterol synthesis: Physiologic and pathophysiologic consequences. *Steroids*. **2011**, *76* (3), 211–215.

[36] a) Stork, G.; Burgstahler, A. W. The Stereochemistry of Polyene Cyclization. *J. Am. Chem. Soc.* **1955**, *77* (19), 5068–5077; (b) Eschenmoser, A.; Ruzicka, L.; Jeger, O.; Arigoni, D. Eine stereochemische Interpretation der biogenetischen Isoprenregel bei den Triterpenen *Helv. Chim. Acta.* **1955**, *38* (7), 1890–1904.

[37] Johnson, W. S.; Gravestock, M. B.; McCarry, B. E. Acetylenic bond participation in biogenetic-like olefinic cyclizations. II. Synthesis of dI-progesterone. *J. Am. Chem. Soc.* **1971**, *93* (17), 4332–4334.

[38] Fish, P. V.; Johnson, W. S. The First Examples of Nonenzymic, Biomimetic Polyene Pentacyclizations. Total Synthesis of the Pentacyclic Triterpenoid Sophoradiol. *J. Org. Chem.* **1994**, *59* (9), 2324–2335.

[39] a) Yoder, R. A.; Johnston, J. N. A Case Study in Biomimetic Total Synthesis: Polyolefin Carbocyclizations to Terpenes and Steroids. *Chem*. *Rev.* **2005**, *105* (12), 4730–4756; b) Barret, A. G. M.; Ma, T. K .; Mies, T. Recent Developments in Polyene Cyclizations and Their Applications in Natural Product Synthesis. *Synthesis.* **2019,** *51* (01), 67–82**.**

[40] Corey, E. J.; Lin, S. A Short Enantioselective Total Synthesis of Dammarenediol II *J. Am. Chem. Soc.* **1996**, *118* (36), 8765–8766.

[41] Ishihara, K.; Nakamura, S.; Yamamoto, H. The First Enantioselective Biomimetic Cyclization of Polyprenoids. *J. Am. Chem. Soc.* **1999,** *121* (20), 4906–4907.

[42] Surendra, K.; Corey, E. J. Highly Enantioselective Proton-Initiated Polycyclization of Polyenes. *J. Am. Chem. Soc.* **2012**, *134* (29), 11992–11994.

[43] Skoda-Földes, R.; Kollár, L. Transition-Metal-Catalyzed reactions in steroid synthesis. *Chem. Rev.* **2003**, *103* (10), 4095–4130.

[44] Geier, M. J.; Gagné, M. R. Diastereoselective Pt Catalyzed Cycloisomerization of Polyenes to Polycycles. *J. Am. Chem. Soc.* **2014**, *136* (8), 3032–3035.

[45] Ronga, Z.; Echaverren, A. M. Broad scope gold(I)-catalysed polyenyne cyclisations for the formation of up to four carbon–carbon bonds. *Biomol. Chem.* **2017**, *15* (10), 2163–2167.

[46] Nising, C. F.; Bräse, S. Highlights in Steroid Chemistry: Total Synthesis versus Semisynthesis. *Angew. Chem. Int. Ed*. **2008**, *47* (49), 9389–9391.

[47] McGee, P.; Brousseau, J.; Barriault, L. Development of New Gold (I)-Catalyzed Carbocyclizations and their Applications in the Synthesis of Natural Products. *Isr. J. Chem.* **2018**, *58* (5), 511–520.

[48] Hashmi, A. S. K. Gold-Catalyzed Organic Reactions. *Chem. Rev*. **2007**, *107* (7), 3180−3211.

[49] Barabé, F.; Levesque, P.; Korobkov, I.; Barriault, L. Synthesis of Fused Carbocycles via a Selective 6-*Endo* Dig Gold(I)-Catalyzed Carbocyclization. *Org. Lett.* **2011**, *13* (20), 5580–5583.

[50] Clayden, J.; Greeves, N.; Warren, S. Organic Chemistry, 2nd ed.; Oxford University Press; Oxford, 2002.

[51] Diels, O.; Alder, K. Synthesen in der hydroaromatischen Reihe. 1928**,** *Justus Liebigs Ann Chem*, **1928**, 460, 98–122.

[52] Alder, K.; Stein, G.; Budedenbrock, F.; Eckardt, W.; Frercks, W.; Schneider, S. Über den sterischen Verlauf von Additions- und Substitutions-reaktionen. *Justus Liebigs Ann. Chem.* **1934**, *514* (1), 1–33.

[53] Nicolaou, K.C.; Snyder S. A.; Montagnon T.; Vassilikogiannakis G. The Diels-Alder reaction in total synthesis. *Angew. Chem., Int. Ed.* **2002**, *41* (10), 1668–1698.

[54] Yates, P.; Eaton, P. Acceleration of the Diels-Alder reaction by aluminium chloride. *J. Am. Chem. Soc.* **1960**, *82* (16), 4436–4437.

[55] Zhang, W.; Loebach, J. L.; Wilson, S. R.; Jacobsen, E. N. Enantioselective epoxidation of unfunctionalized olefins catalyzed by salen manganese complexes. *J. Am. Chem. Soc.* **1990**, *112* (7), 2801–2803.

[56] Huang, Y.; Iwama, T.; Rawal, V. Design and development of highly effective lewis acid catalysts for enantioselective diels-alder reactions. *J. Am. Chem. Soc.* **2002**, *124* (21), 5950–5951.

[57] Wang, W.; Kumar, M.; Hammond, G. B.; Xu, B. Enhanced Reactivity in Homogeneous Gold Catalysis through Hydrogen Bonding. *Org. Lett.* **2014**, *16* (2), 636–639.

[58] a) Fang, W.; Presset, M.; Guérinot, A.; Bour, C.; Bezzenine-Lafollée, S.; Gandon, V. Silver-Free Two-Component Approach in Gold Catalysis: Activation of [LAuCl] Complexes with Derivatives of Copper, Zinc, Indium, Bismuth, and other Lewis Acids. *Chem. Eur. J.* **2014**, *20* (18), 5439–5446; b) Barrio, P.; Kumar, M.; Lu, Z., Han, J.; Xu, B.; Hammond, G. Acidic Co-catalysts in cationic gold catalysis. *Chem. Eur. J.* **2016**, *22* (46), 16410–16414.

[59] Desimoni, G.; Faita, G.; Jorgensen, K. A. C2-symmetric chiral bis(oxazoline) ligands in asymmetric catalysis. *Chem. Rev.* **2006**, *106* (9), 3561–3651.

[60] Corey E. J.; Imai, N.; Zhang, H. Y. Designed catalyst for enantioselective Diels-Alder addition from a c2-symmetric chiral bis(oxazoline)-iron(III) complex. *J. Am. Chem. Soc.* **1991**, *113* (2), 728–729.

[61] Evans, D. A.; Miller, S. J.; Lectka, T. Bis(oxazoline)copper(II) complexes as chiral catalysts for the enantioselective diels-alder reaction. *J. Am. Chem. Soc.* **1993**, *115 (*14), 6460–6461.

[62] Evans, D. A.; Miller, S. J.; Lectka, T.; Matt, P. Chiral bis(oxazoline)copper(II) complexes as lewis acid catalysts for the enantioselective diels-alder reaction. *J. Am. Chem. Soc.* **1999**, *121* (33), 7559–7573.

[63] Ishihaha, K.; Sakakura A. *Comprehensive Organic Synthesis II (Second edition);* Elsevier Ltd., **2014**, 5, 351–408.

[64] a) Yepes, D.; Pérez, P.; Jaque, P.; Fernández, I. Effect of Lewis acid bulkiness on the stereoselectivity of Diels-Alder reactions between acyclic dienes and α,β-enals. *Org. Chem. Front.* **2017**, *4* (7), 1390–1399; b) Lam, Y.-H.; Cheong, P. H.-Y.; Mata, J. M. B.; Stanway, S. J.; Gouverneur, V.; Houk, K. N. Diels-Alder Exo Selectivity in Terminal-Substituted Dienes and Dienophiles: Experimental Discoveries and Computational Explanations. *J. Am. Chem. Soc.* **2009**, *131* (5), 1947–1957.

Chapter 3. Cyclization of enol ethers using gold photocatalysis

3.1 Introduction

3.1.1 Photochemistry

Photochemistry plays an important role in chemical synthesis, giving scientists access to a breadth of reactions that would not otherwise be possible. These reactions involve the excitation of an electron from ultraviolet light, visible light or infrared radiation. The first law of photochemistry, also known as the Grotthuss-Draper law, states that light must be absorbed by a given molecule for a photochemical process to occur. The second law of photochemistry, the Stark-Einstein law, implicates that for every photon absorbed, a single molecule is activated to undergo a chemical process. These processes are well depicted by Jablonski diagrams, illustrating the pathways and electronic states of a molecule when it has reached an excited state.[65]

As demonstrated in **figure 3.1**, upon absorption of a photon, an electron of the excited molecule is promoted in a singlet state from the HOMO to a higher vibrational level of the LUMO, before settling to the most stable one (S_1).[66] This excited state has a short lifetime and will return to the singlet ground state (S_0) by losing energy through various deactivation processes. The electron can first undergo fluorescence and return to the singlet ground state (S_0) by emitting a photon. Alternatively, intersystem crossing (ISC) via a spin flip can lead the electron to a triplet-excited state (T_1). From the triplet state, the electron can reach the S_0 through phosphorescence (P) by emitting a photon, or through internal conversion by vibrational relaxation.

Phosphorescence is considered a longer process than fluorescence because it involves a spin flip to reach the singlet ground state. Accordingly, the triplet excited state has an increased lifetime.

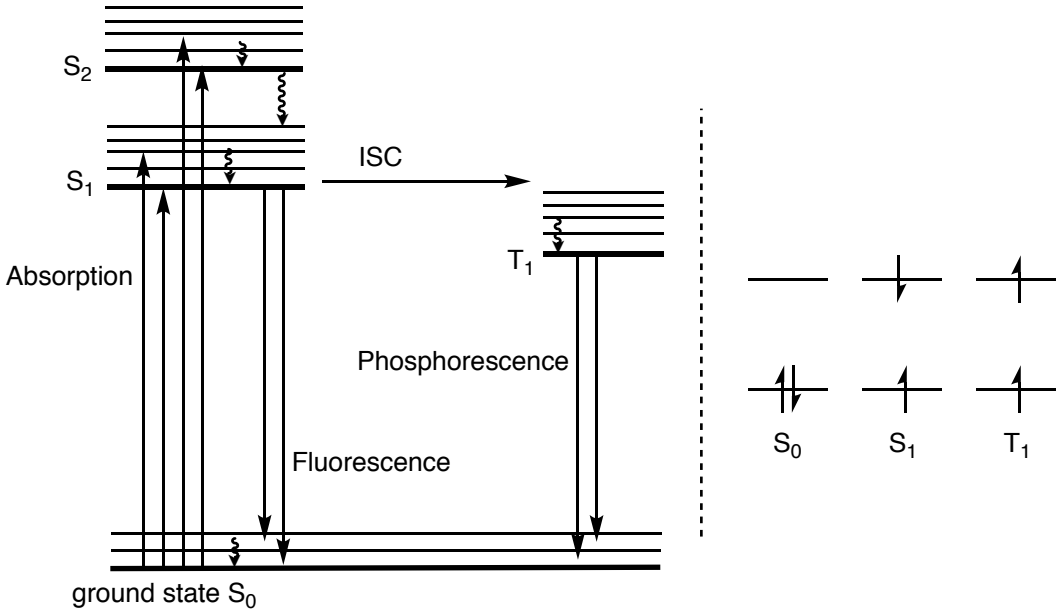

Figure 3.1. *Jablonski diagram.*

The Jablonski diagram illustrates well the physicochemical processes that can occur when a molecule absorbs a photon. However, instead of returning to the singlet ground state following excitation, an excited molecule can also undergo a variety of photochemical transformations, as illustrated in **figure 3.2**.[65]

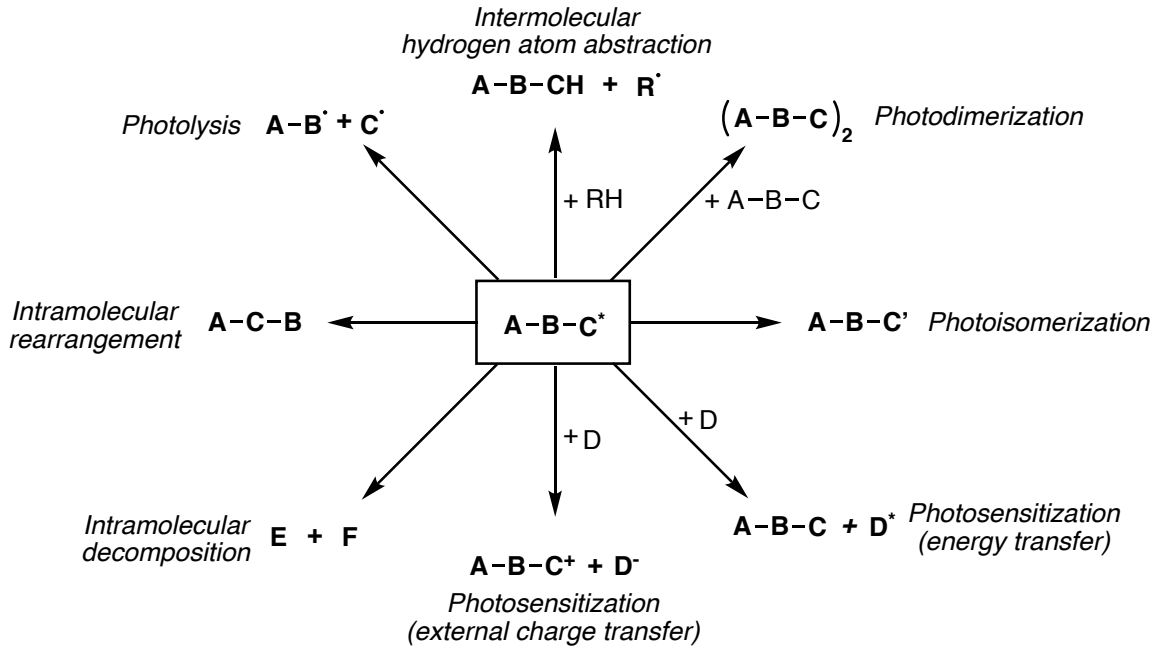

Figure 3.2. *Potential photochemical processes of an excited molecule.*

3.1.2 Photocatalysis

Photochemistry relies first and foremost on the absorption of photons by a molecule at a given wavelength to lead to the desired transformations. Due to the inability of the majority of organic substrates to absorb visible light, photocatalysts have been largely exploited as chromophores, initiating photochemical transformations in a second molecule.

A molecule in its excited state has an increased ability to act as a stronger reductant, as well as a stronger oxidant. Thus, the majority of photocatalytic processes undergo single electron transfer (SET) and can proceed through one of two pathways (**Figure 3.3**). In the reductive quenching cycle, the excited photocatalyst (PC*) receives an electron from a donor substrate (D). The now-reduced

photocatalyst can donate that electron to an acceptor species and regenerate the original active photocatalyst (PC).

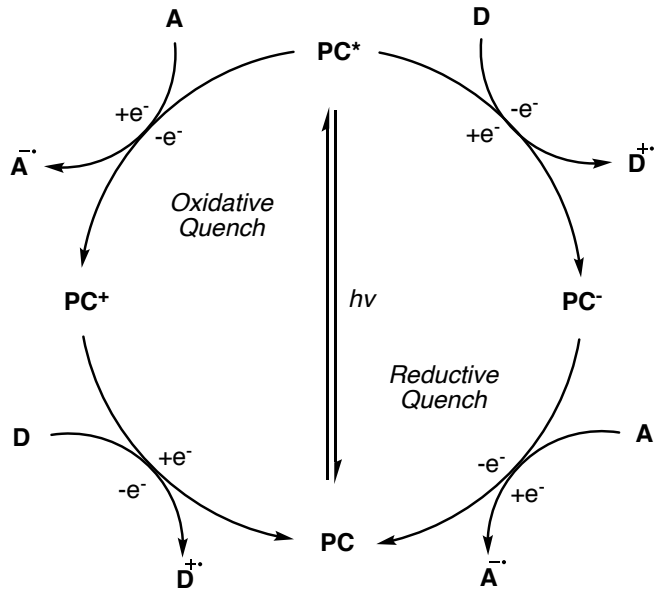

Figure 3.3. *General photocatalytic transformation pathways.*

Alternatively, the oxidative quenching cycle involves the excited photocatalyst being oxidized by an acceptor. The photocatalyst is further regenerated after accepting an electron from a donor molecule. In all cases, redox potentials of the substrate and photocatalyst must be compatible and are extremely influential on whether the transformation will occur through an oxidative or a reductive quenching cycle.[67]

Photocatalysts have the ability to efficiently absorb light at longer wavelengths than most organic molecules. A large number of organic dyes, such as acridiniums and xanthenes, have been explored for this purpose, as well as metal-based catalysts, notably $Ru(bpy)_3Cl_2$ and *fac*-$Ir(ppy)_3$ (**Figure 3.4**).[68,69]

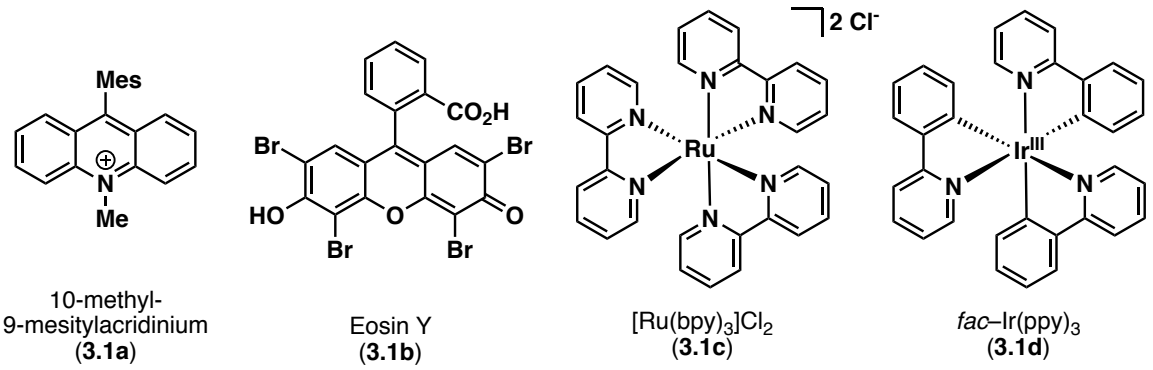

Figure 3.4. *Common organic and metal-based photocatalysts.*

Photocatalysis has many advantages, alongside its ability to generate original reactivity. Photocatalysts are able to realize redox neutral transformations, where the catalyst is employed both as a reductant and an oxidant at distinctive points in the reaction mechanism. This is a large improvement from other synthetic methods, which require stoichiometric quantities of a reductant and an oxidant, often incompatible with each other. Photocatalysis can also be applied under mild conditions and to avoid the use of highly toxic and/or reactive radical initiators. Catalyst loadings in most cases remain very low, near 1 mol% or less, and by-products are few due to the non-reactive nature of most organic reagents under visible light conditions.

In 2008, the group of Stephenson reported a reductive dehalogenation reaction using a ruthenium-based photocatalyst, improving on previous methods which involved toxic tin reagents.[70, 71] The reduction of C–Br and C–Cl bonds was achieved within a scope of 10 examples with high yields and catalyst loadings of 2.5 mol%.

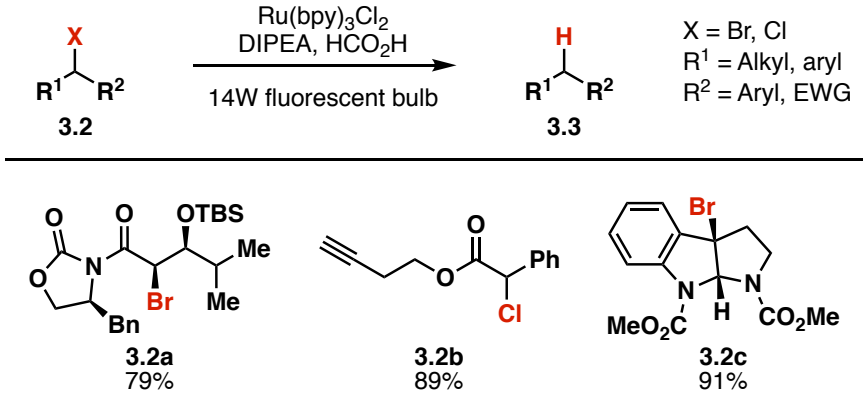

Scheme 3.1. *Reaction scheme for the reductive dehalogenation of C–Cl and C–Br bonds.*

Through a reductive quenching cycle, excited $Ru(bpy)_3^{2+}$ catalyst was quenched by DIPEA through an outer-sphere SET via a metal to ligand charge transfer (MLCT) excited state to generate an aminium cation radical and $Ru(bpy)_3^{+}$ (**Scheme 3.2**). $Ru(bpy)_3^{+}$ was then able to reduce halogenated substrate **3.2** to form a carbon-centered radical species (**3.4**), which subsequently underwent hydrogen atom transfer (HAT) with aminium cation radical species **3.5a**, generating iPr_2EtN^{+} and product **3.3.**

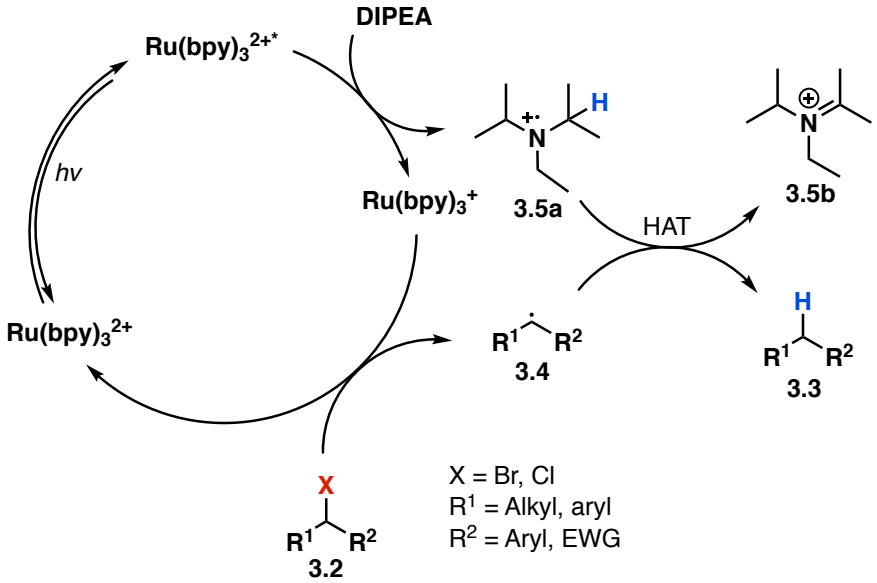

Scheme 3.2. *Proposed photocatalytic cycle for reductive dehalogenation reaction.*

Zhou *et al.* proposed a photocatalytic mechanism for the formation of phenanthrenes via a visible light-induced [4+2] benzannulation using organic photocatalyst eosin Y (EYH_2) (**Scheme 3.3**).[72] Initially, biaryl radical **3.8a** and the radical cation of eosin Y (EYH^{2+}) were generated through single electron transfer between the excited photocatalyst and diazonium salt **3.6**. Addition of the biaryl radical onto an alkyne partner (**3.7**) generated vinylic radical species **3.8b**, which subsequently underwent an intramolecular radical cyclization to generate intermediate **3.8c**. Single electron oxidation of **3.8c** by eosin Y radical cation regenerated the photocatalyst and cationic species **3.8d**. Finally, phenanthrene product (**3.9**) was formed from the deprotonation of **3.8d**.

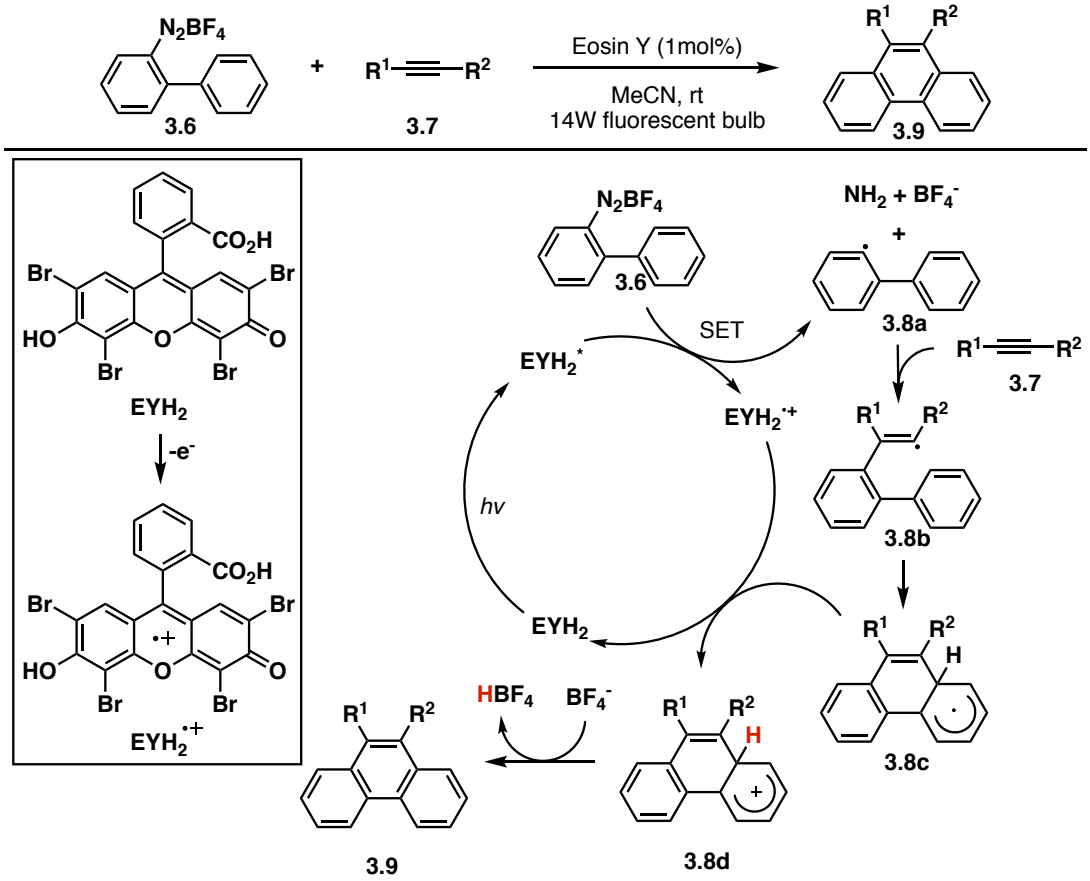

Scheme 3.3. *Proposed photocatalytic mechanism for the formation of phenanthrenes.*

Dual catalytic systems have also been largely explored, where a catalyst that is not necessarily involved in the photochemical mechanism is incorporated into a photocatalytic system.[73] In these methods, the photocatalyst will activate a substrate, while the second catalyst may be necessary to trigger reactivity of generated intermediates. A good example of this is the work completed by MacMillan for the enantioselective α-functionalization of aldehydes.[74] Described in many reports, this reaction has been utilized for the addition of α-carbonyl, fluoroalkyl, α-cyanoalkyl, benzyl, and carbamoyl moieties. The proposed dual catalytic mechanism for the generation of β-cyanoaldehydes is presented in **scheme 3.4**. Condensation of the aldehyde substrate onto chiral secondary amine **3.12** will first form enamine **3.12a**. The photoexcited state of the $Ru(bpy)_3^{2+}$ photocatalyst will quench with a sacrificial quantity of the enamine to form $Ru(bpy)_3^{+}$, which can thereafter reduce the bromonitrile species. The generated cyanoalkyl radical **3.11a** is now able to couple with enamine **3.12a**, leading to α-amino radical intermediate **3.12b**. **3.12b** which is capable of reducing $Ru(bpy)_3^{2+}$ and will form iminium ion **3.12c**. Subsequent hydrolysis of the iminium intermediate will release α-cyanoalkylated aldehyde species **3.13** and regenerate the chiral secondary amine.

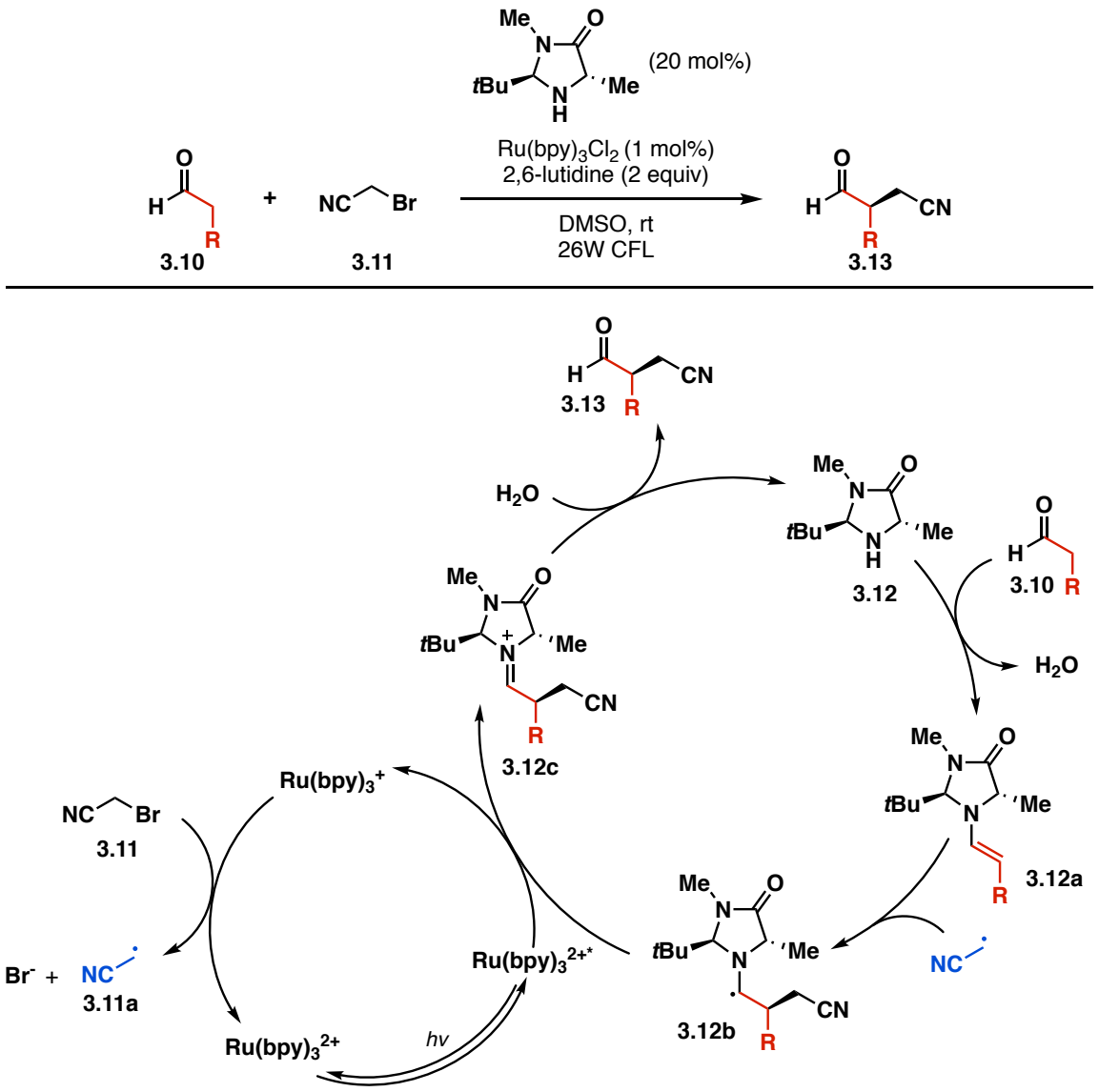

Scheme 3.4. *Proposed dual catalytic mechanism for the enantioselective α-cyanoalkylation of aldehydes.*

3.1.3 Applications of gold photocatalysis

Such as described in chapter 1.5, the Che group carried out a variety of experiments to demonstrate the unique photoluminescent properties of binuclear gold complexes.[75] During their studies, they also completed quenching studies and discovered the ability of the photocatalyst to quench with organic halides. Ever since, a multitude of synthetic studies have been conducted with these catalysts, mainly focusing on substrates with carbon-halide bonds.

One of the most important factors to consider in photocatalysis is compatibility between the photocatalyst and the reacting substrate, determined by their redox potentials. Excited states of the more common $Ru(bpy)_3^{2+}$ and *fac*-$Ir(ppy)_3^{3+}$ catalysts have oxidation potentials of –0.81V[76] and –1.73V[77], respectively, and $*[Au_2(\mu\text{-dppm})_2]^{2+}$ has a potential of –1.63V[78]. Organic halides, more specifically bromoalkanes, are noticeably challenging targets with reduction potentials ranging between -1.9V and -2.5V.[79,80] While they should not be able to engage with currently available photocatalysts, gold(I) dimeric catalysts have demonstrated the ability to quench with these unactivated substrates.[81]

In collaboration with the group of Prof. Scaiano, we have proposed distinct mechanisms by which gold photoactive catalysts undergo photoexcitation.[78] As previously visited, $*[Au_2(\mu\text{-dppm})_2]^{2+}$ is not excited through MLCT like most other catalysts. Instead, an electron is excited from the $5d_{z2}$ anti-bonding orbital to a $6s/6p_z$ bonding orbital, thus allowing interaction with the 4pz orbital of the organohalide to

generate an inner-sphere exciplex. The exciplex then prompts the reductive cleavage of the bromoalkane and oxidative quenching of the catalyst.[82] This mechanistic pathway engages new reactivity by allowing for the exciplex intermediate to interact with bromoalkanes possessing highly negative reduction potentials, which would otherwise be unachievable.

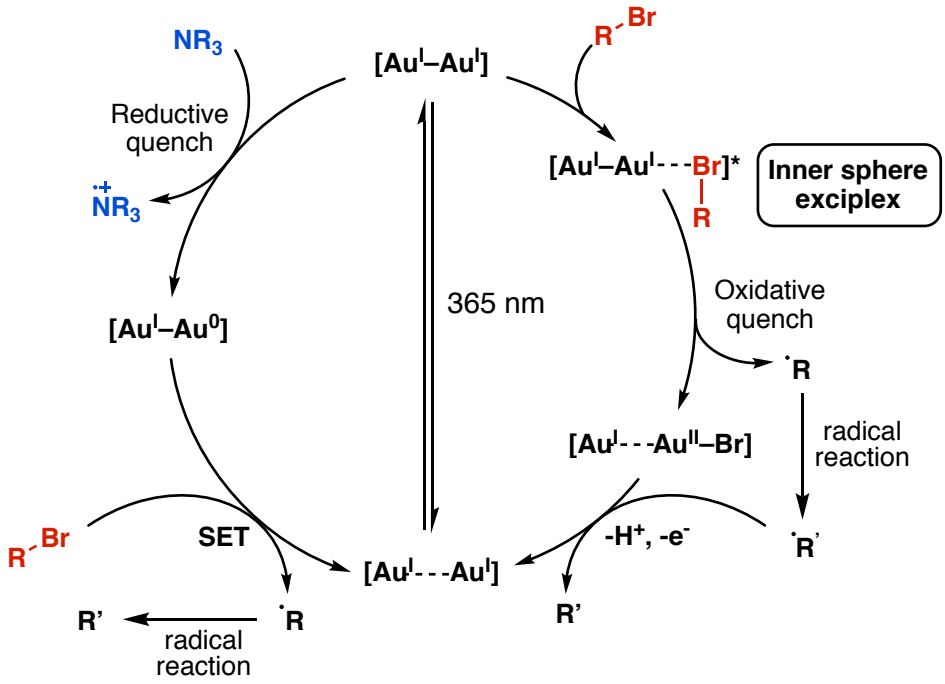

Scheme 3.5. *Proposed photocatalytic reductive and oxidative quenching cycles.*

The mechanism of photochemical transformations involving gold(I) dimeric catalysts are similar to previously visited examples (**Scheme 3.5**). For the oxidative quenching cycle, an inner sphere exciplex is formed, triggering cleavage of the carbon-halide bond and oxidation of the excited catalyst to $[Au^{I}–Au^{II}]^{3+}$. The generated carbon centered radical can undergo radical reactions and subsequently reduce the $[Au^{I}–Au^{II}]^{3+}$ complex, regenerating the ground state dimeric Au(I) catalyst and alkyl functionalized product (where R= alkyl). The photocatalytic pathway can

also go through a reductive quenching cycle, where the excited photocatalyst is reduced by a tertiary amine. Similarly to other trialkylamines, DIPEA has been shown to quench the $[Au^{I}–Au^{I}]^*$ complex at a rate of 2.7×10^7 M^{-1} s^{-1} [78], which is about ten times faster than the quenching with bromoalkanes. The generated $[Au^{1}–Au^{0}]^+$ complex is a strong reductant and can regenerate the ground-state photocatalyst and form a carbon-centered radical through single electron transfer with the bromoalkane. Further radical reactions can occur to form the desired products.

The first demonstration of this reactivity with unactivated alkyl bromides and aryl bromides was demonstrated by our group in 2013 for the cyclization of organobromide substrates.[83] The reaction was optimized from bromoalkane **3.14a** for the formation of radical cyclization product **3.16a** (**Table 3.1**). Initially, the cyclization was completed in sunlight with a $[Au_2(\mu\text{-dppm})_2]X_2$ catalyst and varying counterions. From these first results (entries 1–3), they found that the difference in yield was not significant and further experiments were completed with the more robust and photostable $[Au_2(\mu\text{-dppm})_2]Cl_2$ complex. The absorption maxima of the dimeric gold catalyst is 295nm, however, it also absorbs UVA (315-400nm), allowing for the use of 365nm LEDs and avoiding dependence on weather conditions. Entry 4 shows the use of this new light source and, although the yield showed slight decline, it became a more reliable standard condition. Finally, interesting results that truly demonstrate the impact of this novel photocatalytic system are shown in entries 5–7, where commonly used catalysts are incapable of forming the cyclization product. The

Au(I) dimeric catalyst remarkably stands out from these results as the only catalyst capable of reducing unactivated C–Br bonds.

Table 3.1. *Optimization of photocatalytic cyclization of bromoalkanes.*

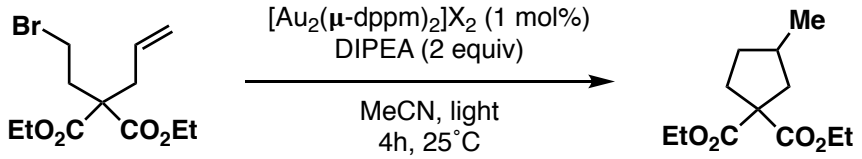

Entry	Catalyst	Light source	Yield (%)
1	$[Au_2(\mu\text{-dppm})_2]OTf_2$ (**3.15a**)	sunlight	94
2	$[Au_2(\mu\text{-dppm})_2]SbF_6$ (**3.15b**)	sunlight	90
3	$[Au_2(\mu\text{-dppm})_2]Cl_2$ (**3.15c**)	sunlight	86
4	$[Au_2(\mu\text{-dppm})_2]Cl_2$(**3.15c**)	UVA (315–400 nm)	74
5[1]	$[Ru(bpy)_3Cl_2]$ (**3.1c**)	23 W CFL/LEDs	s.m.
6[1]	$[Ir(ppy)_2(dtbbpy)]PF_6$ (**3.1e**)	23 W CFL/LEDs	s.m.
7[1]	*fac*-$[Ir(ppy)_3]$ (**3.15d**)	23 W CFL/LEDs	<5

[1]Reaction mixtures were stirred for 36 hours. bpy = 2,2'-bipyridyl, dtbbpy = di-*tert*-butyl-2,2'-bipyridine, ppy = 2-phenylpyridinate, s.m. = starting material.

In this reaction, trialkylamine DIPEA acts as an electron donor to reduce the active photocatalyst (**Scheme 3.6**). The formation of a strongly reducing $[Au^1–Au^0]^+$ complex then allows for reductive cleavage of the organobromide C–Br bond. The generated carbon-centered radical (**3.17a**) can subsequently cyclize in a 5-*exo*-*trig* fashion, leading to radical intermediate **3.17b**. The corresponding product (**3.16a**) is furnished following HAT from the solvent, DIPEA, or formic acid, added in some examples to accelerate the quenching process.

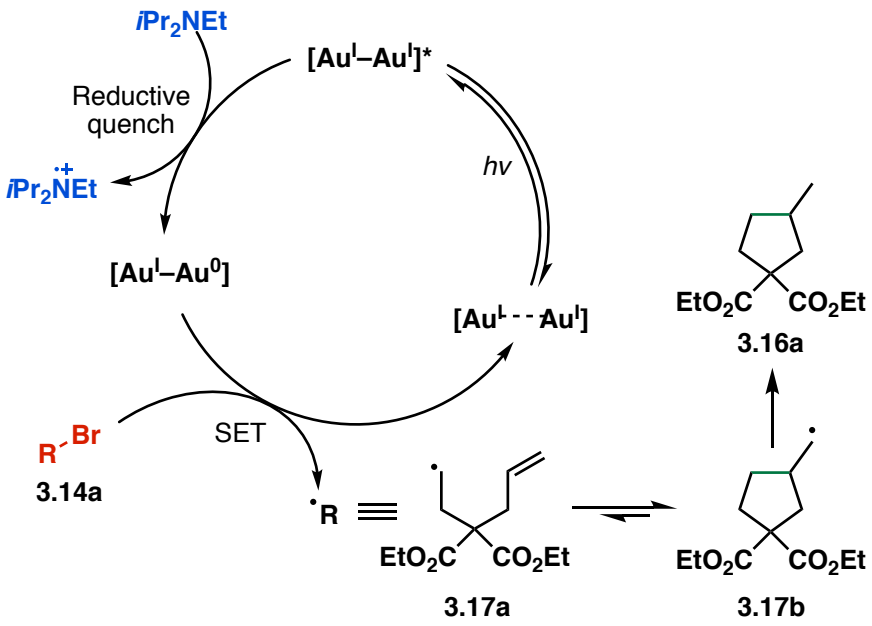

Scheme 3.6. *Proposed photocatalytic mechanism for the cyclization of unactivated bromoalkanes.*

As shown by a limited portion of the completed scope, this method allowed for the cyclization of unactivated alkyl bromide substrates (**Scheme 3.7**). Biaryl substrates were included and generated polycyclic products (**3.16e**) in excellent yields. Bromoaniline was also completely reduced under these reaction conditions with the addition of formic acid (**3.16g**).

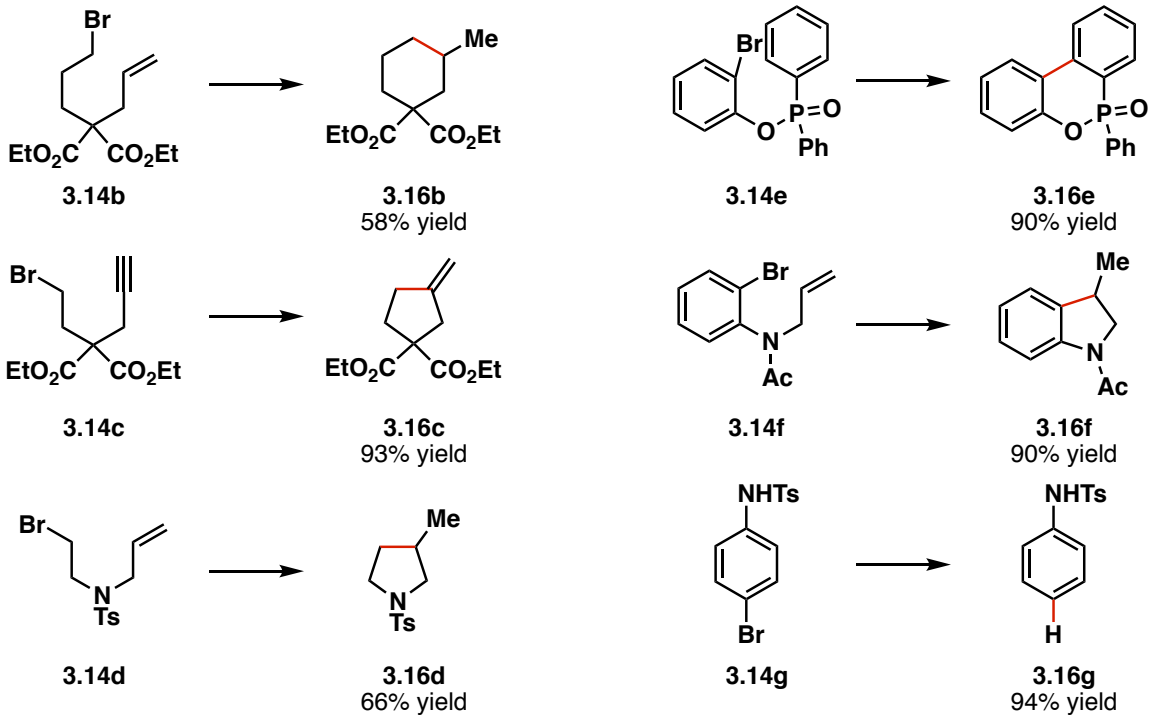

Scheme 3.7. *Scope example for the cyclization of alkyl and arylbromides.*

Later in 2015, the Barriault group reported the functionalization of indoles, photocatalyzed by $[Au_2(\mu\text{-dppm})_2]Cl_2$ via a free-radical cyclization mechanism (**Scheme 3.8**).[84] Like most photocatalytic methods, this reaction overcomes the need for toxic and highly reactive reagents by using stable catalysts and additives under mild conditions. Functionalized indoles were formed in very high yields and a variety of substituents were tolerated at the C^3 position, such as aryl groups and EWGs.

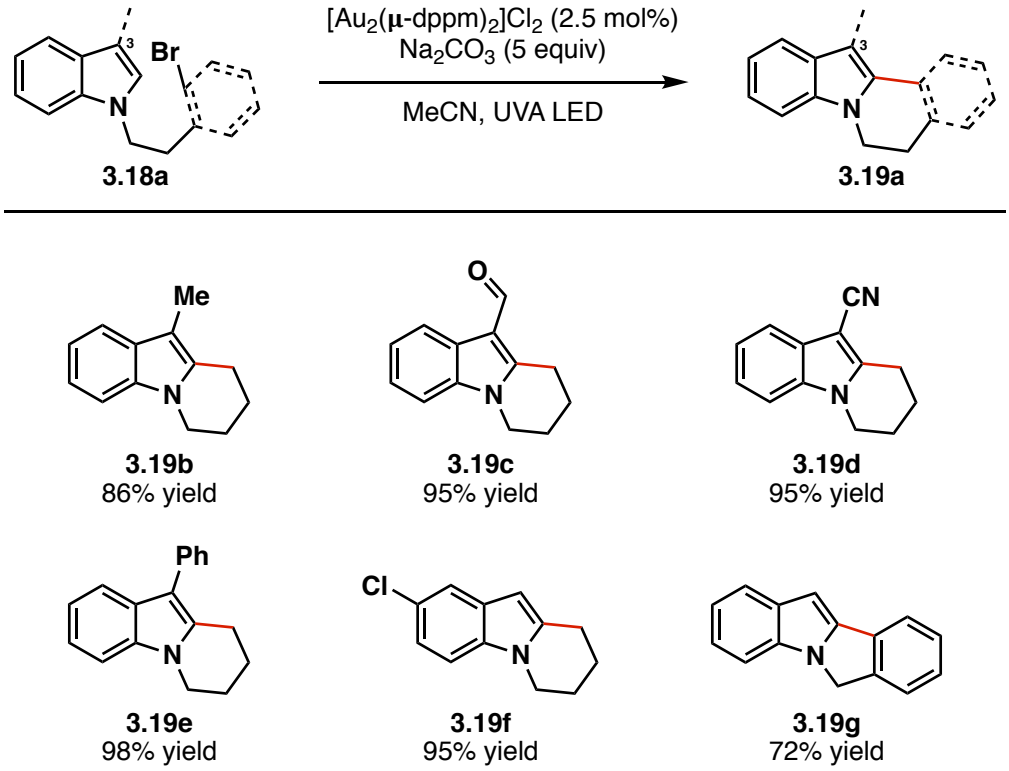

Scheme 3.8. *Functionalization of indoles via gold photoredox catalysis.*

This gold photoredox reaction differs mechanistically from the previous method because it undergoes an oxidative quenching cycle. The incorporation of trialkylamine bases led to undesired reactivity, thus the replacement by inorganic bases was crucial to achieving higher selectivity and yields for the desired product.

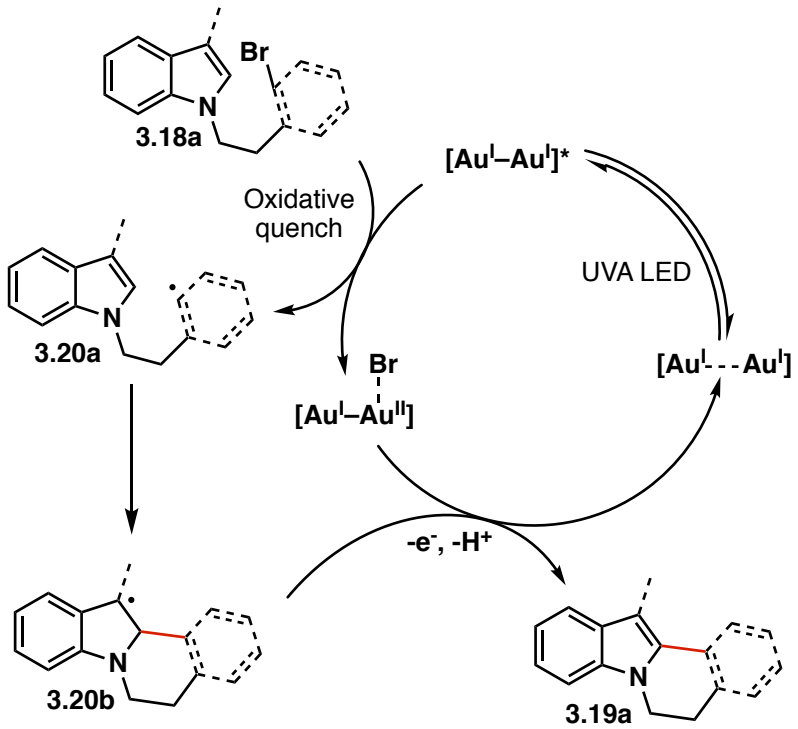

Scheme 3.9. *Proposed photocatalytic mechanism of indole functionalization via free-radical cyclization.*

As shown in **scheme 3.9**, the excited dimeric gold(I) catalyst is oxidatively quenched by the bromoalkane substrate. The formation of a rather nucleophilic radical (**3.20a**) can then lead to intramolecular cyclization onto a heteroarene acceptor, generating a carbon-centered radical intermediate (**3.20b**). The latter can subsequently lose an electron to the [Au^{I}–Au^{II}] complex to complete the catalytic cycle by regenerating the ground-state catalyst. Loss of a proton via deprotonation by an inorganic base, in this case Na_2CO_3, leads to the desired product **3.19a**.

A few years into the application of these gold(I) dimeric photocatalysts to synthetic methods, an intramolecular photoredox arylation using [Au_2(μ-dppm)$_2$]Cl_2

was exploited for the short formal synthesis of (±)-triptolide (**3.21c**) (**Scheme 3.10**).[85] In 2016, the Barriault lab reported the synthesis containing a key radical cyclization step to generate two C–C bonds and the desired polycyclic framework.

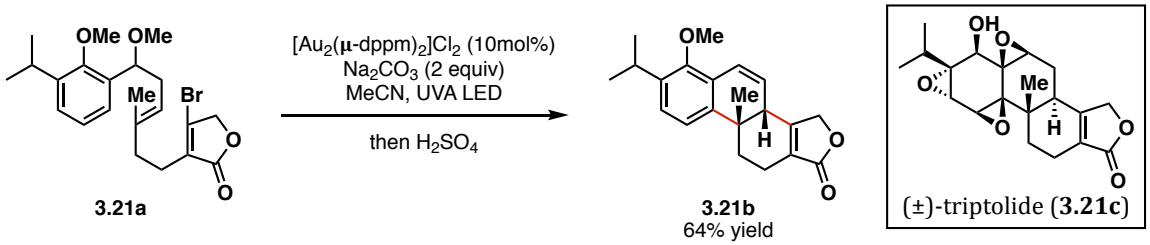

Scheme 3.10. *Photocatalyzed key radical cyclization step in the formal synthesis of (±)-triptolide.*

Studies were initially conducted targeting a reductive quenching pathway, however, due to the complexity and reactivity of the substrate, the formation of byproducts was hindering the success of the reaction. Following multiple attempts using trialkylamine bases, the use of inorganic base Na_2CO_3 was evaluated on a test-substrate and successfully led to the desired cyclization product in good yield.

Building on the studies completed in our lab, a slightly different approach was taken to complete an alkylative semipinacol rearrangement method. Following recent reports of the transformation being accessed via photoredox methods, a photocatalytic system was designed using gold as the catalyst (**Scheme 3.11**).[86] As previously visited, an alkylbromide (**3.23**) can form an inner sphere exciplex with the gold excited catalyst (**3.25a**) and trigger an oxidative quenching pathway to generate a $[Au^{I}–Au^{II}]^{3+}$ species (**3.25b**) and a carbon-centered radical (**3.23b**). What differs in this mechanism is the addition of the radical to the $[Au^{I}–Au^{II}]^{3+}$ complex. This would

result in a $[Au^{I}–Au^{III}–R]^{+}$ intermediate (**3.25c**) which can coordinate to a α-styrenyl substituted alcohol. Lewis acid activation of the substrate would trigger a semipinacol rearrangement via ligand exchange to the gold(III) center (**3.25e**). Reductive elimination would finally generate the ground state catalyst and lead to a functionalized cyclic ketone (**3.24**). The use of a sub-stoichiometric quantity of a DABCO additive was justified by the potential of it resuscitating Au intermediates that may have degraded.

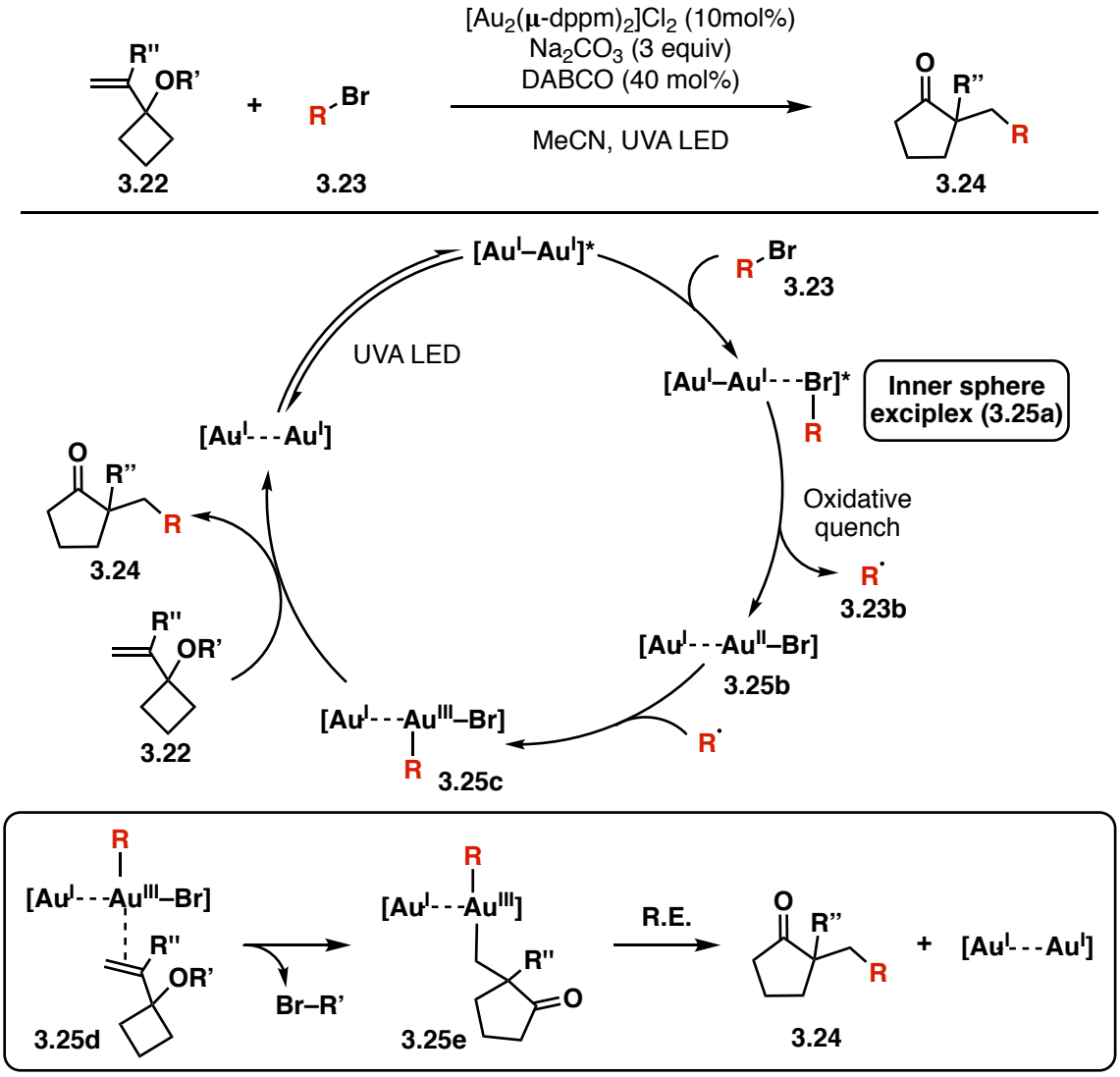

Scheme 3.11. *Proposed mechanism of photocatalytic semipinacol rearrangement via [Au^{I}–Au^{III}] intermediate.*

3.2 Initial investigations

The objective of this project was to apply the photocatalytic method demonstrated in the alkylative semipinacol rearrangement developed by our group. This project would allow continued exploration of this newly discovered process through an intramolecular cyclization between unactivated C–Br bonds and enol ethers. The general reaction scheme of the transformation is demonstrated in **scheme 3.12**. Enol ether **3.27** would be formed through a Diels-Alder reaction, controlling the installation of up to three stereocenters, and would then be submitted to photoredox conditions to form cyclization product **3.28**.

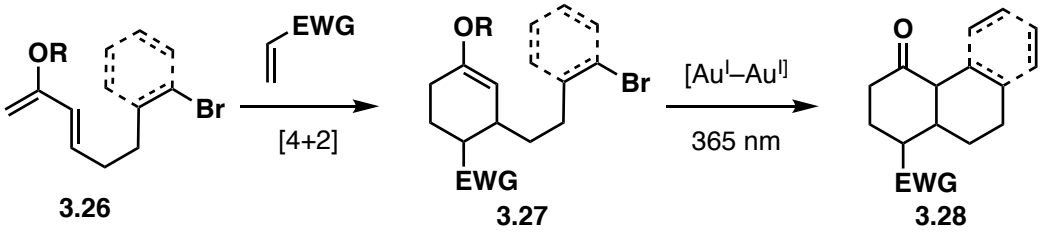

Scheme 3.12. *General reaction scheme.*

Traditionally, radical cyclizations were often completed using a radical initiator, such as AIBN. These initiators do not require light activation and are most often paired with hydrogen atom donor tributyltin hydride. However, in cases where the desired reactivity pathway is slow, premature reduction of the generated radical by the organostannane can lead to unwanted products. The interaction between alkyl radicals and tin hydride occurs with a rate constant of about 2 x 10^6 M^{-1} s^{-1} at room temperature, which is about 1000 times faster than we can expect the 6-*exo-trig* cyclization to occur, with a rate constant around 6 x 10^3 M^{-1} s^{-1}.[66]

The proposed mechanism of the gold-catalyzed photoredox cyclization involves the excitation of the gold dimeric catalyst to its excited state (**Scheme 3.13**). The formation of an inner sphere exciplex with the bromoalkane moiety of the Diels-Alder product triggers oxidative quenching of the excited catalyst, generating a Au^{I}–Au^{II}–Br complex and alkyl radical **3.29a**. Addition of the latter to the Au^{II} center forms a Lewis acidic Au^{III} complex **3.29b**, which simultaneously coordinates to the silyl enol ether moiety. Nucleophilic addition of the silyl enol ether to the Au^{III} center then leads to intermediate **3.29c,** which can subsequently undergo reductive elimination to generate ketone product **3.28.**

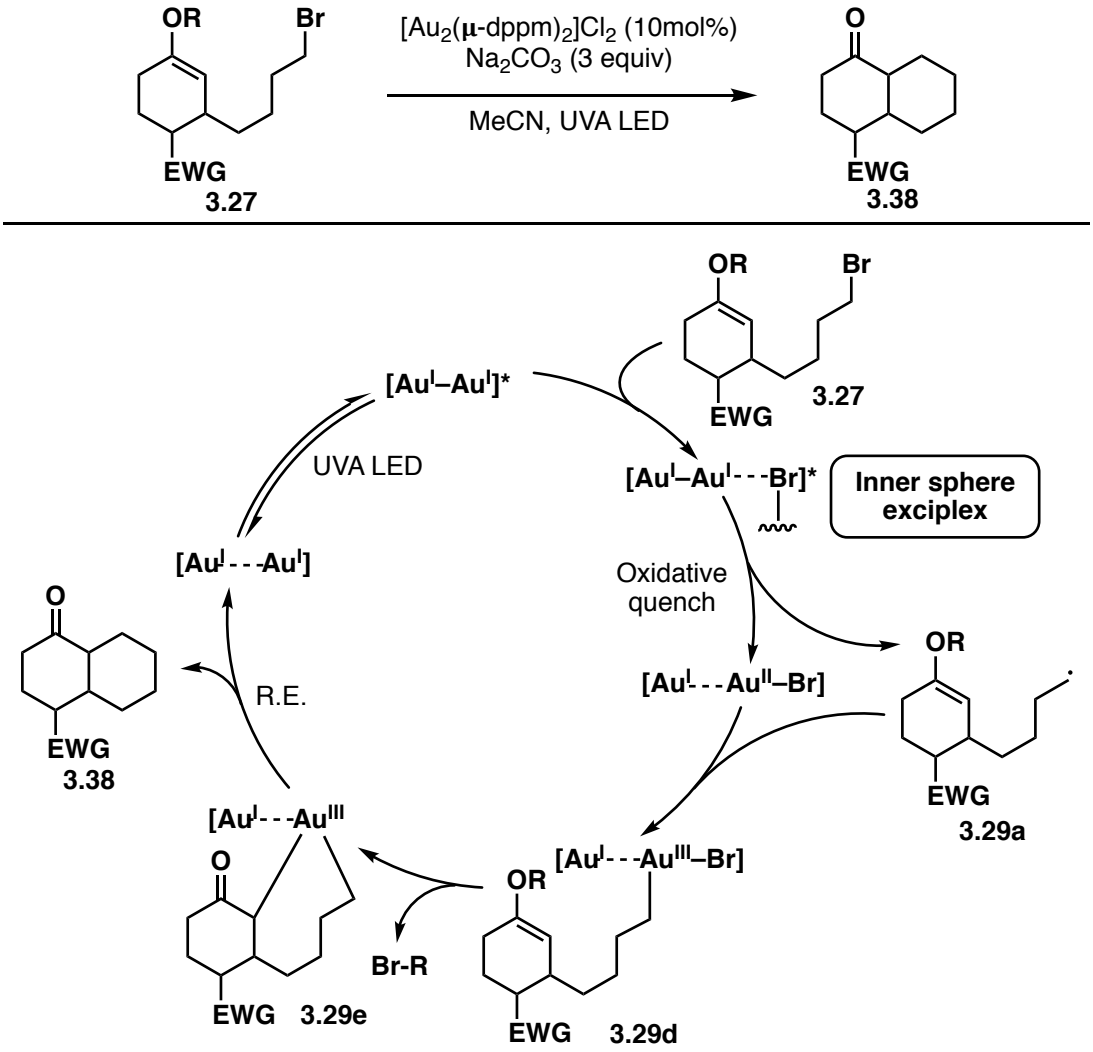

Scheme 3.13. *Proposed radical cyclization mechanism through Au^{III} intermediate.*

The starting material for this method consists of a diene tethered to a bromoalkane, to undergo the Diels-Alder reaction and participate in the radical cyclization. The formation of this scaffold followed a convergent synthesis from diethyl (2-oxopropyl)phosphonate and ethyl 5-bromovalerate (**Scheme 3.14**). The latter was first reduced to 5-bromopentanal (**3.30**) using DIBAL-H, before undergoing a Horner-Wadsworth-Emmons transformation in a second step to

generate ketone **3.31**. Finally, a triisopropyl silyl protecting group was installed to the enone to afford diene starting material **3.26**.

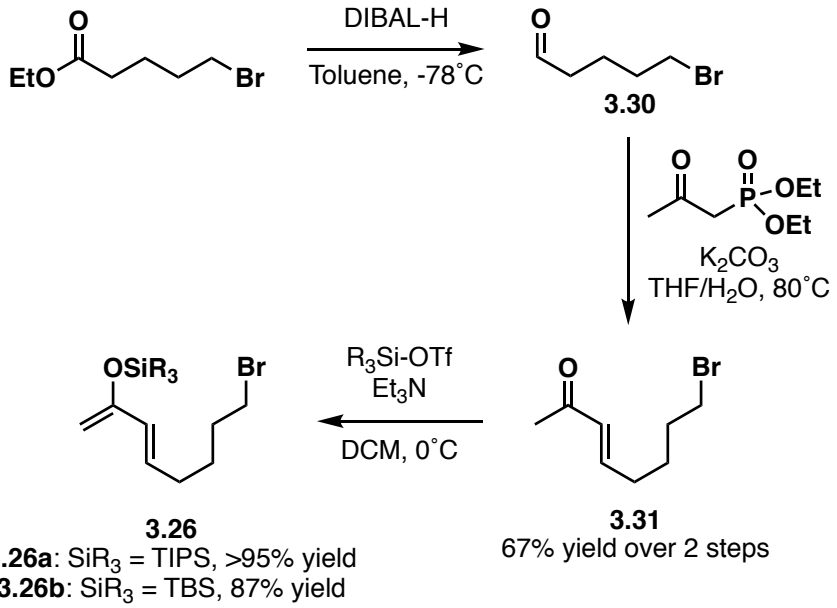

Scheme 3.14. *Substrate synthesis.*

Initial studies for the Diels-Alder reaction were conducted using the TIPS-protected diene substrate. Experiments were completed under Co^{III}-catalyzed conditions, based on the method discussed in Chapter 2. These reactions led to a major *endo* Diels-Alder product with a dr of 6:1 in 88% yield (**Table 3.2**). The Diels-Alder reaction was also attempted under thermal conditions, leading to a 5:1 dr in 91% yield.

Table 3.2. *Diels-Alder reaction.*

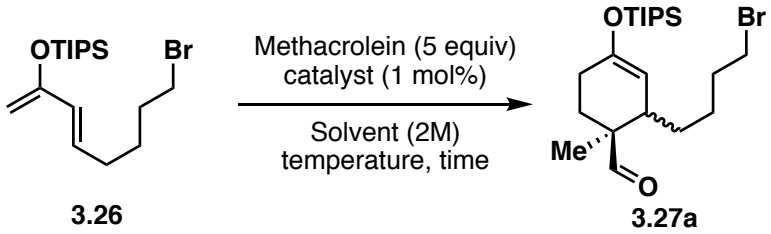

3.26 3.27a

Entry	Catalyst	Solvent	Temperature (°C)	Time (h)	Yield (%)	dr (*endo*:*exo*)
1	**2.31b**	DCM	20	18	88	6:1
2	-	DCE	60	3	91	5:1

Once the silyl enol ether formed, the radical cyclization was attempted under conditions to prompt the Au^{I}/Au^{III} redox cycle. Gold dimeric catalysts with both Cl and NTf_2 counterions were attempted in various solvents, such as toluene, acetonitrile, benzene, dimethylformamide and tetrahydrofuran (**Scheme 3.15**).

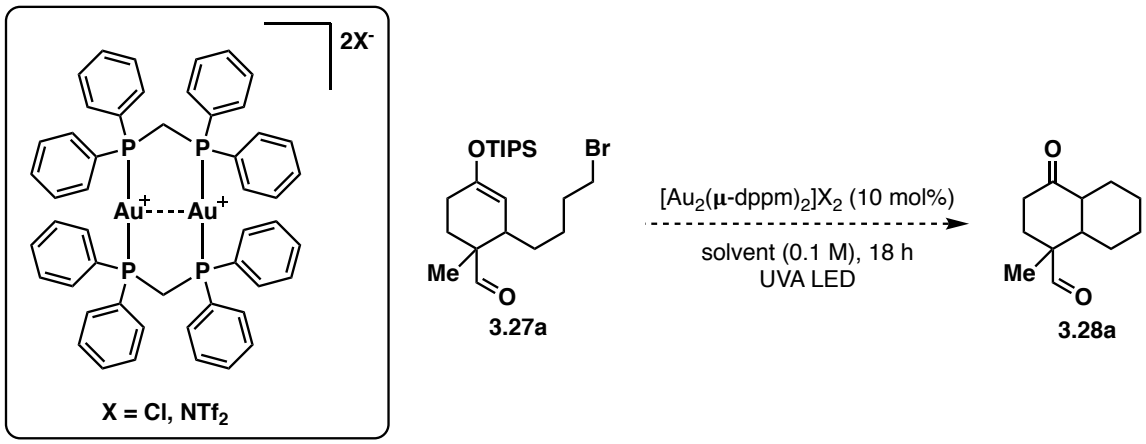

Scheme 3.15. *Initial cyclization reaction studies.*

In all cases, degradation was observed along with the formation of desilylated starting material. At this point, it was unknown whether premature desylilation of the starting material by the gold catalyst was preventing the cyclization, or whether the starting material was simply not converting to product and was being degraded over time. The addition of inorganic bases, such as Na_2CO_3 and K_2CO_3, was attempted to ensure no acidic intermediates were being formed and shutting down the reactivity, however this led to no significant change. Due to the bulkiness of the silyl protecting group, it was hypothesized that the formation of the Au^{III} intermediate was too hindered. In response, the starting material was synthesized using a smaller silyl-protecting agent, TBS. Unfortunately, these modifications did not lead to any improvements when it came to the photochemical reaction. Following a series of unsuccessful reactions, I was unable to generate the desired product through the oxidative quenching cycle.

While our initial objective to utilize a Au^{III} intermediate was unsuccessful, the addition of a trialkylamine base to our reaction conditions would allow us to form the desired product through the reductive quenching cycle. In this case, DIPEA, which quenches ten times faster with the excited catalyst than the bromoalkane, would reduce the active gold species to a [Au^{I}–Au^{0}] complex (**Scheme 3.16**). Reduction of the bromoalkane substrate by the catalyst generates alkyl radical **3.29a,** which can cyclize and form oxonium ion **3.29e** by donating an electron from intermediate **3.29d** to the DIPEA radical cation. Deprotonation and/or loss of the silyl protecting group from a bromine ion can lead to various bicycles.

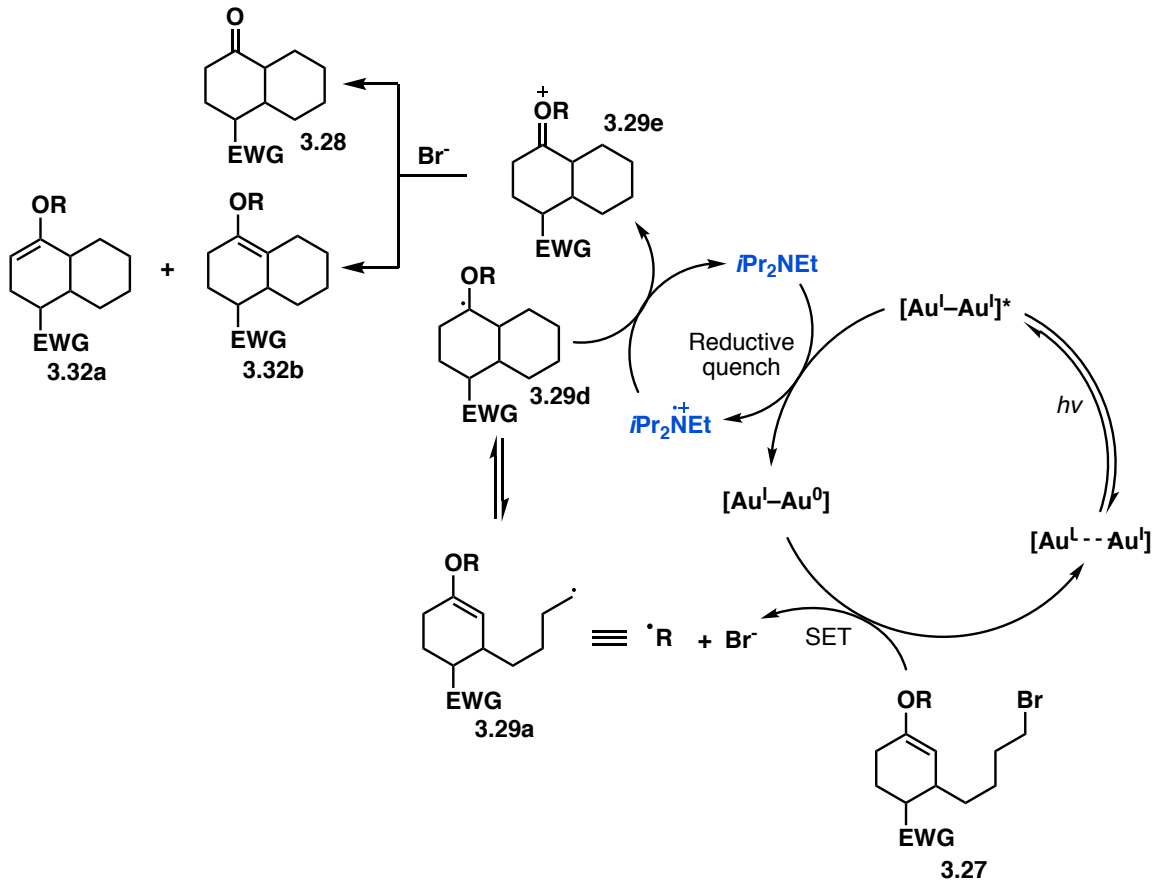

Scheme 3.16. *Proposed photocatalytic mechanism through a reductive quenching cycle.*

The transformation was attempted under reductive quenching conditions with 1.1 equivalents of DIPEA in acetonitrile for 18 hours (**Scheme 3.17**). The disappearance of the bromine and silyl enol ether alkene peaks by NMR, paired with the creation of a new alkene peak, seemed to point to successful product formation in a mixture of diastereoisomers. While the products have not been fully separated and characterized, mass spectroscopy data of the products suggests that **3.32c** was formed under the reaction conditions.

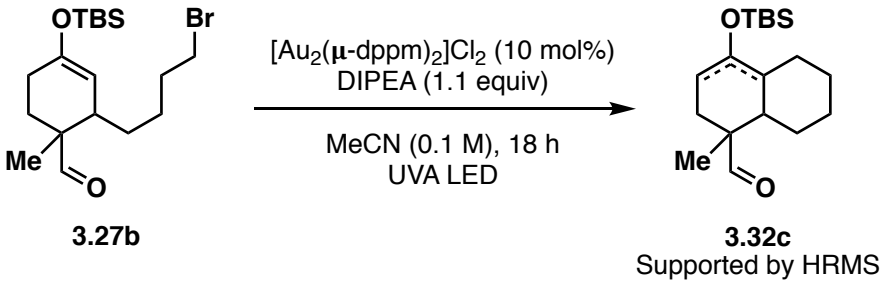

Scheme 3.17. *Cyclization reaction under a reductive quenching pathway.*

3.3 Future work

The cyclization reaction appeared to lead to multiple diastereoisomers of **3.32a** and **3.32b**, which were difficult to separate. To continue this project, hydrolysis of the silyl protecting-group following the cyclization may be necessary to converge the silyl enol ether products to ketone **3.28**, as demonstrated in **scheme 3.18**. Under acidic conditions, we could also expect isomerization of the ring junction to generate the more stable *trans*-decalin **3.33**. The presence of only two diastereoisomers would facilitate the optimization process, which would involve investigations into the solvent, molarity, catalyst counterion, trialkylamine base and reagent equivalents.

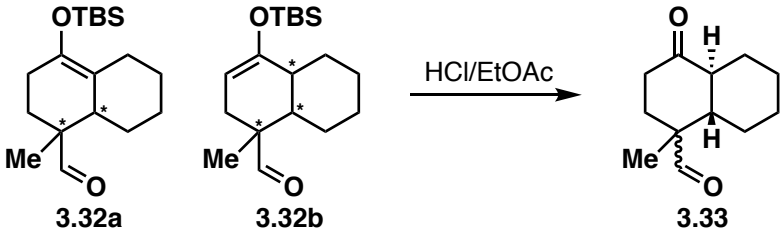

Scheme 3.18. *Hydrolysis of silyl enol ether products to ketone **3.33**.*

Once established, this method could be applied to a large scope of substrates. Some interesting examples are demonstrated in **scheme 3.19**, where the cyclization

of silyl enol ether **3.34** could lead to bridged-ketone **3.35**, and spirocycle **3.37** could be formed upon ring formation from **3.36**.

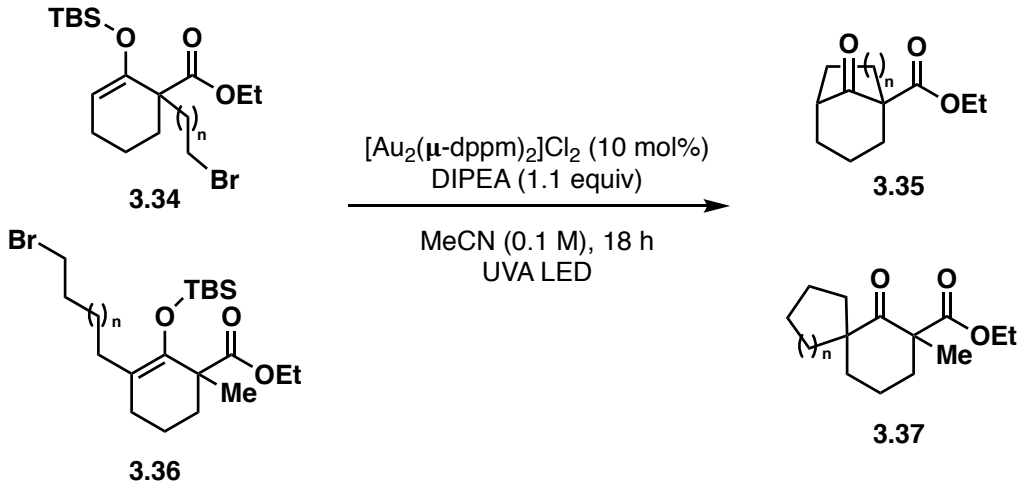

Scheme 3.19. *Formation of bridged-ketone and spirocyclic scaffolds.*

Both of these silyl enol ether substrates can be formed in few steps from commercially available ethyl 2-oxocyclohexanecarboxylate (**Scheme 3.20**). A suggested synthesis first involves the alkylation of the keto ester, generating alkyl bromide **3.37**. Subsequent protection chemistry can lead to target silyl enol ether **3.34**. Additionally, methylation of the keto ester prior to alkylation can generate alkyl bromide **3.38b**, which can be similarly transformed to silyl enol ether **3.36**.

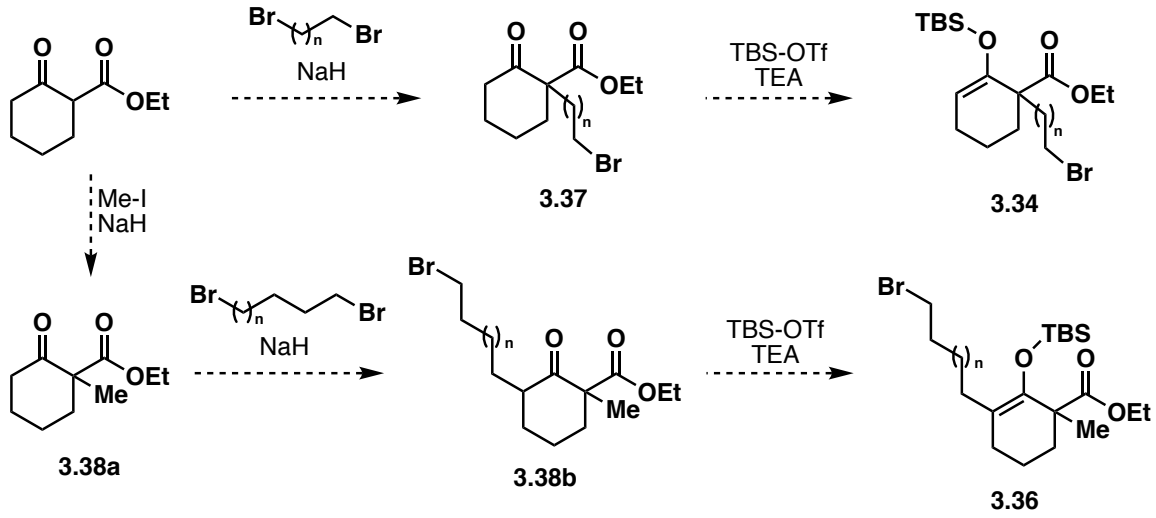

Scheme 3.20. *Suggested synthesis of silyl enol ethers **3.34** and **3.36**.*

3.4. Conclusion

While this project remains in the development phase, it shows good potential for becoming an efficient method to generate C–C bonds between enol ethers and unactivated alkyl bromides. The initially proposed mechanism to obtain cyclized products through a Au^{III} intermediate was not successful, however further investigations suggest that a reductive quenching pathway is a promising alternative.

3.5 References

[65] George, C.; Brüggemann, M.; Hayeck, N.; Tinel, L.; Donaldson, J. Interfacial Photochemistry. *Phys. Chem. Gas-Liquid Interfaces* **2018**, 435–457.

[66] Turro, N.; Ramamurthy, V.; Scaiano, J. C. *Modern Molecular Photochemistry of Organic Molecules*; University Science Books: Sausalito, Calif., 2010.

[67] Pitre, S. P.; McTiernan, C. D.; Scaiano, J. C. Understanding the Kinetics and Spectroscopy of Photoredox Catalysis and Transition-Metal-Free Alternatives. *Acc. Chem. Res.* **2016**, *49* (6), 1320−1330.

[68] Prier, C. K.; Rankic, D. A.; MacMillan, D. W. C. Visible Light Photoredox Catalysis with Transition Metal Complexes: Applications in Organic Synthesis. *Chem. Rev.* **2013**, *113* (7), 5322−5363.

[69] Romero, N. A.; Nicewicz, D. A. Organic Photoredox Catalysis. *Chem. Rev.* **2016**, *116* (17), 10075−10166.

[70] Narayanam, J. M. R.; Tucker, J. W.; Stephenson, C. R. J. Electron-Transfer Photoredox Catalysis: Development of a Tin-Free Reductive Dehalogenation Reaction. *J. Am. Chem. Soc*. **2009**, *131* (25), 8756–8757.

[71] Gong, H.; Andrews, R. S.; Zuccarello, J. L.; Lee, S. J.; Gagné, M. R. Sn-Free Ni-Catalyzed Reductive Coupling of Glycosyl Bromides with Activated Alkenes. *Org. Lett.* **2009**, *11* (4), 879–882.

[72] Xiao, T.; Dong, X.; Tang, Y.; Zhou, L. Phenanthrene Synthesis by Eosin Y-Catalyzed, Visible Light-Induced [4+2] Benzannulation of Biaryldiazonium Salts with Alkynes. *Adv. Synth. Catal.,* **2012**, *354* (17), 3195–3199.

[73] Skubi, K. L.; Blum, T. R.; Yoon, T. P. Dual Catalysis Strategies in Photochemical Synthesis. *Chem. Rev.,* **2016**, *116* (17), 10035−10074.

[74] a) Nicewicz, D. A.; MacMillan, D. W. C. Merging Photoredox Catalysis with Organocatalysis: The Direct Asymmetric Alkylation of Aldehydes. Science, **2008**, *322* (5898), 77−80; b) Nagib, D. A.; Scott, M. E.; MacMillan, D. W. C. Enantioselective α-Trifluoromethylation of Aldehydes via Photoredox Organocatalysis*. J. Am. Chem. Soc*. **2009**, *131* (31), 10875−10877; c) Welin, E. R.; Warkentin, A. A.; Conrad, J. C.; MacMillan, D. W. C. Enantioselective α-

Alkylation of Aldehydes by Photoredox Organocatalysis: Rapid Access to Pharmacophore Fragments from β-Cyanoaldehydes. *Angew. Chem., Int. Ed*. **2015**, *54* (33), 9668–9672; d) Shih, H.-W.; Vander Wal, M. N.; Grange, R. L.; MacMillan, D. W. C. Enantioselective α-Benzylation of Aldehydes via Photoredox Organocatalysis. *J. Am. Chem. Soc*. **2010**, *132* (39), 13600–13603; e) Cecere, G.; Kö nig, C. M.; Alleva, J. L.; MacMillan, D. W. C. Enantioselective Direct α-Amination of Aldehydes via a Photoredox Mechanism: A Strategy for Asymmetric Amine Fragment Coupling. *J. Am. Chem. Soc*. **2013**, *135* (31), 11521–11524.

[75] Li, D.; Che, C.-M.; Kwong, H.-L.; Wing-Wah Yam,V. Photoinduced C–C bond formation from alkyl halides catalysed by luminescent dinuclear gold(I) and copper(I) complexes. *J. Chem. Soc. Dalton Trans.* **1992**, (23), 3325–3329.

[76] Bock, C. R.; Connor, J. A.; Gutierrez, A. R.; Meyer, T. J.; Whitten, D. G.; Sullivan, B. P.; Nagle, J. K. Estimation of excited-state redox potentials by electron-transfer quenching. Application of electron-transfer theory to excited-state redox process. *J. Am. Chem. Soc.* **1979**, *101* (17), 4815–4824.

[77] Flamigni, L.; Barbieri, A.; Sabatini, C.; Ventura, B.; Barigelletti, F. Photochemistry and Photophysics of Coordination Compounds: Iridium. *Top. Curr. Chem*. **2007**, 281, 143–203.

[78] Barriault, L.; Scaiano, J. C.; McTiernan, C. D.; Morin, M.; McCallum, T. Polynuclear Gold(I)(Complexes in Photoredox Catalysis: Understanding their Reactivity through Characterization and Kinetic Analysis. *Cat. Sci. Technol*., **2016**, *6* (1), 201–207.

[79] Fry, A. J.; Krieger, R. L. Electrolyte effects upon the polargraphic reduction of alkyl halides in dimethyl sulfoxide. *J. Org. Chem.,* **1976**, *41* (1), 54–57.

[80] Rondinini, S.; Mussini, P. R.; Muttini, P.; Sello, G. Silver as a Powerful Electrocatalyst for Organic Halide Reduction: The Critical Role of Molecular Structure. *Electrochim. Acta.* **2001**, *46* (20–21), 3245–3258.

[81] McCallum, T.; Rohe, S.; Barriault, L. Thieme Chemistry Journals Awardees – Where Are They Now? What's Golden: Recent Advances in Organic Transformations Using Photoredox Gold Catalysis. *Synlett*. **2017**, *28* (3), 289–305.

[82] Zidan, M.; Rohe, S.; McCallum, T.; Barriault, L. Recent Advances in Mono and Binuclear Gold photoredox Catalysis. *Cat. Sci. Technol.,* **2018**, *8* (23), 6019–6028.

[83] Revol, G.; McCallum, T.; Morin, M.; Gagozs, F.; Barriault, L. Photoredox Transformations via Gold Dimeric Complexes. *Angew. Chem., Int. Ed.* **2013**, *52* (50), 13342–13345.

[84] Kaldas, S. J.; Cannillo, A.; McCallum, T.; Barriault, L. Indole Functionalization via Photoredox Gold Catalysis. *Org Lett.* **2015**, *17* (11), 2864–2866.

[85] Cannillo, A.; Schwantje, T. R.; Bégin, M.; Barabé, F.; Barriault, L. Gold-Catalyzed Photoredox C(sp2) Cyclization: Formal Synthesis of (±)-Triptolide. *Org Lett.* **2016**, *18* (11), 2592–2595.

[86] Zidan, M.; McCallum, T.; Thai-Savard, L.; Barriault, L. Photoredox Meets Gold Lewis Acid Catalysts in the Alkylative Semipinacol Rearrangement: A Photocatalyst with a Dark Side. *Org. Chem. Front.* **2017**, *4* (11), 2092–2096.

Chapter 4. Conclusion

The work presented in this dissertation concentrates on applications of gold catalysis by controlling divergent reactivity pathways, as well as developing new synthetic methods. The first project presented in chapter 2, conducted in collaboration with Huy Tran, put forward our efforts towards the development of one-pot syntheses for the formation of complex polycyclic scaffolds. The divergent nature of gold(I)-catalyzed cyclizations allows access to a range of products, but the challenge to select for a specific pathway remains. Through catalyst modifications, we have successfully developed three one-pot sequences to generate carbocycles **2.14, 2.15** and **2.21** from a diene substrate (**2.12**) prepared in 4 linear steps.

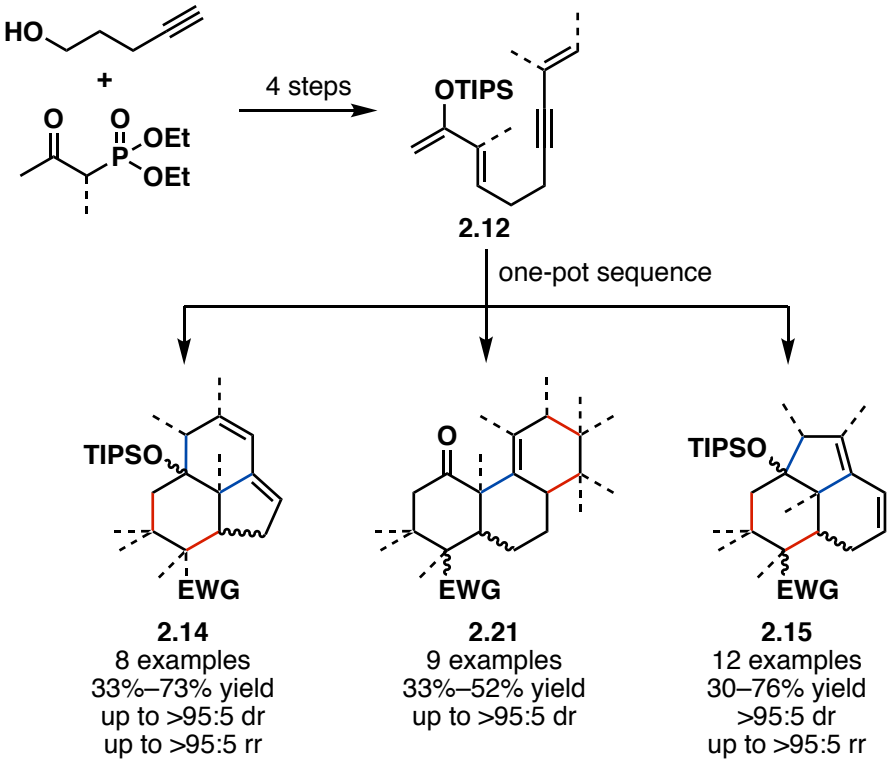

Scheme 4.1. *Divergent one-pot syntheses for the formation of complex polycyclic scaffolds.*

The initial forays into the use of dimeric gold photocatalysis for the intramolecular cyclization of **3.27b** were disseminated in chapter 3. The first objective was to obtain the desired product through an oxidative quenching pathway involving a Au^{III} intermediate, however this approach did not produce the desired product. Further investigations involving a reductive quenching cycle suggest that to obtain **3.32c** additional studies under these new conditions will be required.

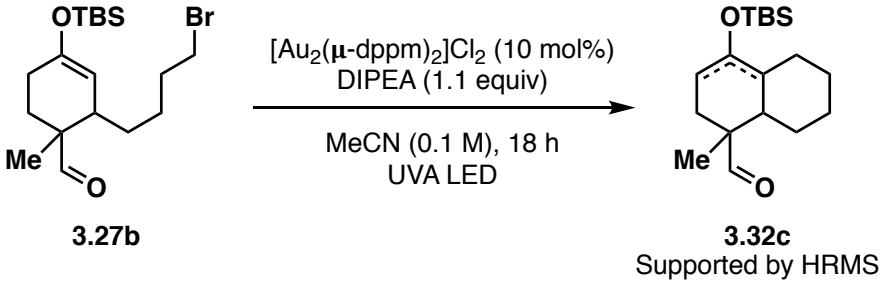

3.27b **3.32c**
Supported by HRMS

Scheme 4.2. *Photocatalytic cyclization of **3.27b** under a reductive quenching cycle.*

Chapter 5. Additional information

5.1 General information

All reactions were performed under argon atmosphere in flame-dried glassware equipped with a magnetic stir bar and capped with a rubber septum, unless otherwise indicated. All commercial reagents were used without further purification, unless otherwise noted. Reactions were monitored by thin layer chromatography (TLC) analysis of reaction aliquots. TLC plates were viewed under UV light and stained with permanganate, vanillin or *p*-anisaldehyde staining solutions. Proton nuclear magnetic resonance (^{1}H NMR) spectra were recorded on a Bruker AMX 400 MHz at room temperature. NMR samples were dissolved in chloroform-*d*, unless specified otherwise, and chemicals shifts are reported in ppm from ppm relative to the residual non-deuterated solvent. Carbon nuclear magnetic resonance (^{13}C NMR) spectra were also recorded on the Bruker AMX 400 MHz at 101 MHz and room temperature. HRMS were obtained on a Kratos Analytical Concept instrument (University of Ottawa Mass Spectrum Centre).

5.2 Experimental procedure chapter 2

General procedure 1: Diene starting material

General Procedure 1a:

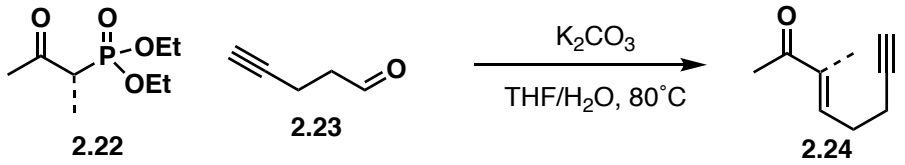

Scheme 5.1. *Synthesis of terminal alkyne substrate.*

Adopted from literature procedure.[87]

To a solution of phosphonate **2.22** in THF (115 ml) was added a solution of potassium carbonate (22.0 g, 160 mmol) in water (57 ml), and crude aldehyde **2.23**. The mixture was heated at 80°C overnight with vigorous stirring. The product was extracted with ethyl acetate (3x50 ml), and the combined organic layers were dried over sodium sulfate and evaporated. The residue was diluted with DMF (250 ml) and added to an extraction funnel. Then, aq. sat. sodium bisulfite (250 ml) was added and shaken for 30 s. The mixture was then extracted with hexanes (250 ml x 3). The combined organic layers were dried (Na_2SO_4), filtered, and concentrated i*n vacuo* to give a crude product which was separated via flash chromatography (5–10% EtOAc in hexanes) to give ketone **2.24**.

General Procedure 1b:

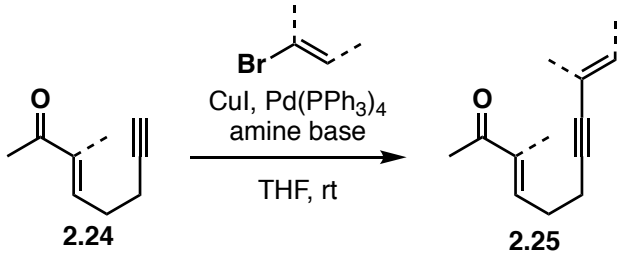

Scheme 5.2. *Synthesis of ketone substrate.*

A flame-dried reaction flask was equipped with a magnetic stir bar and charged with **2.24** (18.2 mmol) in THF (125 ml), followed by Copper(I) Iodide (1.8 mmol) and an amine base (91 mmol). Then, vinyl bromide in THF (1.0 M, 54.6 ml) and palladium tetrakis (0.9 mmol) were added to the solution and stirred overnight. The reaction mixture was filtered through a sintered glass funnel and the mother liquor was collected and evaporated. The residue was then diluted with EtOAc and washed with sat. NH_4Cl. The combined organic layers were dried with Na_2SO_4 and concentrated in vacuo. The crude was filtered through celite (x 3) and a silica plug (x 3) before purification by flash column chromatography, eluted with EtOAc in hexanes to yield **2.25**.

General Procedure 1c:

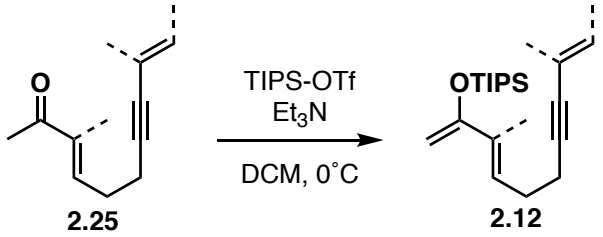

Scheme 5.3. *Synthesis of linear diene substrate.*

To a flame-dried RBF under argon was added **2.25** (2.55 mmol), DCM (12.75 ml) and triethylamine (5.09 mmol). Then, TIPS(OTf) (2.55 mmol) was added at 0˚C. The mixture was stirred at 0˚C for 1 h, then quenched with sat. $NaHCO_3$. The layers were separated and the organic phase collected. The aqueous phase was back-extracted with DCM. Combined organic layers were dried with $MgSO_4$, filtered, and concentrated in vacuo. The crude product was added to a basicified silica gel column and eluted with 1% TEA in hexanes, yielding **2.12**.

General Procedure 2: Salen ligand synthesis

General Procedure 2a:

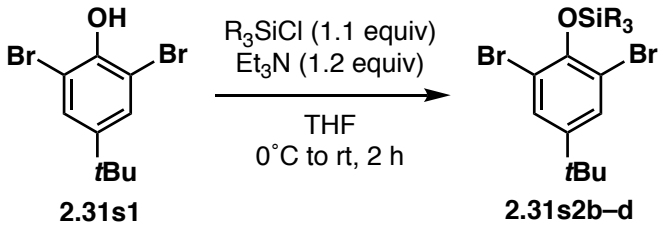

Scheme 5.4. *Synthesis of 2,6-dibromophenol silyl ethers.*

Synthesized according to literature procedure.[88]

A solution of 2,6-dibromo-4-*tert*-butylphenol in THF (1.0 M) was cooled in an ice-bath and treated with triethylamine (1.2 equiv) followed by the dropwise addition of chlorotrimethylsilane (1.1 equiv). The ice-bath was removed and the mixture was allowed to warm up to room temperature over 2 h. The solvent was removed in vacuo and the residue diluted with hexanes. The mixture was then filtered over Celite® and the filtrate was concentrated to afford the silylether products as clear, colorless oils.

General Procedure 2b:

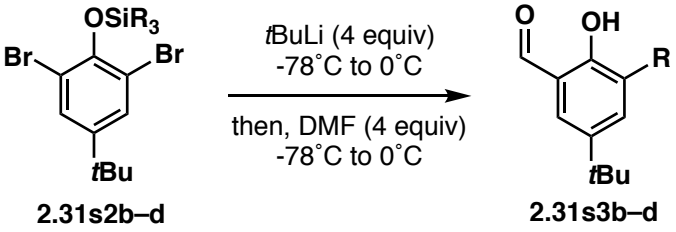

Scheme 5.5. *Synthesis of 3-silylsubstituted salicylaldehydes.*

Synthesized according to literature procedure.[88]

A solution of 2,6-dibromophenol silyl ether **2.31s2** (1.50 mmol) in Et_2O (3.0 ml) was cooled to –78 °C and treated dropwise with *t*BuLi (1.7 M in pentane, 3.53 ml, 6.00 mmol). The reaction mixture was stirred for 1.5 h while warming to 0°C, and another 0.5 h at 0 °C. The mixture was then re-cooled to –78 °C prior to the addition of DMF

(0.465 ml, 6.00 mmol), all at once. The reaction mixture was subsequently stirred for 1 h while warming to 0 °C and then quenched with saturated aq. NH_4Cl (5.0 ml) and diluted with Et_2O (75 ml). The layers were separated, and the organic layer was washed with H_2O (2 x 15 ml) and brine (25 ml), dried ($MgSO_4$), and concentrated in vacuo to afford the crude salicylaldehyde. Flash chromatography (silica gel, EtOAc/hexanes) afforded the pure salicyladehyde **2.31s3**.

General Procedure 2c:

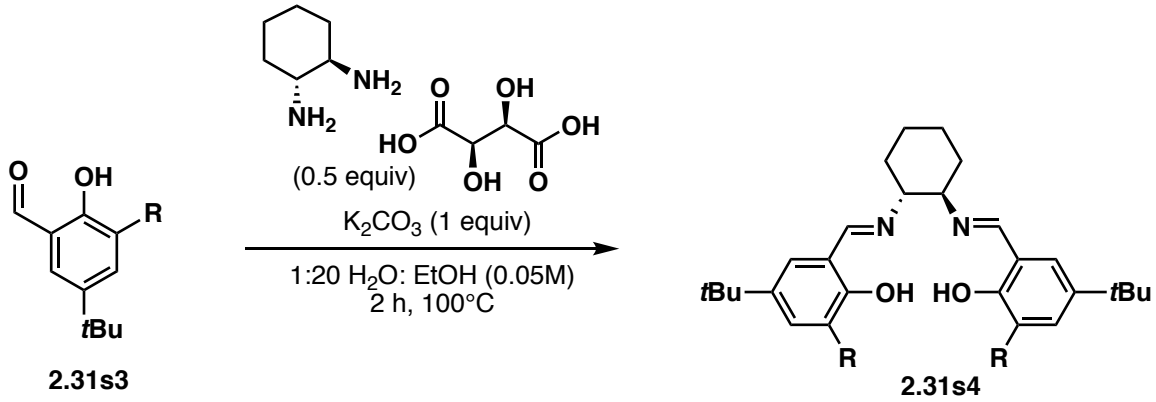

Scheme 5.6. *Salen ligand synthesis from hydroxybenzaldehyde substrate.*

Synthesized according to literature procedure.[88]

A mixture of (1*R*,2*R*)-(+)-1,2-diaminocyclohexane L-tartrate (0.171 mmol) and K_2CO_3 (0.342 mmol) was dissolved in water (0.170 ml). This solution was added to **2.31s3** (1.026 mmol) dissolved in EtOH (3.39 ml). The resulting yellow suspension was heated to 100˚C for 2 h, after which 0.7 ml water was added while hot. The reaction mixture was cooled to room temperature and the yellow precipitate was collected by filtration, yielding **2.31s4**.

General procedure 3: Gold(I) catalysts

General procedure 3a:

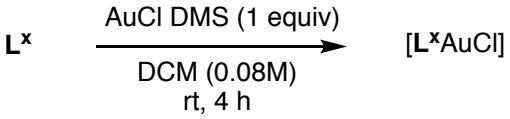

Scheme 5.7. *Preparation of LAuCl complexes with phosphine ligands.*

To a suspension of L_x (0.2 mmol) in DCM (2.58 ml) was added AuCl DMS complex (0.2 mmol). The mixture was stirred at room temperature for 4 h, then filtered through cotton and the solvent was removed in vacuo to yield a crude solid. The crude was added to a silica gel plug and eluted with EtOAc in hexanes to yield [**L**^{x}AuCl].

General Procedure 3b:

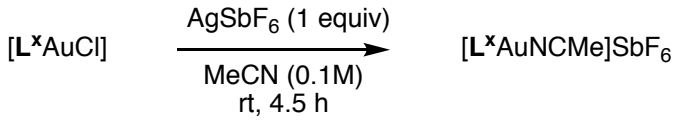

Scheme 5.8. *Preparation of L**x**AuNCMeSbF$_6$ complexes with phosphine ligands.*

To a flame-dried reaction vial under argon was added [**L**^{x}AuCl] (0.146 mmol), MeCN (1.46 ml) and $AgSbF_6$ (0.146 mmol). The mixture was stirred at room temperature for 4.5 h, then filtered through celite. The solution was concentrated in vacuo and eluted on a silica plug to yield [**L**^{x}AuNCMe]SbF_6.

General Procedure 4: Oxazolidinone dienophiles

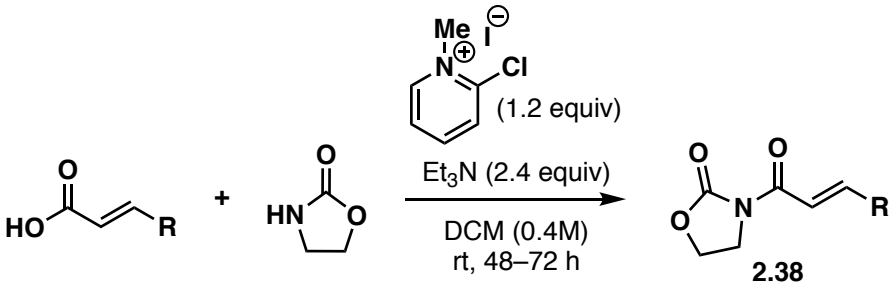

Scheme 5.9. *Oxazolidinone dienophile synthesis.*

Synthesized via modified literature procedure.[89]

To a round-bottomed flask was added acrylic acid (1 eq.), DCM (0.4M), 2-chloro-1-methylpyridin-1-ium iodide (1.2 eq.), oxazolidin-2-one (1.1 eq.), then, triethylamine (2.4 eq.). The mixture was stirred at room temperature for 48–72 hours. The solvent was evaporated, then diluted with EtOAc, and the resulting precipitates were filtered and washed with EtOAc. The mother liquor was evaporated, giving a crude product, which was purified by flash chromatography, yielding oxazolidinone dienophile **2.38**.

General procedure 5: Diels-Alder/6-*endo-dig* cyclization/Diels-Alder

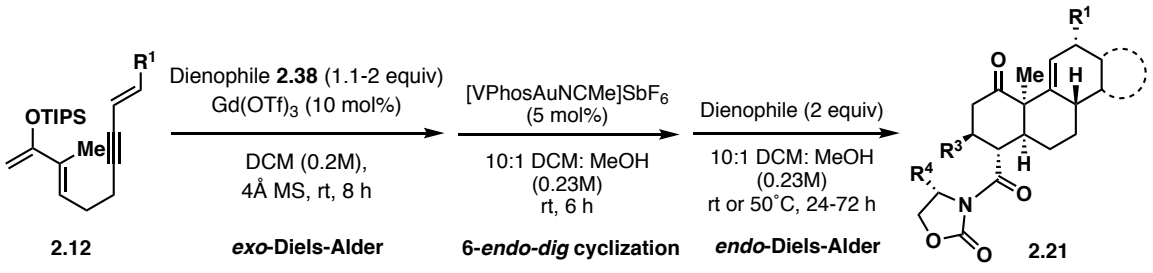

Scheme 5.10. *One-pot reaction cascade for the synthesis of steroid scaffolds.*

To a capped 4 mL oven dried reaction vial was added oxazolidinone dienophile **2.38** (0.300 mmol, 2 eq.), gadolinium(III) trifluoromethanesulfonate (9.1 mg, 0.015 mmol, 10 mol%), DCM (0.750 ml, 0.200M) and 4Å MS (38 mg, 250 mg/mmol). The mixture

was stirred for 3h at room temperature. Then, diene **2.12** (0.150 mmol) was added. The mixture was stirred at room temperature for 18 h.

Then, to the mixture was added MeOH (0.075 ml) and [VPhosAuNCMe]SbF_6 (7.2 mg, 7.50 µmol, 5 mol%). The mixture was stirred at room temperature for 6 h.

Then, a dienophile (0.300 mmol, 2 eq.) was added. The mixture was stirred at room temperature or 50 °C for 18–48 h. The mixture was dry packed in silica, evaporated, and separated by flash chromatography, yielding **2.21.**

General procedure 6: Diels-Alder/6-*endo-dig* cyclization/Prins-type cyclization

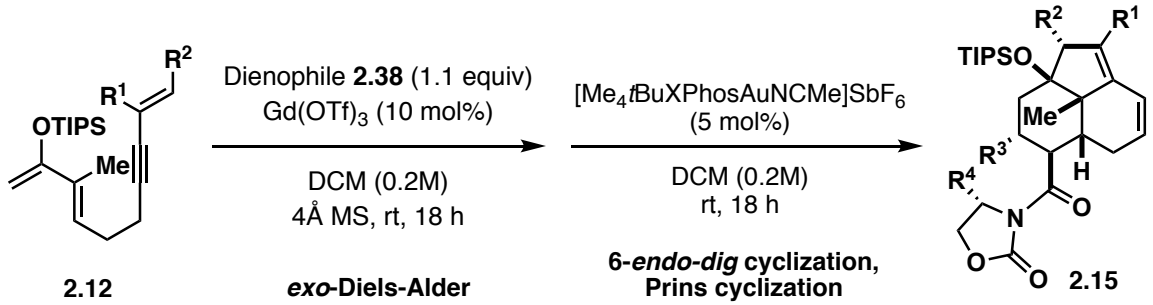

Scheme 5.11. *One-pot Diels-Alder/6-endo-dig cyclization/Prins cyclization sequence.*

To a capped 4 mL oven dried reaction vial was added oxazolidinone dienophile **2.38** (0.165 mmol, 1.1 eq.), gadolinium(III) trifluoromethanesulfonate (9.1 mg, 0.015 mmol, 10 mol%), DCM (0.750 ml, 0.200M) and 4Å MS (38 mg, 250mg/mmol). The mixture was stirred for 3h at room temperature. Then, diene **2.12** (0.150 mmol) was added. The mixture was stirred at room temperature for 18 h.

Then, to the mixture added [Me_4*t*BuXPhosAuNCMe]SbF_6 (7.2 mg, 7.50 µmol, 5 mol%). The mixture was stirred at room temperature for 24–48 h. The mixture was dry packed in silica, evaporated, and separated by flash chromatography, yielding a mixture of regioisomers with **2.15** as the major product**.**

General procedure 7: Diels-Alder/5-*exo-dig* cyclization/Prins-type cyclization

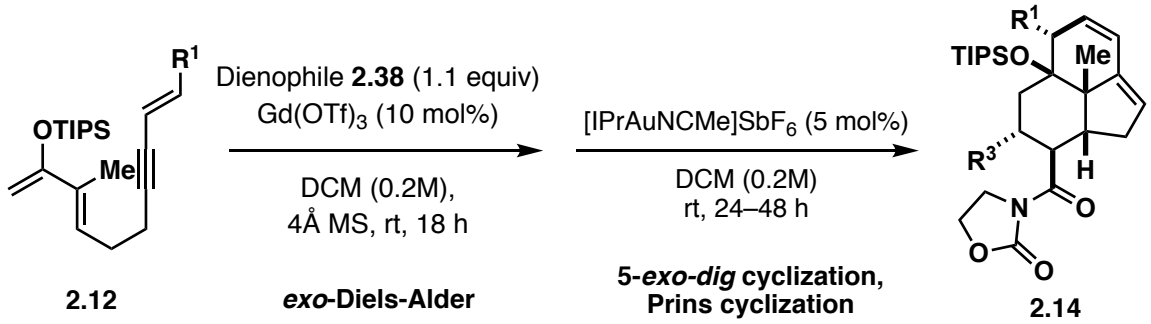

Scheme 5.12. *One-pot Diels-Alder/5-exo-dig cyclization/Prins cyclization sequence.*

To a capped 4 mL oven dried reaction vial was added oxazolidinone dienophile **2.38** (0.165 mmol, 1.1 eq.), gadolinium(III) trifluoromethanesulfonate (9.1 mg, 0.015 mmol, 10 mol%), DCM (0.750 ml, 0.200M) and 4Å MS (38 mg, 250mg/mmol). The mixture was stirred for 3 h at room temperature. Then, diene **2.12** (0.150 mmol) was added. The mixture was stirred at room temperature for 18 h.

Then, to the mixture added [IPrAuNCMe]SbF_6 (7.2 mg, 7.50 μmol, 5 mol%). The mixture was stirred at room temperature for 24–48 h. The mixture was dry packed in silica, evaporated, and separated by flash chromatography, yielding a mixture of regioisomers with **2.14** as the major product**.**

5.3. Characterization data chapter 2

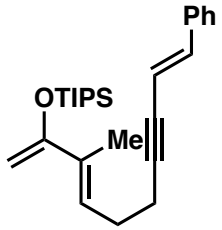

Diene 2.12a

Synthesized according to **general procedure 1c** using ketone **2.25a** in >95% yield (1.173 g).

^{1}H NMR (400 MHz, $CDCl_3$) δ 7.39–7.26 (m, 5H), 6.85 (d, *J* = 16.2 Hz, 1H), 6.23–6.17 (m, 1H), 6.13 (dt, *J* = 16.2, 2.1 Hz, 1H), 4.41 (d, *J* = 1.4 Hz, 1H), 4.30–4.26 (m, 1H), 2.50–2.37 (m, 4H), 1.79 (d, *J* = 1.2 Hz, 3H), 1.31–1.19 (m, 3H), 1.11 (d, *J* = 7.2 Hz, 18H); **^{13}C NMR** (101 MHz, $CDCl_3$) δ 157.6, 140.2, 136.8, 132.2, 128.8, 128.4, 126.5, 126.2, 109.0, 92.5, 90.6, 80.2, 27.9, 20.0, 18.3, 13.6, 13.0; **IR** (neat, cm^{-1}): 2945.6, 2865.6, 2364.2, 2342.2, 1712.1, 1667.8; **HRMS** (EI): m/z calc'd for $C_{26}H_{38}OSi$ [M^+] = 394.2692, found mass = 394.2698.

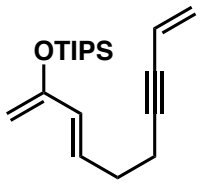

Diene 2.12b

Synthesized according to **general procedure 1c** from ketone **2.25b** in 85% yield (2.875 g).

^{1}H NMR (400 MHz, $CDCl_3$) δ 6.14 (dt, *J* = 15.2, 6.7 Hz, 1H), 5.93 (dq, *J* = 15.2, 1.1 Hz, 1H), 5.76 (ddt, *J* = 17.5, 11.0, 2.1 Hz, 1H), 5.53 (dd, *J* = 17.6, 2.3 Hz, 1H), 5.36 (dd, *J* = 11.0, 2.3 Hz, 1H), 4.23 (d, *J* = 21.0 Hz, 2H), 2.45–2.24 (m, 4H), 1.32–1.18 (m, 3H), 1.11 (d, *J* = 7.4 Hz, 18H); **^{13}C NMR** (101 MHz, $CDCl_3$) δ 155.2, 129.5, 129.2, 125.6, 117.7,

93.8, 90.2, 80.0, 31.4, 19.7, 18.2, 12.9; **IR** (neat, cm^{-1}): 2948, 2869, 1579, 1297; **HRMS** (EI): m/z calc'd for $C_{19}H_{32}OSi$ [M^+] = 304.2222, found mass = 304.2243.

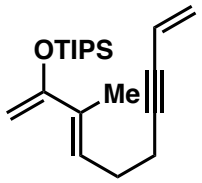

Diene 2.12c

Synthesized according to **general procedure 1c** from ketone **2.25c** in 90% yield (0.226 g).

^{1}H NMR (400 MHz, $CDCl_3$) δ 6.16 (tt, *J* = 5.7, 3.1 Hz, 1H), 5.81–5.68 (m, 1H), 5.53 (dd, *J* = 17.5, 2.3 Hz, 1H), 5.37 (dd, *J* = 11.0, 2.3 Hz, 1H), 4.39 (d, *J* = 1.3 Hz, 1H), 4.27 (t, *J* = 1.0 Hz, 1H), 2.42–2.33 (m, 4H), 1.77 (d, *J* = 1.1 Hz, 3H), 1.29–1.18 (m, 3H), 1.10 (d, *J* = 7.1 Hz, 18H); **^{13}C NMR** (101 MHz, $CDCl_3$) δ 157.6, 132.2, 126.5, 125.7, 117.7, 90.7, 90.6, 79.7, 27.8, 19.7, 18.3, 13.6, 13.0; **IR** (neat, cm^{-1}): 2945.1, 2866.8, 1587.3; **HRMS** (EI): m/z calc'd for $C_{20}H_{34}OSi$ [M^+] = 318.2379, found mass = 318.2380.

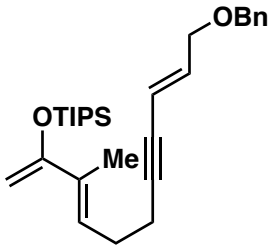

Diene 2.12d

Synthesized according to **general procedure 1c** from ketone **2.25d** in 92% yield (0.283 g).

^{1}H NMR (400 MHz, $CDCl_3$) δ 7.39–7.28 (m, 5H), 6.20–6.04 (m, 2H), 5.72 (dq, *J* = 15.8, 2.0 Hz, 1H), 4.51 (s, 2H), 4.33 (dd, *J* = 50.9, 1.3 Hz, 2H), 4.05 (dd, *J* = 5.7, 1.7 Hz, 2H), 2.38 (d, *J* = 3.8 Hz, 4H), 1.78 (d, *J* = 1.2 Hz, 3H), 1.34–1.16 (m, 3H), 1.10 (d, *J* = 7.1 Hz, 18H); **^{13}C NMR** (101 MHz, $CDCl_3$) δ 157.5, 138.2, 138.1, 128.5, 127.8, 127.8, 126.5,

112.7, 90.8, 90.6, 78.8, 72.2, 70.0, 27.9, 19.8, 18.3, 13.6, 13.0; **IR** (neat, cm^{-1}): 2945.1, 2864.1, 1463.87; **HRMS** (EI): m/z calc'd for $C_{28}H_{42}O_2Si$ [M^+] = 438.2954, found mass = 438.2961.

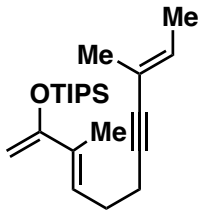

Diene 2.12e

Synthesized according to **general procedure 1c** from ketone **2.25e** in 80% yield (0.257 g).

^{1}H NMR (400 MHz, $CDCl_3$) δ 6.18 – 6.07 (m, 1H), 5.81 (qq, *J* = 7.0, 1.5 Hz, 1H), 4.39 (d, *J* = 1.4 Hz, 1H), 4.28 – 4.21 (m, 1H), 2.36 (d, *J* = 3.4 Hz, 4H), 1.77 (d, *J* = 1.2 Hz, 3H), 1.74 (quint, *J* = 1.2 Hz, 3H), 1.65 (dq, *J* = 7.1, 1.2 Hz, 3H), 1.28 – 1.19 (m, 3H), 1.10 (d, *J* = 7.2 Hz, 18H); **^{13}C NMR** (101 MHz, $CDCl_3$) δ 157.6, 132.1, 131.0, 126.7, 118.9, 90.5, 85.8, 83.9, 28.2, 19.6, 18.3, 17., 14.05, 13.6, 13.0; **IR** (neat, cm^{-1}): 2945.0, 2870.7, 1595.1, 1462.1; **HRMS** (EI): m/z calc'd for $C_{22}H_{38}OSi$ [M^+] = 346.2692, found [M^+] = 346.2701.

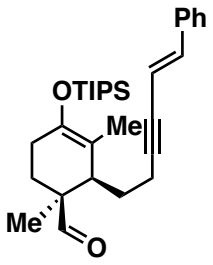

Silyl enol ether 2.13a

To an oven dried reaction tube was added diene **2.12a** (0.15 mmol), methacrolein (0.75 mmol), Co(III) catalyst **2.31b** (1 mol%) and DCM (2M). The reaction mixture was stirred overnight at room temperature and the solvent evaporated in vacuo. The crude product was purified by flash chromatography to yield **2.13a** in 90% yield (0.062 g).

^{1}H NMR (400 MHz, $CDCl_3$) δ 9.66 (s, 1H), 7.42–7.27 (m, 5H), 6.87 (d, *J* = 16.2 Hz, 1H), 6.15 (dt, *J* = 16.2, 2.2 Hz, 1H), 2.38 (m, 2H), 2.19–2.08 (m, 3H), 1.91 (dt, *J* = 13.9, 9.1 Hz, 1H), 1.76 (quint, *J* = 2.2 Hz, 3H), 1.66–1.48 (m, 3H), 1.17–1.05 (m, 24H); **^{13}C NMR** (101 MHz, $CDCl_3$) δ 206.2, 143.4, 140.4, 136.6, 128.8, 128.4, 126.2, 111.55, 108.72, 92.23, 80.70, 48.70, 45.07, 32.34, 26.57, 24.08, 19.71, 19.32, 18.26, 18.24, 16.86, 13.34; **IR** (neat, cm^{-1}): 2942.8, 2865.8, 1723.6, 1459.0, 1317.7, 1215.9, 1177.0, 951.4, 911.2, 882.7, 746.7, 688.1, 679.3; **HRMS** (EI): m/z calc'd for $C_{30}H_{44}O_2Si$ $[M]^+$ = 464.3111, found $[M]^+$ = 464.3126.

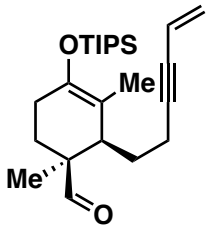

Silyl enol ether 2.13e

To an oven dried reaction tube was added diene **2.12c** (0.15 mmol), methacrolein (0.75 mmol), Co(III) catalyst **2.31b** (1 mol%) and DCM (2M). The reaction mixture was stirred overnight at room temperature and the solvent evaporated in vacuo. The crude product was purified by flash chromatography to yield **2.13e** in 62% yield (0.036 g).

^{1}H NMR (400 MHz, $CDCl_3$) δ 9.62 (s, 1H), 5.76 (ddt, *J* = 17.5, 11.0, 2.1 Hz, 1H), 5.55 (dd, *J* = 17.5, 2.2 Hz, 1H), 5.38 (dd, *J* = 11.0, 2.3 Hz, 1H), 2.30 (qd, *J* = 7.4, 2.2 Hz, 2H), 2.17–2.09 (m, 3H), 1.88 (dt, *J* = 13.8, 9.2 Hz, 1H), 1.72 (t, *J* = 1.9 Hz, 3H), 1.62–1.48 (m, 3H), 1.18–1.02 (m, 24H); **^{13}C NMR** (101 MHz, $CDCl_3$) δ 206.2, 143.4, 126.0, 117.6, 111.5, 90.5, 80.3, 48.7, 45.0, 32.2, 26.6, 24.1, 19.4, 19.3, 18.2, 18.2, 16.8, 13.3; **IR** (neat, cm^{-1}): 2942.3, 2895.6, 2866.2, 1724.0, 1677.3, 1461.2; **HRMS** (EI): m/z calc'd for $C_{24}H_{40}O_2Si$ $[M]^+$ = 388.2798, found mass = 388.2773.

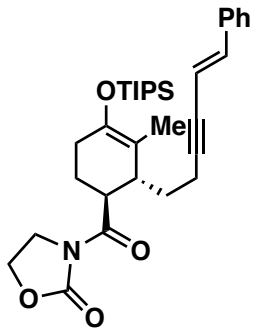

Silyl enol ether (*rac*-2.13f)

To oven dried reaction tube was added gadolinium(III) triflate (0.013 mmol), DCM (0.380 ml), 4Å MS (32 mg, 250mg/1mmol), and oxazolidinone dienophile **2.38a** (0.253 mmol). The mixture was stirred for 3 h at room temperature. Then, a solution of diene **2.12a** (0.127 mmol) in DCM (0.127 ml) was added via syringe. The mixture was then stirred at 20 °C for 18h. The mixture was filtered through celite and evaporated. The crude residue was purified by flash chromatography, yielding *rac*-**2.13f** in 88% yield (0.061 g) as a 95:5 *exo:endo* Diels-Alder cycloadduct mixture.

^{1}H NMR (400 MHz, $CDCl_3$) δ 7.37–7.18 (m, 5H), 6.83 (d, *J* = 16.2 Hz, 1H), 6.12 (dt, *J* = 16.2, 2.3 Hz, 1H), 4.40–4.28 (m, 2H), 4.08–3.91 (m, 2H), 3.74 (ddd, *J* = 9.2, 7.6, 3.3 Hz, 1H), 2.78–2.68 (m, 1H), 2.35–2.18 (m, 3H), 2.14–2.03 (m, 1H), 2.03–1.92 (m, 1H), 1.79–1.65 (m, 3H), 1.66 (s, 3H), 1.18–1.01 (m, 21H); **^{13}C NMR** (101 MHz, $CDCl_3$) δ 175.6, 153.3, 144.8, 140.2, 136.6, 128.8, 128.4, 126.2, 111.3, 108.9, 93.2, 79.9, 61.95, 43.0, 41.6, 39.8, 31.1, 29.5, 25.7, 18.2, 16.1, 14.2, 13.3; **IR** (neat, cm^{-1}): 2943.5, 2865.3, 2209.2, 1774.7, 1697.6, 1383.1, 1175.5; **HRMS** (EI): m/z calc'd for $C_{32}H_{45}NO_4Si$ $[M]^+$ = 535.3118, found $[M]^+$= 535.3088.

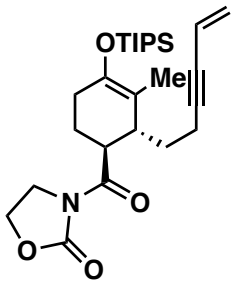

Silyl enol ether 2.13g

To oven dried reaction tube was added gadolinium(III) triflate (0.015 mmol), DCM (0.450 ml), 4Å MS (32 mg, 250mg/1mmol) and oxazolidinone dienophile **2.38a** (0.30 mmol). The mixture was stirred for 3h at room temperature. Then, a solution of diene **2.12c** (0.15 mmol) in DCM (0.15 ml) was added via syringe. The mixture was then stirred at room temperature for 18 h. The mixture was filtered through celite and evaporated. The crude residue was purified by flash chromatography, yielding **2.13g** in 93% yield (0.064 g) as a 95:5 *exo*:*endo* mixture.

^{1}H NMR (400 MHz, $CDCl_3$) δ 5.76 (ddt, *J* = 17.6, 11.0, 2.1 Hz, 1H), 5.53 (dd, *J* = 17.5, 2.3 Hz, 1H), 5.36 (dd, *J* = 11.0, 2.3 Hz, 1H), 4.41 (t, *J* = 8.1 Hz, 2H), 4.09 – 3.95 (m, 2H), 3.72 (ddd, *J* = 9.3, 7.6, 3.4 Hz, 1H), 2.71 (s, 1H), 2.31 – 2.17 (m, 3H), 2.09 (dtt, *J* = 16.3, 5.0, 1.4 Hz, 2H), 1.97 (dtd, *J* = 12.6, 5.3, 3.4 Hz, 1H), 1.71 (m, 2H), 1.65 (s, 3H), 1.15 – 1.03 (m, 21H); **^{13}C NMR** (101 MHz, $CDCl_3$) δ 175.6, 153.3, 144.8, 125.7, 117.7, 111.3, 91.4, 79.5, 62.0, 43.0, 41.6, 39.8, 31.1, 29.4, 25.7, 18.2, 15.7, 14.2, 13.3; **IR:** 2943.6, 2865.9, 1774.5, 1697.7, 1383.2, 1351.2, 1240.4, 1194.2, 1175.9; **HRMS** (EI) m/z calculated for $C_{26}H_{41}NO_4Si$ $[M]^+$ = 459.2805, found $[M]^+$ = 459.2787.

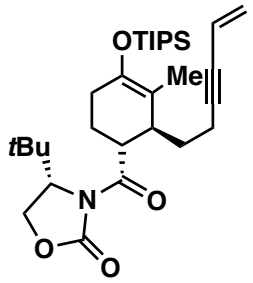

Silyl enol ether 2.13h

To oven dried reaction tube was added gadolinium(III) triflate (0.015 mmol), DCM (0.450 ml), 4Å MS (32 mg, 250mg/1mmol) and oxazolidinone dienophile **2.38b** (0.300 mmol). The mixture was stirred for 3h at room temperature. Then, a solution of diene **2.12c** (0.15 mmol) in DCM (0.15 ml) was added via syringe. The mixture was then stirred at room temperature for 18 h. The mixture was filtered through celite and evaporated. The crude residue was purified by flash chromatography, yielding **2.13g** in 84% yield (0.062 g) as a 95:5 *exo*:*endo* mixture.

^{1}H NMR (400 MHz, $CDCl_3$) δ 5.74 (ddt, *J* = 17.6, 11.0, 2.1 Hz, 1H), 5.50 (dd, *J* = 17.5, 2.3 Hz, 1H), 5.33 (dd, *J* = 11.0, 2.3 Hz, 1H), 4.46 (dd, *J* = 7.7, 1.9 Hz, 1H), 4.30–4.16 (m, 2H), 3.81 (td, *J* = 6.9, 3.8 Hz, 1H), 2.65 (q, *J* = 5.6 Hz, 1H), 2.45–2.34 (m, 1H), 2.34–2.22 (m, 2H), 2.22–2.10 (m, 1H), 1.86 (dtd, *J* = 12.5, 6.2, 3.7 Hz, 1H), 1.76 (ddd, *J* = 13.1, 6.1, 2.6 Hz, 3H), 1.63 (s, 3H), 1.07 (d, *J* = 5.4 Hz, 21H), 0.91 (s, 9H); **^{13}C NMR** (101 MHz, $CDCl_3$) δ 175.6, 154.3, 144.8, 125.3, 117.7, 110.4, 91.2, 79.3, 64.99, 60.8, 41.3, 41.0, 35.7, 32.0, 28.5, 25.6, 23.7, 18.1, 16.1, 14.5, 13.2; **IR** (neat, cm^{-1}): 2945.5, 2867.1, 1777.7, 1706.2, 1381.8, 1216.4, 1176.1; **HRMS** (EI): m/z calc'd for $C_{30}H_{49}NO_4Si$ $[M]^+$ = 515.3431, found $[M]^+$ = 515.3415.

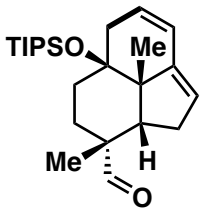

Tricycle 2.14a

To a capped 4 mL oven dried reaction vial was added diene **2.12c** (0.150 mmol, 0.048 g), methacrolein (0.750 mmol,0.062 mL) and DCE (0.750 ml, 0.200M). The mixture was heated to 100 ^{o}C for 18 h. Then, [JohnPhosAuNCMe]SbF_6 was added to the mixture (5.8 mg, 7.50 μmol, 5 mol%). The mixture was stirred at room temperature for 24 h, and then purified according by column chromatography, yielding 53% of (0.031 g) **2.14a** as a 12:1 mixture of diastereoisomers as a colourless oil**.**

^{1}H NMR (400 MHz, $CDCl_3$) δ 9.48 (s, 1H), 6.12 (dd, *J* = 9.7, 3.0 Hz, 1H), 5.72–5.63 (m, 1H), 5.38 (s, 1H), 2.68–2.56 (m, 2H), 2.34 (dd, *J* = 17.3, 3.1 Hz, 1H), 2.18–2.06 (m, 2H), 1.84–1.75 (m, 2H), 1.54 (dd, *J* = 10.9, 3.7 Hz, 1H), 1.42 (dd, *J* = 11.5, 3.7 Hz, 1H), 1.11 (d, *J* = 4.2 Hz, 21H), 1.07 (s, 3H), 0.99 (s, 3H); **^{13}C NMR** (101 MHz, $CDCl_3$) δ 205.5, 149.6, 128.7, 123.6, 122.2, 74.6, 54.7, 52.8, 46.2, 39.4, 31.8, 31.8, 27.0, 25.0, 19.6, 18.7, 18.7, 13.9; **IR** (neat, cm^{-1}): 2941.9, 2865.1, 1712.7, 1449.9; **HRMS** (EI): m/z calc'd for $C_{24}H_{40}O_2Si$ $[M]^+$ = 388.2798, found $[M]^+$ = 388.2816.

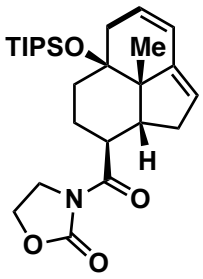

Tricycle 2.14c

Synthesized according to **general procedure 7** using oxazolidinone dienophile **2.38a** and diene **2.12c,** reacting for 24 h during the gold cyclization, yielding 64% (0.044g) of a 5:1 5-*exo-dig* (**2.14c**): 6-*endo-dig* mixture as a white foam**.**

^{1}H NMR (400 MHz, $CDCl_3$) δ 6.19–6.11 (m, 1H), 5.68–5.59 (m, 1H), 5.42–5.36 (m, 1H), 4.42–4.32 (m, 2H), 4.09–3.94 (m, 2H), 3.54–3.42 (m, 1H), 2.70–2.56 (m, 3H), 2.09 (dd, *J* = 17.6, 5.9 Hz, 1H), 1.87–1.46 (m, 5H), 1.14–1.02 (m, 21H); **^{13}C NMR** (101 MHz, $CDCl_3$) δ 176.2, 152.9, 147.5, 127.0, 122.3, 76.6, 74.1, 61.6, 52.4, 44.9, 43.8, 42.9, 39.0, 37.3, 34.6, 23.1, 19.7, 18.5, 18.4, 13.7; **IR** (neat, cm^{-1}): 2943.0, 2867.4, 1778.0, 1698.5, 1385.8, 1107.2, 1055.6; **HRMS** (EI): m/z calc'd for $C_{23}H_{34}NO_4Si$ $[M\text{-}iPr]^+$ = 416.2257, found $[M\text{-}iPr]^+$ = 416.2230.

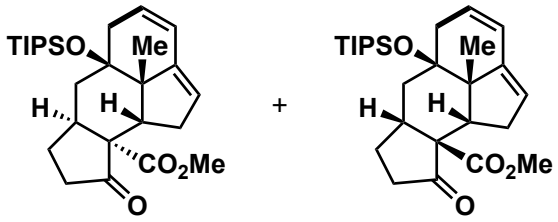

Tricycle 2.14h

Synthesized according to **general procedure 7** using dienophile **2.38h** and diene **2.12c,** reacting for 48 h during the gold cyclization, yielding 33% (0.045 g) a 5:4 mixture of diastereoisomers (**2.14h** = major) as a white foam**.**

Major Diastereoisomer:

^{1}H NMR (400 MHz, $CDCl_3$) δ 6.15 (dd, J = 9.6, 2.9 Hz, 1H), 5.66–5.57 (m, 1H), 5.38 (s, 1H), 3.63 (s, 3H), 2.91–2.83 (m, 1H), 2.83–2.73 (m, 2H), 2.61–2.52 (m, 1H), 2.46 (dt, J = 19.2, 8.8 Hz, 1H), 2.29 (dd, J = 15.1, 9.9 Hz, 1H), 2.26–2.12 (m, 2H), 2.07 (dt, J = 22.0, 3.8 Hz, 1H), 2.03–1.92 (m, 1H), 1.86–1.77 (m, 1H), 1.36 (dd, J = 15.4, 4.2 Hz, 1H), 1.17–1.09 (m, 24H); **^{13}C NMR** (101 MHz, $CDCl_3$) δ 211.9, 170.5, 147.2, 127.4, 123.4, 123.4, 75.4, 63.6, 52.5, 52.4, 44.4, 39.8, 38.0, 35.2, 34.9, 34.2, 27.9, 21.1, 19.4, 19.0, 15.0; **IR** (neat, cm^{-1}): 2944.7, 2867.6, 1759.2, 1728.6**; HRMS** (EI): m/z calc'd for $C_{27}H_{42}O_4Si$ $[M\text{-}iPr]^+$ = 415.2305, found mass = 415.2315.

Minor Diastereoisomer:

^{1}H NMR (400 MHz, $CDCl_3$) δ 6.08 (dd, J = 9.6, 3.0 Hz, 1H), 5.58–5.48 (m, 2H), 3.70 (s, 3H), 3.39 (dd, J = 17.0, 3.4 Hz, 1H), 3.09 (dt, J = 11.8, 6.1 Hz, 1H), 2.70–2.60 (m, 2H), 2.58–2.47 (m, 1H), 2.30–2.07 (m, 3H), 1.91 (dddd, J = 13.0, 10.9, 9.7, 6.2 Hz, 1H), 1.52–1.45 (m, 1H), 1.44–1.40 (m, 2H), 1.12 (d, J = 2.8 Hz, 21H), 1.07 (s, 3H); **^{13}C NMR** (101 MHz, $CDCl_3$) δ 213.2, 172.7, 144.7, 127.1, 125.5, 122.4, 74.0, 61.0, 52.6, 52.6, 49.3, 39.0, 36.9, 36.3, 35.9, 31.3, 24.3, 19.6, 18.5, 18.4, 13.7; **IR** (neat, cm^{-1}): 2941.9, 2865.9, 2359.4, 1754.3, 1729.1, 1463.1; **HRMS** (EI): m/z calc'd for $C_{24}H_{35}O_4Si$ $[M\text{-}iPr]^+$ = 415.2305, found mass = 415.2321.

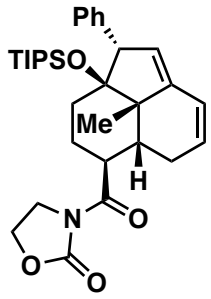

Tricycle 2.15a

Synthesized according to **general procedure 6** using oxazolidinone dienophile **2.38a** and diene **2.12a,** reacting for 24 h during the gold cyclization, and yielding 76% (0.061 g) of a 12:1 6-*endo-dig* (**2.15a**): 5-*exo-dig* mixture as a white foam**.**

^{1}H NMR (400 MHz, $CDCl_3$) δ 7.32–7.18 (m, 5H), 6.22 (dd, *J* = 9.9, 2.8 Hz, 1H), 5.70–5.62 (m, 1H), 5.49–5.43 (m, 1H), 4.39 (t, *J* = 8.3 Hz, 2H), 4.26–4.22 (m, 1H), 4.10–3.94 (m, 2H), 3.59 (td, *J* = 11.6, 3.3 Hz, 1H), 2.56 (dq, *J* = 18.9, 2.7 Hz, 1H), 2.34 (dd, *J* = 11.7, 5.9 Hz, 1H), 2.00 (td, *J* = 14.1, 3.9 Hz, 1H), 1.81 (dd, *J* = 19.4, 5.9 Hz, 1H), 1.68–1.51 (m, 2H), 1.30 (s, 3H), 1.15–1.08 (m, 1H), 1.05–0.95 (m, 21H); **^{13}C NMR** (101 MHz, $CDCl_3$) δ 176.5, 153.1, 144.3, 139.3, 130.5, 127.9, 126.9, 126.9, 126.1, 123.3, 87.8, 61.9, 59.1, 50.6, 43.3, 42.9, 36.5, 31.9, 28.1, 25.7, 19.9, 18.8, 14.3; **IR** (neat, cm^{-1}): 2966.9, 2944.5, 2866.7, 1777.9, 1697.5, 1387.9, 1239.3, 1131.2; **HRMS** (EI): m/z calc'd for $C_{32}H_{45}NO_4Si$ $[M]^+$= 535.3118, found $[M]^+$= 535.3112.

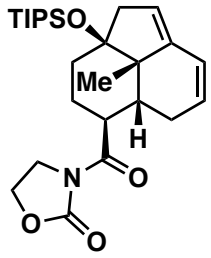

Tricycle 2.15b

Synthesized according to **general procedure 6** using oxazolidinone dienophile **2.38a** and diene **2.12c**, reacting for 24 h during the gold cyclization, yielding 55% (0.038 g) of a 2:1 6-*endo-dig* (**2.15b**): 5-*exo-dig* mixture as a white foam**.**

^{1}H NMR (400 MHz, $CDCl_3$) δ 6.15 (dd, *J* = 9.9, 2.9 Hz, 1H), 5.63–5.53 (m, 1H), 5.40–5.33 (m, 1H), 4.38 (t, *J* = 8.1 Hz, 2H), 4.10–3.93 (m, 3H), 3.58–3.44 (m, 1H), 2.74–2.64 (m, 1H), 2.24 (dd, *J* = 11.7, 5.9 Hz, 1H), 2.14 (dd, *J* = 15.6, 3.6 Hz, 1H), 1.97–1.85 (m, 1H), 1.83–1.74 (m, 2H), 1.67–1.59 (m, 2H), 1.13–1.05 (m, 24H); **^{13}C NMR** (101 MHz, $CDCl_3$) δ 176.6, 153.1, 144.7, 126.4, 123.4, 121.4, 82.5, 61.9, 49.4, 44.6, 43.2, 42.9, 36.5, 36.4, 28.0, 26.1, 20.8, 18.6, 18.5, 13.6; **IR** (neat, cm^{-1}): 2943.7, 2866.9, 1777.7, 1698.1, 1389.2, 1221.6; **HRMS** (EI): m/z calc'd for $C_{23}H_{34}NO_4Si$ $[M\text{-}iPr]^+$= 416.2257, found $[M\text{-}iPr]^+$= 416.2282.

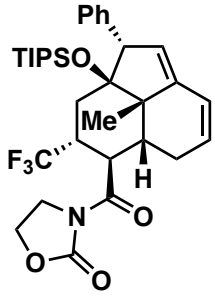

Tricycle 2.15c

Synthesized according to **general procedure 6** using oxazolidinone dienophile **2.38g** and diene **2.12a**, reacting for 24 h during the gold cyclization, yielding 49% (0.044g) of **2.15c** as the sole isomer, and as a white foam**.**

^{1}H NMR (400 MHz, $CDCl_3$) δ 7.29 (tt, J = 15.1, 7.1 Hz, 5H), 6.27 (dd, J = 9.8, 2.8 Hz, 1H), 5.79–5.64 (m, 1H), 5.47 (s, 1H), 4.41 (ddd, J = 9.4, 7.4, 2.9 Hz, 2H), 4.31 (s, 1H), 4.23 (t, J = 11.4 Hz, 1H), 4.14–3.95 (m, 2H), 2.89–2.74 (m, 1H), 2.60–2.49 (m, 1H), 2.32 (dd, J = 11.6, 5.9 Hz, 1H), 2.06 (t, J = 13.8 Hz, 1H), 1.78 (dd, J = 19.2, 5.9 Hz, 1H), 1.44–1.35 (m, 1H), 1.30 (s, 3H), 1.11–0.97 (m, 21H); **^{13}C NMR** (101 MHz, $CDCl_3$) δ 175.6, 152.8, 143.3, 138.2, 130.3, 128.1, 127.2, 126.8, 126.1, 122.8, 86.9, 61.7, 59.0, 50.3, 43.0, 40.8, 40.6 (q, *J* = 25.7 Hz), 38.9, 30.6, 27.2, 19.5, 18.6, 18.4, 13.7; **^{19}F NMR** (282 MHz, $CDCl_3$) δ -69.89 (d, *J* = 7.8 Hz); **IR** (neat, cm^{-1}): 2945.6, 2869.2, 1780.4, 1698.8, 1387.8, 1166.1, 1119.1; **HRMS** (EI): m/z calc'd for $C_{30}H_{37}F_3NO_4Si$ $[M\text{-}iPr]^+$ = 560.2444, found $[M\text{-}iPr]^+$ = 560.2432.

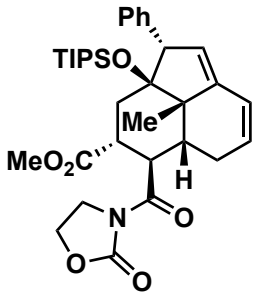

Tricycle 2.15f

Synthesized according to **general procedure 6** using oxazolidinone dienophile **2.38f** and diene **2.12a,** reacting for 24 h during the gold cyclization, yielding 57% (0.051 g) of a 6:1 6-*endo-dig* (**2.15f**): 5-*exo-dig* mixture as a white foam**.**

^{1}H NMR (400 MHz, $CDCl_3$) δ 7.32–7.18 (m, 5H), 6.22 (dd, *J* = 9.8, 2.7 Hz, 1H), 5.76–5.66 (m, 1H), 5.45–5.38 (m, 1H), 4.45–4.31 (m, 2H), 4.28–4.23 (m, 1H), 4.23–4.14 (m, 1H), 4.07–3.98 (m, 2H), 3.49 (s, 3H), 3.06 (ddd, *J* = 13.7, 11.1, 2.6 Hz, 1H), 2.56–2.44 (m, 1H), 2.19 (dd, *J* = 11.8, 5.8 Hz, 1H), 2.05 (t, *J* = 13.9 Hz, 1H), 1.83 (dd, *J* = 19.1, 5.9 Hz, 1H), 1.49 (dd, *J* = 14.3, 2.6 Hz, 1H), 1.26 (s, 3H), 1.17–1.06 (m, 3H), 1.05–0.97 (m, 18H); **^{13}C NMR** (101 MHz, $CDCl_3$) δ 177.5, 175.1, 153.2, 143.7, 138.8, 130.5, 128.0, 127.2, 127.1, 125.9, 122.8, 87.9, 61.7, 59.1, 52.1, 50.9, 43.4, 43.1, 42.4, 39.4, 34.6, 27.2, 19.6, 18.8, 18.7, 13.9; **IR** (neat, cm^{-1}): 2943.6, 2867.3, 1781.3, 1733.9, 1696.1, 1388.4; **HRMS** (EI): m/z calc'd for $C_{34}H_{47}NO_6Si$ $[M]^+$ = 593.3173, found $[M]^+$ = 593.3190.

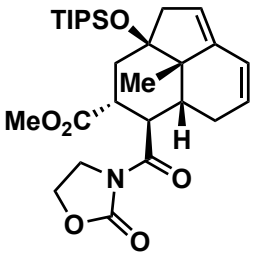

Tricycle 2.15g

Synthesized according to **general procedure 6** using oxazolidinone dienophile **2.38f** and diene **2.12c,** reacting for 24 h during the gold cyclization, yielding 42% (0.042 g) of a 2:1 6-*endo-dig* (**2.15g**): 5-*exo-dig* mixture as a white foam**.**

^{1}H NMR (400 MHz, $CDCl_3$) δ 6.18 (dd, *J* = 9.9, 2.8 Hz, 1H), 5.70–5.62 (m, 1H), 5.35 (s, 1H), 4.39 (td, *J* = 8.0, 5.9 Hz, 2H), 4.04 (t, *J* = 8.1 Hz, 2H), 3.59 (s, 3H), 3.12 (ddd, *J* = 13.8, 11.2, 3.0 Hz, 1H), 2.74 (d, *J* = 15.7 Hz, 1H), 2.51–2.39 (m, 1H), 2.23–2.09 (m, 3H), 1.95 (t, *J* = 13.7 Hz, 1H), 1.81 (dd, *J* = 19.1, 5.8 Hz, 1H), 1.73–1.57 (m, 1H), 1.16–1.10 (m, 21H), 1.09 (s, 3H); **^{13}C NMR** (151 MHz, $CDCl_3$) δ 177.5, 175.1, 153.2, 144.2, 126.8, 122.9, 121.0, 82.6, 61.7, 52.0, 49.5, 44.3, 43.1, 42.4, 39.4, 38.8, 27.2, 20.5, 18.6, 18.5, 13.5, 13.5; **IR** (neat, cm^{-1}): 2942.9, 2867.0, 2359.2, 2342.2, 1781.5, 1732.1, 1691.6, 1386.1; **HRMS** (EI): m/z calc'd for $C_{25}H_{36}NO_6Si$ $[M\text{-}iPr]^+$ = 474.2312, found $[M\text{-}iPr]^+$ = 474.2317.

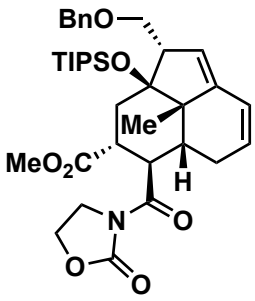

Tricycle 2.15i

Synthesized according to **general procedure 6** using oxazolidinone dienophile **2.38f** and diene **2.12d,** reacting for 24 h during the gold cyclization, yielding 55% (0.040 g) of an 8:1 6-*endo-dig* (**2.15i**): 5-*exo-dig* mixture as a white foam**.**

^{1}H NMR (400 MHz, $CDCl_3$) δ 7.40–7.26 (m, 5H), 6.18 (dd, J = 9.9, 2.7 Hz, 1H), 5.74–5.59 (m, 1H), 5.47 (s, 1H), 4.60 (d, J = 12.1 Hz, 1H), 4.46 (d, J = 12.1 Hz, 1H), 4.39 (td, J = 8.1, 5.7 Hz, 2H), 4.15–4.06 (m, 1H), 4.03 (t, J = 8.1 Hz, 2H), 3.74 (dd, J = 8.4, 3.3 Hz, 1H), 3.58 (s, 3H), 3.32 (dd, J = 10.1, 8.4 Hz, 1H), 3.20 (d, J = 10.0 Hz, 1H), 3.06 (ddd, J = 12.7, 11.1, 3.4 Hz, 1H), 2.44 (dd, J = 19.4, 5.7 Hz, 1H), 2.11 (dd, J = 11.7, 5.8 Hz, 1H), 1.96–1.75 (m, 3H), 1.12–1.03 (m, 24H); **^{13}C NMR** (101 MHz, $CDCl_3$) δ 174.9, 153.2, 143.2, 138.4, 128.5, 128.0, 127.8, 126.9, 123.4, 122.8, 84.8, 73.7, 68.6, 61.7, 52.5, 52.1, 50.4, 43.1, 42.2, 39.2, 34.3, 27.1, 20.1, 18.7, 18.6, 13.8; **IR** (neat, cm^{-1}): 2963.9, 2867.2, 2362.6, 2338.7, 1780.6, 1734.3, 1696.7, 1388.1; **HRMS** (EI): m/z calc'd for $C_{33}H_{44}NO_7Si$ $[M\text{-}iPr]^+$ = 594.2887, found $[M\text{-}iPr]^+$ = 594.2884.

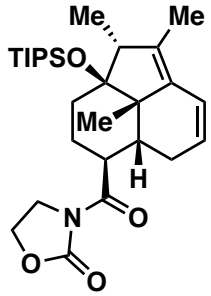

Tricycle 2.15j

Synthesized according to **general procedure 6** using oxazolidinone dienophile **2.38a** and diene **2.12e,** reacting for 24 h during the gold cyclization, yielding 39% (0.028 g) of **2.15j** as the sole isomer and as a white foam**.**

^{1}H NMR (400 MHz, $CDCl_3$) δ 6.24 (dd, *J* = 10.0, 2.8 Hz, 1H), 5.57–5.46 (m, 1H), 4.38 (t, *J* = 8.1 Hz, 2H), 4.10–3.94 (m, 2H), 3.50–3.38 (m, 1H), 2.97–2.87 (m, 1H), 2.55–2.42 (m, 1H), 2.24 (dd, *J* = 11.7, 6.0 Hz, 1H), 1.76 (dd, *J* = 19.3, 5.9 Hz, 1H), 1.72–1.52 (m, 4H), 1.61 (s, 3H), 1.15–1.05 (m, 21H), 1.06 (s, 3H), 1.00 (d, *J* = 7.3 Hz, 3H); **^{13}C NMR** (101 MHz, $CDCl_3$) δ 176.7, 153.1, 135.3, 132.5, 124.3, 120.9, 84.4, 61.9, 49.5, 49.1, 43.3, 42.9, 36.5, 31.5, 28.0, 26.0, 20.1, 18.8, 14.0, 11.7, 10.5; **IR** (neat, cm^{-1}): 2966.8, 2945.3, 2867.2, 1777.2, 1697.7, 1389.0; **HRMS** (EI): m/z calc'd for $C_{28}H_{45}NO_4Si$ $[M]^+$ = 487.3118, found $[M]^+$ = 487.3092.

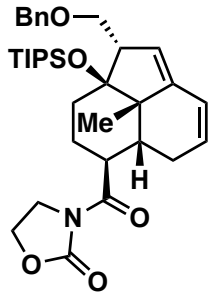

Tricycle 2.15l

Synthesized according to **general procedure 6** using oxazolidinone dienophile **2.38a** and diene **2.12d,** reacting for 24 h during the gold cyclization, yielding 55% (0.048 g) of a 6:1 6-*endo-dig* (**2.15l**): 5-*exo-dig* mixture as a white foam**.**

^{1}H NMR (400 MHz, $CDCl_3$) δ 7.40–7.24 (m, 5H), 6.15 (dd, *J* = 9.9, 2.8 Hz, 1H), 5.63–5.54 (m, 1H), 5.51–5.46 (m, 1H), 4.59 (d, *J* = 12.0 Hz, 1H), 4.45 (d, *J* = 12.1 Hz, 1H), 4.37 (t, *J* = 8.1 Hz, 2H), 4.09–3.92 (m, 2H), 3.70 (dd, *J* = 8.4, 3.3 Hz, 1H), 3.47 (td, *J* = 11.4, 3.3 Hz, 1H), 3.31 (dd, *J* = 10.4, 8.4 Hz, 1H), 3.21–3.11 (m, 1H), 2.54–2.42 (m, 1H), 2.24 (dd, *J* = 11.7, 5.8 Hz, 1H), 1.85 (td, *J* = 13.4, 3.8 Hz, 1H), 1.82–1.71 (m, 1H), 1.68–1.51 (m, 2H), 1.50–1.40 (m, 1H), 1.12 (s, 3H), 1.10–0.98 (m, 21H); **^{13}C NMR** (101 MHz, $CDCl_3$) δ 176.4, 153.1, 143.7, 138.4, 128.5, 128.1, 127.8, 126.6, 123.7, 123.4, 84.7, 73.7, 68.8, 61.9, 52.6, 50.3, 43.1, 42.9, 36.3, 31.7, 27.9, 25.8, 20.3, 18.7, 18.7, 13.8; **IR** (neat, cm^{-1}): 2944.5, 2866.7, 1777.6, 1697.7, 1389.0; **HRMS** (EI): m/z calc'd for $C_{31}H_{42}NO_5Si$ $[M\text{-}iPr]^+$ = 536.2832, found $[M\text{-}iPr]^+$ = 536.2804.

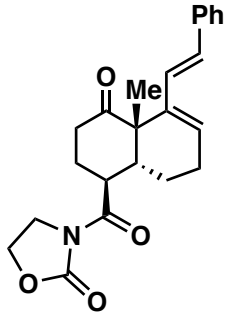

Diene 2.17c

To an oven dried reaction tube was added silyl enol ether **2.13f** (0.15 mmol), [VPhosAuNCMe]SbF_6 (7.50 μmol, 5 mol%), MeOH (0.075 ml) and DCM (0.75 ml, 0.2M). The mixture was stirred at room temperature for 6 h. The crude mixture was dry packed in silica, evaporated, and separated by flash chromatography, yielding **2.17c** in 76% (0.042 g) yield**.**

^{1}H NMR (400MHz, $CDCl_3$) δ = 7.35–7.20 (m, 4 H), 7.20–7.12 (m, 1 H), 6.50 (d, J = 16.4 Hz, 1 H), 6.38 (d, J = 16.4 Hz, 1 H), 6.06–6.01 (m, 1 H), 4.40 (t, J = 8.1 Hz, 2 H), 4.34 (dt, J = 3.9, 11.8 Hz, 1 H), 4.06–3.95 (m, 2 H), 2.65–2.53 (m, 1 H), 2.37 (td, J = 3.1, 11.4 Hz, 1 H), 2.34–2.15 (m, 4 H), 1.93–1.81 (m, 1 H), 1.78–1.64 (m, 1 H), 1.52 - 1.42 (m, 1 H), 1.40 (s, 3 H); **^{13}C NMR** (101MHz, $CDCl_3$) δ = 214.1, 175.0, 153.2, 137.3, 137.1, 128.5, 128.2, 127.9, 127.4, 127.1, 126.3, 61.9, 52.1, 45.0, 42.8, 39.8, 38.9, 31.0, 23.0, 22.0, 20.8; **IR** (neat, cm^{-1}): 2968.5, 2926.0, 2871.0, 1774.2, 1702.4, 1386.2; **HRMS** (EI): m/z calc'd for $C_{23}H_{25}NO_4$ $[M]^+$ =379.1784, found $[M]^+$=379.1764.

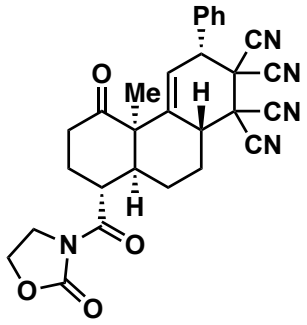

Tricycle 2.21a

In a capped 4 mL oven dried reaction vial, tetracyanoethylene (2 equiv) was added to diene **2.17c** in DCE (0.2M). The mixture was stirred at 60˚C overnight and purified by flash chromatography. Tetracycle **2.21a** was formed in 73% yield (0.054 g).

^{1}H NMR (400 MHz, $CDCl_3$) δ 7.58–7.36 (m, 5H), 5.73 (t, *J* = 1.9 Hz, 1H), 4.54 (td, *J* = 8.8, 2.5 Hz, 2H), 4.40 (t, *J* = 2.1 Hz, 1H), 4.25–4.14 (m, 1H), 4.03 (ddd, *J* = 11.1, 8.3, 6.4 Hz, 1H), 3.70–3.62 (m, 1H), 3.26–3.03 (m, 2H), 2.48–2.30 (m, 5H), 2.27–2.13 (m, 2H), 1.82–1.65 (m, 1H), 1.45 (s, 3H); **^{13}C NMR** (101 MHz, $CDCl_3$) δ 211.6, 176.1, 153.3, 140.6, 133.8, 130.2, 129.6, 129.4, 120.1, 111.3, 111.0, 110.1, 62.3, 56.4, 49.1, 46.8, 43.7, 43.1, 42.8, 42.1, 42.0, 35.6, 31.7, 29.8, 23.1, 22.0; **IR** (neat, cm^{-1}): 2967.7, 2921.4, 2854.0, 2364.0, 2360.3, 1774.7, 1698.3, 1388.1, 1362.5, 1250.1, 1221.0; **HRMS** (ESI): m/z calc'd for $C_{29}H_{25}N_5O_4Na$ [M+Na] = 530.1804, found [M+Na] = 530.1792.

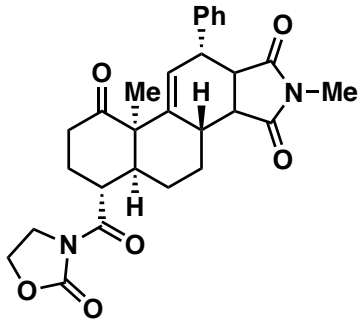

Tetracycle 2.21b

In a capped 4 mL oven dried reaction vial, *N*-methylmaleimide (2 equiv) was added to diene **2.17c** in DCE (0.2M). The mixture was stirred at 60˚C overnight and purified by flash chromatography. Tetracycle **2.21b** was formed in 79% yield (0.056 g).

^{1}H NMR (400 MHz, $CDCl_3$) δ = 7.40 – 7.27 (m, 3H), 7.25 – 7.19 (m, 2H), 5.75 (t, *J* = 3.4 Hz, 1H), 4.46 (ddd, *J* = 8.7, 7.4, 2.6 Hz, 2H), 4.25 (td, *J* = 11.2, 3.4 Hz, 1H), 4.15 – 4.00 (m, 2H), 3.60 (ddd, *J* = 6.3, 4.2, 1.5 Hz, 1H), 3.26 (dd, *J* = 8.4, 6.5 Hz, 1H), 3.15 (dd, *J* = 8.4, 6.2 Hz, 1H), 2.86 (s, 1H), 2.82 (s, 3H), 2.69 (td, *J* = 14.0, 6.0 Hz, 1H), 2.53 (ddd, *J* = 12.4, 8.2, 3.9 Hz, 1H), 2.31 (tt, *J* = 15.6, 3.6 Hz, 2H), 2.20 – 2.05 (m, 3H), 1.79 (tdd, *J* = 13.3, 11.4, 4.1 Hz, 1H), 1.50 (dt, *J* = 7.6, 3.7 Hz, 1H), 1.20 (s, 3H); **^{13}C NMR** (101 MHz, $CDCl_3$) δ = 210.0, 178.1, 176.0, 174.9, 153.6, 142.8, 138.8, 128.9, 128.4, 127.3, 126.5, 62.1, 53.2, 46.4, 46.4, 43.8, 42.9, 42.4, 41.9, 37.4, 32.4, 29.5, 25.0, 24.6, 22.2, 19.9; **IR** (neat, cm^{-1}): 2949.0, 2364.5, 1774.2, 1698.4, 1386.7, 1220.4; **HRMS** (ESI): m/z calc'd for $C_{28}H_{30}N_2O_6$ $[M]^+$ = 490.2104, found $[M]^+$ = 490.2096.

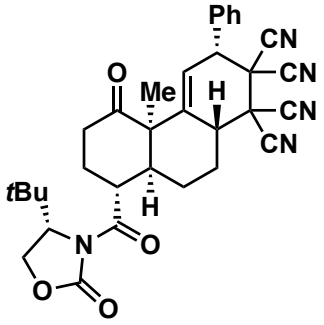

Tricycle 2.21c

Synthesized according to **general procedure 5** using oxazolidinone dienophile **2.38b** and diene **2.12a** for the first DA step, and tetracyanoethylene and reacting at room temperature for 18 h for the final DA step, yielding 46% (0.039 g) of **2.21c** as a sole diastereoisomer and as an off-white solid**.**

^{1}H NMR (400 MHz, $CDCl_3$) δ 7.56–7.38 (m, 5H), 5.79–5.69 (m, 1H), 4.53 (dd, *J* = 7.7, 1.6 Hz, 1H), 4.44–4.35 (m, 2H), 4.31 (dd, *J* = 9.4, 7.7 Hz, 1H), 3.61–3.51 (m, 1H), 3.29–3.11 (m, 2H), 2.63–2.52 (m, 1H), 2.47–2.29 (m, 4H), 2.31–2.10 (m, 2H), 1.79–1.66 (m, 1H), 1.53 (s, 3H), 1.03 (s, 9H); **^{13}C NMR** (101 MHz, $CDCl_3$) δ 211.6, 175.9, 154.7, 140.7, 133.7, 130.2, 129.5, 129.4, 120.1, 111.2, 111.0, 110.1, 110.0, 65.8, 61.8, 56.2, 49.0, 46.8, 43.6, 42.8, 42.0, 42.0, 35.8, 35.7, 31.2, 29.4, 25.9, 24.7, 23.9, 23.3; **IR** (neat, cm^{-1}):

2925.7, 2361.7, 2339.8, 1774.3, 1707.6; **LRMS** (APCI-): calc'd for $C_{33}H_{32}N_5O_3$ $[M-H]^+$ = 562.2, found $[M-H]^+$ = 562.3; **Optical Rotation:** $[\alpha]_d^{24}$ = +139° (c 0.2, DCM).

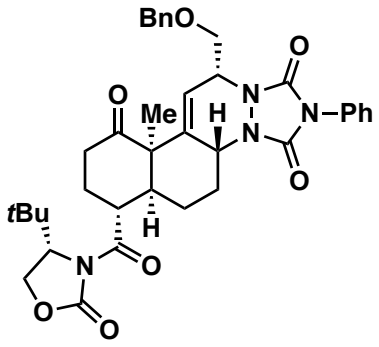

Tetracycle 2.21e

Synthesized according to **general procedure 5** using oxazolidinone dienophile **2.38b** and diene **2.12d** for the first DA step, and using 4-Phenyl-1,2,4-triazoline-3,5-dione and reacting at room temperature for 18 h for the final DA step, yielding 39% of **2.21e** as a sole diastereoisomer and as a white foam**.**

^{1}H NMR (400 MHz, $CDCl_3$) δ 7.52–7.41 (m, 4H), 7.39–7.23 (m, 6H), 5.81–5.75 (m, 1H), 4.77–4.69 (m, 1H), 4.63–4.49 (m, 3H), 4.39–4.24 (m, 3H), 3.92 (dd, *J* = 9.8, 5.0 Hz, 1H), 3.79 (dd, *J* = 9.8, 6.0 Hz, 1H), 3.53–3.47 (m, 1H), 3.24–3.11 (m, 1H), 2.73 (dq, *J* = 12.0, 3.8 Hz, 1H), 2.53–2.43 (m, 1H), 2.42–2.29 (m, 2H), 2.28–2.11 (m, 2H), 1.80–1.64 (m, 1H), 1.62–1.47 (m, 1H), 1.52 (s, 3H), 1.00 (s, 9H); **^{13}C NMR** (101 MHz, $CDCl_3$) δ 212.3, 176.5, 154.9, 151.7, 151.1, 139.5, 137.9, 131.5, 129.2, 128.6, 128.1, 127.9, 127.6, 125.7, 118.2, 73.4, 69.9, 65.8, 61.9, 55.7, 54.6, 53.4, 49.4, 42.3, 36.0, 35.8, 31.6, 29.7, 26.0, 23.8, 23.6; **IR** (neat, cm^{-1}): 2962.4, 2859.4, 2360.0, 1777.1, 1708.7, 1420.7; **HRMS** (EI): m/z calc'd for $C_{37}H_{43}N_4O_7$ $[M]^+$ = 654.3053, found $[M]^+$ = 654.3075; **Optical Rotation:** $[\alpha]_d^{24}$ = +11° (c 0.4, DCM).

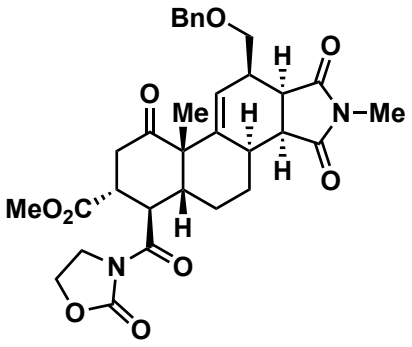

Tetracycle 2.21i

Synthesized according to **general procedure 5** using oxazolidinone dienophile **2.38f** and diene **2.12d** for the first DA step, and using *N*-methylmaleimide and reacting at 50˚C for 48 h for the final DA step, yielding 43% (0.038 g) of **2.21i** as a 9:1 mixture of diastereoisomers and as a white foam**.**

^{1}H NMR (400 MHz, $CDCl_3$) δ 7.32 (d, *J* = 3.4 Hz, 4H), 7.29–7.25 (m, 1H), 5.17 (t, *J* = 3.3 Hz, 1H), 4.62–4.36 (m, 5H), 4.13–4.01 (m, 2H), 3.97 (dd, *J* = 9.2, 7.2 Hz, 1H), 3.71 (dd, *J* = 9.2, 7.9 Hz, 1H), 3.61 (s, 3H), 3.17 (dd, *J* = 8.5, 6.1 Hz, 1H), 3.09 (td, *J* = 10.9, 5.5 Hz, 1H), 3.05 (s, 1H), 2.84 (t, *J* = 14.1 Hz, 1H), 2.82 (s, 3H), 2.72 (d, *J* = 6.8 Hz, 1H), 2.66 (dd, *J* = 14.2, 4.3 Hz, 1H), 2.58–2.43 (m, 2H), 2.14 (m, *J* = 11.2, 3.6 Hz, 2H), 2.02–1.92 (m, 1H), 1.41 (ddd, *J* = 13.6, 7.0, 3.4 Hz, 1H), 1.04 (s, 3H); **^{13}C NMR** (101 MHz, $CDCl_3$) δ 207.7, 178.4, 176.9, 175.0, 172.0, 153.7, 141.3, 138.1, 128.3, 127.8, 127.6, 126.4, 73.3, 69.9, 61.8, 52.5, 52.3, 46.2, 45.9, 44.3, 42.9, 42.4, 41.3, 38.8, 37.5, 31.4, 24.4, 23.9, 21.0, 18.5; **IR** (neat, cm^{-1}): 2928.3, 1776.8, 1697.1, 1385.1, 1219.6; **HRMS** (ESI): m/z calc'd for $C_{32}H_{36}N_2O_9Na$ [M+Na] = 615.2318, found [M+Na] = 615.2329.

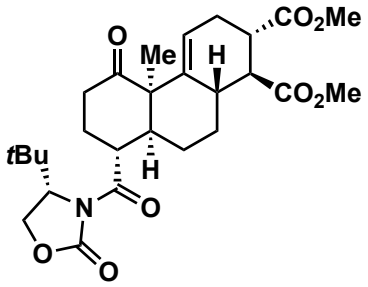

Tricycle 2.21k

Synthesized according to **general procedure 5** using oxazolidinone dienophile **2.38b** and diene **2.12c** for the first DA step, and using dimethyl fumarate and reacting at 50˚C for 48 hours for the final DA step, yielding 37% (0.029 g) of **2.21k** as a 3:1 mixture of diastereoisomers and as a white foam**.**

^{1}H NMR (400 MHz, $CDCl_3$) δ 5.45 (dt, *J* = 5.2, 2.2 Hz, 1H), 4.48 (dd, *J* = 7.6, 1.6 Hz, 1H), 4.32 (dd, *J* = 9.3, 1.6 Hz, 1H), 4.24 (dd, *J* = 9.3, 7.6 Hz, 1H), 3.91 (q, *J* = 6.6 Hz, 1H), 3.70 (s, 3H), 3.66 (s, 3H), 2.99 (td, *J* = 11.7, 5.4 Hz, 1H), 2.72–2.60 (m, 2H), 2.55–2.41 (m, 2H), 2.40 (dd, *J* = 11.7, 10.1 Hz, 1H), 2.35–2.28 (m, 1H), 2.19 (dddd, *J* = 17.9, 11.7, 4.0, 2.3 Hz, 1H), 2.04 (qd, *J* = 8.6, 7.4, 3.6 Hz, 2H), 1.98–1.86 (m, 1H), 1.49 (ddt, *J* = 13.7, 10.7, 6.7 Hz, 1H), 1.37 (s, 3H), 1.36–1.23 (m, 2H), 0.97 (s, 9H); **^{13}C NMR** (101 MHz, $CDCl_3$) δ 211.5, 176.1, 174.9, 174.8, 154.6, 139.9, 121.3, 65.5, 61.7, 54.2, 52.1, 52.0, 50.1, 45.9, 44.1, 41.9, 37.0, 36.6, 36.0, 28.7, 27.9, 27.0, 26.3, 26.0, 25.1; **IR** (neat, cm^{-1}): 2956.4, 2875.3, 1778.6, 1736.2, 1702.1; **HRMS** (ESI): m/z calc'd for $C_{27}H_{37}NO_8Na$ [M+Na] = 526.2417, found [M+Na] = 526.2437; **Optical Rotation:** $[\alpha]_d^{24}$ = +19^o (c 0.17, DCM).

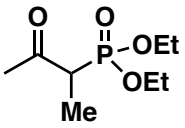

diethyl (3-oxobutan-2-yl)phosphonate 2.22a

Synthesized according to literature procedure.[87]

Spectral data in accordance with reported literature.[90]

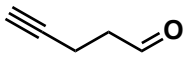

pent-4-yn-1-al 2.23

Adopted from literature procedure.[87]

To a flame-dried round-bottom flask under argon was added PCC (29.1 g, 135 mmol), 1 PCC mass equivalent of silica gel (29 g), and DCM (400 ml). Then pent-4-yn-1-ol (8.37 ml, 90 mmol) in DCM (200 ml) was added via addition funnel over 30 min and stirred at room temperature for 1h. The reaction mixture was filtered through a silica plug (~200 ml) and was eluded with DCM. The filtrate was collected and carefully rotary evaporated (low bath temperature at ~35˚C), yielding crude **2.23** as a clear oil, which was used without further purification. Spectral data in accordance with reported literature.[89]

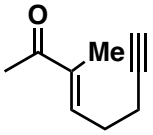

Terminal alkyne 2.24a

Synthesized according to **general procedure 1a** in 32% yield (4.91 g) over three steps. Characterized according to reported literature.[87]

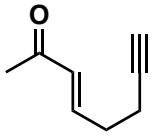

Terminal alkyne 2.24b

Synthesized according to **general procedure 1a** 71% (2.34 g) yield over two steps. Characterized according to reported literature.[87]

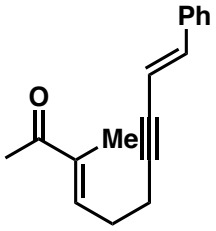

Enone 2.25a

Synthesized according to **general procedure 1b** from **2.24a** (1.50 g, 11.0 mmol), diisopropylamine (6.17 ml, 44.1 mmol), 2-bromovinylbenzene (4.74 g, 25.9 mmol), and $Pd(PPh_3)_4$ (0.318 g, 2.5 mol%) yielding **2.25a** in 74% (1.94 g).

^{1}H NMR (400 MHz, $CDCl_3$) δ 7.39–7.21 (m, 5H), 6.87 (d, *J* = 16.2 Hz, 1H), 6.68 (tt, *J* = 5.6, 1.3 Hz, 1H), 6.14 (dt, *J* = 16.3, 2.0 Hz, 1H), 2.56–2.47 (m, 4H), 2.33 (s, 3H), 1.83–1.78 (m, 3H); **^{13}C NMR** (101 MHz, $CDCl_3$) δ 199.7, 141.1, 140.7, 138.7, 136.4, 128.7, 128.5, 126.1, 108.4, 91.1, 80.7, 28.4, 25.5, 19.1, 11.4; **IR** (neat, cm^{-1}): 3027.0, 2962.1, 2924.8, 1664.7; **HRMS** (EI): m/z calc'd for $C_{17}H_{18}O$ $[M]^+$ = 238.1358, found $[M]^+$ = 238.1325.

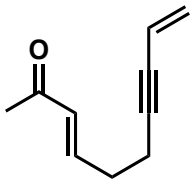

Enone 2.25b

Synthesized according to **general procedure 1b** from **2.24b** (2.477 g, 16.22 mmol), diisopropylamine (11.37 ml, 81 mmol), vinyl bromide 1.0 M in THF (48.7 ml, 48.7 mmol), and $Pd(PPh_3)_4$ (0.937 g, 5 mol%) as a clear oil in 69% yield (1.655 g).

^{1}H NMR (400 MHz, $CDCl_3$) δ 6.89–6.72 (m, 1H), 6.13 (dt, *J* = 16.0, 1.4 Hz, 1H), 5.76 (ddt, *J* = 17.5, 11.0, 1.9 Hz, 1H), 5.62–5.47 (m, 1H), 5.40 (dd, *J* = 11.0, 2.2 Hz, 1H), 2.52–2.41 (m, 4H), 2.26 (s, 3H); **^{13}C NMR** (101 MHz, $CDCl_3$) δ 198.6, 145.8, 132.3, 126.4, 117.4, 89.0, 80.6, 31.6, 27.1, 18.5; **IR** (neat, cm^{-1}): 2920.0, 1671.1, 1626.1; **HRMS** (EI): m/z calc'd for $C_{10}H_{12}O$ $[M-H]^+$ = 147.0810, found $[M-H]^+$ = 147.0825.

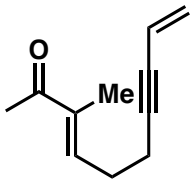

Enone 2.25c

Synthesized according to **general procedure 1b** from **2.24a** (0.300 g, 2.20 mmol), diisopropylamine (1.54 ml, 11.0 mmol), vinyl bromide 1M in THF (6.61 ml, 6.61 mmol), and $Pd(PPh_3)_4$ (0.064 g, 2.5 mol%) as an orange oil in 63% yield (0.226 g).

^{1}H NMR (400 MHz, $CDCl_3$) δ 6.71–6.61 (m, 1H), 5.77 (ddt, J = 17.5, 11.0, 2.1 Hz, 1H), 5.56 (dd, J = 17.5, 2.2 Hz, 1H), 5.41 (dd, J = 11.0, 2.2 Hz, 1H), 2.53–2.44 (m, 4H), 2.32 (s, 3H), 1.79 (d, J = 1.2 Hz, 3H); **^{13}C NMR** (101 MHz, $CDCl_3$) δ 199.9, 141.1, 138.9, 126.3, 117.4, 89.4, 80.3, 28.4, 25.6, 18.8, 11.4; **IR** (neat, cm^{-1}): 2924.0, 1665.7; **HRMS** (EI): m/z calc'd for $C_{11}H_{13}O$ $[M-H]^+$ = 161.0961, found $[M-H]^+$ = 161.0968.

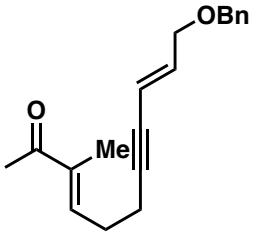

Enone 2.25d

Synthesized according to **general procedure 1b** from **2.24a** (0.219 g, 1.61 mmol), diisopropylamine (1.12 ml , 44.1 mmol), (E)-(((3-bromoallyl)oxy)methyl)benzene (0.729 g, 3.21 mmol), and $Pd(PPh_3)_4$ (0.093 g, 2.5 mol%) as a clear oil in 57% yield (0.260 g).

^{1}H NMR (400 MHz, $CDCl_3$) δ 7.40–7.25 (m, 5H), 6.69 – 6.63 (m, 1H), 6.14 (dt, *J* = 15.9, 5.6 Hz, 1H), 5.78–5.71 (m, 1H), 4.52 (s, 2H), 4.05 (dd, *J* = 5.6, 1.7 Hz, 2H), 2.53–2.45 (m, 4H), 2.32 (s, 3H), 1.83–1.77 (m, 3H); **^{13}C NMR** (101 MHz, $CDCl_3$) δ 199.9, 141.2, 138.8, 138.7, 138.2, 128.6, 127.8, 127.8, 112.1, 89.5, 79.5, 72.4, 70.0, 28.4, 25.6, 18.9, 11.5; **IR** (neat, cm^{-1}): 2927.4, 2360.6, 2341.3, 1666.9; **HRMS** (ESI): m/z calc'd for $C_{19}H_{22}O_2Na$ $[M+Na]^+$ = 305.1517, found $[M+Na]^+$ = 305.1519.

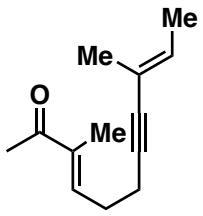

Enone 2.25e

Synthesized according to **general procedure 1b** from ketone **2.24a** (0.150 g, 1.10 mmol), diethylamine (0.570 ml, 5.50 mmol), (E)-2-Bromo-2-butene (0.340 ml, 3.30 mmol), and $Pd(PPh_3)_4$ (0.064 g, 5 mol%) as an orange oil in 30% yield (0.063 g).

^{1}H NMR (400 MHz, $CDCl_3$) δ 6.69–6.59 (m, 1H), 5.78 (m, 1H), 2.43 (d, *J* = 3.3 Hz, 4H), 2.28 (s, 3H), 1.79–1.72 (m, 3H), 1.74–1.68 (m, 3H), 1.62 (m, 3H); **^{13}C NMR** (101 MHz, $CDCl_3$) δ 199.7, 141.5, 138.6, 131.4, 118.5, 84.6, 84.5, 28.6, 25.5, 18.7, 17.1, 14.0, 11.3; **IR** (neat, cm^{-1}): 2920.6, 2858.9, 1667.1, 1644.2, 1432.0; **HRMS** (EI): m/z calc'd for $C_{12}H_{15}O$ $[M\text{-}H\text{-}Me]^+$ = 175.1117, found $[M\text{-}H\text{-}Me]^+$ = 175.1108

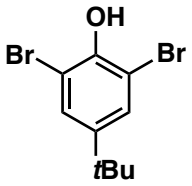

2.31s1

Synthesized according to literature procedure.[90]

Spectral data in accordance with reported literature.[91]

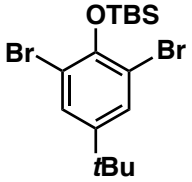

2.31s2b

Synthesized according to **general procedure 2a.** Used directly in **general procedure 2b** for the formation of salicylaldehyde **2.31s3b**.

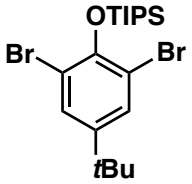

2.31s2c

Synthesized according to **general procedure 2a** in 82% yield (3.08 g).

Spectral data in accordance with reported literature.[88]

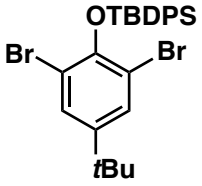

2.31s2d

Synthesized according to **general procedure 2a.** Used directly in **general procedure 2b** for the formation of salicylaldehyde **2.31s3d**.

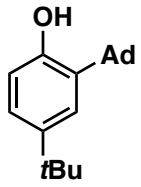

2.31s2e

Synthesized according to literature procedure.[91]

Spectral data in accordance with reported literature.[92]

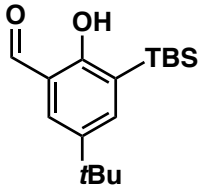

2.31s3b

Synthesized according to **general procedure 2b** in 49% yield over 2 steps (1.26 g).

Spectral data in accordance with reported literature.[88]

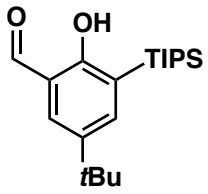

2.31s3c

Synthesized according to **general procedure 2b** in 62% yield (1.38 g).

Spectral data in accordance with reported literature.[88]

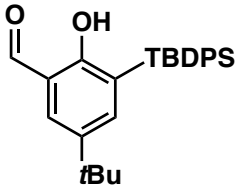

2.31s3d

Synthesized according to **general procedure 2b** in 31% yield over 2 steps (1.05 g).

Spectral data in accordance with reported literature.[88]

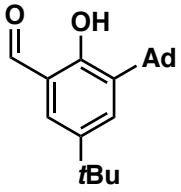

2.31s3e

Synthesized and characterized according to reported literature.[92]

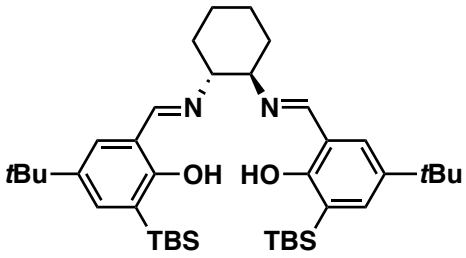

Silyl salen ligand 2.31s4b

Synthesized in accordance to **general procedure 2c** in 79% yield (0.461 g).

Spectral data in accordance with reported literature.[88]

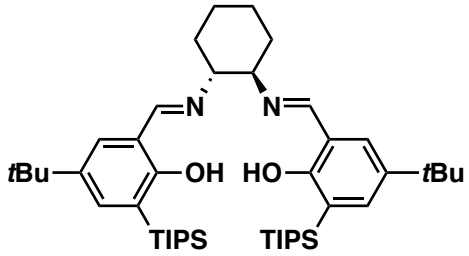

Silyl salen ligand 2.31s4c

Synthesized in accordance to **general procedure 2c** in 93% yield (0.416 g).

Spectral data in accordance with reported literature.[88]

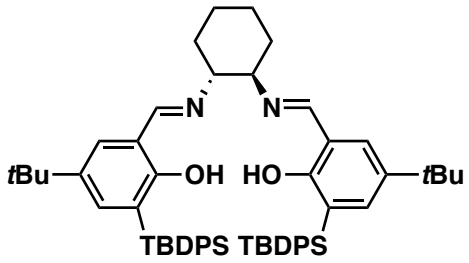

Silyl salen ligand 2.31s4d

Synthesized in accordance to **general procedure 2c** in 76% yield (0.333 g).

Spectral data in accordance with reported literature.[88]

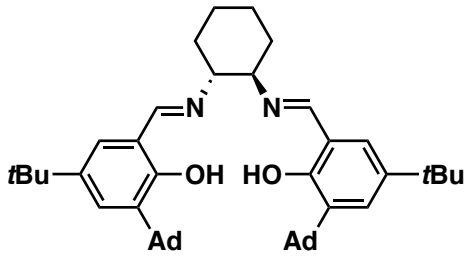

Adamantyl salen ligand 2.31s4e

Synthesized in accordance to **general procedure 2c** in 67% yield (0.183 g).

Spectral data in accordance with reported literature.[95]

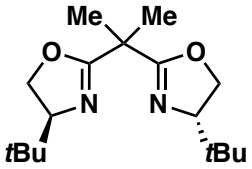

Chiral BOX ligand 2.37b

Synthesized and characterized according to reported literature.[96]

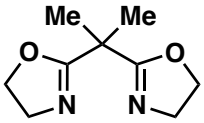

Achiral BOX ligand 2.37d

Synthesized and characterized according to reported literature.[97]

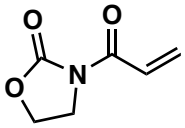

Dienophile 2.38a

Synthesized and characterized according to reported literature.[98–99]

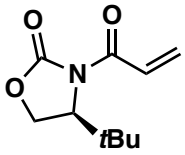

Dienophile 2.38b

Synthesized and characterized according to reported literature.[100]

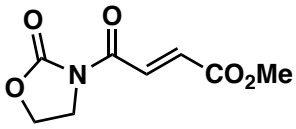

Dienophile 2.38f

Synthesized according to **general procedure 4** from mono-methyl fumarate (15.4 mmol), and reacting for 48 h, in 90% yield (2.76 g).

Spectral data in accordance with reported literature.[98]

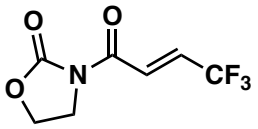

Dienophile 2.38g

Synthesized according to **general procedure 4** from (E)-4,4,4-trifluorobut-2-enoic acid (1.43 mmol) and reacting for 72 h, in 76% yield (0.228 g).

Spectral data in accordance with reported literature.[101]

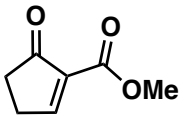

Dienophile 2.38h

Synthesized and characterized according to reported literature.[102]

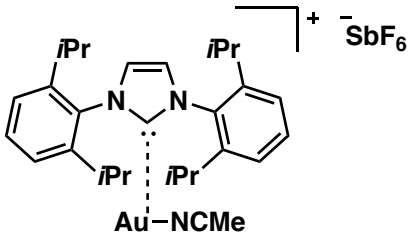

[L²AuNCMe]SbF₆ (L² = IPr)

Synthesized and characterized according to reported literature.[103]

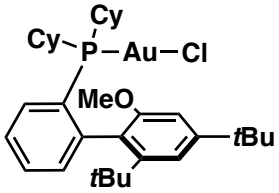

L⁵AuCl (L⁵ = VPhos)

Synthesized according to **general procedure 3a** in >95% yield (0.390 g).

¹H NMR (400 MHz, $CDCl_3$) δ 7.54–7.38 (m, 3H), 7.35 (d, *J* = 1.7 Hz, 1H), 7.31 (ddd, *J* = 6.8, 3.3, 1.6 Hz, 1H), 6.77 (d, *J* = 1.7 Hz, 1H), 3.61 (s, 3H), 2.41 (q, *J* = 11.6, 11.1 Hz, 1H), 2.16–1.93 (m, 4H), 1.91–1.61 (m, 8H), 1.43 (s, 9H), 1.43–1.23 (m, 6H), 1.15 (s, 12H);

^{13}C NMR (101 MHz, $CDCl_3$) δ 156.2, 152.4, 147.7, 146.5, 146.4, 134.2, 134.1, 131.3, 131.2, 129.9, 129.9, 128.9, 128.3, 126.8, 126.7, 125.6, 125.6, 119.2, 104.8, 55.0, 53.4, 38.2, 37.9, 37.3, 35.2, 34.0, 34.0, 33.7, 33.5, 31.6, 31.2, 31.2, 29.8, 29.8, 27.9, 27.8, 27.5, 27.4, 27.0, 27.0, 26.7, 26.6, 26.4, 26.2, 26.0, 26.0, 25.6, 25.6. (The observed complexity is due to the P–C splitting.); **^{31}P NMR** (121 MHz, $CDCl_3$) δ 34.43; **IR** (neat, cm^{-1}): 2929.4, 2854.3, 2360.7, 2342.3; **HRMS** (ESI): m/z calc'd for $C_{33}H_{49}AuOP$ $[M\text{-}Cl]^+$ = 689.3206, found $[M\text{-}Cl]^+$ = 689.3187.

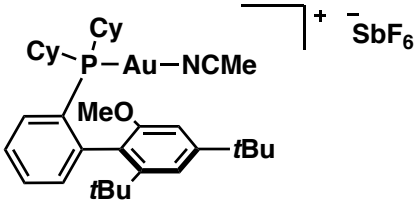

[L^{5}AuNCMe]SbF$_6$ (L^5 = VPhos)

Synthesized according to **general procedure 3b** in 78% yield (1.75 g) as a white solid.

^{1}H NMR (600 MHz, $CDCl_3$) δ 7.49–7.42 (m, 3H), 7.26 (d, *J* = 1.7 Hz, 1H), 7.22 (ddd, *J* = 7.8, 4.1, 1.8 Hz, 1H), 6.78 (d, *J* = 1.7 Hz, 1H), 3.58 (s, 3H), 2.47–2.37 (m, 1H), 2.31 (s, 3H), 2.06–1.90 (m, 4H), 1.90–1.77 (m, 3H), 1.77–1.70 (m, 1H), 1.70–1.56 (m, 3H), 1.58–1.46 (m, 1H), 1.42–1.24 (m, 14H), 1.21–1.07 (m, 4H), 1.05 (s, 9H); **^{13}C NMR** (151 MHz, $CDCl_3$) δ 156.9, 152.7, 148.8, 145.7, 145.6, 134.2, 134.2, 131.3, 131.3, 131.0, 127.7, 127.6, 126.5, 126.1, 126.0, 126.0, 119.6, 118.6, 105.3, 55.3, 38.4, 38.2, 37.6, 35.4, 34.4, 34.3, 33.8, 33.7, 33.6, 33.5, 31.8, 31.6, 31.6, 30.4, 27.9, 27.8, 27.4, 27.4, 27.0, 26.9, 26.7, 26.6, 26.4, 26.3, 25.8, 25.5, 2.7. (The observed complexity is due to the P–C splitting.); **^{31}P NMR** (121 MHz, $CDCl_3$) δ 31.60; **IR** (neat, cm^{-1}): 2934.2, 2858.0, 1602.3, 1560.5, 1450.3, 1405.1; **HRMS** (ESI) m/z calc'd for $C_{35}H_{52}AuNOP$ $[M\text{-}SbF_6]^+$ = 730.3452, found $[M\text{-}SbF_6]^+$ = 730.3474.

5.4 General procedures chapter 3

General procedure 8: Synthesis of alkyl bromide starting material

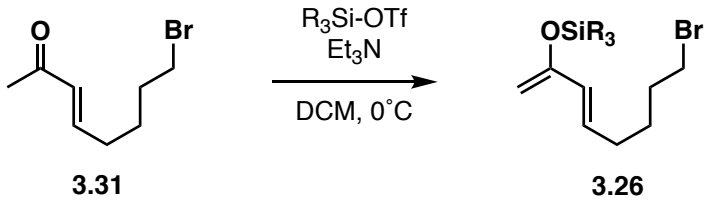

Scheme 5.13. *Synthesis of diene starting material **3.26**.*

To a flame-dried RBF under argon was added **3.31** (2.5 mmol), DCM (12.5 ml) and triethylamine (5.0 mmol). Then, R_3SiOTf (2.5 mmol) was added at 0˚C. The mixture was stirred at 0˚C for 1 h, then quenched with sat. $NaHCO_3$. The layers were separated and the organic phase collected. The aqueous phase was back-extracted with DCM. Combined organic layers were dried with $MgSO_4$, filtered, and concentrated *in vacuo*. The crude product was added to a basicified silica gel column and eluted with 1% TEA in hexanes, yielding **3.26**.

5.5 Characterization chapter 3

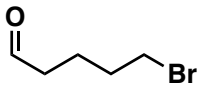

Aldehyde 3.30

Adopted from literature procedure.[104]

DIBAL-H (25% w/w in hexanes, 62.5 mmol) was added dropwise to a solution of ethyl 5-bromovalerate (50 mmol) in PhMe (250 ml) at -78˚C. The reaction remained at -78˚C and was stirred for 2 h before being quenched by addition of aq. HCl (5%). The mixture was allowed to warm to rt and stirred vigorously for 1 h. The layers were separated and the organic phase was washed with water, dried ($MgSO_4$) and concentrated *in vacuo*. The crude aldehyde was used in the next step without further purification. Spectral data in accordance with reported literature.[105]

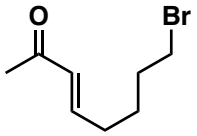

Enone 3.31

Adopted from literature procedure.[87]

To a solution of diethyl (2-oxopropyl)phosphonate in THF (115 ml) was added a solution of potassium carbonate (22.0 g, 160 mmol) in water (57 ml), and crude 5-bromopentanal (**3.30**). The mixture was then heated overnight at 80°C with vigorous stirring. The product was extracted with ethyl acetate, and the combined organic layers were dried over sodium sulfate and evaporated. The crude product was purified by flash chromatography isolating enone **3.31** in 80% yield (0.512 g).

^{1}H NMR (400 MHz, $CDCl_3$) δ 6.75 (dt, *J* = 15.5, 6.8 Hz, 1H), 6.06 (ddd, *J* = 15.9, 2.3, 1.3 Hz, 1H), 3.39 (t, *J* = 6.7 Hz, 2H), 2.28 – 2.19 (m, 5H), 1.86 (quint, *J* = 6.6 Hz, 2H), 1.61 (quint, *J* = 7.4 Hz, 2H); **^{13}C NMR** (101 MHz, $CDCl_3$) δ 198.46, 147.20, 131.75, 33.26, 32.12, 31.52, 27.02, 26.63; **IR** (neat, cm^{-1}): 3005.1, 2937.2, 2863.3, 1697.4, 1671.8,

1671.5, 1625.8, 1359.6, 1251.7, 976.3, 732.4; **HRMS** (EI): m/z calc'd for $C_8H_{13}BrO$ $[M]^+$= 204.0150, found mass 204.0153.

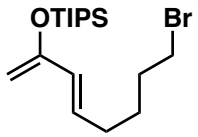

Diene 3.26a

Prepared according to **general procedure 8** in >95% yield (3.376 g).

^{1}H NMR (400 MHz, $CDCl_3$) δ 6.04 (dt, *J* = 15.2, 6.9 Hz, 1H), 5.88 (dt, *J* = 15.2, 1.4 Hz, 1H), 4.20 (d, *J* = 20.4 Hz, 2H), 3.41 (t, *J* = 6.8 Hz, 2H), 2.14 (qd, *J* = 7.2, 1.3 Hz, 2H), 1.88 (dt, *J* = 14.8, 6.8 Hz, 2H), 1.56 (quint, *J* = 7.5 Hz, 2H), 1.29 – 1.18 (m, 3H), 1.11 (d, *J* = 7.2 Hz, 18H); **^{13}C NMR** (101 MHz, $CDCl_3$) δ 155.3, 130.7, 128.7, 93.4, 33.8, 32.4, 31.3, 27.8, 18.2, 13.0; **IR** (neat, cm^{-1}): 2942.7, 2893.7, 2866.5, 1589.0, 1463.4, 677.5; **HRMS** (EI): m/z calc'd for $C_{17}H_{33}BrOSi$ $[M]^+$= 360.1484, found mass = 360.1497.

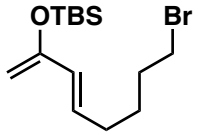

Diene 3.26b

Prepared according to **general procedure 8** in 87% yield (1.81 g).

^{1}H NMR (400 MHz, $CDCl_3$) δ 6.02 – 5.84 (m, 2H), 4.24 – 4.18 (m, 2H), 3.41 (t, *J* = 6.8 Hz, 2H), 2.13 (quint, *J* = 7.1 Hz, 2H), 1.92 – 1.82 (m, 2H), 1.60 – 1.50 (m, 2H), 0.97 (s, 9H), 0.17 (s, 6H); **^{13}C NMR** (101 MHz, $CDCl_3$) δ 155.1, 130.8, 128.6, 94.3, 33.8, 32.4, 31.3, 27.8, 26.0, 18.5, -4.5; **IR** (neat, cm^{-1}): 2930.2, 2857.5, 1591.8, 692.0; **HRMS** (EI): m/z calc'd for $C_{14}H_{27}BrOSi$ $[M]^+$= 318.1015, found mass 318.1006.

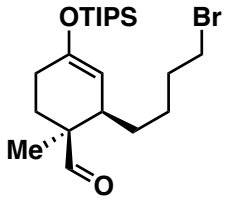

Silyl enol ether 3.27a

To an oven dried reaction tube was added diene **3.26a** (0.2 mmol), methacrolein (1 mmol), Co(III) catalyst **2.31b** (0.002 mmol, 1 mol%) and DCM (2M). The reaction mixture was stirred overnight at room temperature and the solvent evaporated in vacuo. The crude product was purified by flash chromatography to yield **3.27a** in 88% yield (0.076 g), dr 6:1 (*endo*:*exo*).

^{1}H NMR (400 MHz, $CDCl_3$) δ 9.64 (s, 1H), 4.92 (d, *J* = 3.9 Hz, 1H), 3.38 (tq, *J* = 5.9, 3.1 Hz, 2H), 2.18–2.04 (m, 3H), 1.94–1.73 (m, 4H), 1.57 (tt, *J* = 15.7, 8.5 Hz, 2H), 1.46–1.28 (m, 2H), 1.26–1.11 (m, 3H), 1.11–0.99 (m, 21H); **^{13}C NMR** (101 MHz, $CDCl_3$) δ 206.6, 150.6, 104.2, 47.5, 41.3, 33.7, 32.8, 32.1, 27.3, 26.7, 26.4, 20.0, 18.1, 12.8; **IR** (neat, cm^{-1}): 2943.8, 2866.6, 1774.8, 1702.4, 677.3; **HRMS** (ESI) m/z calc'd for $C_{21}H_{39}BrO_2SiNa$ [M+Na] = 453.1800, found mass = 453.1777.

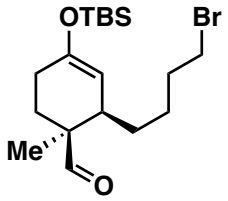

Silyl enol ether 3.27b

To an oven dried reaction tube was added diene **3.26b** (0.2 mmol), methacrolein (1 mmol), Co(III) catalyst **2.31b** (0.002 mmol, 1 mol%) and DCM (2M). The reaction mixture was stirred overnight at room temperature and the solvent evaporated in vacuo. The crude product was purified by flash chromatography to yield **3.27b** in 84% yield (0.065 g), dr 5:1 (*endo*:*exo*).

^{1}H NMR (400 MHz, $CDCl_3$) δ 9.64 (s, 1H), 4.96 – 4.87 (m, 1H), 3.39 (tq, *J* = 7.3, 3.2 Hz, 2H), 2.15–1.97 (m, 3H), 1.94–1.73 (m, 3H), 1.57 (m, 2H), 1.44–1.31 (m, 2H), 1.27–1.14

(m, 1H), 1.08 (d, *J* = 4.5 Hz, 3H), 0.93–0.87 (m, 9H), 0.13 (d, *J* = 5.1 Hz, 6H); **^{13}C NMR** (101 MHz, $CDCl_3$) δ 206.5, 150.5, 105.5, 47.5, 41.3, 33.7, 32.8, 32.0, 27.3, 26.7, 26.5, 25.8, 20.0, 18.1, -4.2; **IR** (neat, cm^{-1}): 2930.0, 2929.7, 2857.2, 1723.6, 1664.8j, 682.3; **HRMS** (EI): m/z calc'd for $C_{14}H_{24}BrO_2Si$ [M-*t*Bu]= 331.0729, found mass 331.0754.

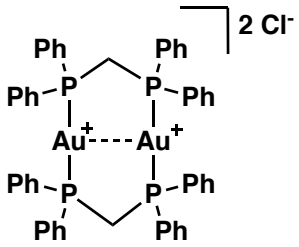

$[Au_2(\mu\text{-dppm})_2]Cl_2$

Synthesized and characterized according to reported literature.[106]

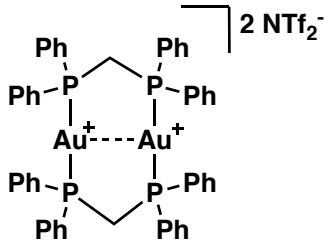

$[Au_2(\mu\text{-dppm})_2]NTf_2$

Synthesized and characterized according to reported literature.[106]

5.6 References:

[87] Han, Y.; Zhu, L.; Gao, Y.; Lee, C.-S. A Highly Convergent Cascade Cyclization to *cis*-Hydrindanes with All-Carbon Quaternary Centers and Its Application in the Synthesis of the Aglycon of Dendronobiloside A. *Org. Lett.* **2011**, *13* (4), 588–591.

[88] Thadani, A. V.; Huang, Y.; Rawal, V. H. Expedient, High-Yielding Synthesis of Silyl-Substituted Salen Ligands, *Org. Lett.* **2007**, *9* (20), 3873–3876.

[89] Ho, G.-J.; Mathre, D. J. Lithium-Initiated Imide Formation. A Simple Method for N-Acylation of 2-Oxazolidinones and Bornane-2,10-Sultam. *J. Org. Chem.* **1995**, *60* (7), 2271–2273.

[90] Lili, L.; Huang, W.; Chen, L.; Dong, J.; Ma, X.; Peng, Y. Silver-catalyzed oxidative C(sp^3)–P bond formation through C–C and P–H bond cleavage. *Angew. Chem., Int. Ed.* **2017**, *56* (35), 10539–10544.

[91] Phillips, E. M.; Mesganaw, T.; Patel, A.; Duttwyler, S.; Mercado, B. Q.; Houk, K. N.; Ellman, J. A. Synthesis of *ent*-ketorfanol [4] Thadani, A. V.; Huang, Y.; Rawal, V. H. Expedient, High-Yielding Synthesis of Silyl-Substituted Salen Ligands, *Org. Lett.* **2007**, *9* (20), 3873–3876.

[92] Ay, S.; Nieger, M.; Bräse, S. Co-metal-free enantioselective conjugate addition reactions of zinc reagents. *Chem. Eur. J.* **2008**, *14* (36), 11539–11556.

[93] Zeng, C.; Yuan, D.; Zhao, B.; Yao, Y. Highly enantioselective epoxidation of α,β-Unsaturated Ketones Catalyzed by Rare-Earth Amides $[(Me_3Si)_2N]_3RE(\mu\text{-}Cl)Li(THF)_3$ with Phenoxy-Functionalized Chiral Prolinols *Org. Lett.* **2015**, *17* (9), 2242–2245.

[94] Lam, F.; Chan, K.S. Synthesis of acyclic dinucleating Schiff base-pyridine and schiff base-phosphine ligands. *Tetrahedron. Lett.* **1995**, *36* (6), 919–922.

[95] Mehrkhodavandi, P.; Aluthge, D. D. Mononuclear salen indium catalysts and methods of manufacture and use thereof. US 2017/0137442 A1, May 18, 2017.

[96] Evans, D.; Peterson, G.; Johnson, J.; Barnes, D.; Campos, K.; Woerpel, K. An Improved Procedure for the Preparation of 2,2-Bis[2-[4(*S*)- *tert*-butyl-1,3-oxazolinyl]]propane [(*S,S*)-*tert*-Butylbis(oxazoline)] and Derived Copper(II) Complexes. *J. Org. Chem.* **1998**, *63* (13), 4541–4544.

[97] Paderes, M. C.; Chemler, S. R. Stereoselective Copper-Catalyzed Intramolecular Alkene Aminooxygenation: Effects of Substrate and Ligand Structure on Selectivity. *Eur. J. Org. Chem.* **2011**, *2011 (*20–21), 3679–3684.

[98] Knol, J.; Feringa, B. L. Direct Coupling Procedure for the Synthesis of N-Acyl-2-oxazolidinones Derived from α,β-Unsaturated Carboxylic Acids. *Synth. Commun.* **1996**, *26* (2), 261–268.

[99] Buzas, Andrea K.; Istrate, Florin M.; Gagosz, F. Gold-catalyzed rearrangements of propargylic *tert*-butyl carbonates. *Tetrahedron*, **2009**, *65* (9), 1889–1901.

[100] Cannizzaro, C. E.; Ashley, J. A.; Janda, K. D.; Houk, K, N. Experimental determination of the absolute enantioselectivity of an antibody-catalyzed diels-alder reaction and theoretical explorations of the origins of stereoselectivity. *J. Am. Chem. Soc.*, **2003**, *125* (9), 2489–2506.

[101] Harada, S.; Morikawa, T.; Nishida, A. Chiral Holmium Complex-Catalyzed Diels–Alder Reaction of Silyloxyvinylindoles: Stereoselective Synthesis of Hydrocarbazoles. *Org. Lett.,* **2013**, *15* (20), 5314–5317.

[102] Lebold, T. P.; Gallego, G. M.; Marth, C. J.; Sarpong, R. Synthesis of the Bridging Framework of Phragmalin-Type Limonoids. *Org. Lett.* **2012**, *14* (8), 2110–2113.

[103] de Frémont, P.; Marion, N.; Nolan, S. P. Cationic NHC–gold(I) Complexes: Synthesis, Isolation, and Catalytic Activity. *J. Org. Chem.* **2009**, *694* (4), 551–560.

[104] Paterson, I.; Coster, M. J.; Chen, D. Y.-K.; Aceña, J. L.; Bach, J.; Keown, L. E.; Trieselmann, T. The Stereocontrolled Total Synthesis of Altohyrtin A/Spongistatin 1: the Southern Hemisphere EF Segment. *Org. Biomol. Chem.* **2005**, *3* (13), 2420–2430.

[105] Pearson, W. H.; Hutta, D. A.; Fang, W.-K. Azidomercurations of Alkenes: Mercury-Promoted Schmidt Reactions. *J. Org. Chem.* **2000**, *65* (24), 8326–8332.

[106] Revol, G.; McCallum, T.; Morin, M.; Gagozs, F.; Barriault, L. Photoredox Transformations via Gold Dimeric Complexes. *Angew. Chem., Int. Ed.* **2013**, *52* (50), 13342–13345.

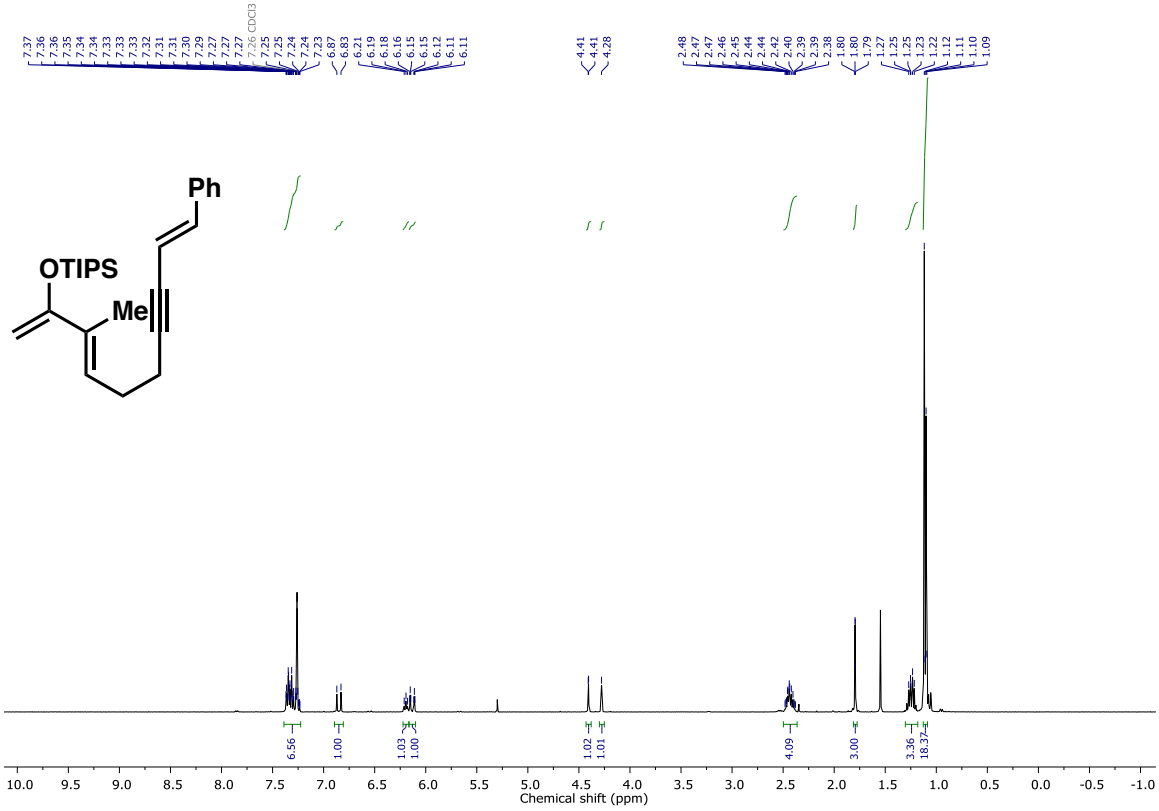
Ph
OTIPS
Me
Chemical shift (ppm)

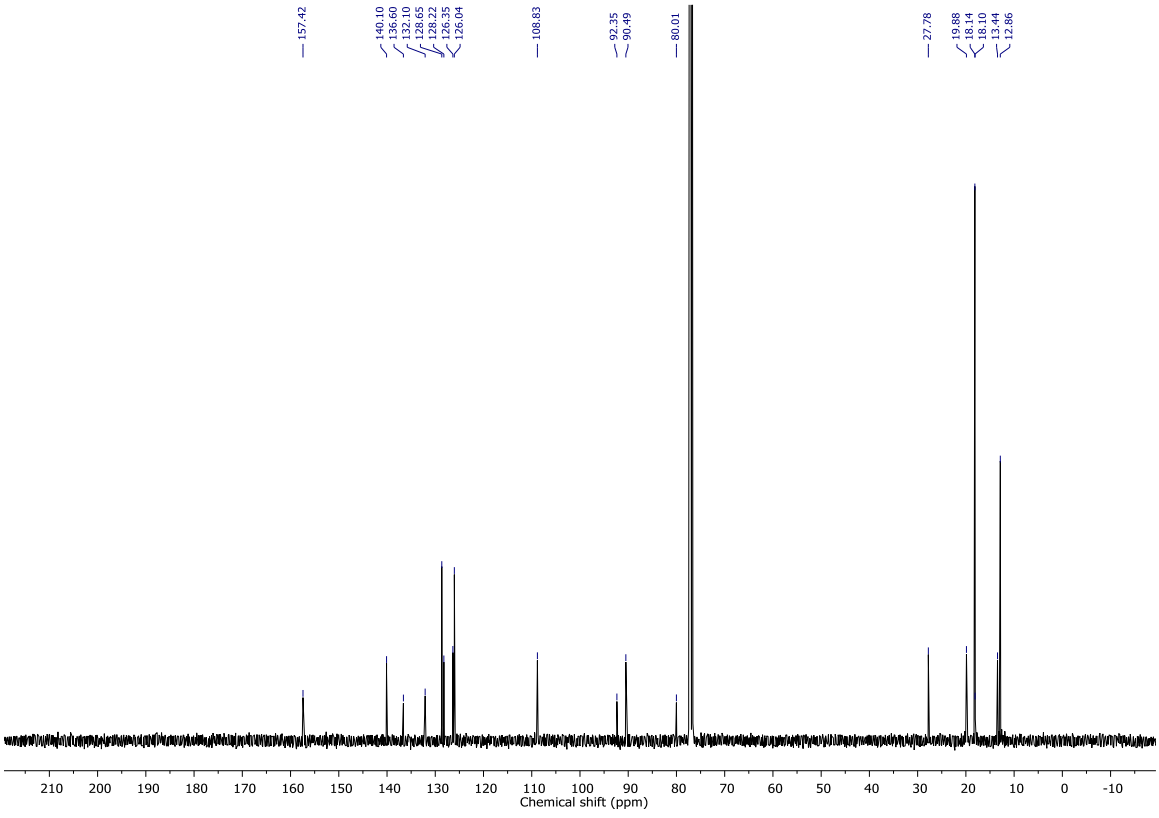
Chemical shift (ppm)

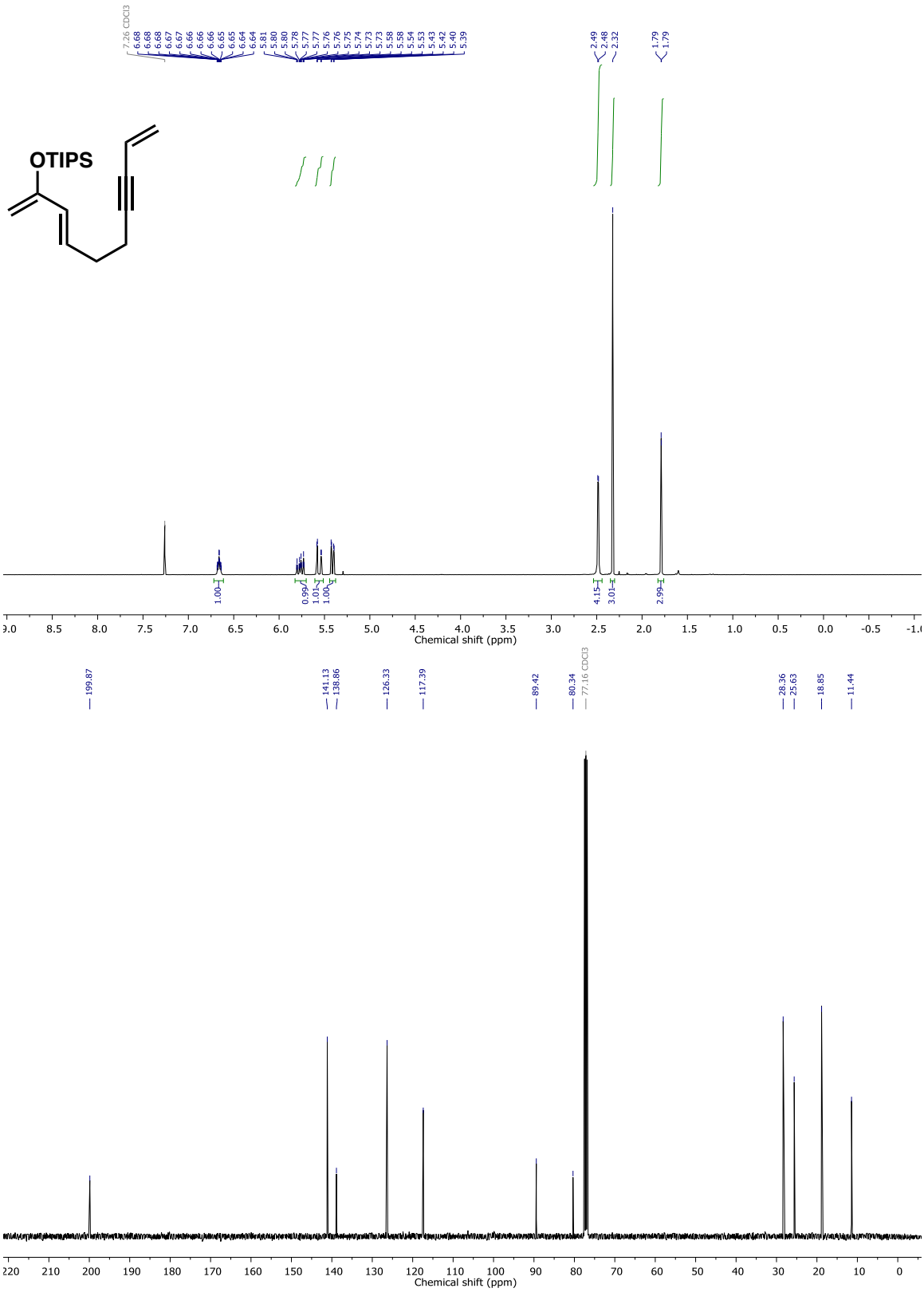
OTIPS
7.26 CDCl3
6.68
6.68
6.68
6.67
6.67
6.66
6.66
6.66
6.65
6.65
6.64
6.64
5.81
5.80
5.80
5.78
5.77
5.77
5.76
5.76
5.75
5.74
5.73
5.73
5.58
5.58
5.54
5.53
5.43
5.42
5.40
5.39
2.49
2.48
2.32
1.79
1.79
1.00
0.99
1.01
1.00
4.15
3.01
2.99
Chemical shift (ppm)
199.87
141.13
138.86
126.33
117.39
89.42
80.34
77.16 CDCl3
28.36
25.63
18.85
11.44
Chemical shift (ppm)

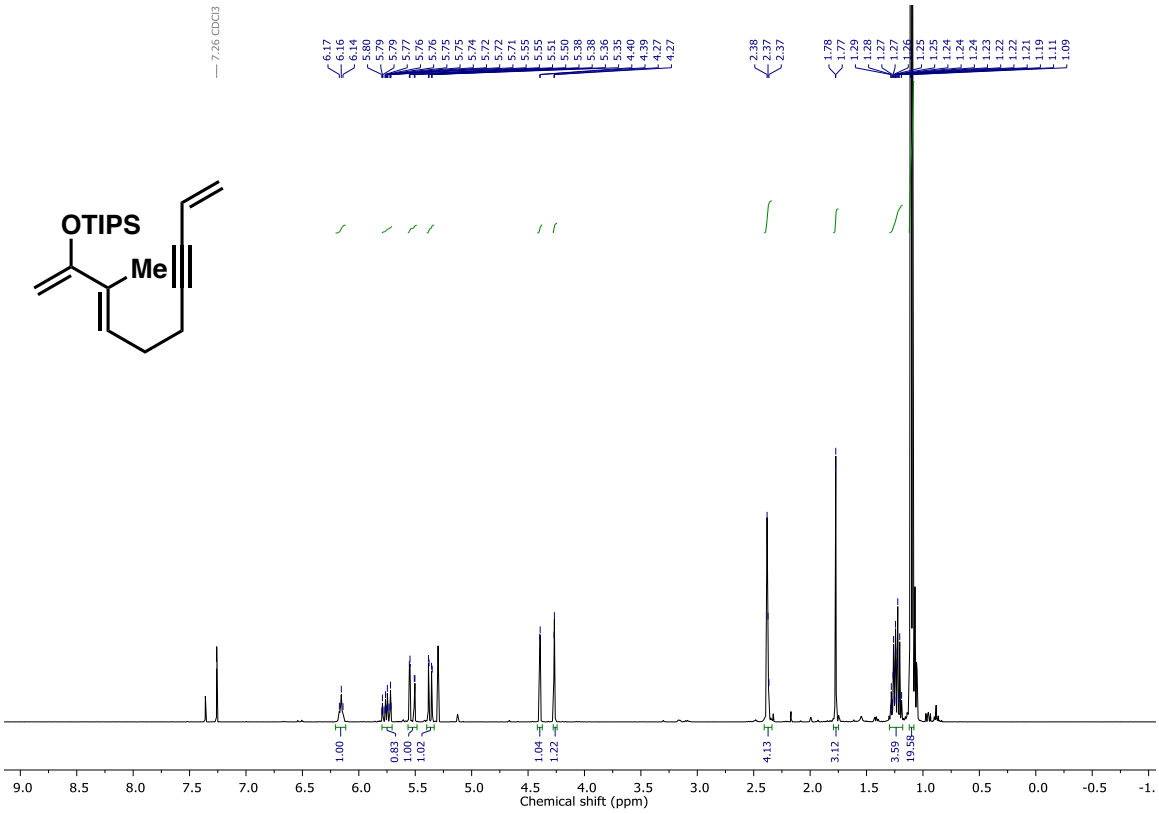
OTIPS
Me
7.26 CDCl3
6.17
6.16
6.14
5.80
5.79
5.79
5.77
5.76
5.76
5.75
5.75
5.74
5.72
5.72
5.71
5.55
5.55
5.51
5.50
5.38
5.38
5.36
5.35
4.40
4.39
4.27
4.27
4.27
2.38
2.37
2.37
1.78
1.77
1.29
1.28
1.27
1.27
1.26
1.25
1.25
1.24
1.24
1.24
1.23
1.22
1.22
1.21
1.19
1.11
1.09
1.00
0.83
1.00
1.02
1.04
1.22
4.13
3.12
3.59
19.58
Chemical shift (ppm)

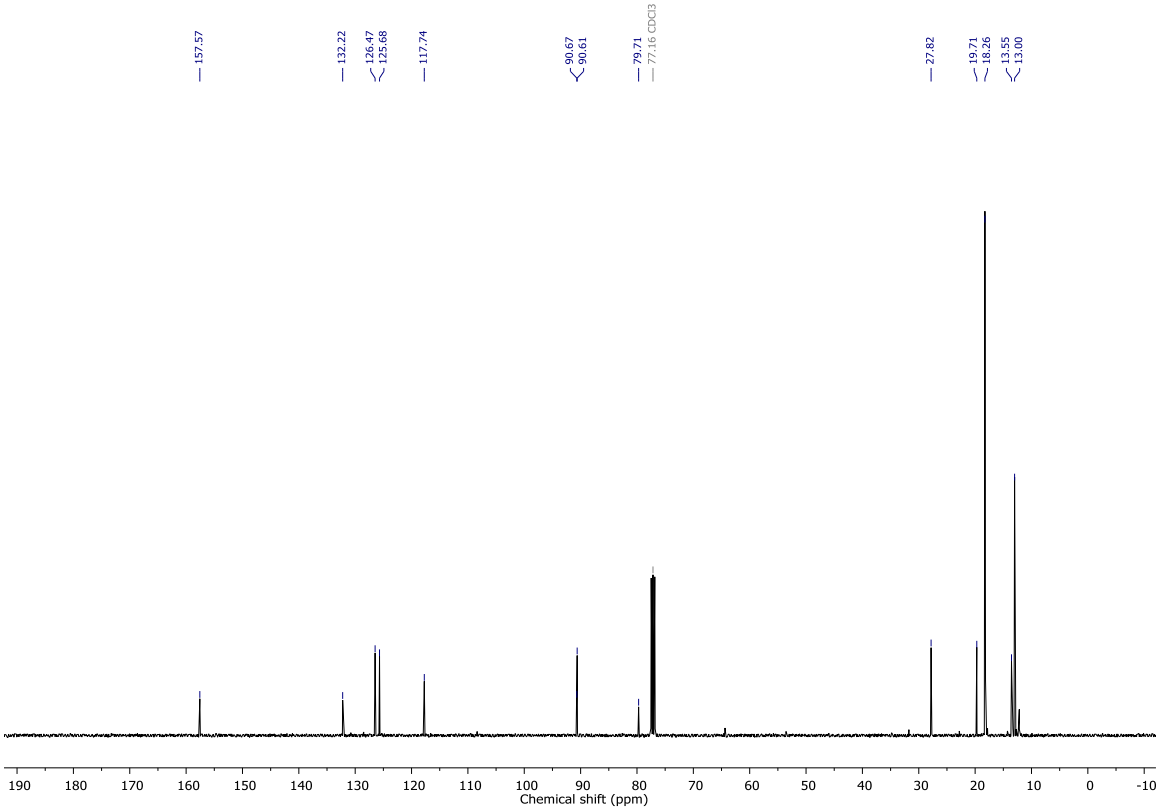
157.57
132.22
126.47
125.68
117.74
90.67
90.61
79.71
77.16 CDCl3
27.82
19.71
18.26
13.55
13.00
Chemical shift (ppm)

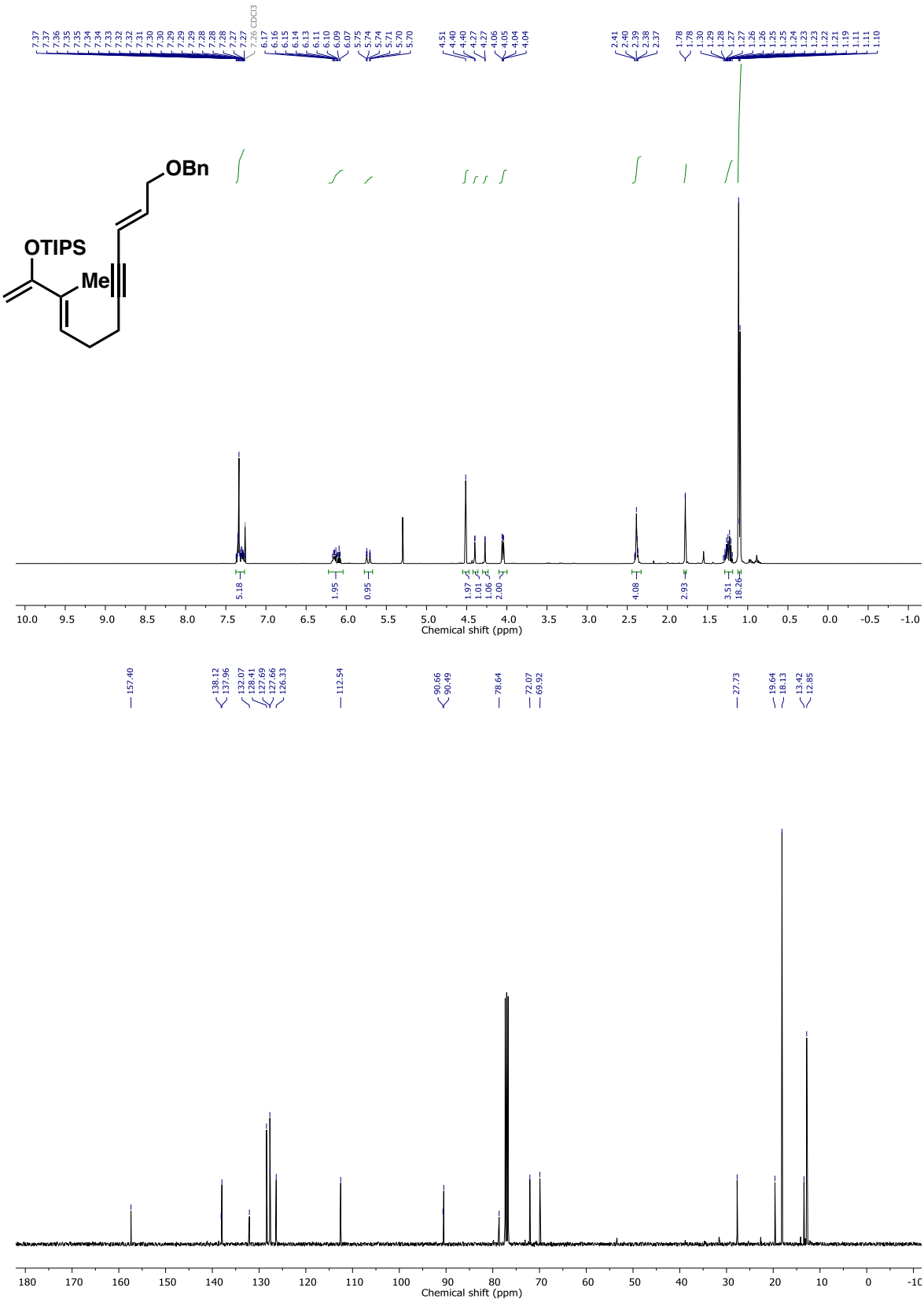
OBn
OTIPS
Me
CDCl3
Chemical shift (ppm)
Chemical shift (ppm)

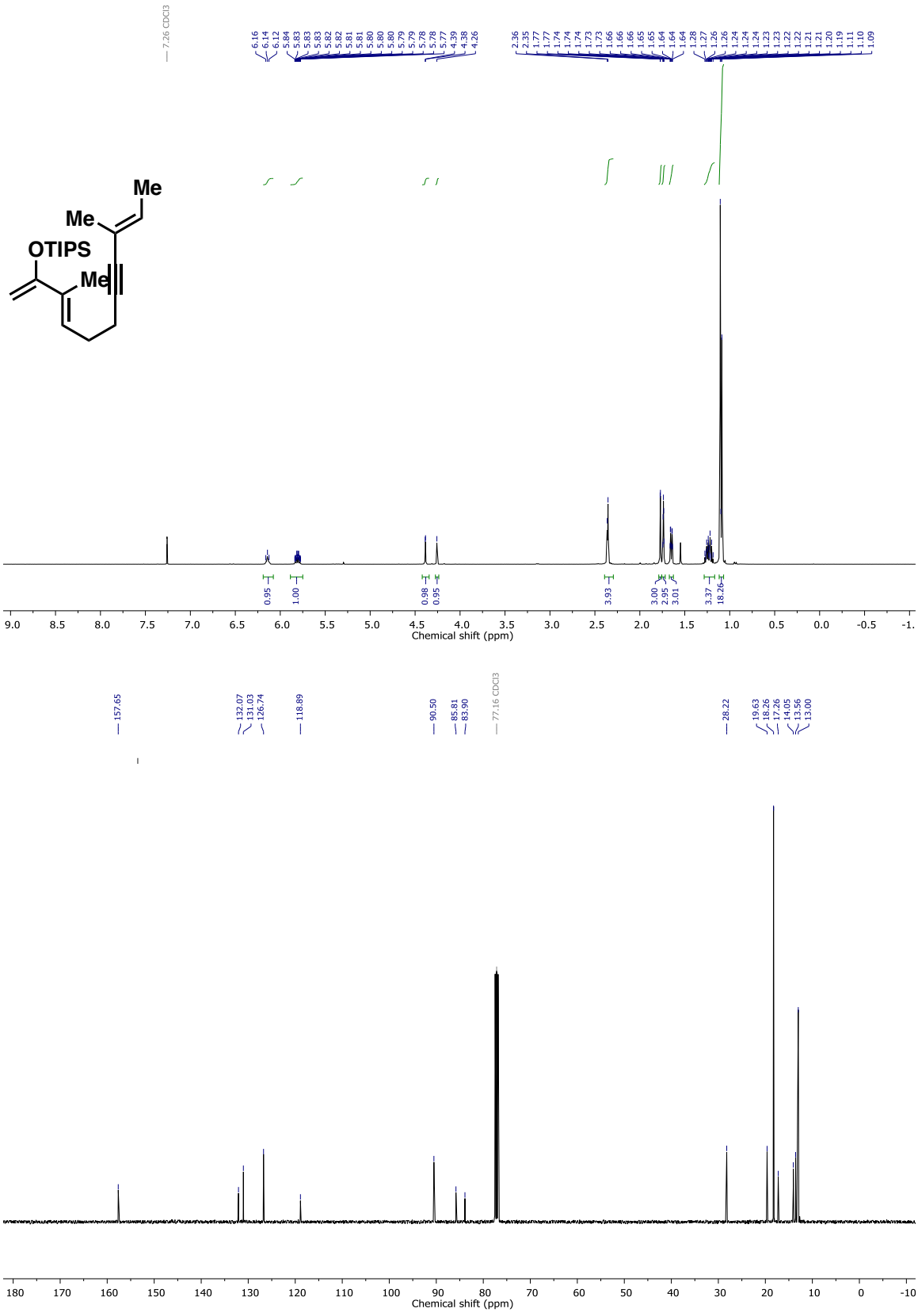
Me
Me
OTIPS
Me
7.26 CDCl3
6.16
6.14
6.12
5.84
5.83
5.83
5.83
5.82
5.82
5.81
5.81
5.80
5.80
5.80
5.79
5.79
5.78
5.78
5.77
4.39
4.38
4.26
2.36
2.35
1.77
1.77
1.74
1.74
1.74
1.73
1.73
1.66
1.66
1.66
1.65
1.65
1.64
1.64
1.64
1.28
1.27
1.26
1.26
1.24
1.24
1.24
1.23
1.23
1.22
1.22
1.21
1.21
1.20
1.19
1.11
1.10
1.09
0.95
1.00
0.98
0.95
3.93
3.00
2.95
3.01
3.37
18.26
Chemical shift (ppm)
157.65
132.07
131.03
126.74
118.89
90.50
85.81
83.90
77.16 CDCl3
28.22
19.63
18.26
17.26
14.05
13.56
13.00
Chemical shift (ppm)

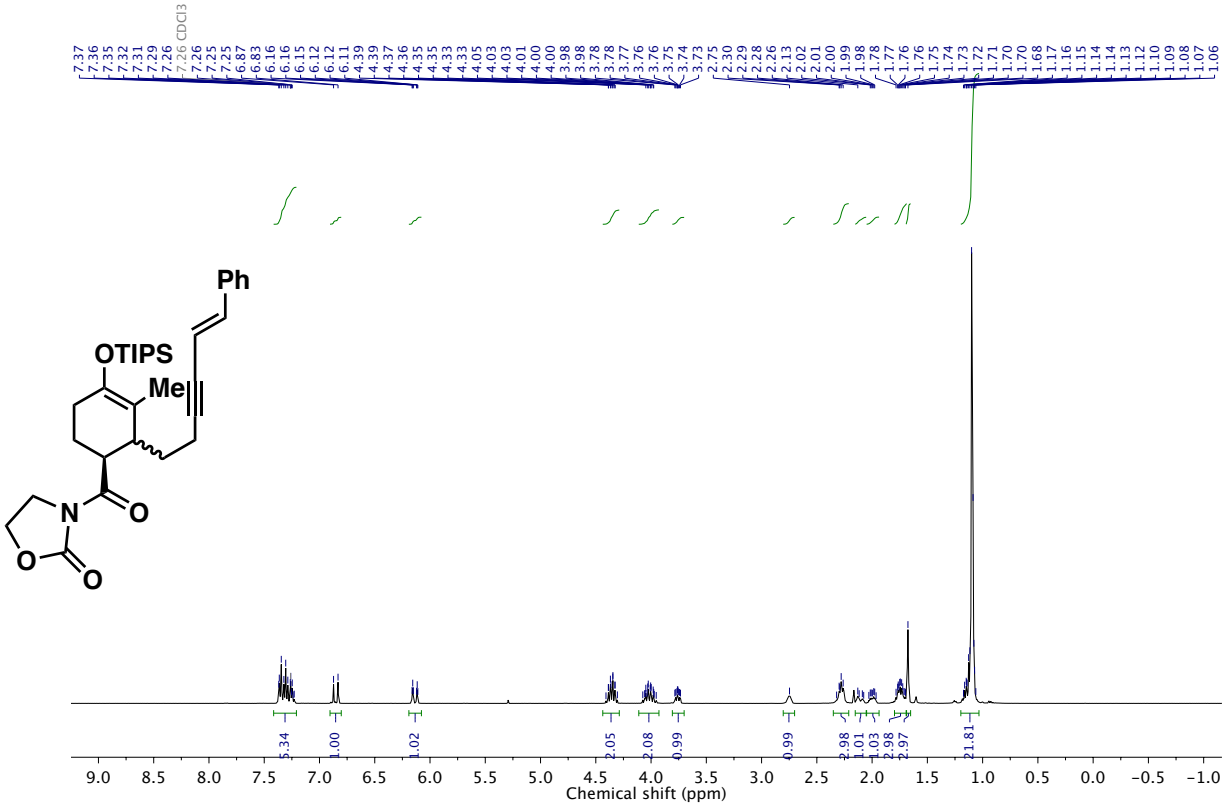
Ph
OTIPS
Me
N
O
O
O
Chemical shift (ppm)

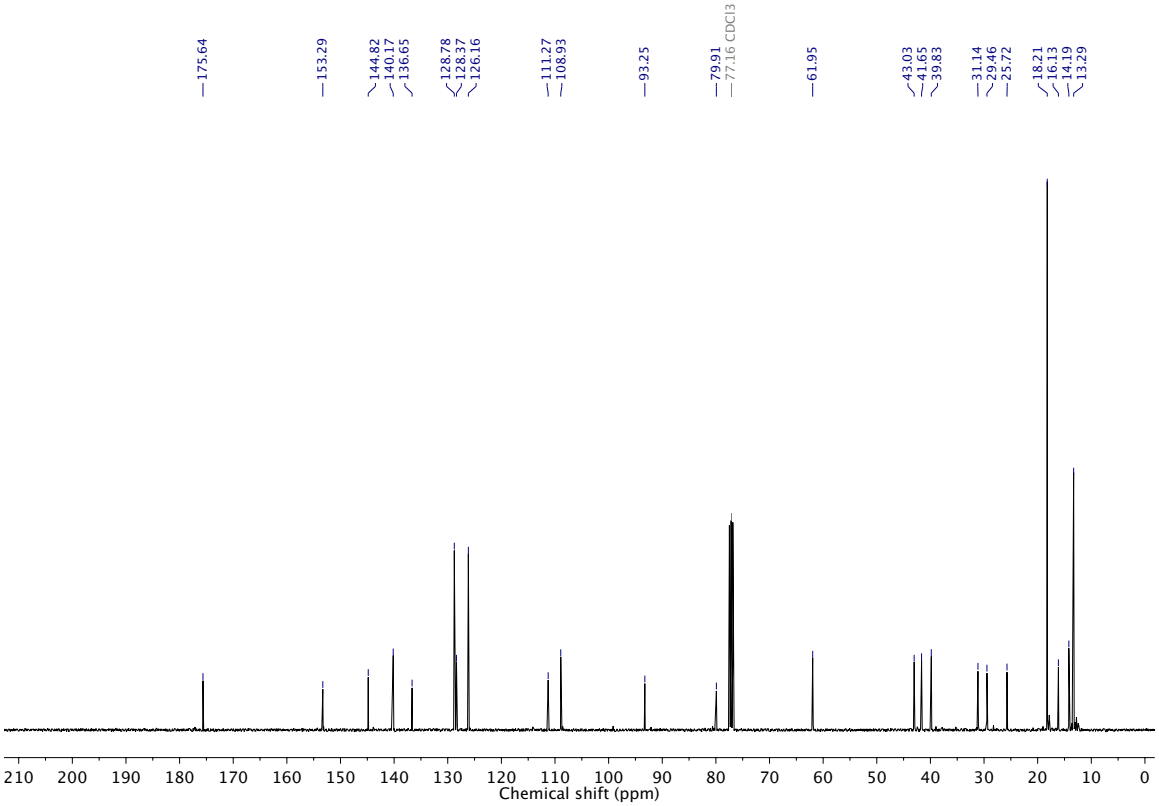
Chemical shift (ppm)

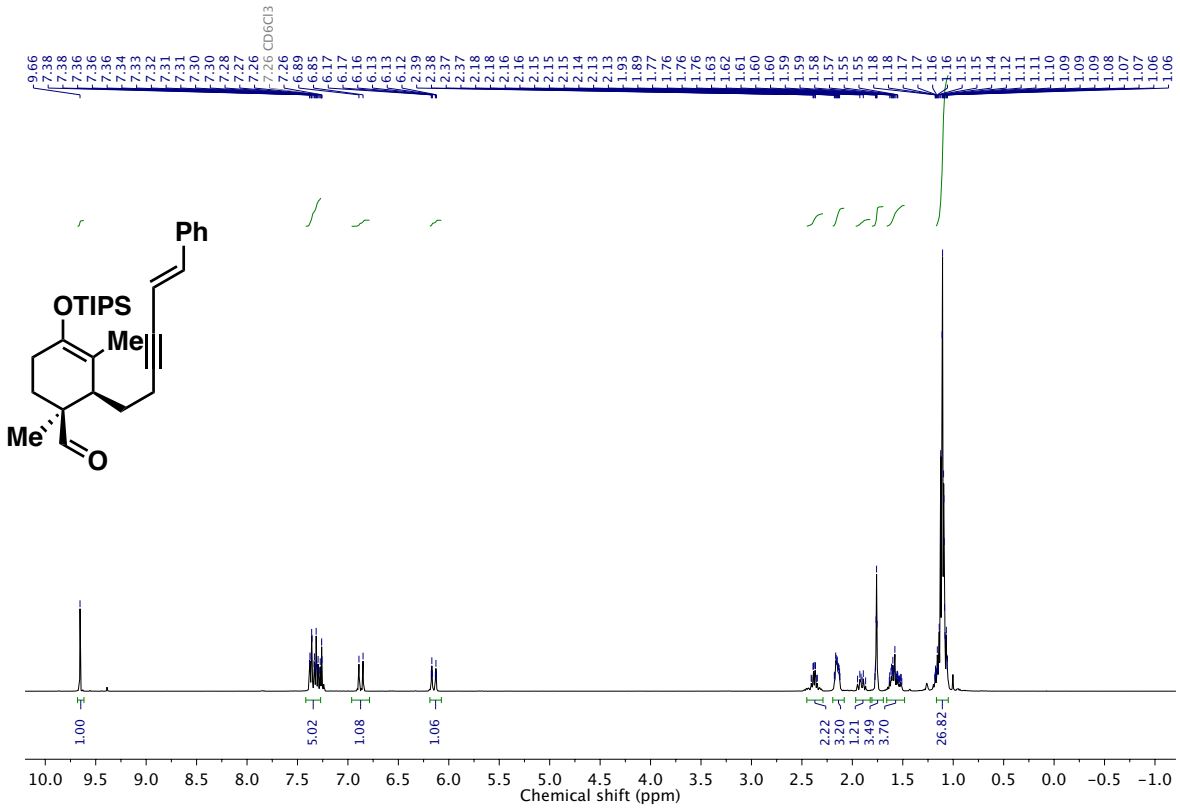
Ph
OTIPS
Me
Me
O
Chemical shift (ppm)

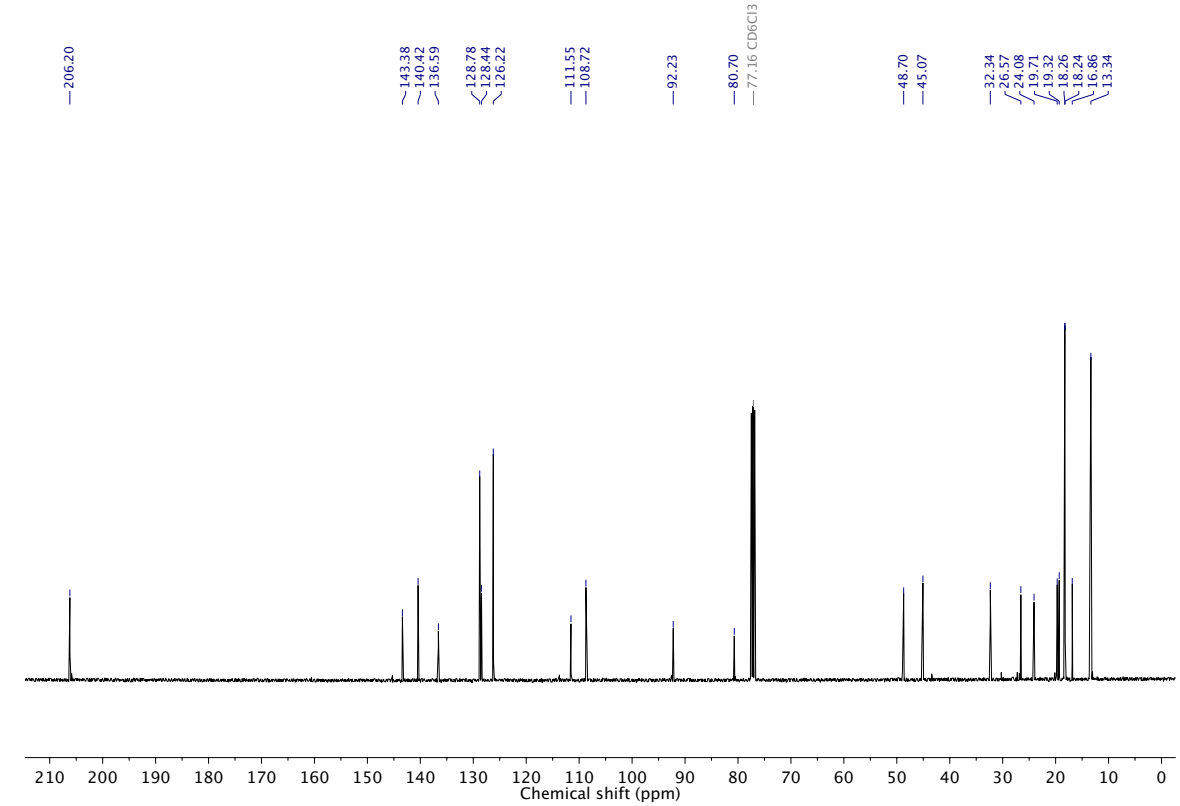
Chemical shift (ppm)

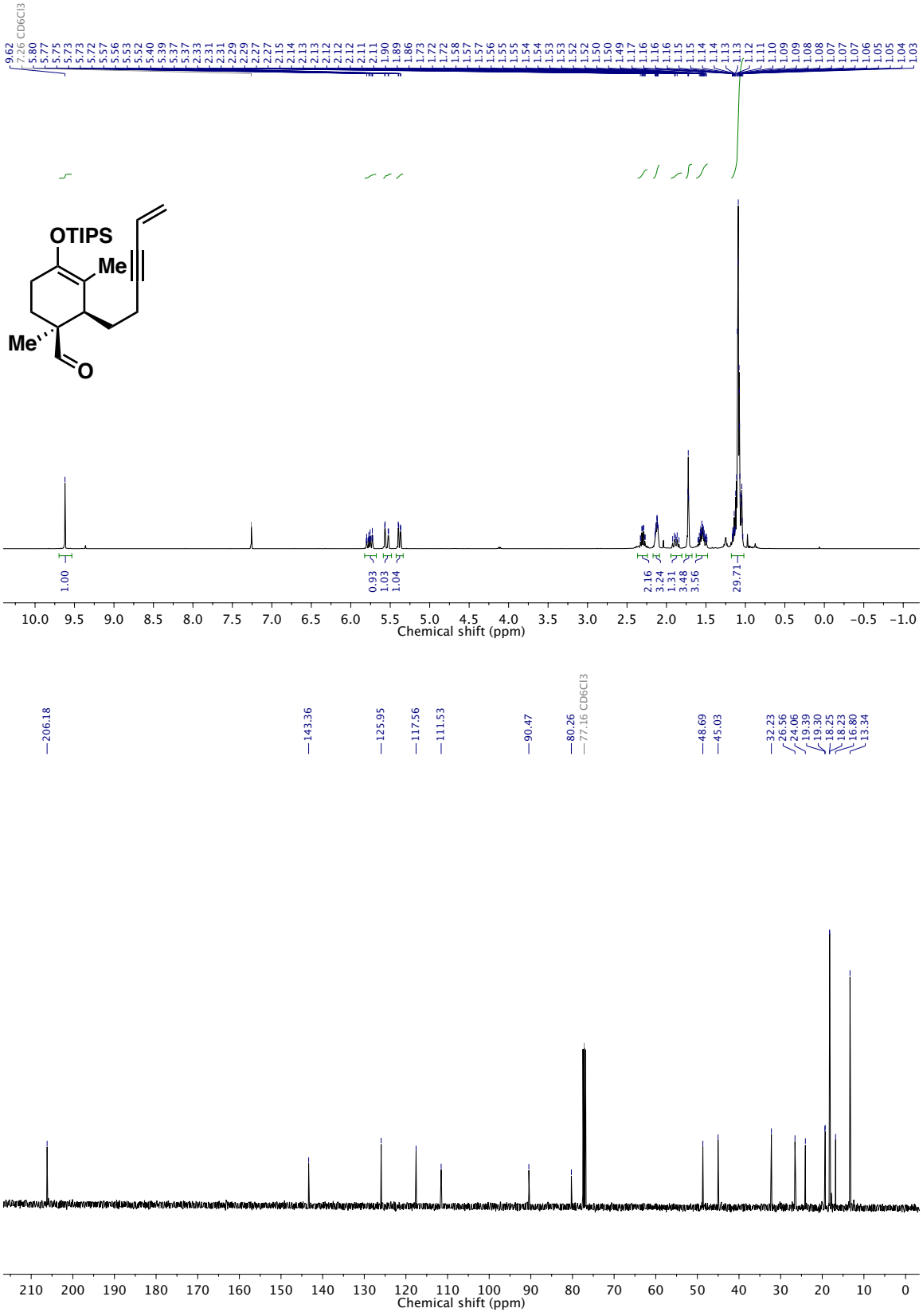
OTIPS
Me
Me
O
Chemical shift (ppm)
Chemical shift (ppm)


OTIPS
Me
N
O
O
O
Chemical shift (ppm)
Chemical shift (ppm)

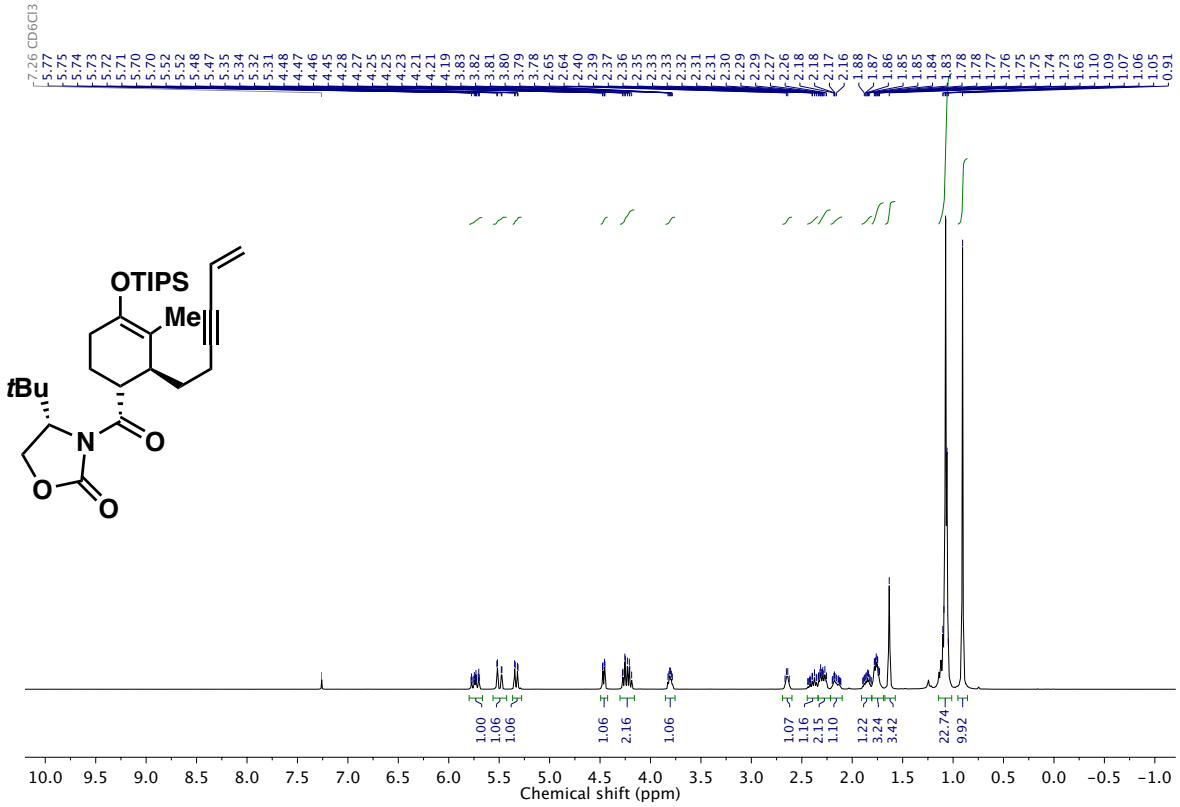
OTIPS
Me
tBu
N
O
O
O
Chemical shift (ppm)

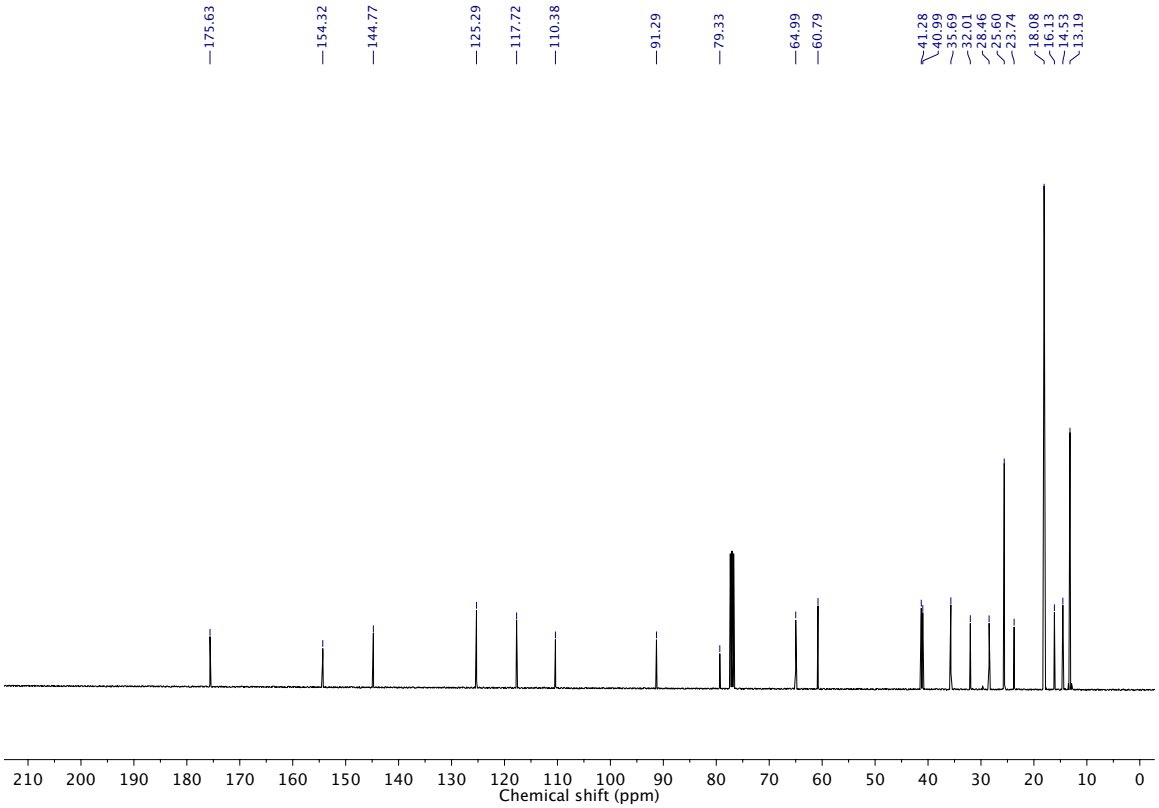
Chemical shift (ppm)

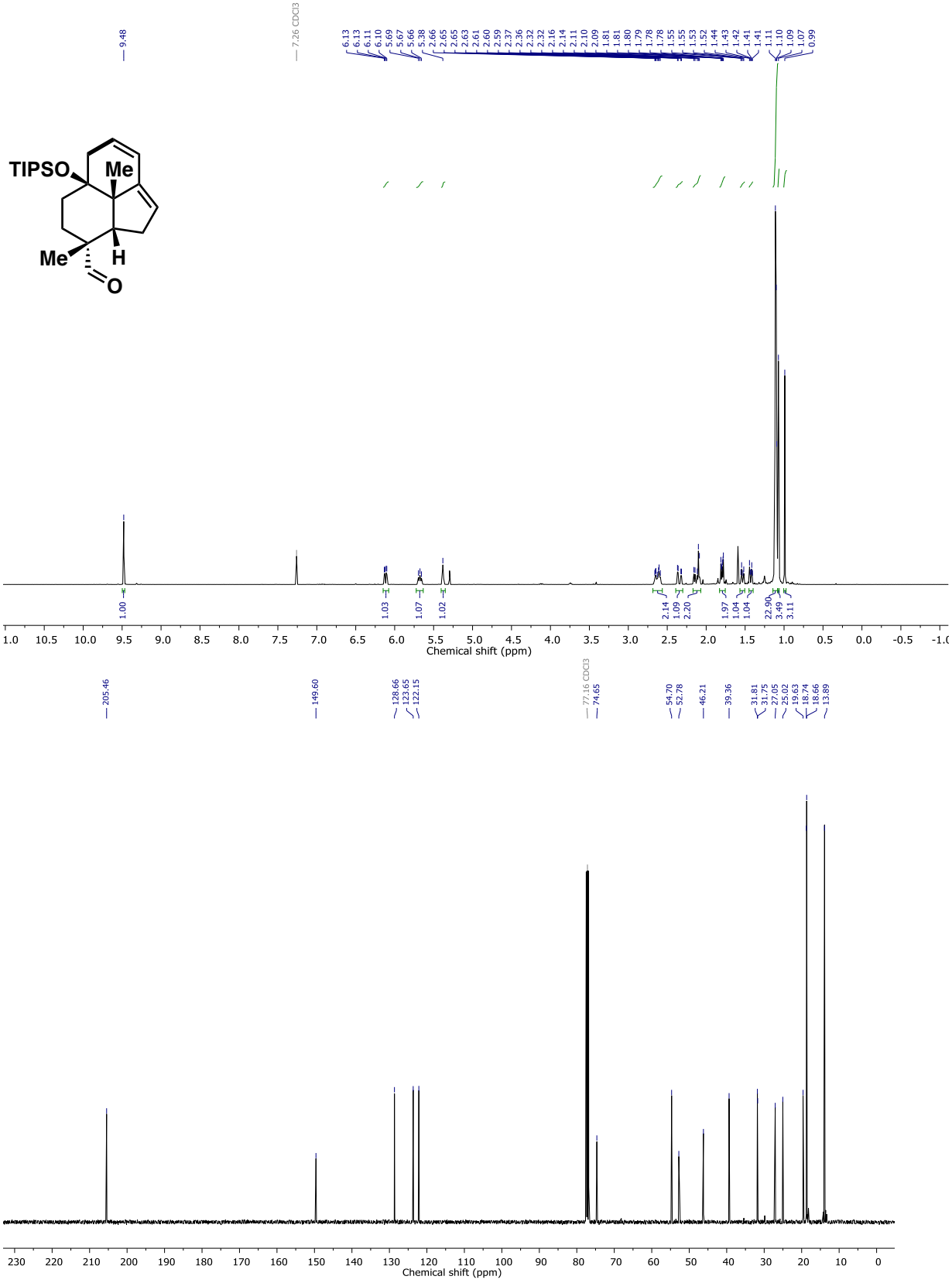
TIPSO
Me
Me
H
O
9.48
7.26 CDCl3
6.13
6.13
6.11
6.10
5.69
5.67
5.66
5.38
2.66
2.65
2.65
2.63
2.61
2.60
2.59
2.37
2.36
2.32
2.32
2.16
2.14
2.11
2.10
2.09
1.81
1.81
1.80
1.79
1.78
1.78
1.55
1.55
1.53
1.52
1.44
1.43
1.42
1.41
1.41
1.11
1.10
1.09
1.07
0.99
1.00
1.03
1.07
1.02
2.14
1.09
2.20
1.97
1.04
1.04
22.90
3.49
3.11
Chemical shift (ppm)
205.46
149.60
128.66
123.65
122.15
77.16 CDCl3
74.65
54.70
52.78
46.21
39.36
31.81
31.75
27.05
25.02
19.63
18.74
18.66
13.89
Chemical shift (ppm)

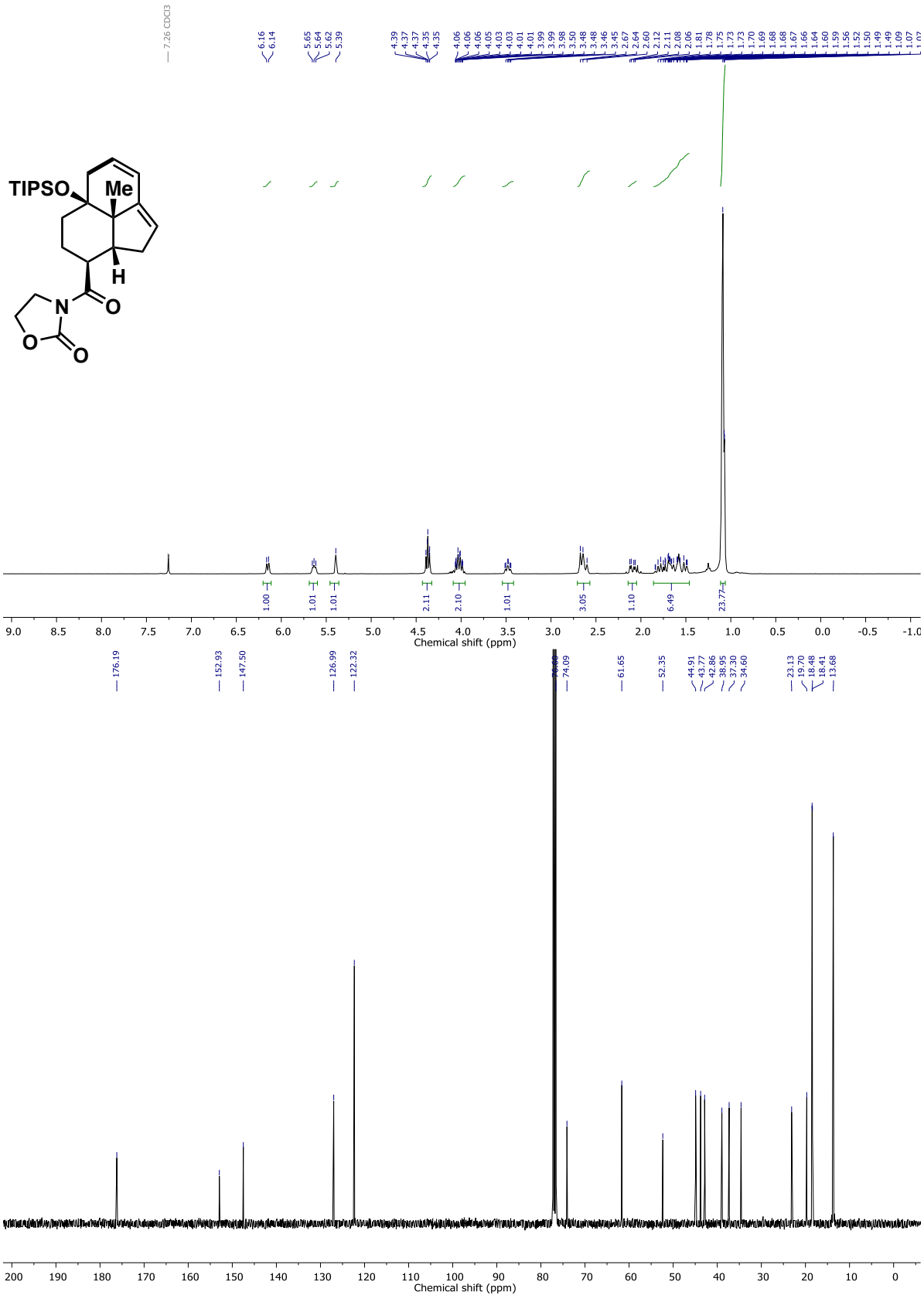
TIPSO
Me
H
N
O
O
O
7.26 CDCl3
6.16
6.14
5.65
5.64
5.62
5.39
4.39
4.37
4.37
4.35
4.35
4.06
4.06
4.06
4.05
4.03
4.01
4.01
3.99
3.99
3.98
3.50
3.48
3.48
3.46
3.45
2.67
2.64
2.60
2.12
2.11
2.08
2.06
1.81
1.78
1.75
1.73
1.73
1.70
1.69
1.68
1.68
1.67
1.66
1.64
1.60
1.59
1.56
1.52
1.50
1.49
1.49
1.09
1.07
1.00
1.01
1.01
2.11
2.10
1.01
3.05
1.10
6.49
23.77
9.0 8.5 8.0 7.5 7.0 6.5 6.0 5.5 5.0 4.5 4.0 3.5 3.0 2.5 2.0 1.5 1.0 0.5 0.0 -0.5 -1.0
Chemical shift (ppm)
176.19
152.93
147.50
126.99
122.32
74.09
61.65
52.35
44.91
43.77
42.86
38.95
37.30
34.60
23.13
19.70
18.48
18.41
13.68
200 190 180 170 160 150 140 130 120 110 100 90 80 70 60 50 40 30 20 10 0
Chemical shift (ppm)

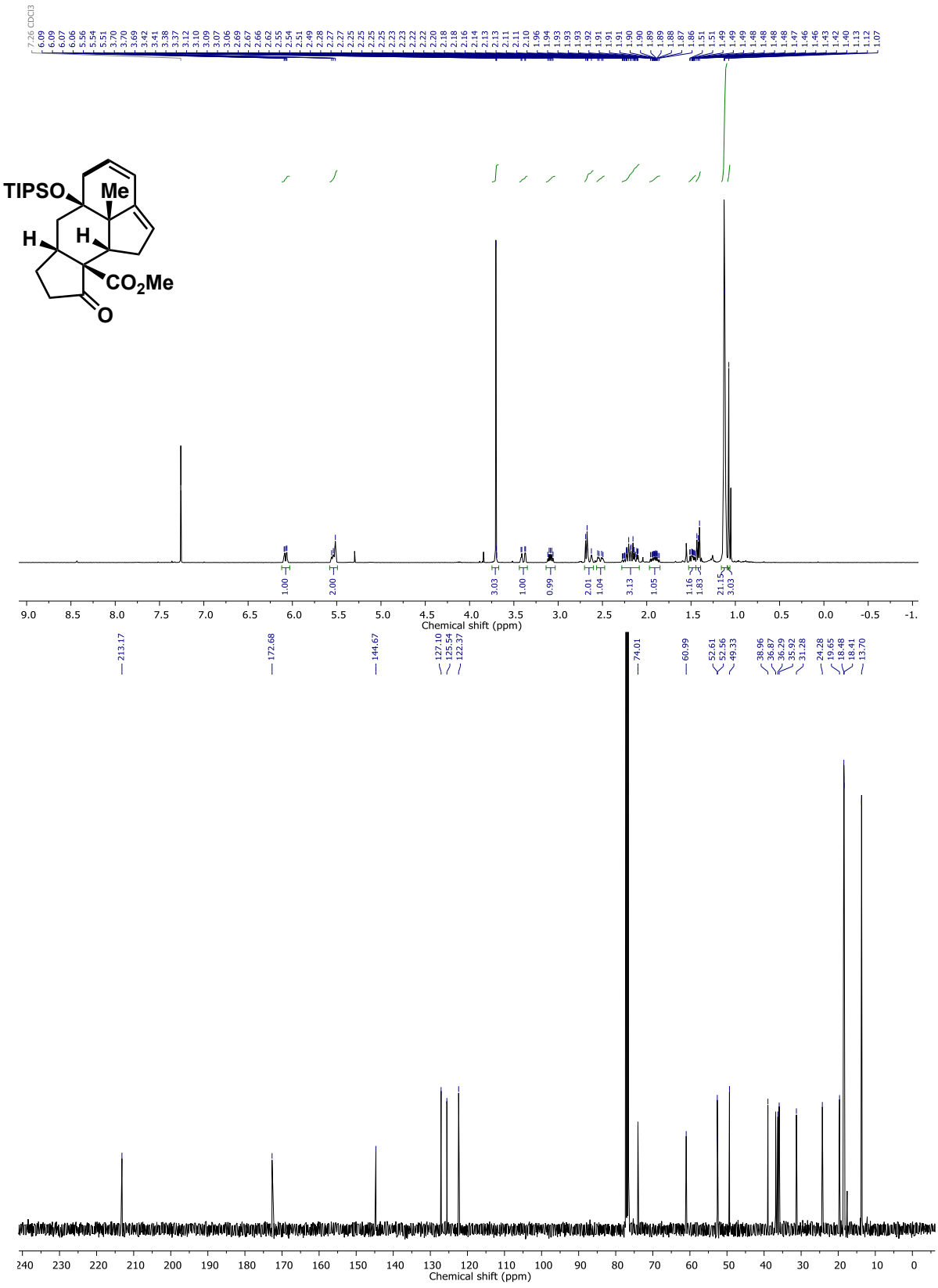
TIPSO
Me
H
H
CO2Me
O
Chemical shift (ppm)
Chemical shift (ppm)

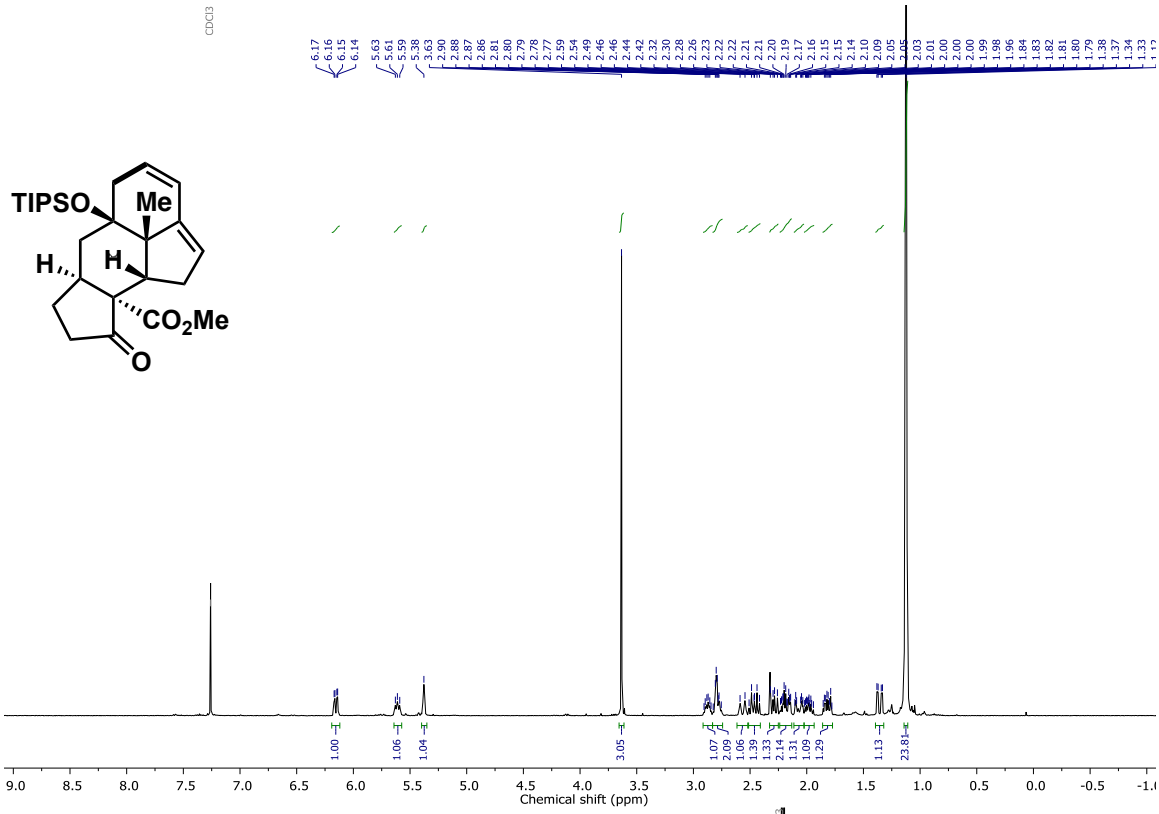
TIPSO
Me
H
H
CO2Me
O
CDCl3
Chemical shift (ppm)

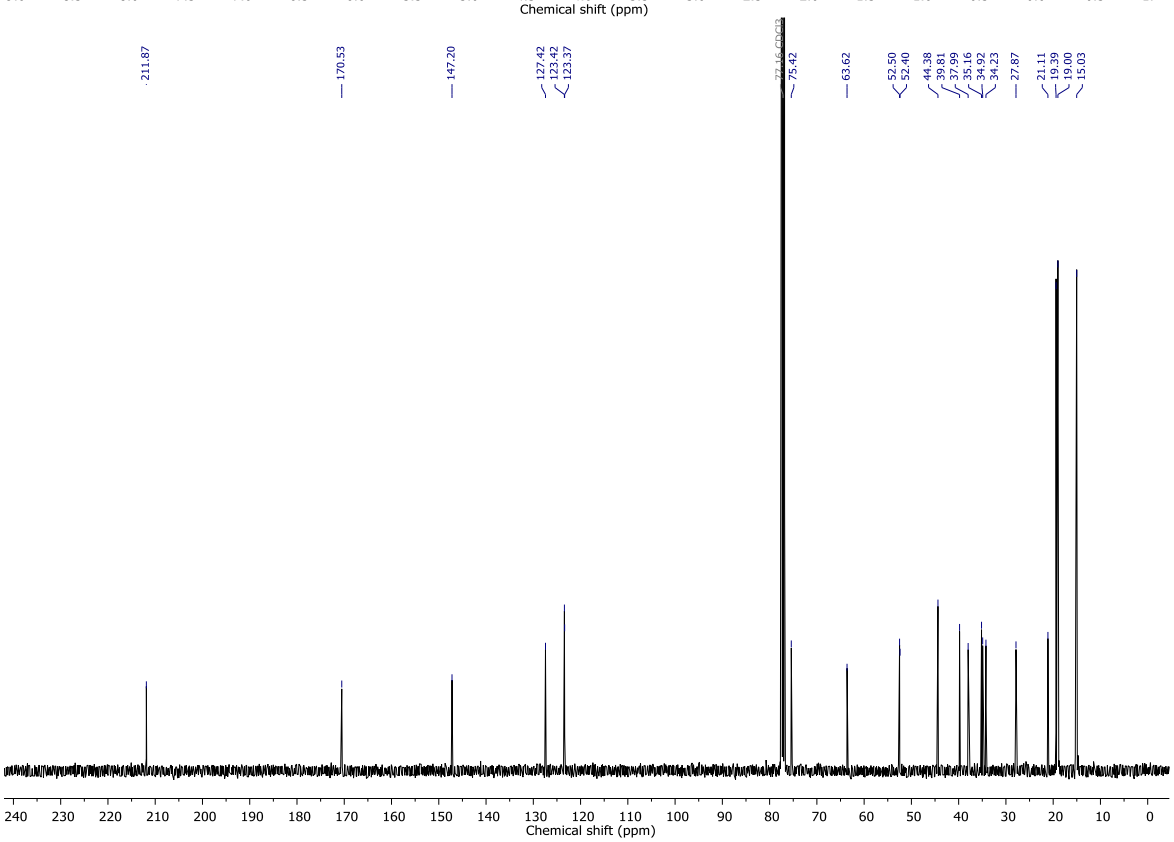
211.87
170.53
147.20
127.42
123.42
123.37
77.16 CDCl3
75.42
63.62
52.50
52.40
44.38
39.81
37.99
37.16
34.92
34.23
27.87
21.11
19.39
19.00
15.03
Chemical shift (ppm)

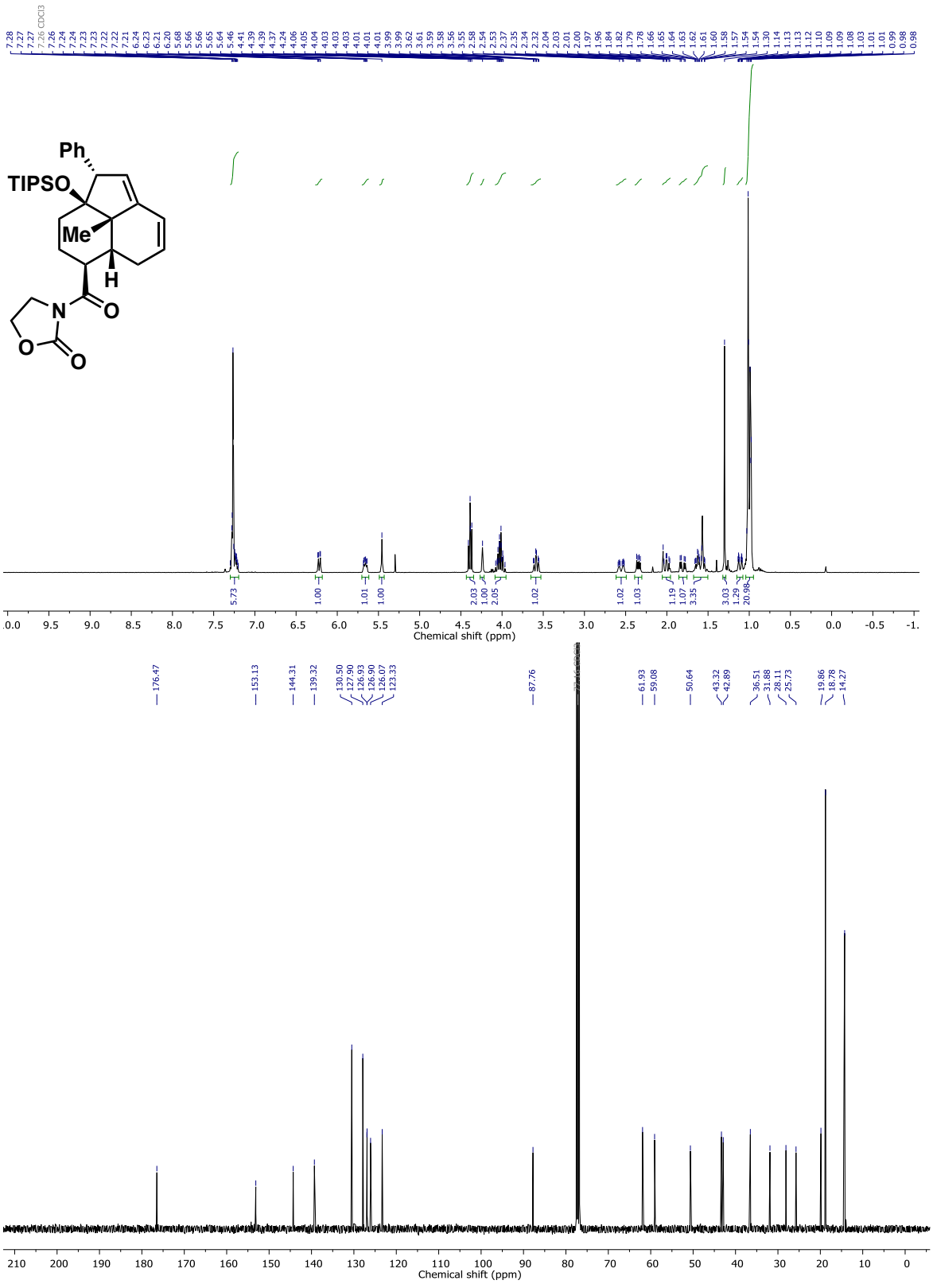
Ph
TIPSO
Me
H
N
O
O
O
Chemical shift (ppm)
Chemical shift (ppm)

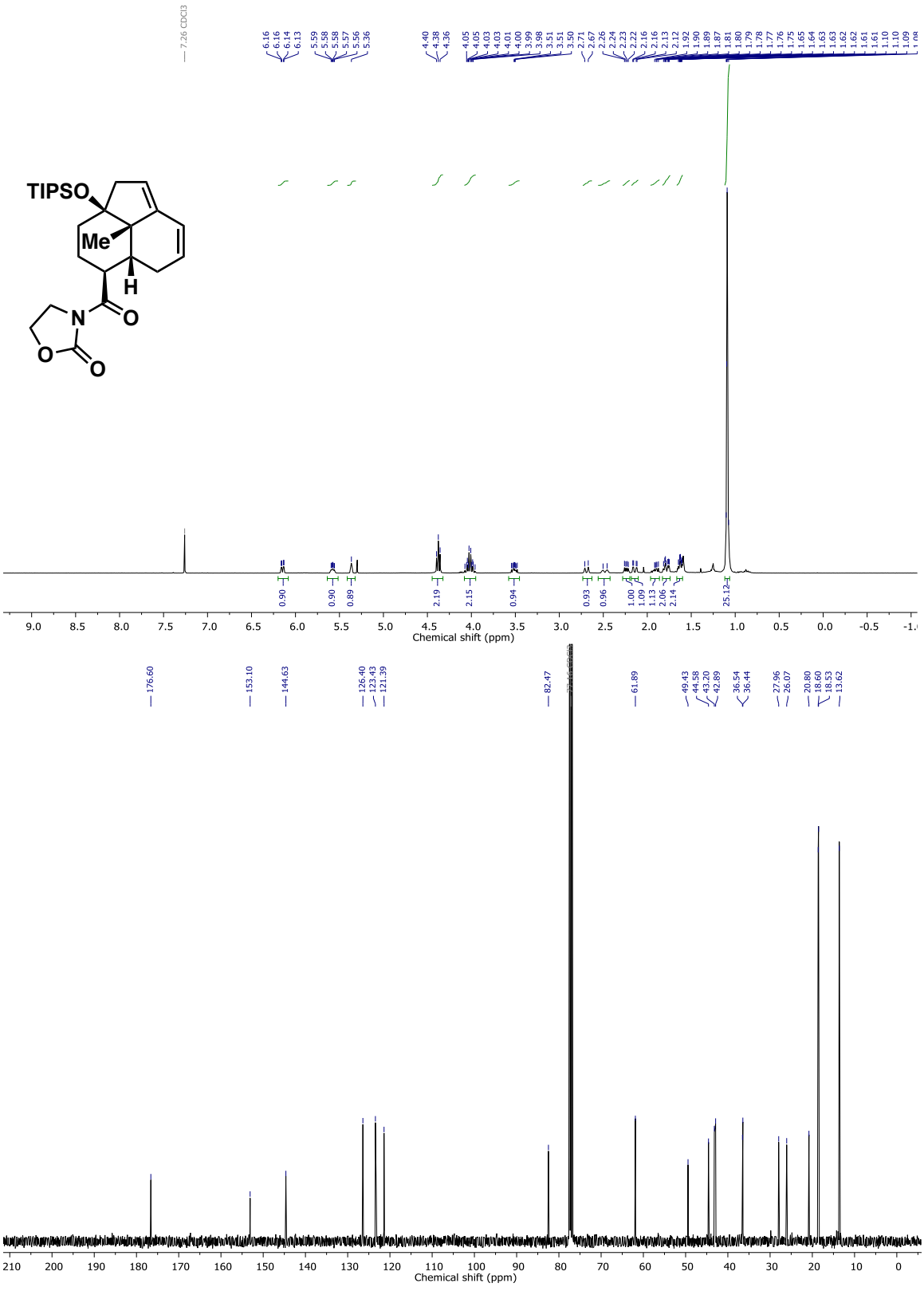
TIPSO
Me
H
N
O
O
O
Chemical shift (ppm)
Chemical shift (ppm)

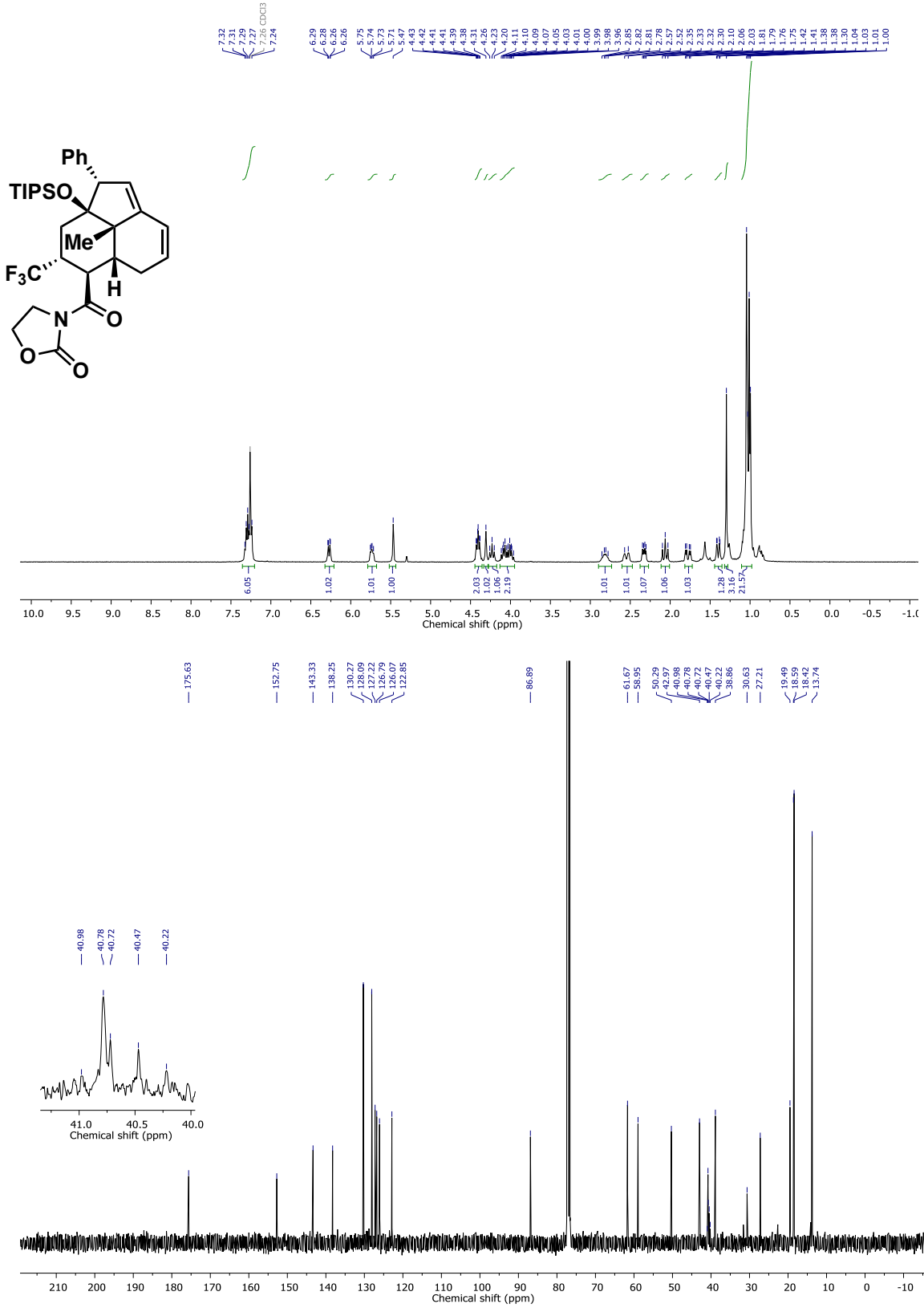
Ph
TIPSO
Me
F3C
H
N
O
O
O
Chemical shift (ppm)
Chemical shift (ppm)
Chemical shift (ppm)

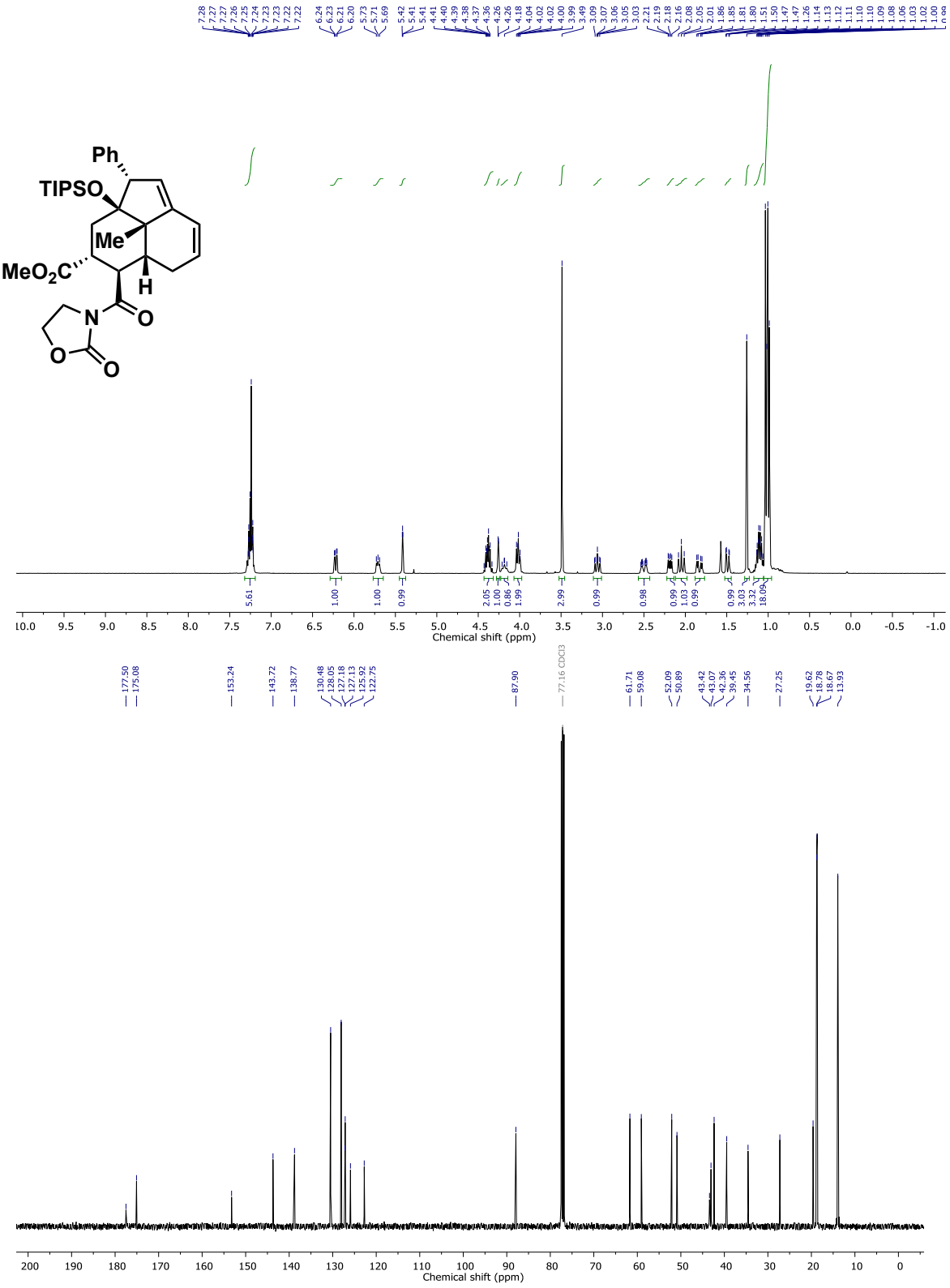
Ph
TIPSO
Me
MeO2C
H
N
O
O
O
Chemical shift (ppm)
Chemical shift (ppm)

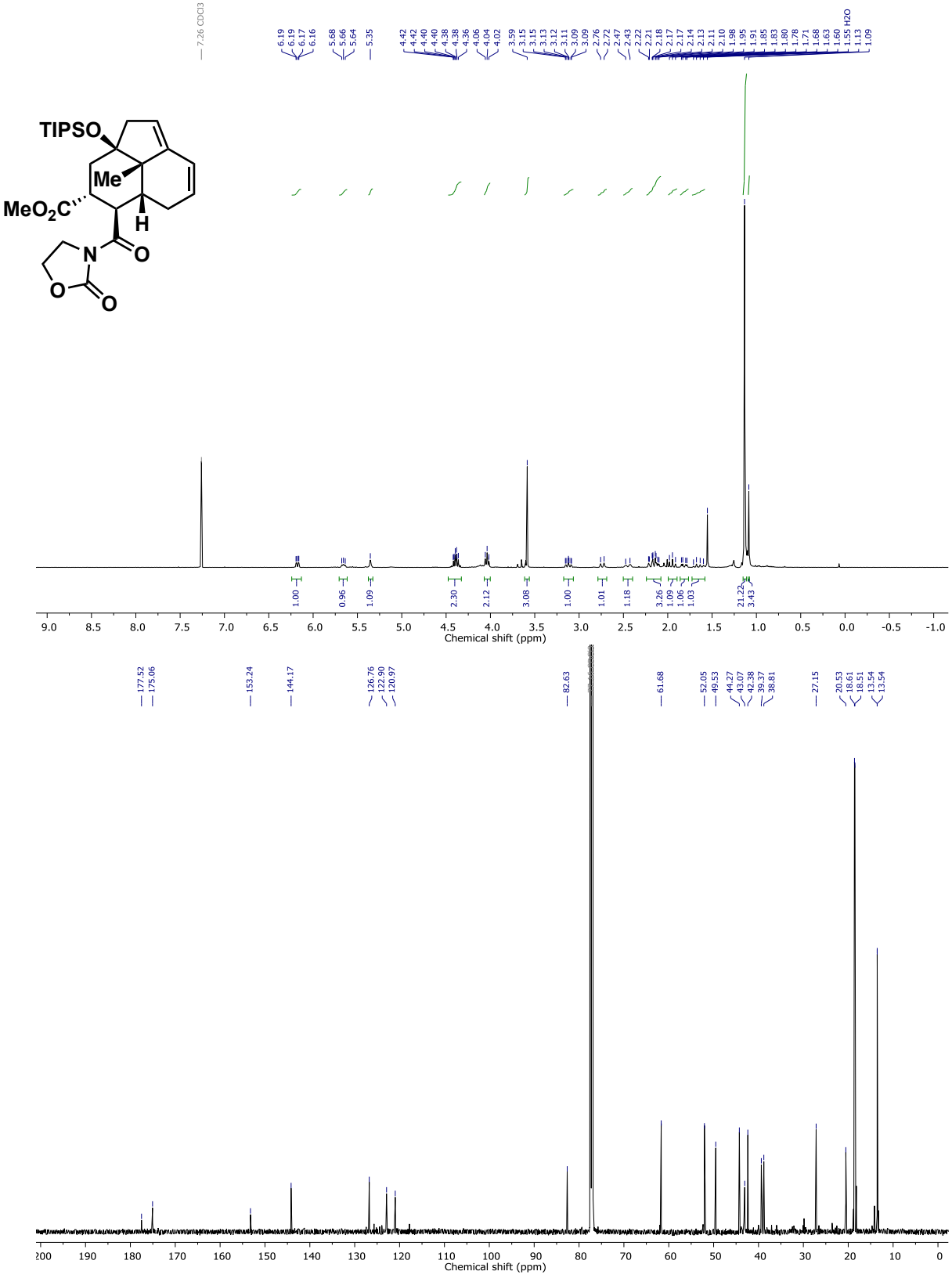
TIPSO
Me
MeO2C
H
N
O
O
O
Chemical shift (ppm)
Chemical shift (ppm)

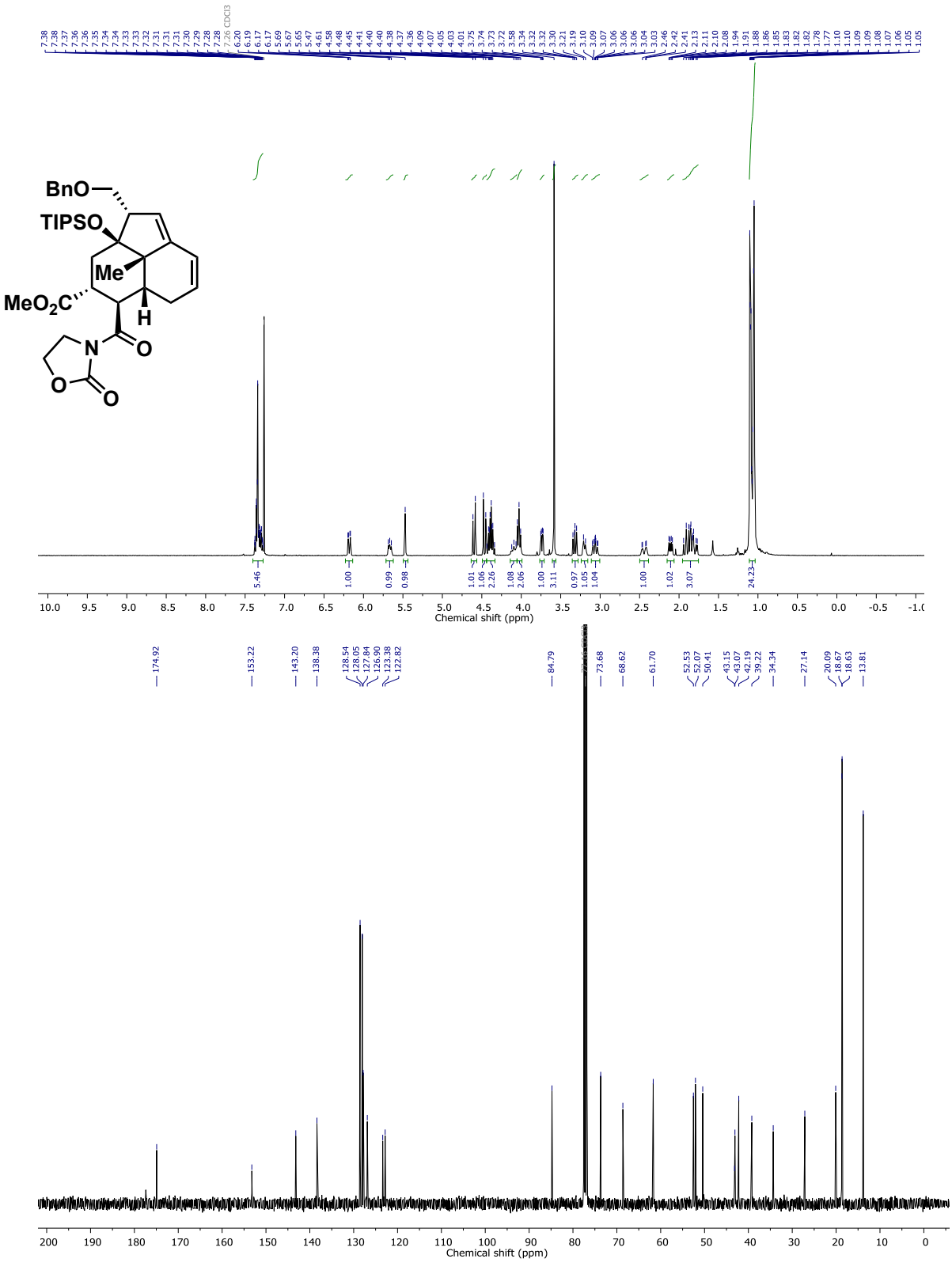
BnO
TIPSO
Me
MeO2C
H
N
O
O
O
Chemical shift (ppm)
Chemical shift (ppm)

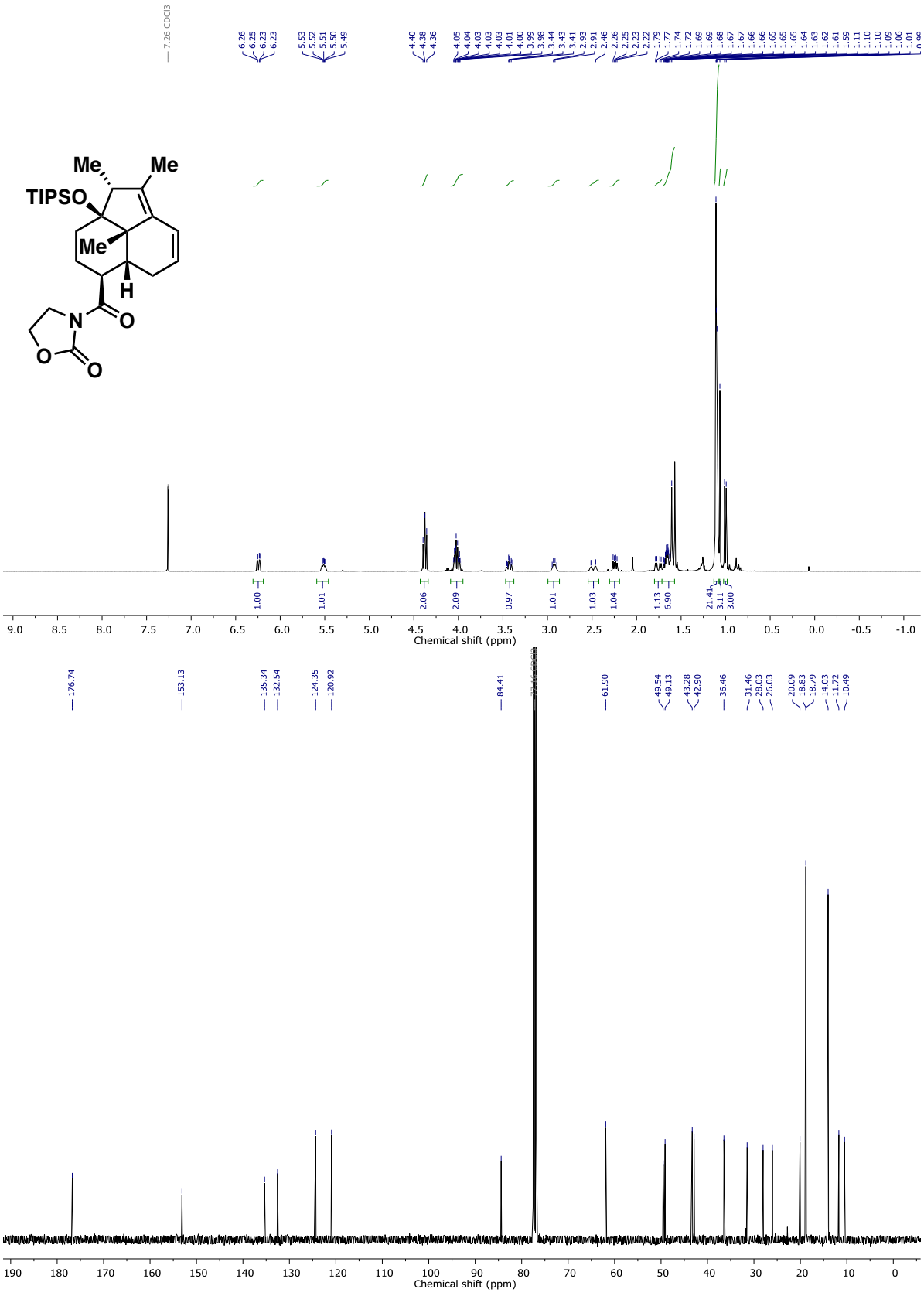
Me
Me
TIPSO
Me
H
N
O
O
O
Chemical shift (ppm)
Chemical shift (ppm)

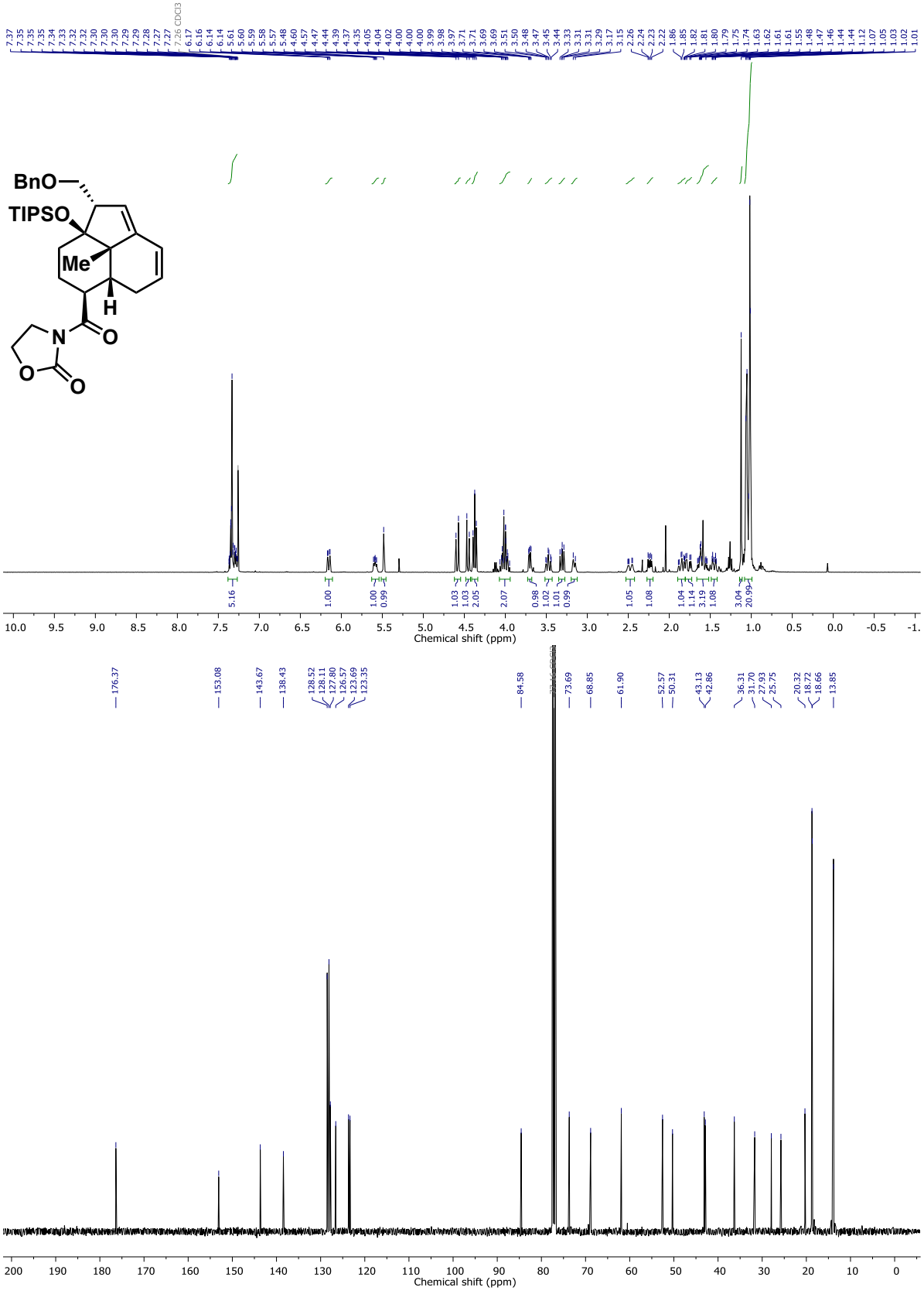
BnO
TIPSO
Me
H
N
O
O
O
Chemical shift (ppm)
Chemical shift (ppm)

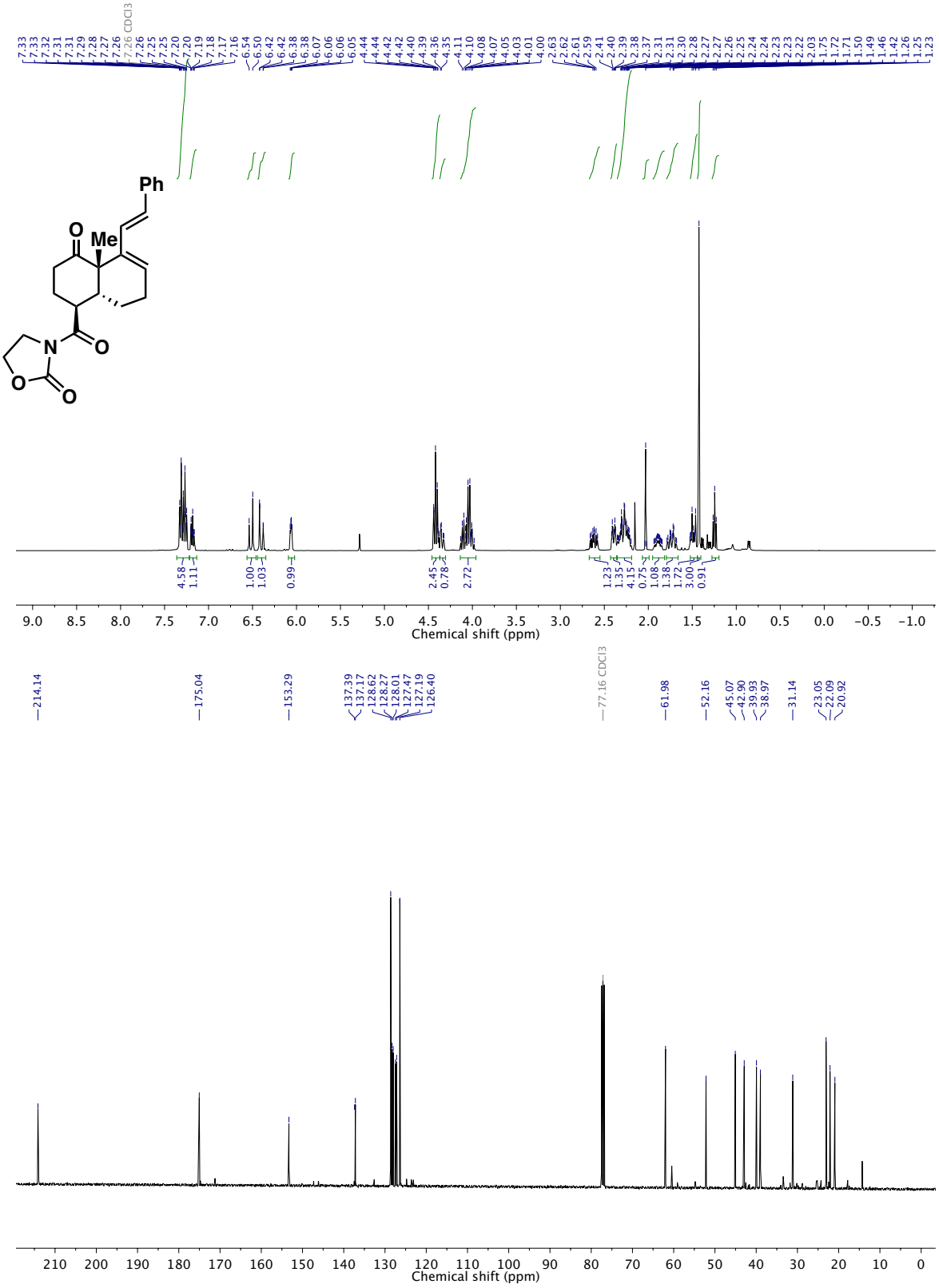
Ph
O
Me
O
N
O
O
O
Chemical shift (ppm)
Chemical shift (ppm)

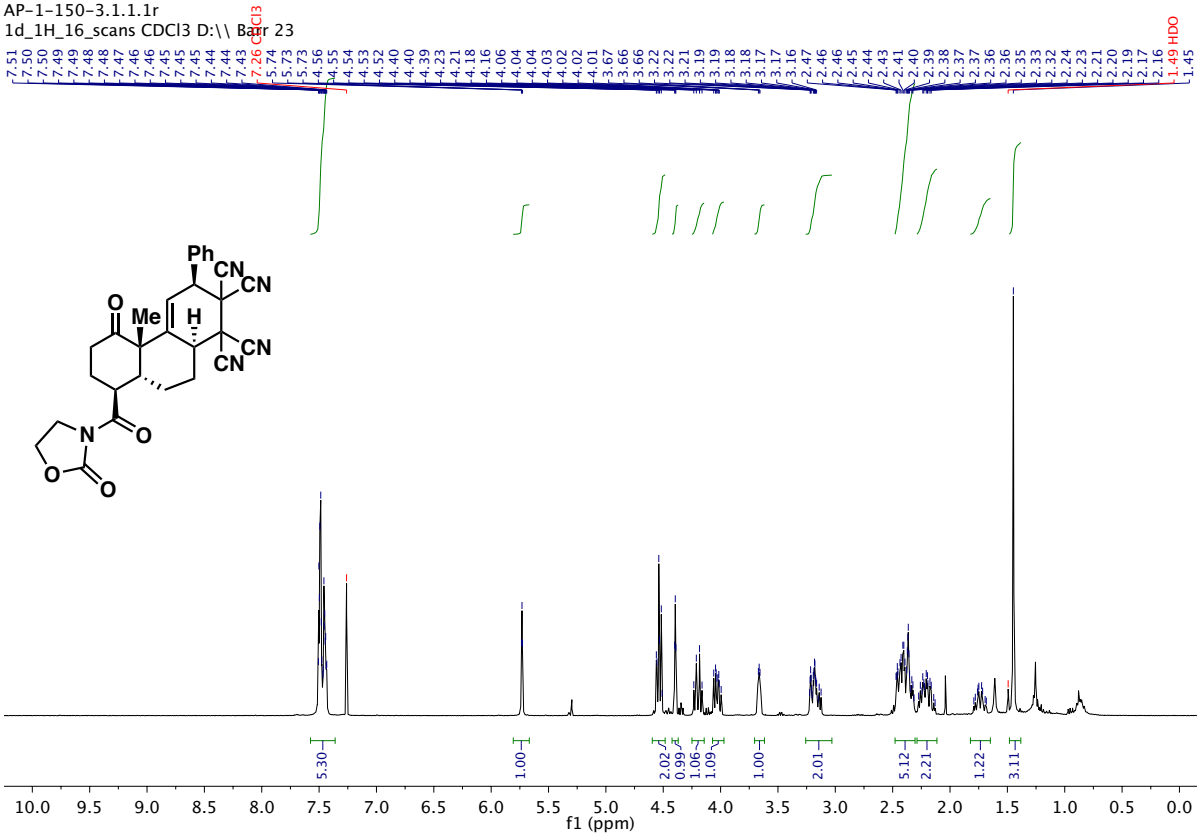
AP-1-150-3.1.1.1r
1d_1H_16_scans CDCl3 D:\\ Barr 23
Ph
CN
CN
CN
CN
O
Me
H
N
O
O
O
5.30
1.00
2.02
0.99
1.06
1.09
1.00
2.01
5.12
2.21
1.22
3.11
f1 (ppm)

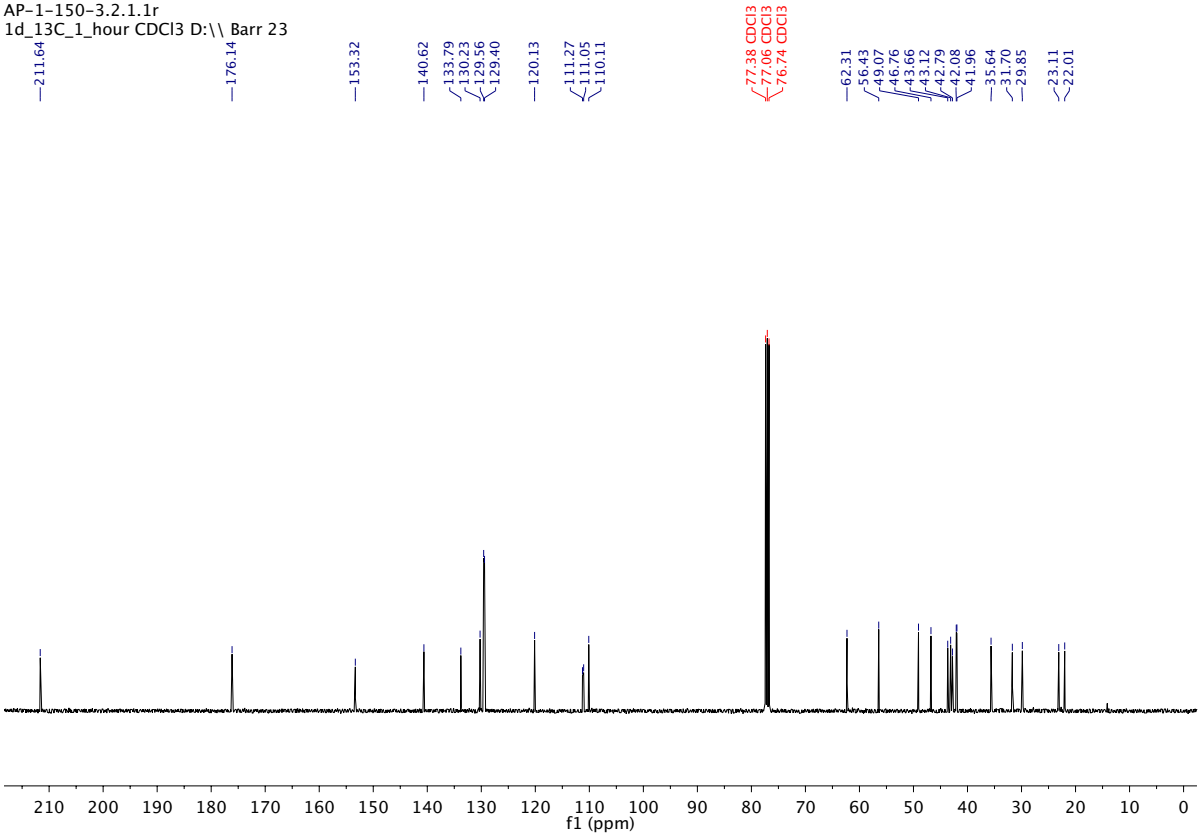
AP-1-150-3.2.1.1r
1d_13C_1_hour CDCl3 D:\\ Barr 23
211.64
176.14
153.32
140.62
133.79
130.23
129.56
129.40
120.13
111.27
111.05
110.11
77.38 CDCl3
77.06 CDCl3
76.74 CDCl3
62.31
56.43
49.07
46.76
43.66
43.12
42.79
42.08
41.96
35.64
31.70
29.85
23.11
22.01
f1 (ppm)

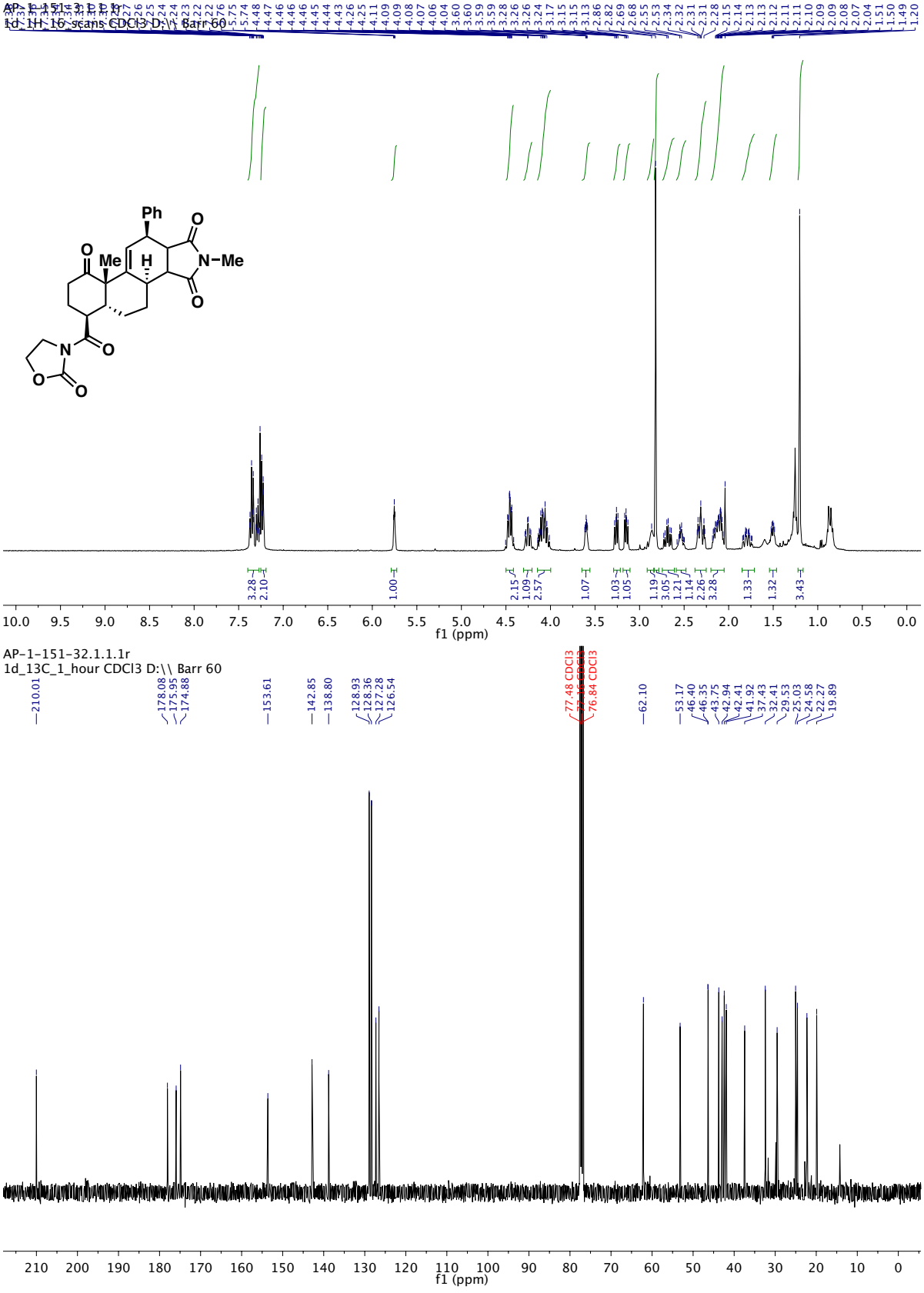
AP-1-151-3.1.1.1r
1d_1H_16 scans CDCl3 D:\\ Barr 60
Ph
O
Me
H
N-Me
O
O
N
O
O
O
3.28
2.10
1.00
2.15
1.09
2.57
1.07
1.03
1.05
1.19
3.05
1.21
1.14
2.26
3.28
1.33
1.32
3.43
f1 (ppm)
AP-1-151-32.1.1.1r
1d_13C_1_hour CDCl3 D:\\ Barr 60
210.01
178.08
175.95
174.88
153.61
142.85
138.80
128.93
128.36
127.28
126.54
77.48 CDCl3
76.84 CDCl3
62.10
53.17
46.40
46.35
43.75
42.94
42.41
41.92
37.43
32.41
29.53
25.03
24.58
22.27
19.89
f1 (ppm)

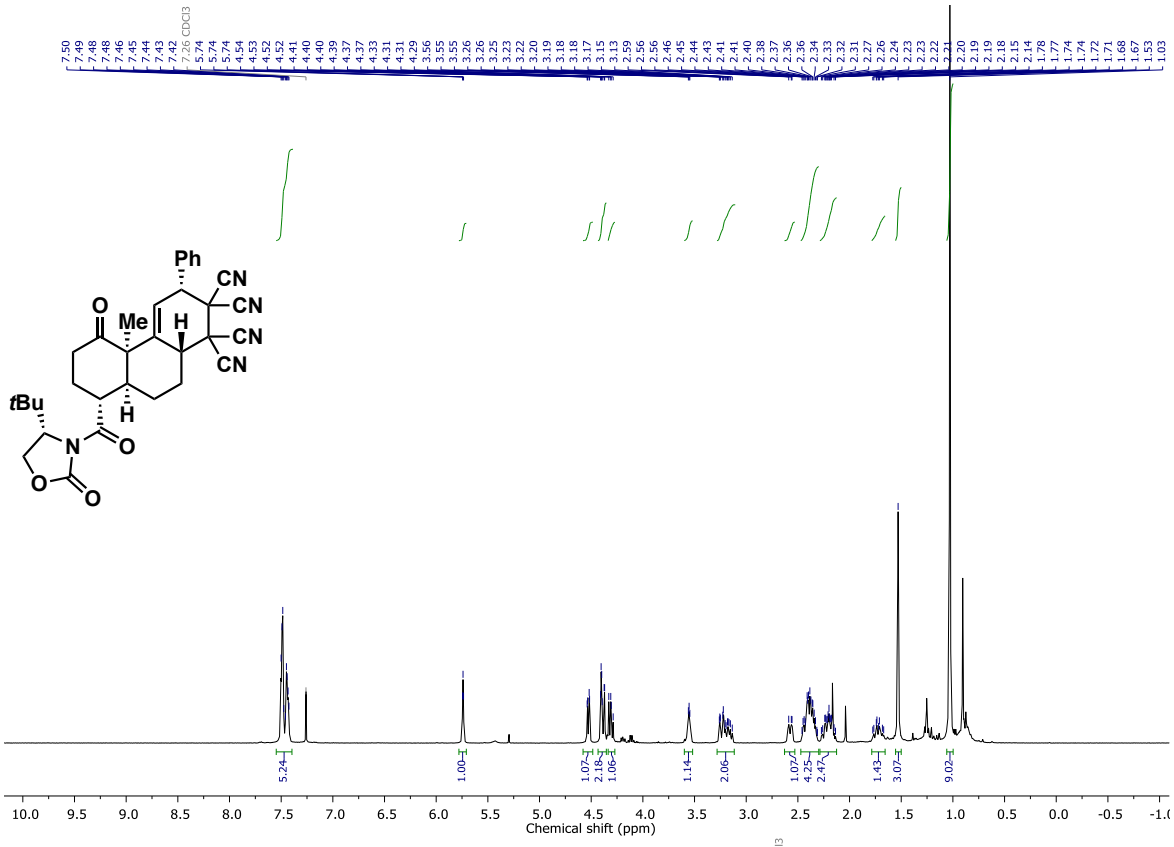
Ph
CN
CN
CN
CN
O
Me
H
H
tBu
N
O
O
O
Chemical shift (ppm)

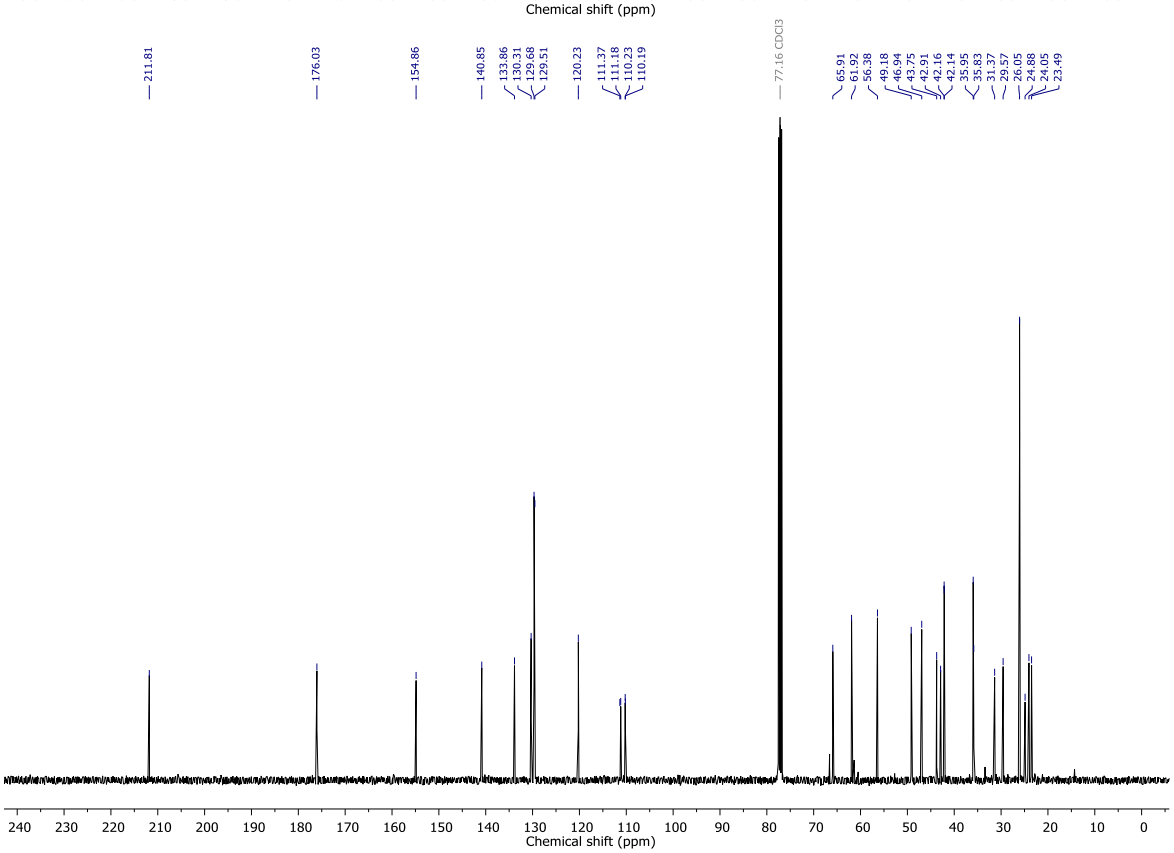
211.81
176.03
154.86
140.85
133.86
130.31
129.68
129.51
120.23
111.37
111.18
110.23
110.19
77.16 CDCl3
65.91
61.92
56.38
49.18
46.94
43.75
42.91
42.16
42.14
35.95
35.83
31.37
29.57
26.05
24.88
24.05
23.49
Chemical shift (ppm)

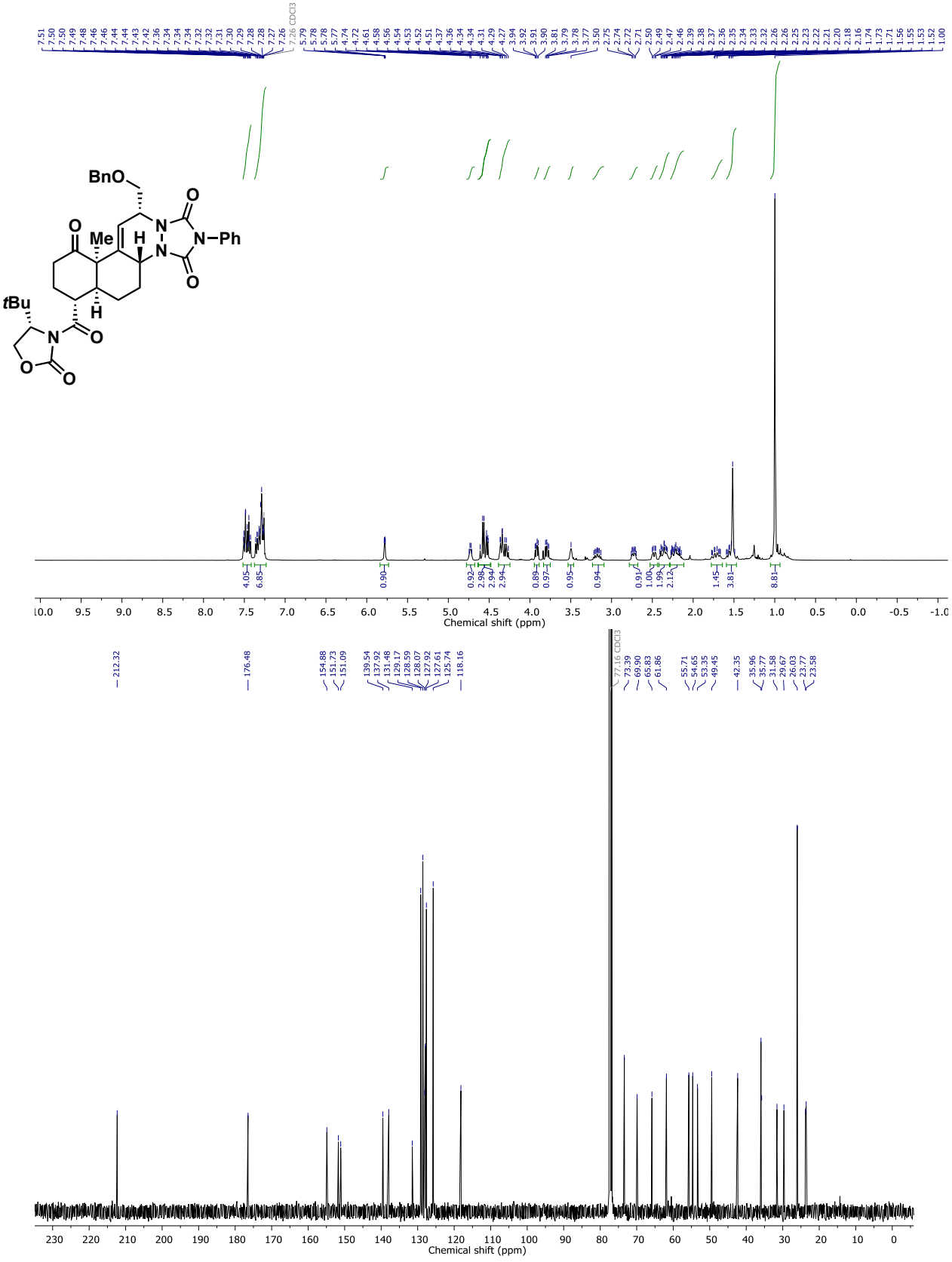
BnO
O
Me
H
N
N
N–Ph
O
O
H
tBu
N
O
O
O
Chemical shift (ppm)
Chemical shift (ppm)

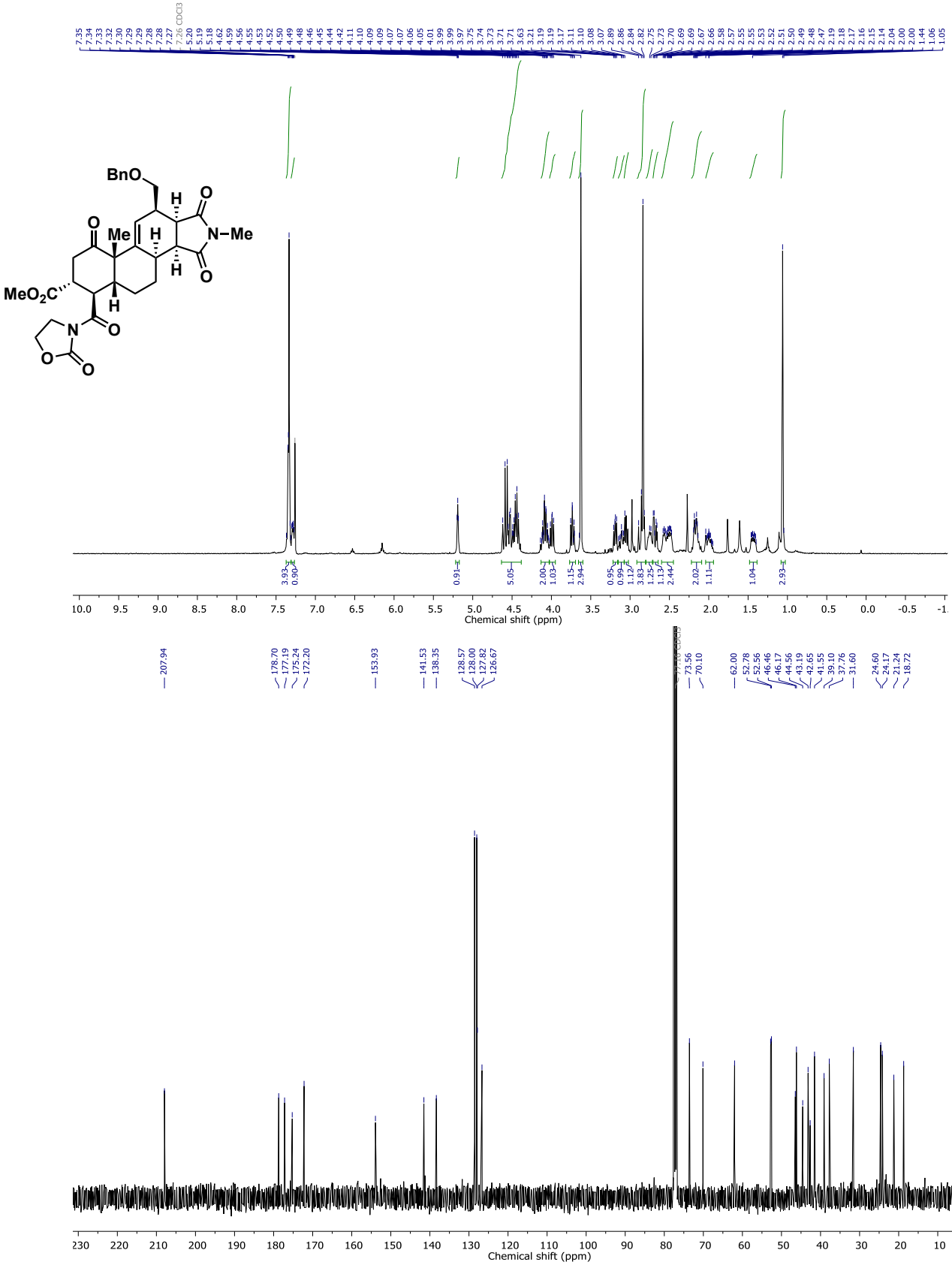
BnO
H
O
O
Me
H
N–Me
H
O
MeO2C
H
N
O
O
O
Chemical shift (ppm)
Chemical shift (ppm)

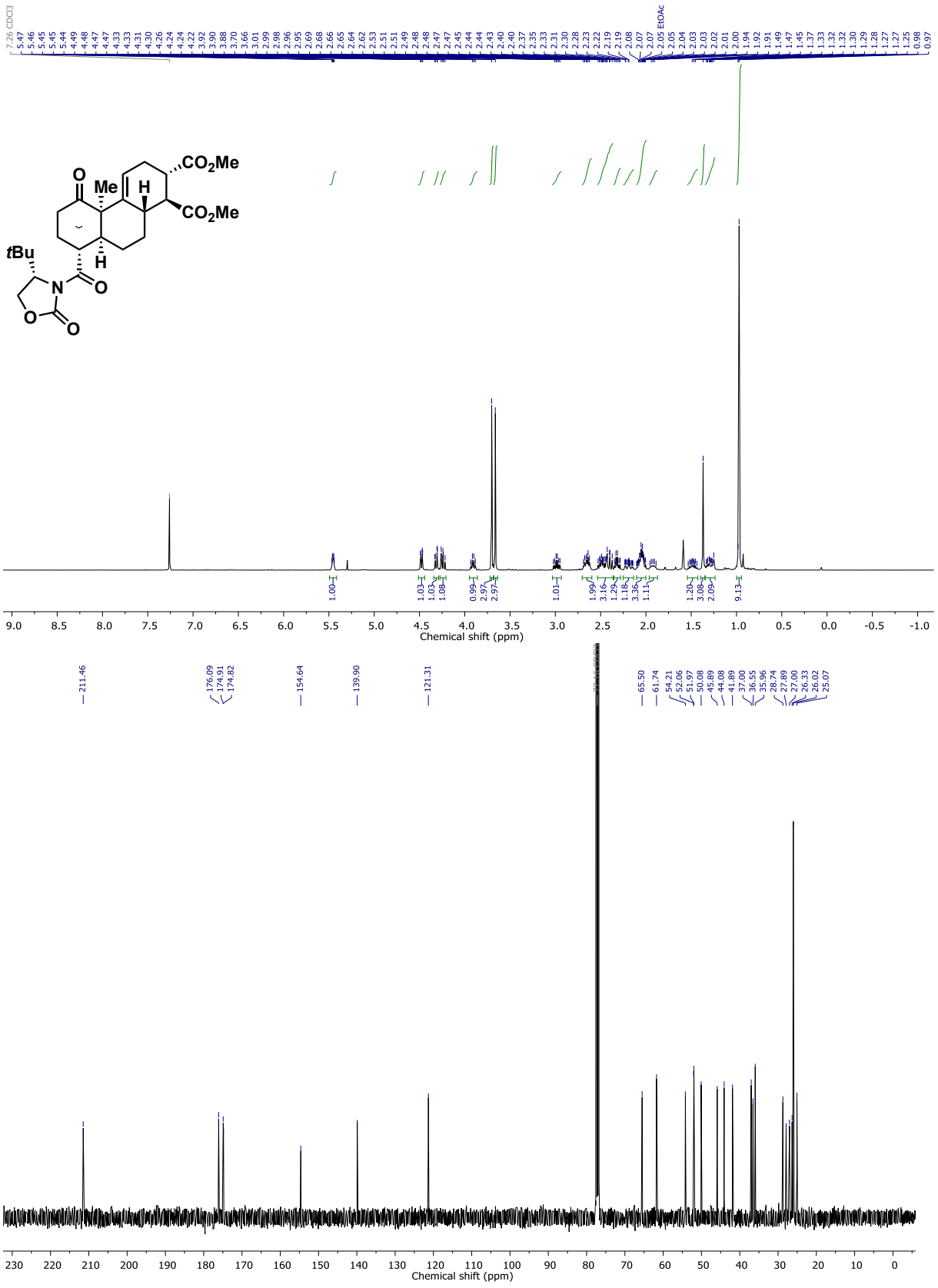
CDCl3
EtOAc
Me
H
CO2Me
CO2Me
tBu
N
O
O
O
O
H
Chemical shift (ppm)
211.46
176.09
174.91
174.82
154.64
139.90
121.31
77.16
65.50
61.74
54.21
52.06
51.97
50.08
45.89
44.08
41.89
37.00
36.55
35.96
28.74
27.89
27.00
26.33
26.02
25.07
Chemical shift (ppm)

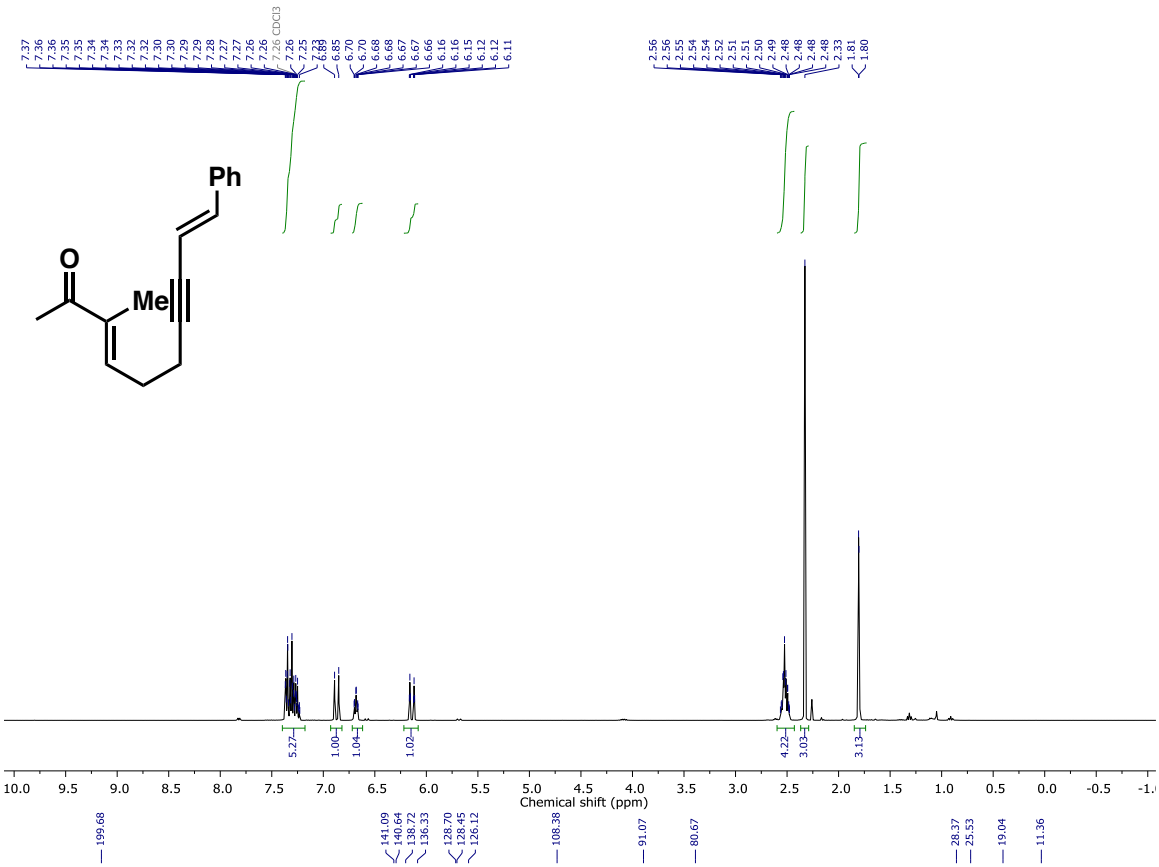
Ph
O
Me
Chemical shift (ppm)

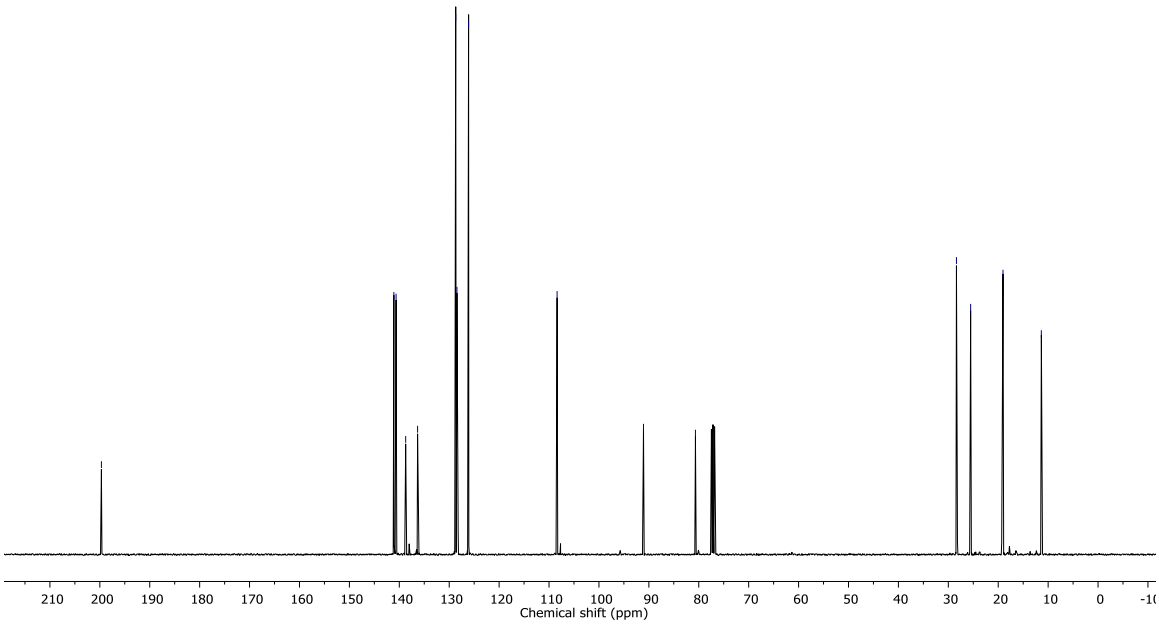
Chemical shift (ppm)

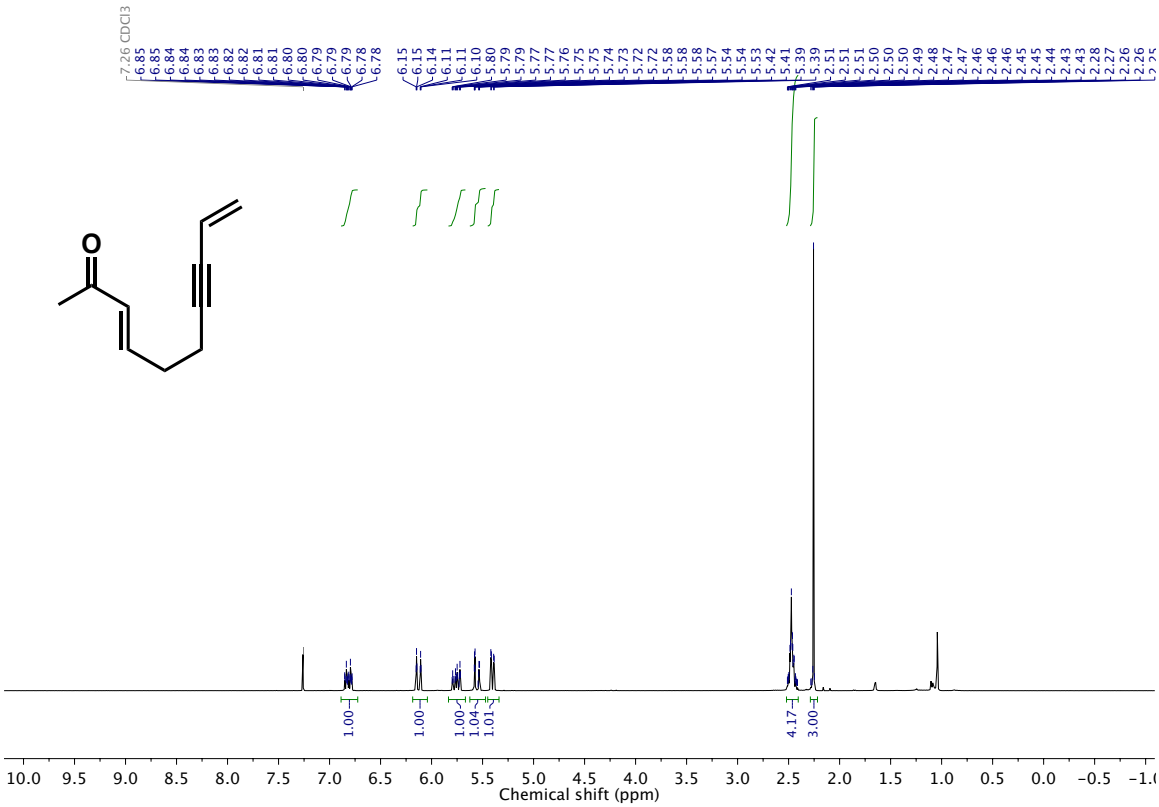
7.26 CDCl3
O
1.00
1.00
1.00
1.04
1.01
4.17
3.00
Chemical shift (ppm)

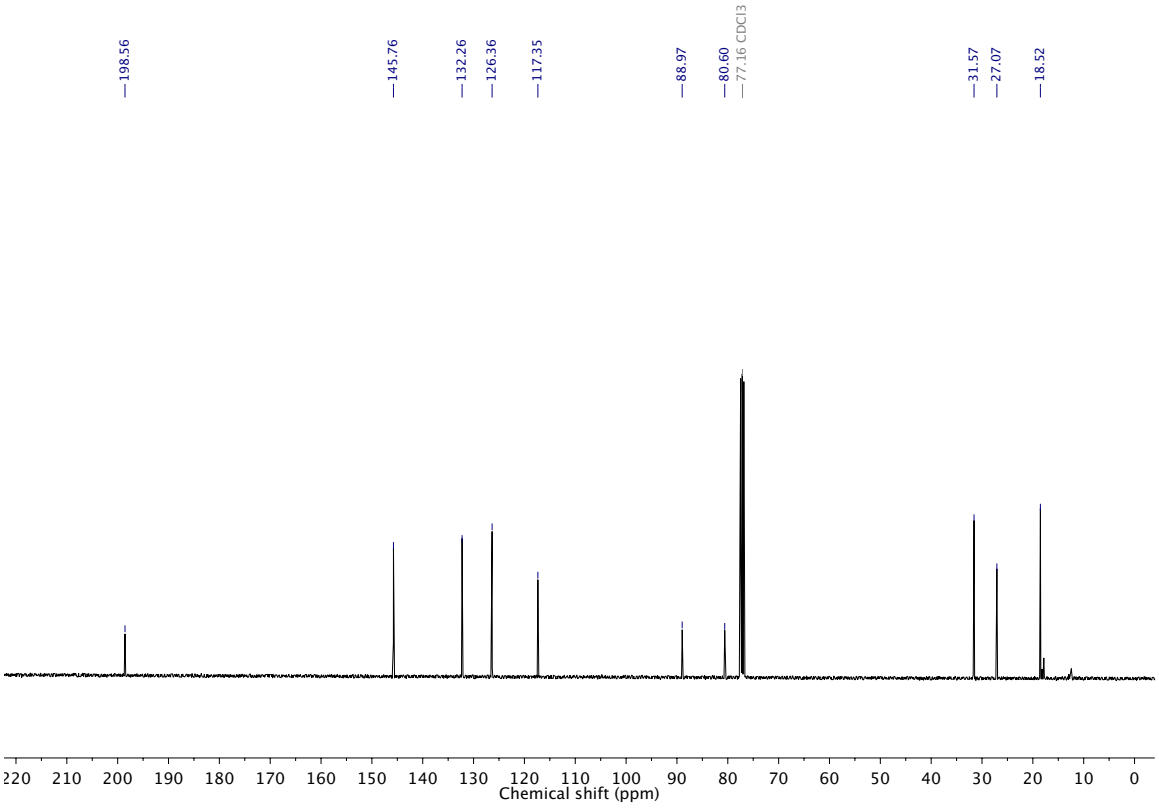
198.56
145.76
132.26
126.36
117.35
88.97
80.60
77.16 CDCl3
31.57
27.07
18.52
Chemical shift (ppm)

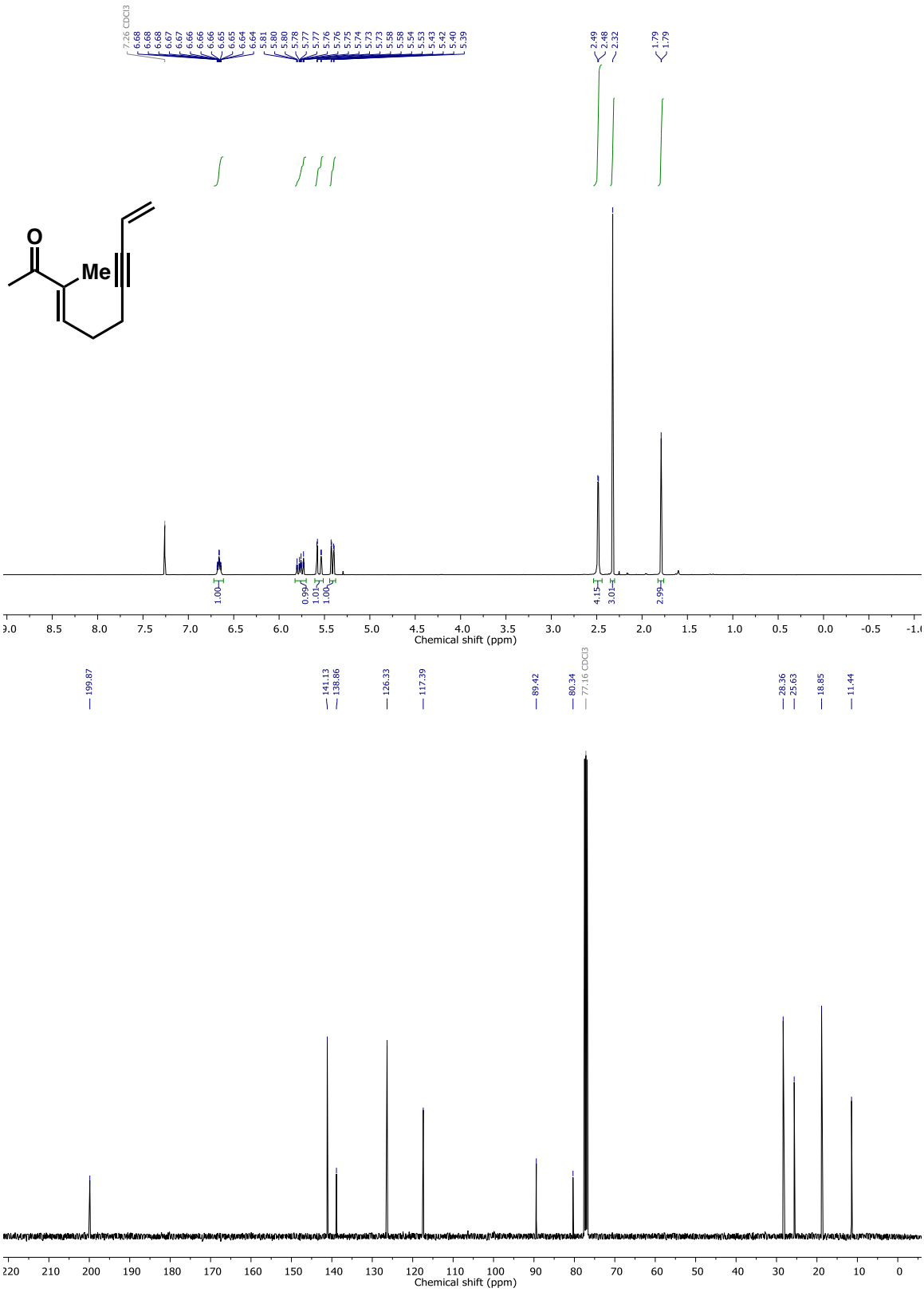
7.26 CDCl3
6.68
6.68
6.68
6.67
6.67
6.66
6.66
6.66
6.65
6.65
6.64
6.64
5.81
5.80
5.80
5.78
5.77
5.77
5.76
5.76
5.75
5.74
5.73
5.73
5.58
5.58
5.54
5.53
5.43
5.42
5.40
5.39
2.49
2.48
2.32
1.79
1.79
O
Me
1.00
0.99
1.01
1.00
4.15
3.01
2.99
Chemical shift (ppm)
199.87
141.13
138.86
126.33
117.39
89.42
80.34
77.16 CDCl3
28.36
25.63
18.85
11.44
Chemical shift (ppm)

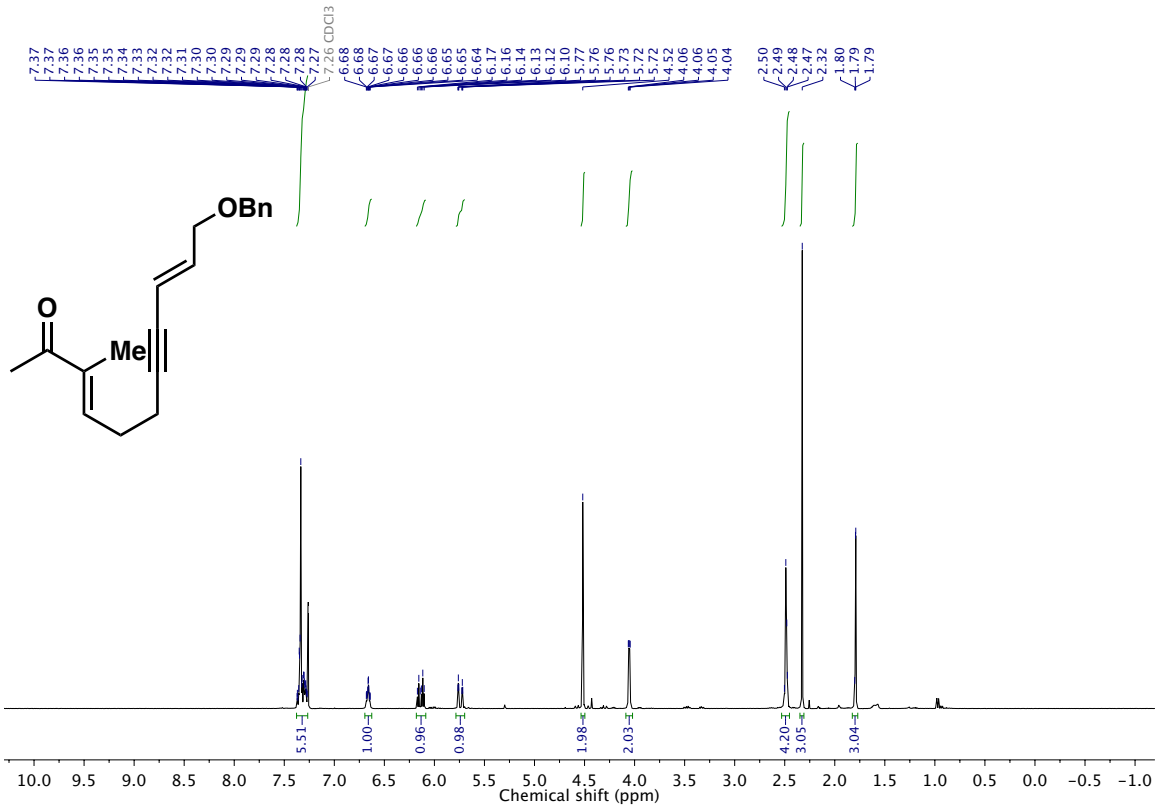
OBn
O
Me
Chemical shift (ppm)

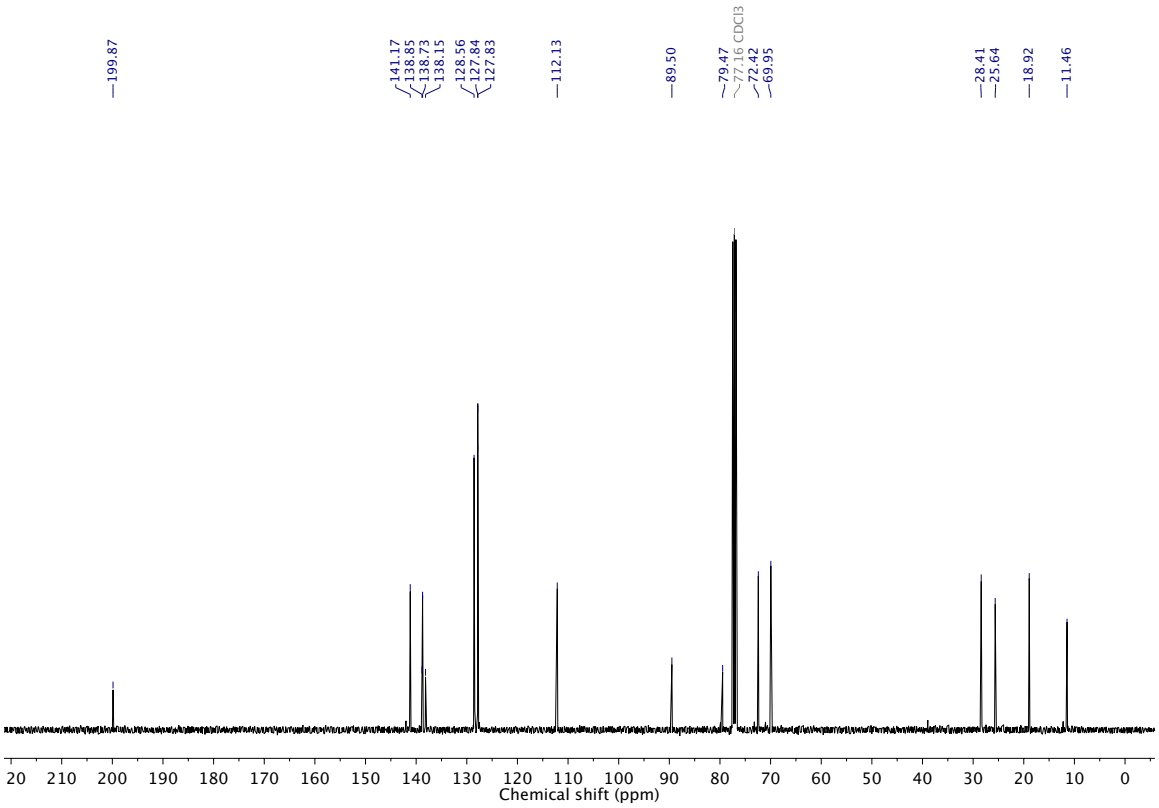
Chemical shift (ppm)

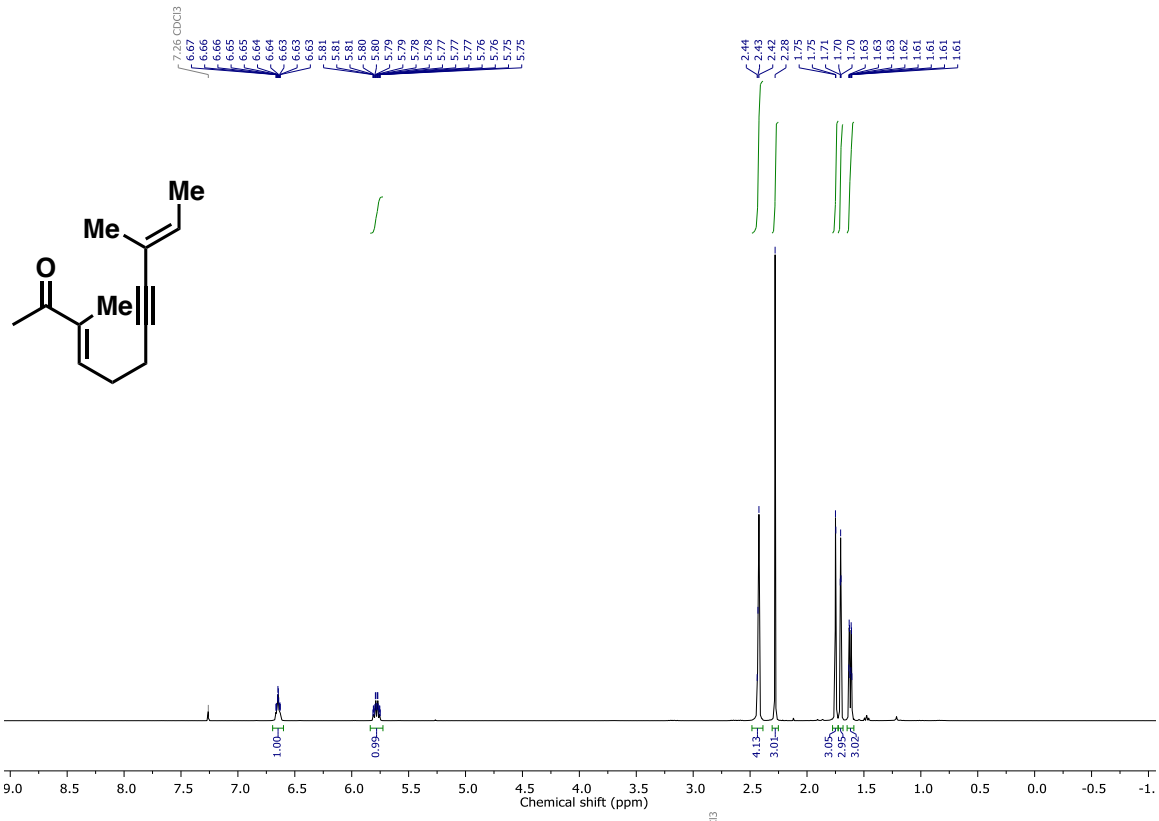
Me
Me
O
Me
Chemical shift (ppm)

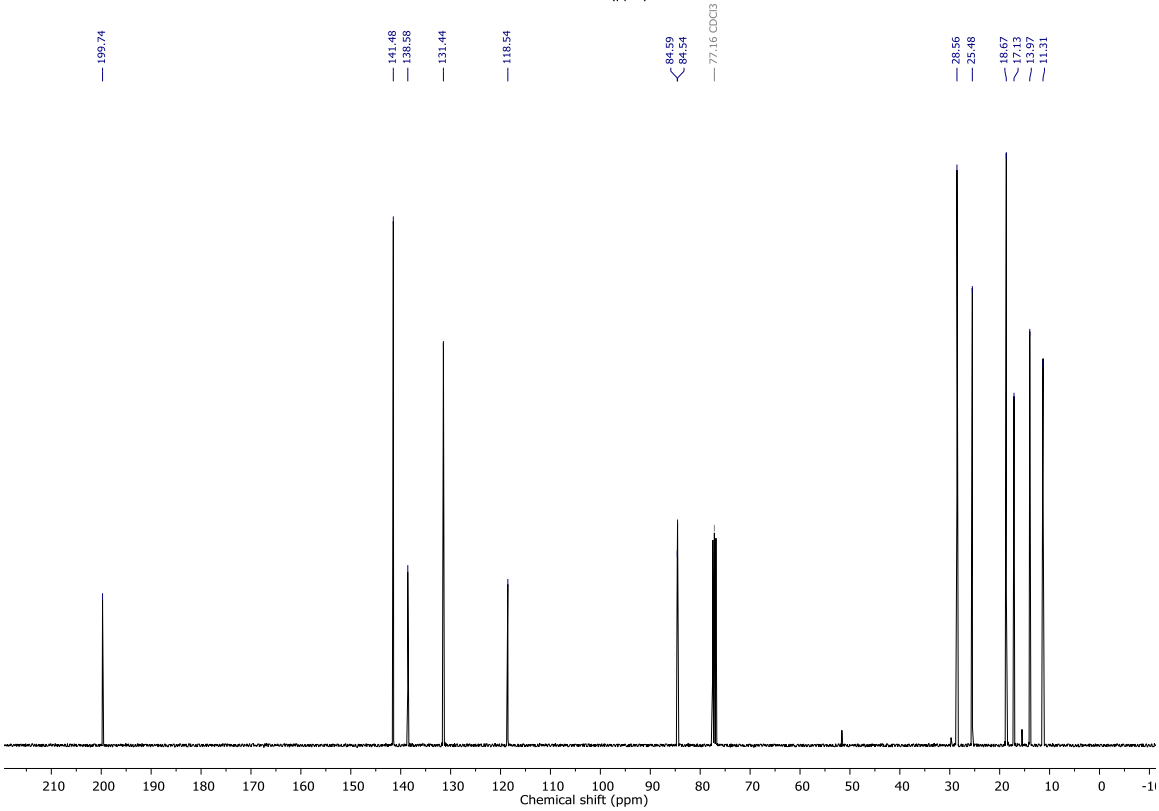
Chemical shift (ppm)

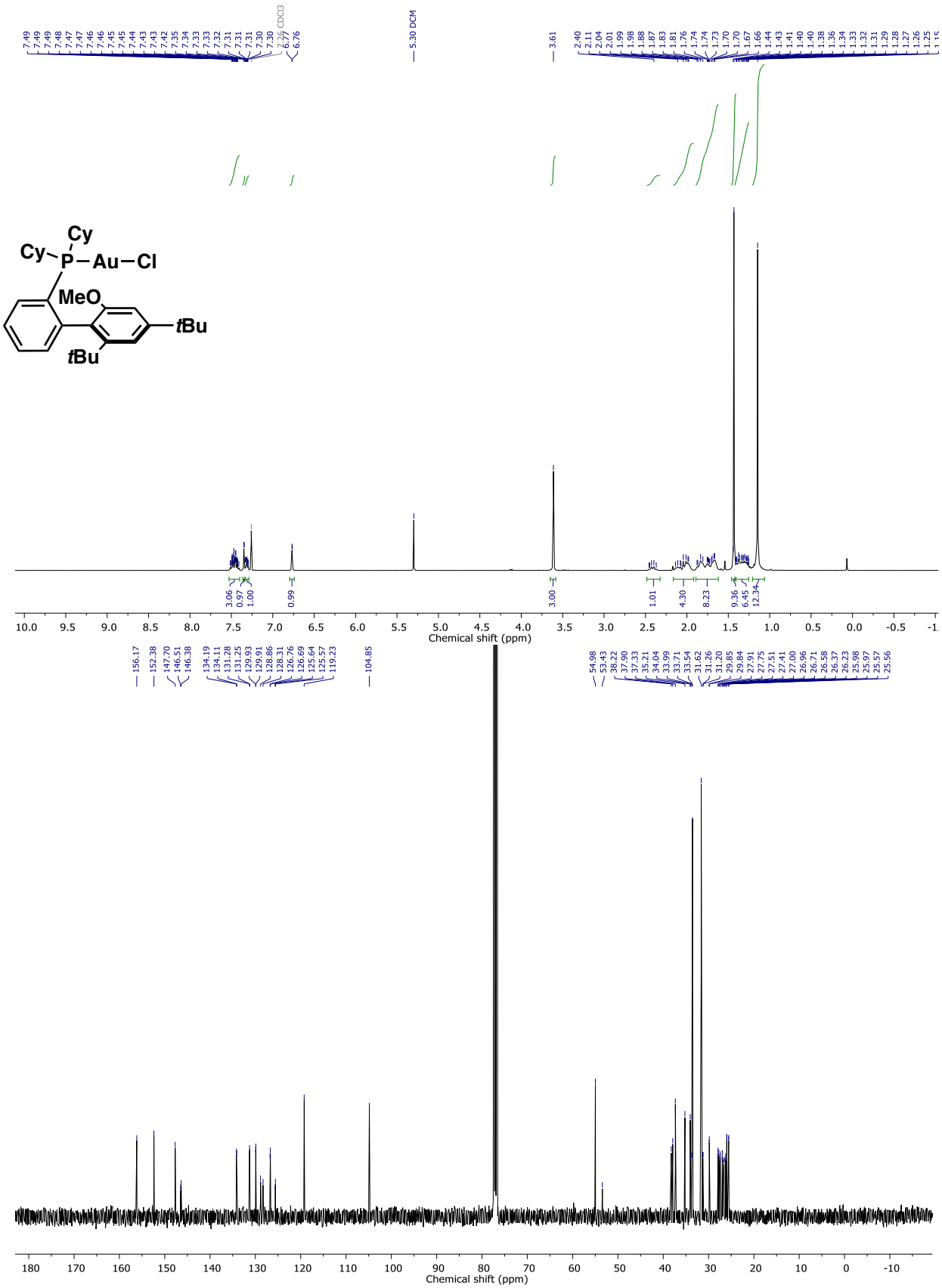
Cy
Cy
P
Au
Cl
MeO
tBu
tBu
Chemical shift (ppm)
Chemical shift (ppm)

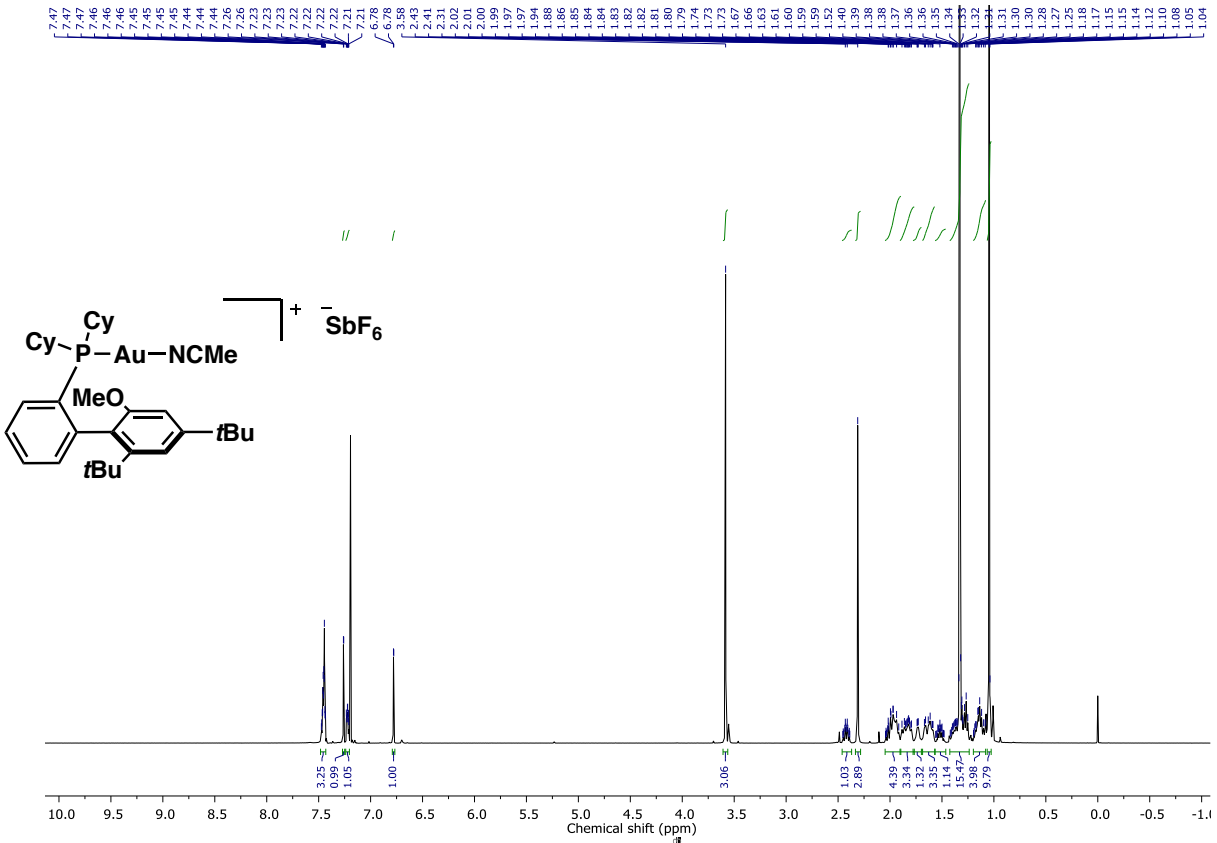
Cy
Cy
P
Au
NCMe
MeO
tBu
tBu
+
SbF6
Chemical shift (ppm)

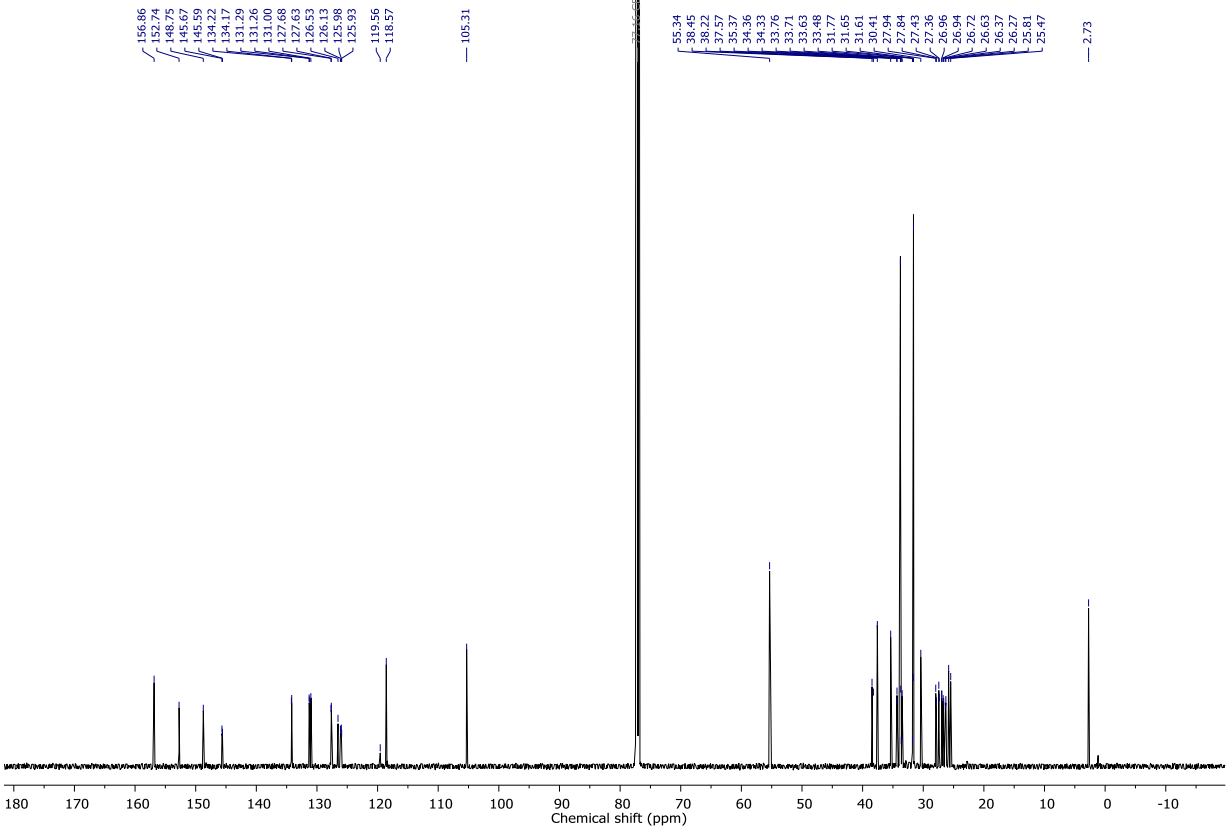
Chemical shift (ppm)

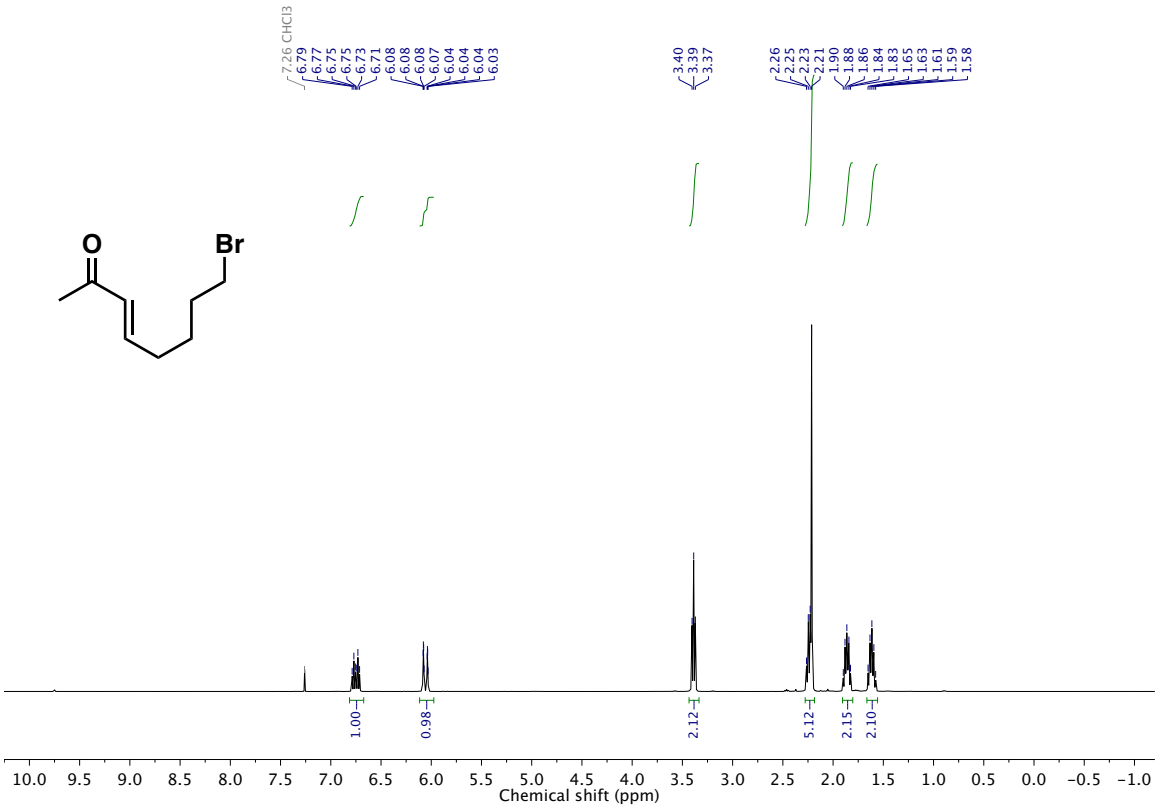
7.26 CHCl3
6.79
6.77
6.75
6.75
6.73
6.71
6.08
6.08
6.08
6.07
6.04
6.04
6.04
6.03
3.40
3.39
3.37
2.26
2.25
2.23
2.21
1.90
1.88
1.86
1.84
1.83
1.65
1.63
1.61
1.59
1.58
O
Br
1.00
0.98
2.12
5.12
2.15
2.10
10.0 9.5 9.0 8.5 8.0 7.5 7.0 6.5 6.0 5.5 5.0 4.5 4.0 3.5 3.0 2.5 2.0 1.5 1.0 0.5 0.0 -0.5 -1.0
Chemical shift (ppm)

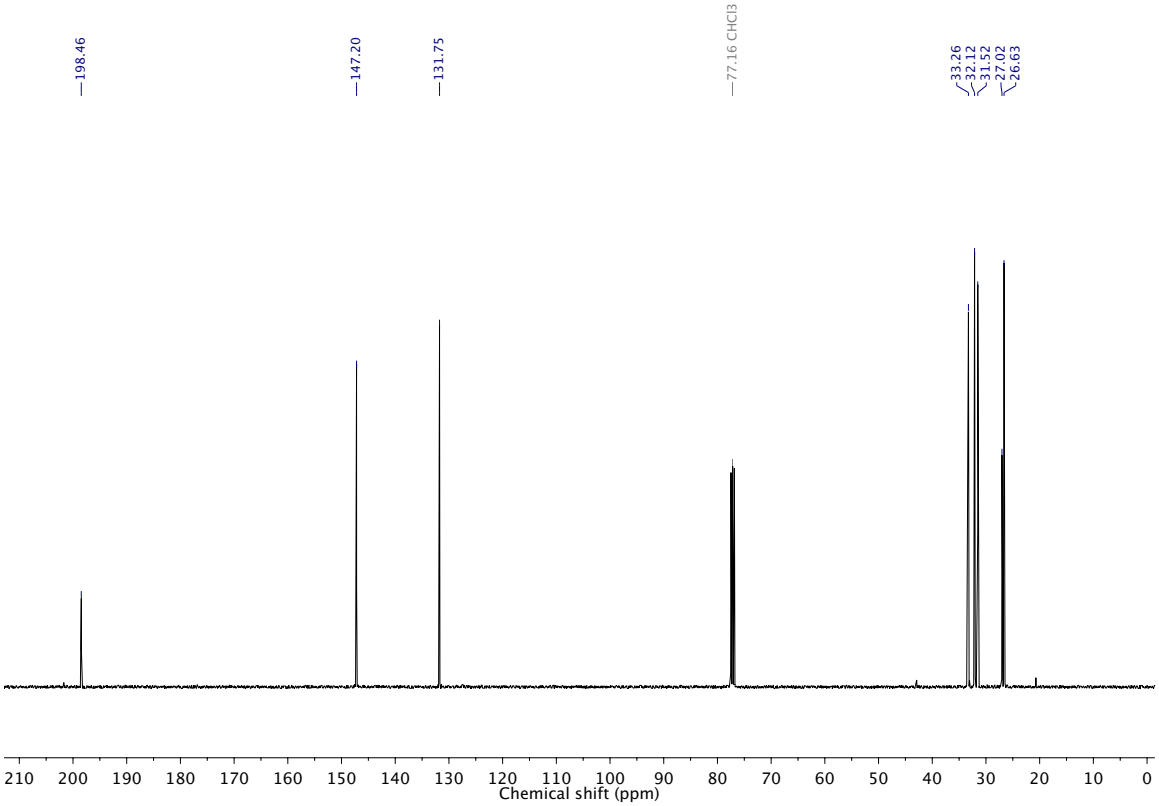
198.46
147.20
131.75
77.16 CHCl3
33.26
32.12
31.52
27.02
26.63
210 200 190 180 170 160 150 140 130 120 110 100 90 80 70 60 50 40 30 20 10 0
Chemical shift (ppm)

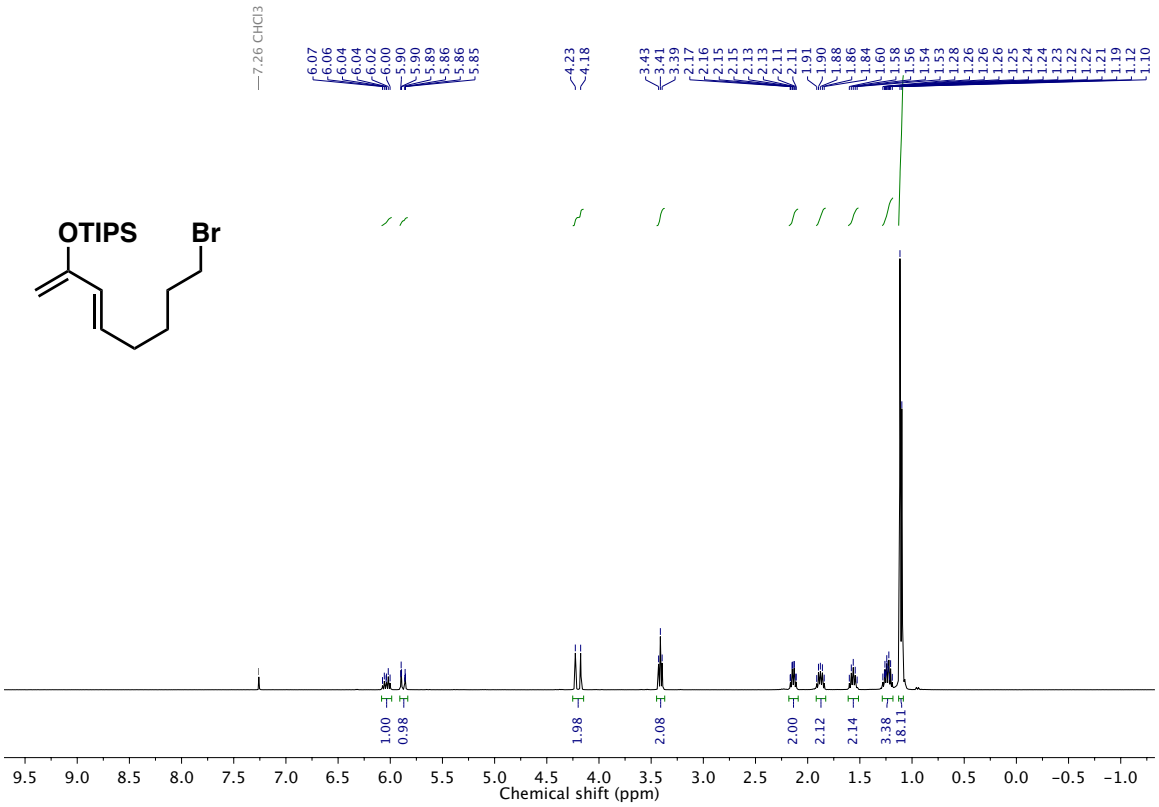
OTIPS
Br
7.26 CHCl3
6.07
6.06
6.04
6.04
6.02
6.00
5.90
5.90
5.89
5.86
5.86
5.85
4.23
4.18
3.43
3.41
3.39
2.17
2.16
2.15
2.15
2.13
2.13
2.11
2.11
1.91
1.90
1.88
1.86
1.84
1.60
1.58
1.56
1.54
1.53
1.28
1.26
1.26
1.26
1.25
1.24
1.24
1.23
1.22
1.22
1.21
1.19
1.12
1.10
1.00
0.98
1.98
2.08
2.00
2.12
2.14
3.38
18.11
Chemical shift (ppm)

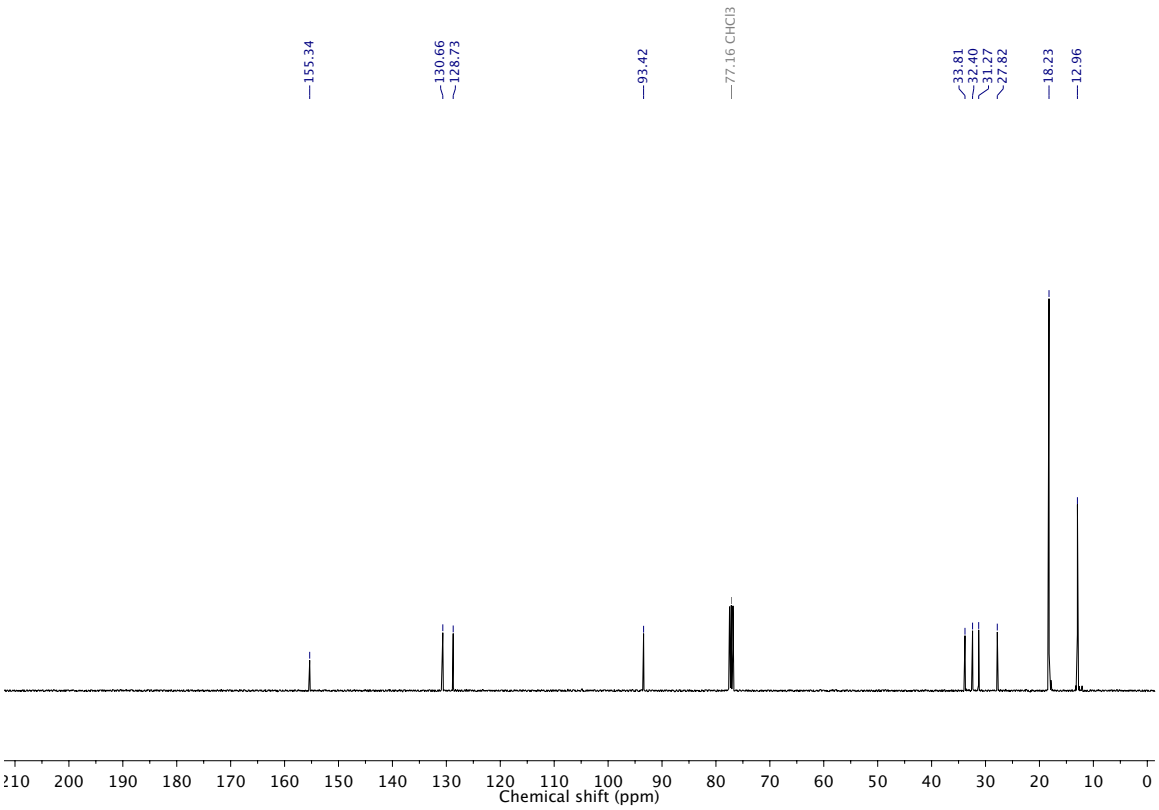
155.34
130.66
128.73
93.42
77.16 CHCl3
33.81
32.40
31.27
27.82
18.23
12.96
Chemical shift (ppm)

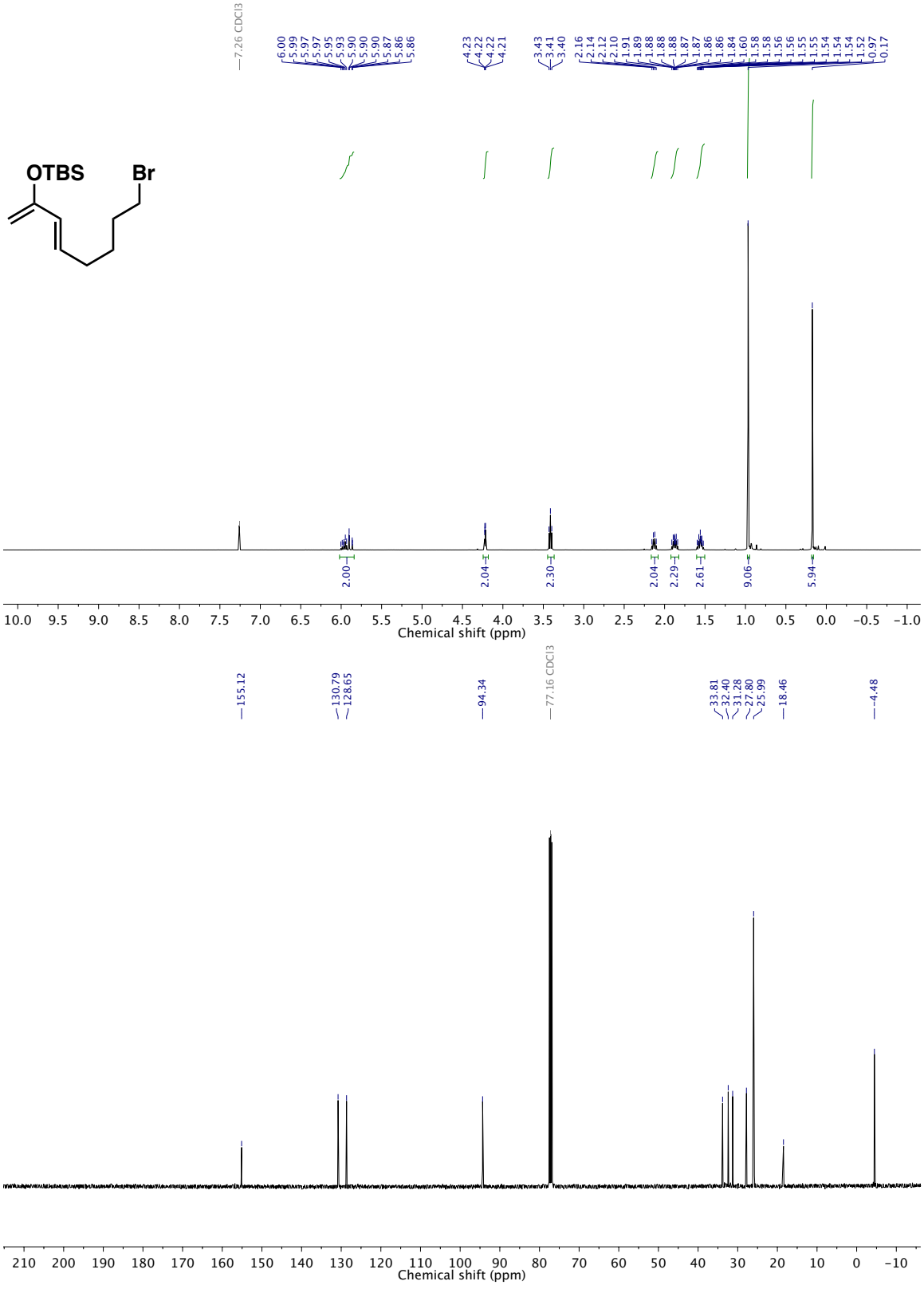
OTBS
Br
7.26 CDCl3
6.00
5.99
5.97
5.97
5.95
5.93
5.90
5.90
5.90
5.87
5.86
5.86
4.23
4.22
4.22
4.21
3.43
3.41
3.40
2.16
2.14
2.12
2.10
1.91
1.89
1.88
1.88
1.88
1.87
1.87
1.86
1.86
1.84
1.60
1.58
1.58
1.56
1.56
1.55
1.55
1.54
1.54
1.54
1.52
0.97
0.17
2.00
2.04
2.30
2.04
2.29
2.61
9.06
5.94
Chemical shift (ppm)
155.12
130.79
128.65
94.34
77.16 CDCl3
33.81
32.40
31.28
27.80
25.99
18.46
-4.48
Chemical shift (ppm)

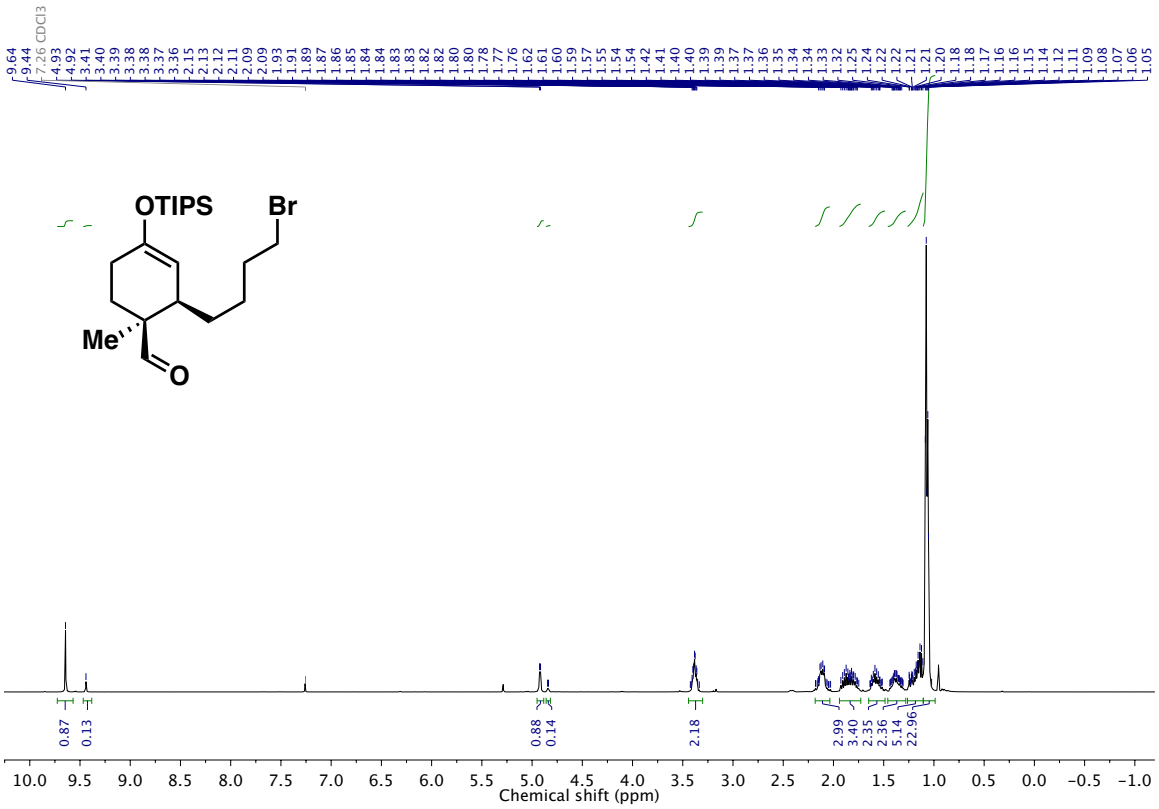
OTIPS
Br
Me
O
Chemical shift (ppm)

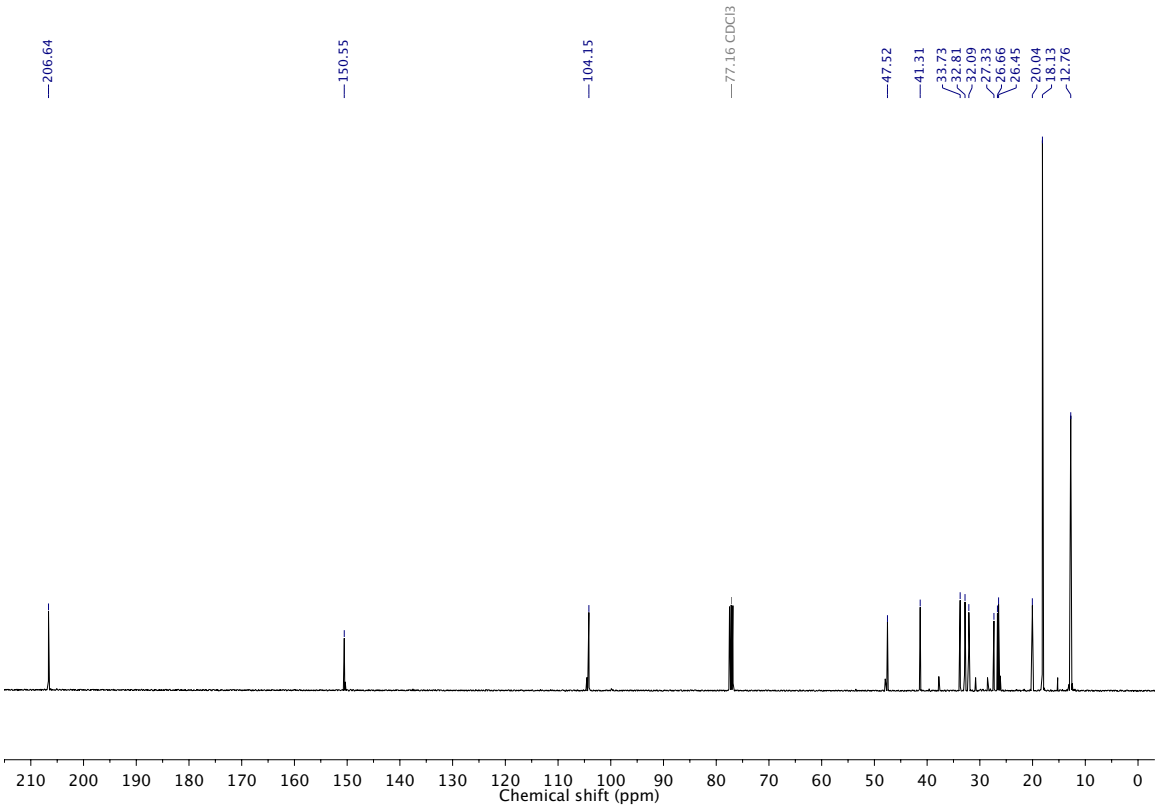
Chemical shift (ppm)

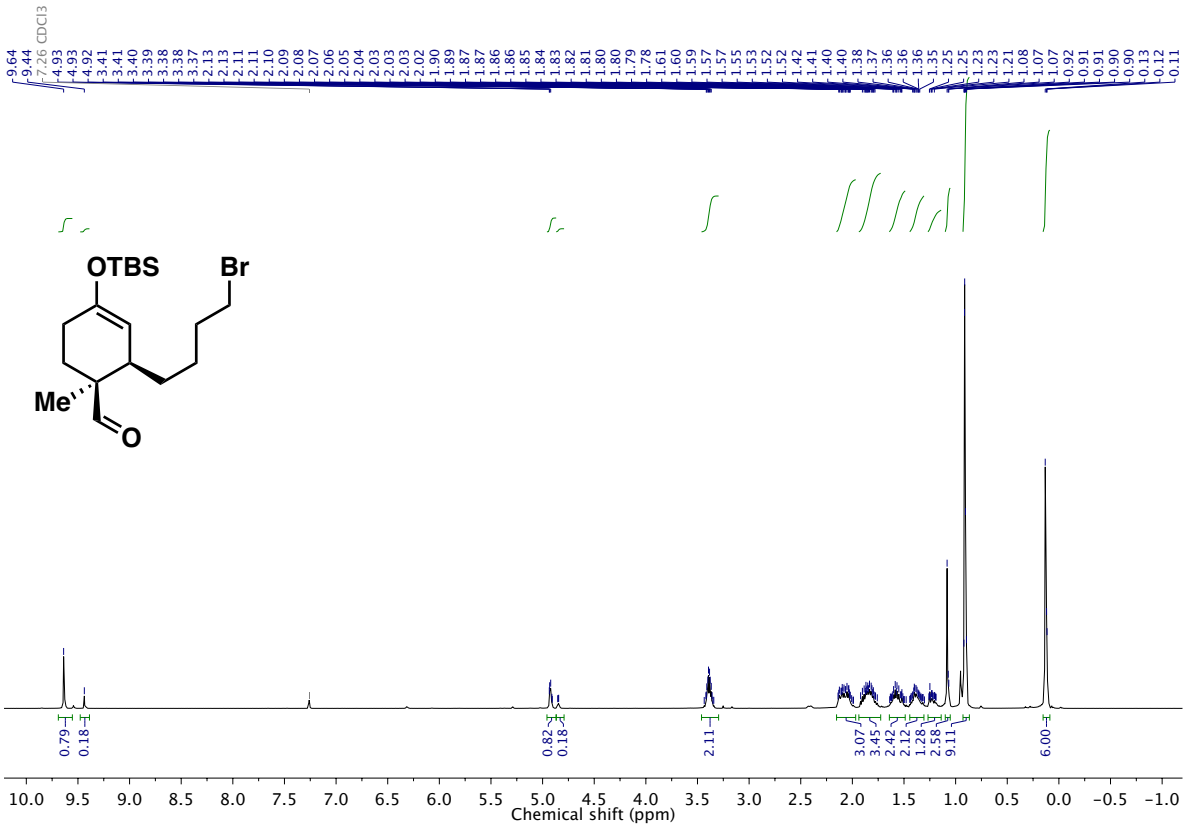
OTBS
Br
Me
O
Chemical shift (ppm)

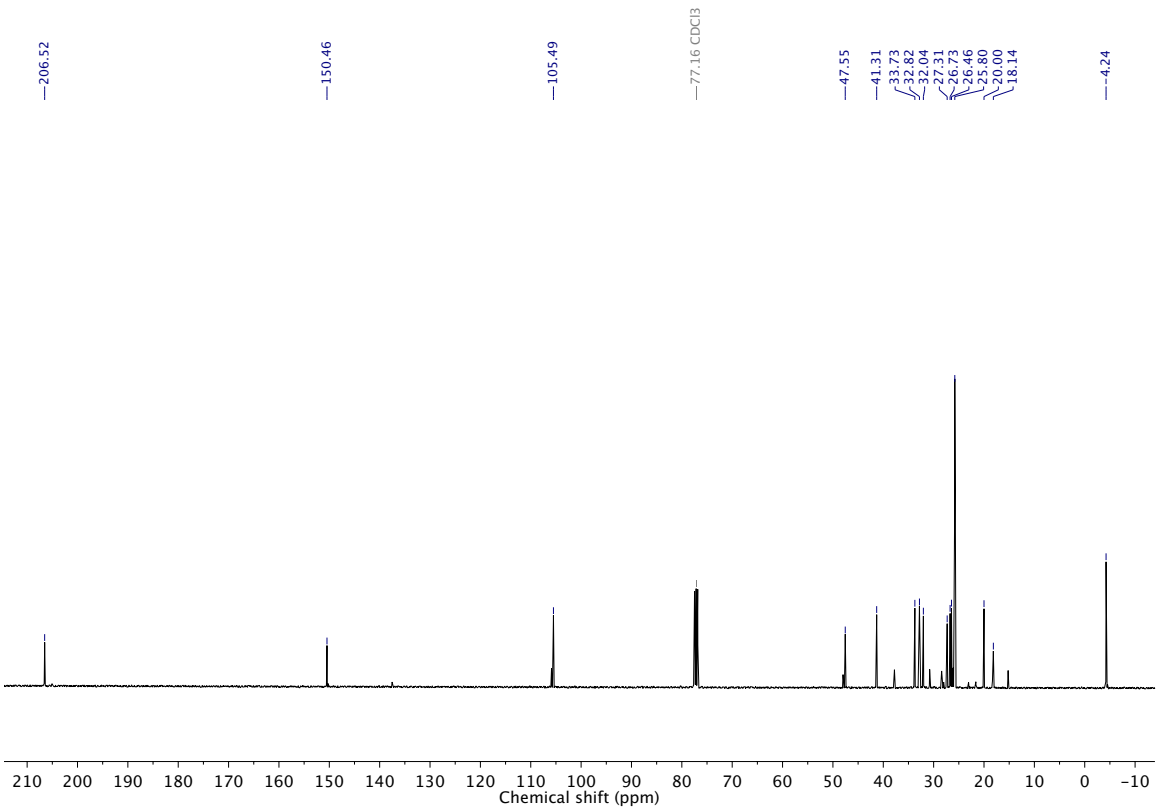
Chemical shift (ppm)